2017

Fabrication of flexible, biofunctional architectures from silk proteins

Ramendra K. Pal

Fabrication of flexible, biofunctional architectures from silk proteins

A dissertation submitted in partial fulfillment of the requirements for the degree of Doctor of Philosophy at Virginia Commonwealth University

by

Ramendra Kishor Pal

Master of Technology in Chemical Engineering- Indian Institute of Technology-Kharagpur, 2013

Advisor: Vamsi K. Yadavalli, Ph.D.

Associate Professor of Chemical and Life Science Engineering

Virginia Commonwealth University

Richmond, Virginia

August 2017

Acknowledgements

The dissertation work would not have been successful without the contributions of numerous colleagues and mentors involved in all stages from idea generation to implementation.

First and foremost, I would like to express my sincere gratitude to my advisor Dr. Vamsi K Yadavalli for the continuous support of my Ph.D. study and research, for his patience, motivation, enthusiasm, and immense knowledge. His leading by example nature has influenced me greatly. His guidance helped me in all the time of research and writing of this thesis. I could not have imagined having a better advisor and mentor for my Ph.D. study. The joy and enthusiasm he has for research are contagious and motivational for me, even during tough times in the Ph.D. pursuit. I am also thankful for his efforts in giving right direction to my academic career.

In addition, I would like to thank Dr. Maryanne Collinson and Dr. Ahmed Farghaly (Department of Chemistry, Virginia Commonwealth University, Richmond, Virginia) for teaching me electroanalytical techniques and assisting with experimental design and troubleshooting. I would also like to thank Dr. Ümit Özgür (Department of Electrical and Computer Engineering, Virginia Commonwealth University, Richmond, Virginia) for guiding me with electrical characterization and providing me unabridged access to his optics lab. The later part of the work would not have been possible without Dr. Ram B Gupta and his students Dr. Muslum Demir, Dylan Rodene, Matthew DeCuir and Dr. Sushil Saraswat (Department of Chemical and Life Science Engineering, Virginia Commonwealth University, Richmond, Virginia) for allowing me to use their potentiostat

whenever required. I would like to thank my thesis committee member Dr. Christina Tang (Department of Chemical and Life Science Engineering, Virginia Commonwealth University, Richmond, Virginia) for her encouragement, insightful comments, and probing questions. My sincere thanks also go to Dr. Christopher Ehrhardt (Department of Forensic Science, Virginia Commonwealth University, Richmond, Virginia), Dr. Ning Zhang (Department of Biomedical Engineering, Virginia Commonwealth University, Richmond, Virginia), and Dr. Xuejun Wen (Department of Chemical and Life Science Engineering, Virginia Commonwealth University, Richmond, Virginia) for providing me access to their lab and leading me to finish works on time. I would like to thank my fellow lab-dwellers in the Bionano Laboratory: Dr. Nicholas Kurland, Dr. Congzhou Wang, and Mahmood Moustafa, Benjamin Chalfant, Emigdio Turner, Songnian Liu, Lokesh Narayan and Sayantan Pradhan for their immense help with my experiments and stimulating discussions. I would like to extend my regards to my friends: Md. Rezaul Karim Khan, Alesio Bucciarelli, Shopan Hafeez, William Clavijo and Chenyang Jiyang for their support in accomplishing my research.

Last but not the least, I would like to thank my parents: Ram Prasad Pal and Geeta Rani Pal, for giving birth to me at the first place and supporting me in my all endeavors throughout life.

Table of Contents

Abstract

FABRICATION OF FLEXIBLE, BIOFUNCTIONAL ARCHITECTURES FROM SILK PROTEINS

By Ramendra Kishor Pal

A dissertation submitted in partial fulfillment of the requirements of the degree of Doctor of Philosophy at Virginia Commonwealth University.

Virginia Commonwealth University, 2017

Major Director: Vamsi K. Yadavalli, Ph.D., Associate Professor of Chemical and Life Science Engineering

Advances in the biomedical field require functional materials and processes that can lead to devices that are biocompatible, and biodegradable, while maintaining high performance and mechanical conformability. In this context, a current shift in focus is towards natural polymers as not only the structural, but also functional components of such devices. This poses material-specific functionalization and fabrication related questions in the design and fabrication of such systems. Silk protein biopolymers from the silkworm show tremendous promise in this regard due to

intrinsic properties: mechanical performance, optical transparency, biocompatibility, biodegradability, processability, and the ability to entrap and stabilize biomolecules. The unique ensemble of properties indicates opportunities to employ this material into numerous biomedical applications. However, specific processing, functionalization, and fabrication techniques are required to make a successful transition from the silk cocoon to silk-based devices. This research is focused on these challenges to form silk-based functional material and devices for application in areas of therapeutics, bio-optics, and bioelectronics.

To make silk proteins mechanically conformable to biological tissues, the first exploration is directed towards the realization of precisely micropatterned silk proteins in flexible formats. The optical properties of silk proteins are investigated by showing angle-dependent iridescent behavior of micropatterned proteins, and developing soft micro-optical devices for light concentration and focusing. The optical characteristics and fabrication process reported in the work can lead to future application of silk proteins in flexible optics and electronics.

The microfabrication process of silk proteins is further extended to form shape-defined silk protein microparticles. Here, the specificity of shape and the ability to form monodisperse shapes can be used as shape encoded efficient cargo and contrast agents. Also, these particles can efficiently entrap and stabilize biomolecules for drug delivery and bioimaging applications.

Next, a smart confluence of silk sericin and a synthetic functional polymer PEDOT:PSS is shown. The composite materials obtained have synergistic effects from both polymers. Silk proteins

impart biodegradability and patternability, while the intrinsically conductive PEDOT:PSS imparts electrical conductivity and electrochemical activity. Conductive microarchitectures on rigid as well as flexible formats are shown via a green, water-based fabrication process. The applications of the composite are successfully demonstrated by realizing biosensing and energy storage devices on rigid or flexible forms. The versatility of the approach will lead to the development of a variety of applications such as in bio-optics, bio-electronics, and in the fundamental study of cellular bio electrogenic environments.

Finally, to expand the applicability of reported functional polymers and composites beyond the microscale, a method for silk nano-patterning via electron beam lithography is explored. The technique enables one-step fabrication of user defined structures at the submicron and nano-scales. By virtue of acrylate chemistry, a very low energetic beam and dosage is required to form silk nano-architectures. Also, the process can form both positive and negative features depending on the dosage. The fabrication platform can also form nanoscale patterns of the conductive composite. The conductive measurements confirm the formation of conductive nanowires and the ability of silk sericin to entrap PEDOT:PSS particles in nanoscale features.

CHAPTER 1

INTRODUCTION

1.1 INTRODUCTION

Applications in the life sciences require devices which can interface and interact with biological systems.[2] Such devices can be external, wearable, implanted or delivered, and can be further classified as passive or active. Broadly defined, passive systems primarily perform structural functions, and do not require an energy source for their function. Examples include tissue scaffolds, intraocular lenses for cataract treatment, vascular grafts, artificial joints and valves.[3-6] In contrast, active systems perform complex functions such as controlling or activating specific biological functions, often requiring energy sources. Examples include pacemakers to control heart rhythms, cochlear implants with electromagnetic transducers for restoring hearing loss, biochemical sensors, and probes to record and stimulate physiological functions.[7-9] For both modalities, extensive efforts are underway to develop both the materials and technologies required. In addition to the functional characteristics needed for a particular application (mechanical strength, stimulus response, mechano-transduction, electrical conductivity, optical properties etc.), desirable intrinsic or design properties of materials include biocompatibility (*i.e.* materials do not invoke adverse reactions in biological systems), controlled biodegradability (*i.e.* stable during the operational period, but capable of degrading in a benign fashion afterwards), compatibility with conventional microfabrication process for miniaturization, and mechanical stability [10, 11]

To date, materials such as metals, ceramics, and polymers have been identified for these diverse biomedical applications. While metals and ceramics are extensively applied in orthopedic and dental applications where mechanical strength and hardness is of prime importance, polymeric biomaterials have been key in developing “softer”, functional tissue scaffolds and drug delivery vehicles.[12, 13] The use of conventional materials in bio-electronics and optoelectronics is a challenge. Such devices operate in environments that are non-planar, soft and flexible, and the use of hard and rigid materials can not only cause problems in conforming to the underlying substrata, but can also prove detrimental to delicate tissues - invoking adverse inflammatory response and scar tissue formation, eventually resulting in improper function and tissue damage.[14, 15] Therefore, there is great interest in materials that are soft, flexible, and can overcome the mechanical mismatch between the biological milieu and implanted devices.[16, 17] Elastomeric polymers provide suitable attributes, such as low cytotoxic response, high stability in physiological environments, and mechanical similarity to soft tissues, which can be exploited to develop flexible and tactile devices.[17] The development of polymeric biomaterials is further improved by their ability to be easily chemical functionalized, or adapted to microfluidics and micro/nano-fabrication techniques. The ability to degrade provides additional advantages for passive or active biomedical applications.

Material selection is generally guided by: (1) mechanical conformability, (2) biocompatibility, (3) biodegradability, (4) performance, and (5) sustainable and reproducible fabrication.[2] Since they mostly serve as structural components, the choice is often based upon the range of functionalities available to address application-specific needs. Broadly, two classes of polymeric materials are in use - synthetics including poly lactic acid (PLA), poly-glycolic acid (PGA), poly lactic-co-glycolic

acid (PLGA) copolymers, and polycaprolactone (PCL); naturally derived materials, including polysaccharides (starch, alginate, chitosan, hyaluronic acid derivatives), proteins (soy, collagen, fibrin, gels, silks), polynucleotides (DNA, RNA), and biofibers.[18] To date, synthetic polymers have been the materials of choice because of their low cost, design flexibility, mechanical strength and overall processability.[19] However, synthetic polymers are typically not usable in a sustainable manner, or are not degradable. In contrast, naturally-derived biomaterials are renewable resources, and offer fundamental compatibility with the host's complex biological systems due to their similar chemical structure. Natural polymers are therefore gaining attention, driven by their intrinsic value as renewable and sustainable materials.[19] While there have been significant efforts to realize high performance and next generation active devices using synthetic polymers, efforts to employ natural biopolymers have been relatively fewer.

Significant challenges hinder the incorporation of natural biomaterials in active systems. These include - (1) material integration into micro/nano-fabrication techniques, (2) performance issues, and (3) long-term stability. In general, natural systems tend to have poor performance characteristics in comparison to synthetic materials (for instance electroactivity). Nonetheless, due to biocompatibility, biodegradability, and environmental concerns, strategies which enable natural polymers to be used as substrates, templates, dispersants, and even as functional components for organic devices are desirable.[20] In addition to silk proteins discussed in this work, to date, some efforts to realize functional architectures and devices using natural polymers include chitosan-polyaniline composites as immunosensors,[21] and cellulosic paper based devices used for biosensing, energy storage and energy harvesting.[22, 23] Realization of sustainable strategies for the formation of natural polymer-based functional micro-architectures continues to be an ongoing

challenge.

Among various bio-derived materials, silk proteins stand out due to exceptional mechanical properties, optical transparency, chemical stability, and biocompatibility. They can be tailored for controlled bio-resorption and are available at low cost.[24] Owing to their controlled processability using well-developed protocols, diverse applications of silk proteins from various sources have been reported.[25] These include tissue scaffolds, drug delivery vehicles, optical devices, and stimuli responsive materials.[26] Silk proteins can be blended with other synthetic materials to form composite architectures like electrospun fibrous mats, hydrogels, sponges, microtubes.[1, 25] These composites can offer better biocompatibility, biodegradability, or processing over synthetic biomaterials. However, blending often results in moderation of the intrinsic properties of silk proteins.[1] Another approach to ensure functional behavior is to use controlled chemical modification.[27] Of interest is the recent chemical modification strategy of silk proteins obtained from *Bombyx mori* developed by our group.[28, 29] Chemical conjugation is used to alter the proteins into photoreactive forms without attenuating their intrinsic properties, while improving mechanical stability under biological conditions. These modified proteins are utilized to create high resolution microarchitectures via conventional photolithography techniques, opening up new applications. **This research is focused on the development of next generation bio-derived and bio-inspired functional architectures and devices based on silk protein precursors.**

1.1.1 Significance/Research Objective

The above discussion enumerates the advantages in using natural polymers to realize functional architectures and active devices. Research into fully integrated devices that are flexible, soft,

biocompatible, biodegradable, without compromising performance metrics, is in its nascent stages. These criteria require new materials and novel fabrication approaches. Since silk proteins already fulfil many criteria for biomedical purposes, they are suitable for developing integrated functional systems. While initial studies demonstrated patterning on conventional, rigid substrates like glass and silicon, the versatile properties of silk proteins are also ideal for developing *flexible* functional devices.[30] Coupling micropatterning strategies with mechanically flexible substrates has the potential to broaden application areas, as well as address the mismatch issues discussed above. For instance, it is possible to form optoelectronic devices with controllable stability, biocompatibility and bioresorption characteristics. Devices can detect, record and/or stimulate physiological activities directly or indirectly while being implanted or as wearable systems. The proteins can be complexed with other functional materials to obtain novel functional composites where both materials synergistically complement properties. For example, conducting polymers and carbon based materials can provide a combination of electrical and electrochemical properties.[31] **The objective of this research is to investigate the micropatterning of silk proteins and composites to fabricate smart architectures, and flexible devices capable of functions such as light manipulation, biosensing, and flexible energy storage.** This research will explore ways to develop modular materials and architectures based on silk proteins, and expand the repertoire of silks to flexible sensors, electronics, optoelectronics, and energy storage systems for the development of integrated active devices.

1.2. SPECIFIC AIMS

Issues related to formation of biodegradable functional morphologies and hybrids, mechanical stability, and integration with fabrication tools, prevent the widespread use of silk proteins for

flexible optical and bioelectronic systems. It is hypothesized that electronic and functional materials can be integrated with silk proteins to form novel functional biocomposites for developing flexible, biodegradable, optical, and bioelectronic devices. Modifications to earlier developed silk protein photolithography protocols can be made without hampering the fidelity and structural resolution. The hypothesis will be tested by following aims:

1. Development of micropatterning techniques to form structures on flexible substrates for soft optics and bioelectronics.
2. Development of shape defined silk particles for drug delivery applications.
3. Development of micropatterning strategies to enable conductive behavior in flexible formats and utilize them for biosensing and energy storage.
4. Translation of lithography techniques for silk proteins to the nanoscale.

1.2.1. Silk protein photolithography techniques to realize patterning on flexible substrates

Micropatterning of silk proteins on flexible substrates is essential to realize flexible organic devices. The first part of the study comprises development of protocols to enable the manufacture of flexible protein (fibroin and sericin) micropatterns using photolithography. These architectures utilize the optical transparency of silk proteins for soft micro-optics and photonics. The study will show the interaction of light with protein microstructures and provide a platform to establish the potential of silk proteins to be used as optical and electronic materials.

1.2.2 Fabrication of precisely shaped particles using silk protein lithography

The developed process will provide a sustainable approach to form shape defined silk microparticles from silk fibroin and sericin. Manufacturing of high fidelity, shape-specific (i.e. non-spherical) particles of silk proteins in large quantities can open up application areas where physical characteristics such as particle shape, size, mechanical properties, permeability, surface charge, and surface chemistry of the particles are of importance.

1.2.3 Micropatterning strategies to enable conductive behavior in flexible formats

Conducting polymers have great potential to be used as active transducers, flexible biosensors and bioelectronic devices. An engineering approach to form composites of the conducting polymer - PEDOT:PSS with silk proteins will be studied. These composites will enable processing using benign conditions for photolithographic micropatterning. Further, processes will be developed to realize rigid, flexible and biodegradable conductive microarchitectures.

1.2.4 Fabrication of biosensors towards different kinds of targets

These techniques are then translated to form biosensors to potentially monitor activities in physiological systems and detecting biological analytes. However, improvement of biosensor sensitivity with benign material and processes is a challenge. Also, there are challenges in translating biosensing electrodes to soft, flexible formats (for example, wearable or implantable devices) suitable for real time monitoring. This research will investigate the application of silk based conductive composites in development of rigid as well as flexible and biodegradable

electrochemical biosensors. The goal of the work will be to show simultaneous detection of biomolecules in rigid format and highly sensitive detection of various bioanalytes without using conventional metal, metal oxide or carbon crystal based electrodes.

1.2.5 Flexible and biodegradable energy storage devices for biomedical applications

Another aspect in development of integrated active systems is to develop power storage and delivery systems that are stable over the useful lifetime of the device. Electrochemical micro supercapacitors (SCs) are considered as viable alternatives due to their fast charging-discharging rates, high power density, higher cycling stability as well as possibility to form in thin-film configuration. This aim of the work will be to develop a completely green, silk protein based SC which should be stable for a month. The modulation of capacitive properties will be done by incorporating graphene in the system.

1.2.6 Nanoscale patterning of silk proteins/conducting polymer for device miniaturization

While the above tasks are focused on microscale architectures, high fidelity fabrication of biopolymers such as silk proteins at nanoscale resolutions can open further avenues of research in miniaturization to form biosensors, or to pursue fundamental studies related to the interactions of nanoscale patterned surfaces with physiological environments. Patterning of conducting polymers at the nanoscale can be exploited to form miniaturized devices and circuits. In this work, e-beam lithography is developed to realize a low energy based, photoresist-free, green process to obtain nanoscale features and wires.

Accomplishment of these aims will provide new knowledge and utility to use silk proteins in conjunction with other functional materials to realize high performance devices for optics and bioelectronics in benign and sustainable manner. The fundamental electrochemical study on silk-based conductive materials provides additional insight into the design and behavior of biocomposites, and leads the way for further improvements in electrical and electrochemical properties. The approaches used in this work may be applicable to other natural and/or synthetic biomaterials being pursued towards similar applications. The devices and techniques developed may be used to develop all polymer, biodegradable, and integrated opto-electronic devices for sensing, therapeutics, and health monitoring.

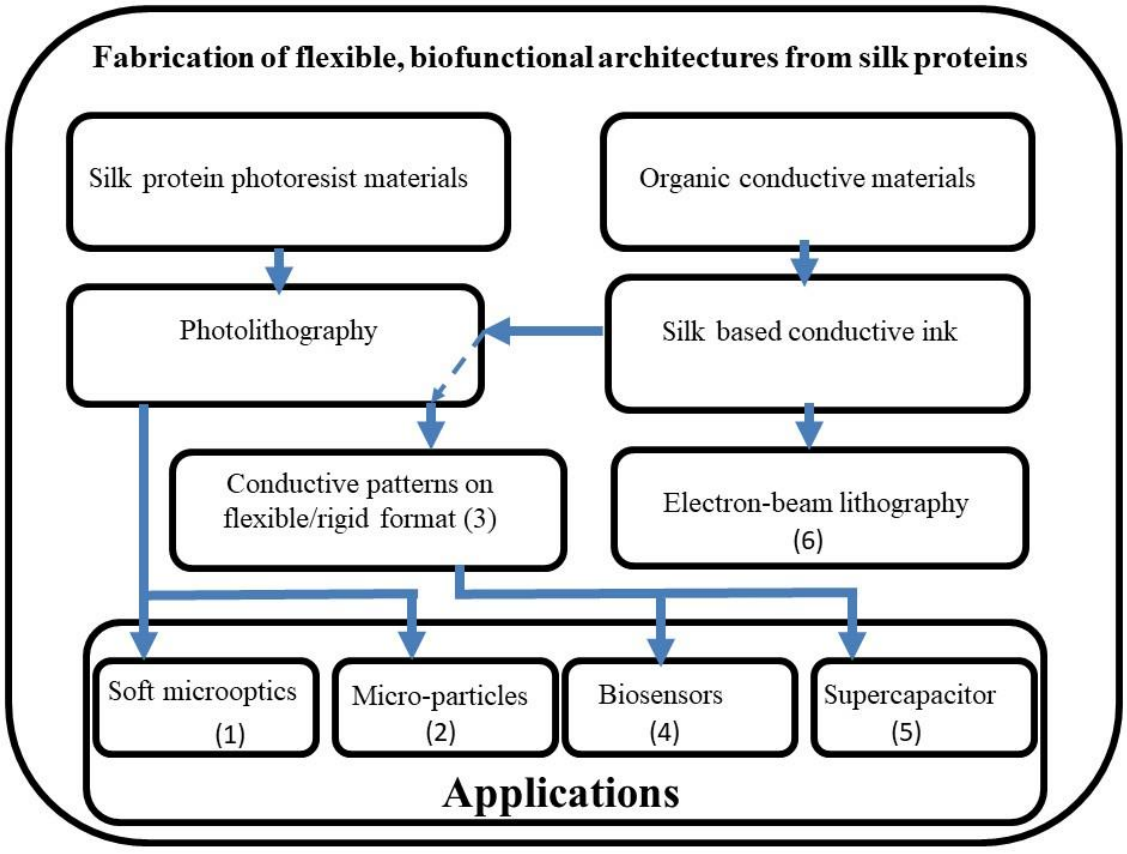

Figure 1.1 *Summary of specific aims and workflow*

1.3. BACKGROUND AND SIGNIFICANCE

This doctoral dissertation is focused on the development of silk protein-based architectures as functional components of integrated bioelectronic devices. To achieve the specific aims outlined above, new materials, techniques and process strategies are needed. Fundamental and applied studies are conducted on silk proteins and other conductive materials employing multidisciplinary approaches of physical, and chemical techniques. This section will lay out the background and significance of the research, first putting together the intrinsic capabilities of silk proteins and conductive polymers, and then expanding into proposed approaches to realize functional silk protein devices.

1.3.1. Biomaterials based on silk proteins

Silk is a commonly used term to imply protein fibers spun by many arthropod family species such as silkworms, spiders, scorpions, mites and flies.[19] Silks have been known to humanity since the 4^{th} millennium BCE.[26] Traditional uses have been in the production of textiles due to its fibrous nature, mechanical strength, luster and durability. With excellent biocompatibility, silks were used by the ancient Egyptians in medical applications such as sutures. Over the two decades, silk has emerged as an important natural biomaterial due to a high abundance, relatively low-cost, exceptional mechanical and biological properties, and well-developed processing [19]

Silk proteins from the domesticated mulberry silkworm, *Bombyx mori,* are most abundant. Spiders form another important source of silk proteins. Even though spider silk is mechanically far superior to the silk from silkworms, they tend to have diverse composition owing to the multiplicity of their

functions, including prey capture, sensing and serving as draglines. Moreover, owing to the predatory and territorial nature of spiders, production of spider silks in large quantities is difficult and expensive. Methods like recombinant DNA technology can be used, which are still in a nascent stage.[32] On the other hand, silk obtained from *B. mori* is easily obtained, enjoys more uniform properties, and has been well characterized physically and biochemically by many independent groups.[33] Thus, silk proteins from *B. mori* form the material of choice for this work.

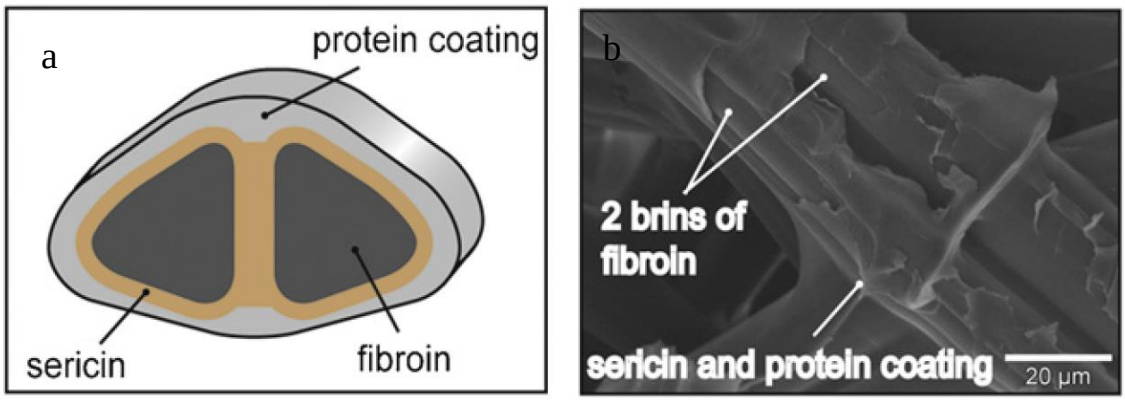

Figure 1.2. *Self-assembled configuration of silk protein fiber where sericin and a protein form a coated envelope for fibroin (a) Schematic and (b) SEM image.[1]*

Natural silk proteins are extruded as self-assembled biopolymers from the glands of the silk worm. The *B. mori* cocoon is made up of 10-20 µm fibers - primarily composed of two proteins: fibroin (70%) which composes the core of the silk fiber, and a glue-like glycoprotein sericin (~30% of fiber) surrounds this core. Sericin combines fibroin fibrils into microscale silk fibrous subunits (Figure 1.2). This unique configuration results from distinct amino acid compositions—the relative strength of fibroin is derived from an abundance of Gly-Ala-rich repeats arranged into β-sheet rich regions, while sericin presents a significant quantity of hydrophilic amino acids, enabling the formation of a soluble protein coat.[34] This makes it possible to form a single, high tensile

strength (> 0.5 GPa), high elasticity (5 – 12 GPa) fiber from the additive contributions of multiple single fibroin subunits.[35]

1.3.1.1 Silk fibroin

Silk fibroin protein is a leading biopolymer in modern biomaterials research, due to an exceptional set of properties such as high tensile strength and elasticity, in addition to native biocompatibility.[36] It was accepted as a biomaterial by the US Food and Drug Administration (FDA) in 1993.[36] Fibroin from *B. mori* is obtained by a process called degumming which involves boiling of cocoons in salt or detergent. To understand the unique properties of fibroin, it is necessary to first study the structure and chemistry of fibroin. Silk fibroin proteins from *B. mori*, are primarily composed of a light chain (~ 26 kDa) and a heavy chain (~ 390 kDa), which are present in a 1 to 1 ratio and linked by a single disulfide bond.[33] The light chain consists of a non-repetitive, more hydrophilic sequence. On the other hand, the amino acid sequence of the heavy chain consists of repetitive hydrophobic blocks of Gly-Ala-Gly-Ala-Gly-Ser and repeats of Gly–Ala/Ser/Tyr dipeptides, which form 12 crystalline domains (Table 1). The high glycine content arranges chains to a tight packing into extremely stable β-sheet nanocrystals structures. The crystalline domains consist of a header and terminal sequence, and are linked by 11 spacers with 42–43 residues, each of which are in near identical structure formation. The predominant molecular interactions among crystalline β-sheets are hydrogen bonds that are largely responsible for the high rigidity and tensile strength. By virtue of fibroin's nano-confinement, the crystals are loaded in uniform shear and rupture, followed by a slip–stick motion as the strand slides and re-forms hydrogen bonds, which leads to their most efficient use. Reforming those weak H-bonds gives fibroin the ability to self-assemble and self-heal. Fibroin can self-assemble into larger fibrous

structures which are characterized by a high degree of hierarchical molecular order and their enhanced mechanical properties.[37] Moreover, silk has higher strength and elasticity than most other biodegradable polymers commonly employed in biomedical applications, such as collagen and poly(L-lactic acid), and even chemically-crosslinked collagen. *B. mori* silk demonstrates an ultimate tensile strength of 500 MPa and an elastic modulus of 5 – 12 GPa after degumming, an enhancement in these mechanical properties is demonstrated in comparison to native silk.[37, 38]

Fibroin is therefore a mechanically-robust biopolymer for biomedical applications. In addition, it is intrinsically biodegradable and biocompatible. The biocompatibility of fibroin is mainly attributed to its chemical composition and structure. Use of fibroin as a biomaterial was first studied in 1995, showing the attachment and growth of fibroblast cells on *B. mori* SF matrices.[39] Later, fibroin was shown to evoke minimal inflammatory response and low overall immunogenicity when utilized in the purified state.[39] Due to its bioresorption properties various commercial biomedical products have surfaced (e.g. *Seriscaffold*®(surgical mesh), *SeriACL*®(ligament graft), and chronic wound dressing mats.[37]) Biodegradability is an important issue when used as scaffolds, drug delivery carriers, and for implanted device applications. Controlled manipulation of protein structures and their effect on biodegradation characteristics have been one of the prime goals of early studies. Many independent studies indicate that fibroin can be readily degraded by proteolytic degradation by a variety of enzymes such as protease XIV, alpha-chymotrypsin and collagenase IA.[40] Since fibroin β-sheets degrade to amyloid β-fibrils which have been associated to Alzheimer disease, some concerns were raised over safe biodegradation. However, in a study, fibroin degradation products did not show any cytotoxicity to neuronal cells.[40] The biodegradation rate of the fibroin is mainly dependent on the water-

soluble silk I and water-insoluble silk II structures. Therefore, the degree of β-sheet crystallinity present in the system is the controlling factor of biodegradation rate.

Silk fibroin is therefore an ideal candidate for the fabrication of biocompatible, mechanically robust devices that may be tuned to the structural properties of the host tissue, yet are able undergo predictable biodegradation. However, the current processing methods of silk fiber only utilizes silk fibroin and discards sericin as a waste, which creates waste disposal issues. This protein itself has excellent properties as a biomaterial discussed in detail next.

1.3.1.2 Silk sericin

Silk fibers from *B. mori*. contain 25-30% of sericin which envelops the fibroin fiber with successive adhesive-like layers which facilitates the formation of the cocoon. Typically, sericin is being considered as an undesired waste product, and is usually removed while processing of natural silk to isolate fibroin for both textile and research applications. Even though silk sericin is found co-existing with fibroin, it is both chemically and structurally distinct. The molecular weight of silk sericin varies between ~10 to 400 kDa.[41] It is a water-soluble glycoprotein, composed of 18 amino acids most of which have polar pendant groups such as hydroxyl, carboxyl, and amino groups (Table 1.1).[42] The amino acids serine and aspartic acid constitute approximately 33% and 17% respectively of the overall structure. Sericin is comprised of amorphous random coils and β-sheets creating amorphous and crystalline regions respectively, with little or no α-helical content. It displays a high degree of water-solubility due to the abundance of amorphous regions.[43]
Historically, native silk fibers were used for suturing open wounds. However, significant inflammatory response and severe allergic reactions were observed. The high immunogenic

response was observed in the form of macrophage activity and the formation of IgE and IgG antibodies to native silk peptides.[44] Initially, this response was attributed to the presence of the sericin. Sericin was previously overlooked due to an earlier study which suggested that it elicited an immune response, which was later shown to be triggered when sericin is associated with fibroin in their native state.[45, 46] However, silk has now been demonstrated to be effective across a range of clinical applications in the purified state. Elaborate studies indicate that the allergic response is primarily caused by the native fibroin-sericin structure, but neither fibroin nor sericin *alone* invoke allergic reactions.[45, 47] Sericin is now considered as a potential biomaterial.[48] Indeed, sericin was reported to have numerous biological functions such as anti-oxidation, anti-bacterial, anti-coagulation, while promoting cell growth and differentiation.[47] In a recent study sericin has been found to be facilitating wound healing in a rat model.[49] Even though silk sericin protein lack the mechanical strength of fibroin, its water solubility makes it an important biomaterial. By virtue of biodegradability and hydrophilicity with many polar side-groups, sericin can be successfully copolymerized, crosslinked and blended with other polymers to form scaffolds for applications such as skin regeneration.[50] To date, sericin based 2D films, fragile gels and 3D sponge-like structures have been made.[42, 50]

The successful extraction of both fibroin and sericin from silk cocoons, provides two materials with distinct properties: biocompatibility, antibacterial activity, oxidation resistance, and controllable degradation, in addition to processability and mechanical strength exceeding comparable synthetic materials. [51, 52]

Table 1.1 *Amino acid compositions of fibroin and sericin.[42, 53]*

Amino acid	Sericin	Fibroin
Alanine	6.7	30.23
Arginine	3.12	0.48
Aspartic acid	18.38	1.66
Glutamic acid	5.74	1.57
Glycine	17.85	43.29
Histidine	1.32	0.2
Isoleucine	1.02	0.57
Leucine	1.49	0.36
Lysine	2.08	0.21
Phenylalanine	0.67	0.69
Serine	25.5	10.58
Threonine	7.47	0.88
Tyrosine	3.1	4.76
Valine	4.05	1.88
Cysteine	0.38	0.01
Proline	0.81	0.17
Methionine	0.31	_

1.3.2 Functionalization of silk proteins

To date, most reports involving silk proteins have utilized them as bulk and passive materials to form gels, sheets, fibers and 3D scaffolds. To diversify their application, it is imperative to incorporate properties and functions that are *not intrinsically present*. A key advantage of protein-based materials is the potential to directly impart specific function via diverse approaches - physical (non-covalent), chemical (covalent), and doping/entrapment. In this section, a discussion on different functionalization methods for silk proteins will be discussed.

1.3.2.1 Physical functionalization

Physical functionalization of silk proteins occurs primarily by surface modification - irradiation, physical adsorption, and coating of functional materials facilitated by non-covalent interactions. To incorporate electrical conductivity, fibers and microspheres of *B. mori* fibroin and spider silk have been coated with multi-wall carbon nanotubes (MWNTs) by immersion of the fibers or microspheres in aqueous suspensions of the MWNTs, followed by washing and drying.[54-56] Such coatings were stable to both extensive washing and sonication due to formation of H-bonds between the fibroin and the carboxylic acids on the surface of the nanotubes. Another example of coating involves conducting polymers such as poly(3,4-ethylenedioxythiophene) polystyrene sulfonate (PEDOT:PSS) by first adsorbing monomers on the surface of silk protein fibers, and then polymerizing those monomers by chemical or electrochemical polymerization. [57, 58] Silk fibers and scaffolds has also been imparted magnetic properties by coating and adsorption of magnetic nanoparticles from a Fe_3O_4 and ferrofluid poly-D,L-aspartic acid solutions respectively.[59, 60] Mechanical characterization of magnetite-silk composite reveal negligible differences in mechanical properties due to the coating. Fluorescent properties were imparted in spider silk fibers by coating with alternating layers of polyelectrolyte (PE) and cadmium telluride (CdTe) nanocrystals.[61] Layers in the form of PE/CdTe/PE generated fibers emitting bright fluorescence in the near-infrared band with a slight decrease in mechanical properties.

Depending on the isoelectric point, hydrophobicity and pH of the solution, proteins can be attracted or repelled by silk proteins. Attraction between silk and other compounds have been utilized for drug delivery using simple absorption. Examples include silk particles loaded with small model drugs (Alcian blue, Rhodamine B and Crystal violet).[62] Drug release characteristics were highly

dependent upon the secondary structure of protein particles. Another study of physical adsorption on spider silk protein (eADF4 (C16)) particles used to adsorb lysozyme protein (up to 30% loading) via electrostatic interactions. However, it was found that the lysozyme was not only adsorbed to the surface of the microspheres, but also diffused into the protein matrix.[63]

1.3.2.2 Chemical functionalization

Due to covalent bond formation, chemical functionalization is way more stable than physical functionalization. The capability to incorporate unique chemical functionalities to proteins is valuable for a variety of applications, including protein immobilization,[64] therapeutic drug delivery,[65] tissue engineering,[66] and imaging.[67] Inserting chemical functionalities into proteins in a site-specific manner is often preferred over nonspecific modifications to provide uniformly modified protein populations while minimizing potential deleterious effects on native protein activity.[68] Silk proteins have a wide range of amino acid side groups which can be conjugated with chemical moieties to incorporate distinct functional characteristics. A range of bioconjugation reactions can be used to change the properties of proteins as dictated by the application.[69] Chemical functionalization allows the formation of chemical handles on silk side chains for the attachment of growth factors, cell binding domains and other polymers to silk.

Several chemically modified silk proteins have been used for the investigation of surface chemistry or biomolecule conjugation for tissue engineering applications. Incorporation of poly(D, L-lactic acid) in silk side chains was found to increase the hydrophilicity of silk fibroin, resulting in increased attachment and proliferation of osteoblasts.[70] Similarly, modification of silk fibroin

with poly (ethylene glycol) chains was also found to increase the hydrophilicity significantly. However, these derivatives caused a decrease in cell attachment of fibroblast cells (L-929).[71] In another study, fibroin films covalently attached with integrin-binding laminin peptide motifs (YIGSR and GYIGSR) demonstrated that the peptide sequence and nature of functionalization steer the differentiation of bone marrow-derived human mesenchymal stem cells (hMSCs). The covalently functionalized fibroin scaffolds with GYIGSR hexapeptide (CL2-SFF) supported hMSC proliferation and maintenance in an undifferentiated pluripotent state and directed the differentiation of hMSCs into neuron-like cells in the presence of a biochemical cue, on-demand.[72] Chemical modification of silk sericin protein has been reported, wherein 4-cyanophenyl isocyanate was reacted with the nucleophilic groups.[73] Similar chemical modification will be discussed in detail later which will render the silk proteins photoreactive.

1.3.2.3 Functionalization by physical blending

The development of new composite materials by physical incorporation such as blending or doping of other functional materials with silk proteins, has been driven by the necessity to address the shortcomings of natural silk fibers which could not be achieved by chemical or physical functionalization. There has been plethora of reports of silk composites by combining with synthetic polymers, natural polymers, inorganic nanoparticles, and other biomolecules. For instance, silk proteins have been formulated for controlled release using various types of drugs and model compounds such as other large proteins, synthetic dyes, cell growth factors, chemotherapeutics, antibiotics, and small molecule drugs.[74] Fibroin films containing various enzymes have been found to retain their catalytic activities over a number of days with minimal leaching of enzyme *in vitro*.[75, 76] Incorporation of silver nanoparticles in silk films resulted in

silk based antimicrobial films. The silk fibroin-silver nanoparticle composite had an effective antibacterial activity against the methicillin-resistant *Staphylococcus aureus* (*S. aureus*) and inhibits the biofilm formation caused by the bacterium. Moreover, a pre-existing methicillin-resistant *S. aureus* biofilm can be also destroyed by the silk fibroin-silver nanoparticle composite, which meets the demand of clinical application.[76] Gold nanoparticles entrapped in silk fibroin films have been shown to fabricate biocompatible surface enhanced Raman scattering (SERS) substrates, [77] and temperature sensitive photonic sensors.[78] Graphene doping has been used to form composite fibers by wet spinning and improve the mechanical and the antibacterial property of silk fibroin.[79] Doping of silk proteins with conducting polymers, which forms one of the key aspects of this work is discussed in detail below.

1.3.2.4 Discussion

The wide variety of functionalization studies of silk proteins display the great promise for the further development of functional composite materials. The above discussion also suggests that the incorporation of conductive/electroactive properties in silk proteins have been relatively unexplored. Therefore, the research opportunity is to investigate novel fabrication strategies that can expand application of silk proteins towards smart silk architectures and bioelectronic devices. However, conventional bulk fabrication methods to process silk proteins are not sufficient for such applications. Developing micro and nanoscale fabrication tools for silk proteins are needed to provide additional functionality by incorporating function specific structures in precise forms. In the next section, a few micro/nano-fabrication strategies involving silk proteins are explored.

1.3.3 Micro/nanofabrication approaches of silk proteins

1.3.3.1 Dry Etching and Direct Printing

In dry etching, a metal mask is used to define the etch geometry.[80] Silk proteins are sensitive to oxygen plasma treatment and the organic bonds can break down at high power dosage. Here the plasma can be used to form precise structures. However, the procedure is hampered by the complex procedure and rough surface. Direct printing techniques such as femtosecond laser machining, and two and three-photon interference lithography have been reported but are quite expensive.[81, 82]

1.3.3.2 Soft lithography and nanoimprinting

Soft lithography is a popular micropatterning technique where the transfer of micro and nanoscale pattern into a material is performed by contact printing or replica molding using an elastomeric master.[83] In nanoimprinting, silk films are placed on top of a hard metal or silicon master pattern. Heat and pressure are then used to form a positive replica of the master pattern.[84] These indirect methods require the formation of master patterns that can then be transferred to the biomaterial.[81, 85, 86]

1.3.3.3 E-beam lithography

E-beam lithography is a direct write technique, where patterns are formed by an incident electron beam. The advantage of the process is this method is that it can form both negative and positive tone features by the modulation of electron beam energy.[87] However, the disadvantage of the reported e-beam lithography process is that it uses very high energy dosage to form patterns

making it unsuitable with enzymes or other biomacromolecules entrapped in the protein.

1.3.3.4 Photolithography

Photolithography is widely used microfabrication technique.[88] Here the patterns are formed by either chemical crosslinking or by breakage of polymer bonds by incident UV radiation. Typically, photolithography was used with synthetic photoreactive polymers and photoresists. Use of this technique with proteins has not been widespread. Our group developed a technique to adopt the technique to silk proteins as discussed below.

1.3.3.5 "Protein photoresists" based on silk

The development of protein "photoresist" materials is based on the chemical functionalization of silk proteins. In this approach, the native proteins are chemically converted to a photoreactive material by incorporating pendant methacrylate groups in the protein chains. The silk photoreactive proteins therefore act as a negative 'photoresist-like' materials – (fibroin protein photoresist (FPP) and sericin protein photoresist (SPP)), and can be patterned by following conventional photolithographic protocols.[28, 29]

A negative photoresist polymer contains pendant acrylate groups, which in presence of a photo initiator and specific wavelength UV light, can crosslink by vinyl double bond. Therefore, the inclusion of methacrylate pendant moieties without disrupting the overall silk structures forms the core of the idea behind the development of silk photoresists. Bioconjugation of the methacrylate

groups is briefly discussed here. Isocyanate groups (-N=C=O) can specifically react with nucleophilic amine-, hydroxyl-, sulfhydrl-, and carboxylic acid groups. These reactions are primarily hydrolysis reactions. The isocyanate containing reagent, 2-isocyanatoethyl methyl-methacrylate (IEM, MW= 155.15) is used here. The presence of the methacrylate terminal group enables photopolymerization, and isocyanate group should react with available nucleophilic groups in silk protein chain. Isocyanate groups also react with water and produce carbon dioxide. Therefore, the conjugation reaction is done in a nitrogen purged environment to remove water formation during synthesis. The basic reaction mechanisms of isocyanates with nucleophilic amino acids are shown in Figure 1.3. The product obtained following consecutive washing and lyophilizing steps, is photoreactive in nature and can be pursued with conventional UV photolithography protocols.

The photolithography process comprises of several steps (Figure 1.4): [88]

1. Substrate preparation to improve photoresist adhesion (such as thermal oxidation or piranha treatment).
2. Formation of uniform layer of photoresist on substrate by drop casting or spin coating.
3. Removal of excess solvent by soft baking.
4. Exposure (UV or visible light) through photomask to induce photoresist crosslinking on exposed areas.
5. Removal of exposure artifacts by post-exposure bake.
6. Development of patterns to remove unexposed photoresist and reveal the micropatterns.

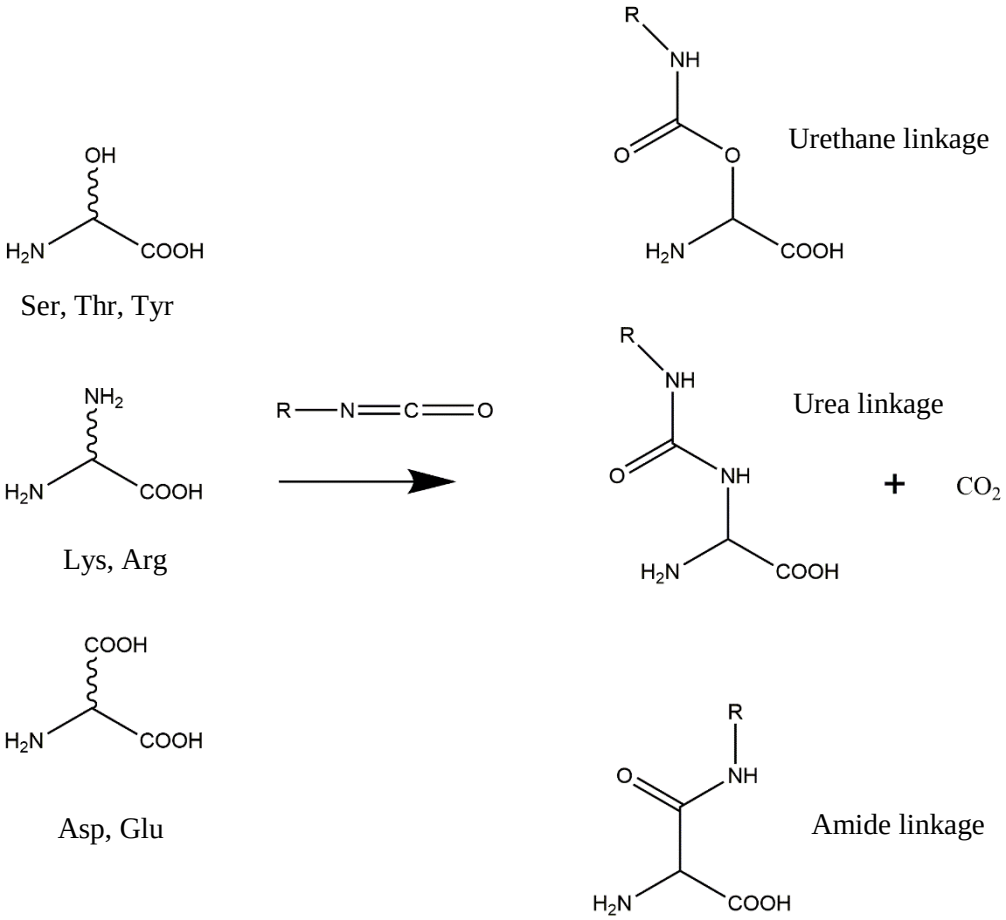

Figure 1.3 *Reaction of isocyanates with nucleophilic amino acids pendant groups.*

This process is relatively benign and the patterning process can be performed at the benchtop at room temperature. The incorporation of methacrylate groups has minimal effect on the native structure, and both mechanical properties and biological stability of silk proteins improve after crosslinking. The process is highly reproducible and high fidelity silk microstructures can be made over large area (cm scale) with microscale spatial resolution. Therefore, this technique has a huge potential to augment the prospects of using silk proteins for biomedical applications, where microscale resolution patterns are required.

This research primarily focuses on the development of next generation functional devices (optical,

electronic, and electrochemical) for life science applications using the silk protein photolithography platform. The objective is to utilize the photoresist-like silk proteins to create micropatterned functional architectures which can be applied to these applications, particularly in flexible formats. The research will also show how protein properties can be engineered to form functional devices and improve their interfaces with biological environments.

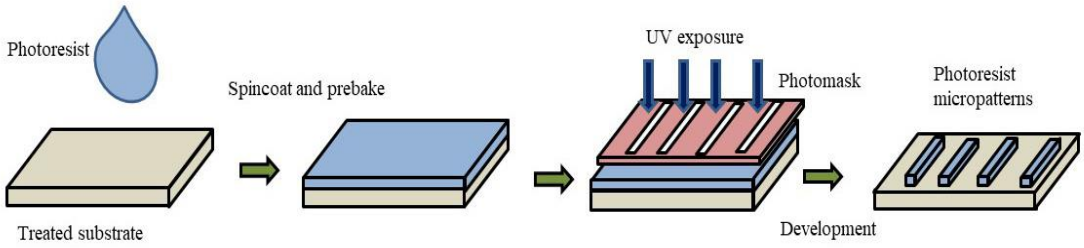

Figure 1.4 *Conventional UV photolithography process schematic.*

1.3.3.6 Comment on the biofriendly nature of the process

A brief comparison between reported techniques used for high-resolution patterning of functional materials is provided. Nanoimprint lithography employs high temperature (~120°C for silk) and pressure (~50 psi) processing to reach the glass transition temperature and allow reflow of silk proteins into a mold to form patterns.[84] The EBL process reported for patterning silk proteins require very high dosage (25,000 μC cm^{-2}). With such doses, functionalization of silk proteins with other biomolecules would be very difficult.[87] Cellulose has been shown to be patterned by soft lithography.[89] However, to dissolve the cellulose, dilute hydrochloric acid was used and the processing also required multiple steps to obtain microscale structures. Thus, the use of such a solvent system is not suitable for many biological applications. Adapting traditional lithographic techniques to the biological context often requires indirect strategies using additional resists. This

makes lithography more complex and involves the use of toxic chemicals that may negatively affect the biological matter (e.g. encapsulated enzymes or antibodies). Such examples can be found in the patterning of functional materials like gold, aluminum, and silicon on biodegradable polymers such as silk proteins and PLGA. [90, 91] Here, patterns are first formed on a hard silicon substrate by following conventional cleanroom multistep techniques which involve toxic resists, harsh solvents and high temperature processing. At the end of formation, the patterns are transferred to biopolymer films. In comparison, the silk protein photolithography (SPL) process developed in this research is a room temperature, bench top technique. High fidelity patterns of silk proteins can be obtained in one step. Even though silk fibroin patterning involves HFIP, recent work from our group has shown the suitability of formic acid. Importantly, sericin can be patterned via all water based techniques. Therefore, the possibility of choosing one protein over another based on the specific requirements is possible. Similar flexibility is difficult to find in other strategies. Therefore, it can be concluded that the SPL is significantly more biofriendly than other existing techniques.

1.3.4 Conductive materials for bioelectronics applications

Successful development of bioelectronic devices relies on the choice of compatible conductive materials to either form circuitry on silk proteins or form composites with silk proteins. The chosen material is responsible for detecting, transducing and modulating electrical cues. Therefore, integration of electrical functionality and chemical stability with conformability and biocompatibility are essential parameters. Due to these stringent selection criteria, only few materials have been found suitable for such applications.

1.3.4.1 Bioresorbable metals

Magnesium (Mg), zinc (Zn), iron (Fe), tungsten (W), and molybdenum (Mo) are few metals being currently studied as dissolvable conductors for transient electronics. All these metals are important to biological functions and have potential to be used in biomedical implants.[92] For instance, Mg, Mg alloys, and Fe have been shown for the development of bioresorbable implants, such as vascular stents, due to their good biocompatibility and favorable mechanical properties.[93] However, highly reactive nature of these materials generate device survival issues, and hydrogen evolution from degradation can have deleterious effects on tissue.[94]

1.3.4.2 Silicon

Semiconducting materials such as silicon have been crucial to the development of solid state electronics. Since the realization of dissolution properties of silicon nanomembranes, this is played an important role in development of transient electronics. Monocrystalline silicon (Si) nanomembranes (NMs) can serve as semiconductors in circuits, and silicon oxide has been applied to form transistor devices such as inverters and gates.[95] However, formation of oxidation layer in biological environments causes a significant decrease in conductive performance of the device.[96] Further, fabrication of metal and silicon based semiconducting materials require complex fabrication protocols and intensive cleanroom usage.

1.3.4.3 Conducting Polymers

To impart electrochemical function to the silk proteins, this research relies on the use of intrinsically conducting polymers. A brief introduction to this emerging field is provided here. Polymers are traditionally excellent electrical insulators leading to their usage in insulating electrical wires and devices. In 1977, a group of scientists at the University of Pennsylvania first showed a conductive form of polyaniline by doping with oxidizing agents(p-type) such as I_2, AsF_5, $NOPF_6$ or reducing agents(n-type) such as sodium napthalide.[97] The discovery was well appreciated in the scientific community and in the year 2000 Drs. Heeger, MacDiarmid and Shirakawa were awarded the Nobel Prize in Chemistry.[98][1] Since the initial discovery, there has been an accelerated development of conducting polymers.

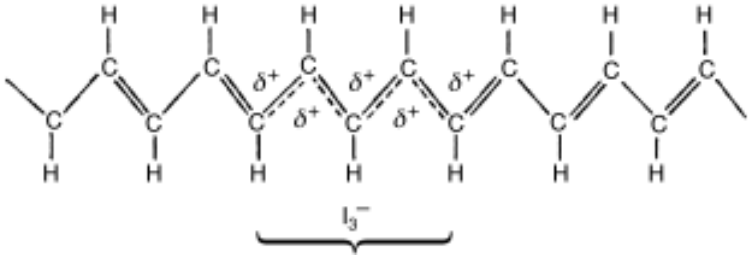

Figure 1.5 *Positive charge hopping in polyacetylene backbone in presence of iodine.[98]*

Conducting polymers (CPs) also called conjugated conducting polymers contain a π-electron backbone having single and double bonds alternating along the polymer chain. Even though the conduction mechanism involves complex concepts such as solitons, polarons and bipolarons,[99] fundamentally, doping causes the enhancement of conductivity by several orders of magnitude and in most cases research is focused on improving conductivity by using better dopants. The process of hole hopping (*p*-doping or partial oxidation) in trans-polyacetylene in presence of a oxidizing agent such as iodine is shown in Figure 1.5. [98]

[1] https://www.nobelprize.org/nobel_prizes/chemistry/laureates/2000/

CPs are now gaining importance as a material of choice for sensing, stimulation, recording applications owing to their flexibility.[100] There are now a variety of CPs and their derivatives available for various applications. CPs can be employed for reversible chemical, electrochemical reactions governed by doping/de-doping process. The electrical doping not only affects the electrical properties of the film, but also causes a dramatic changes in optical and mechanical properties.[96] This effect has been utilized for developing new electrochromic displays and actuators for artificial muscles. Ion exchange does not only occur in between the biological milieu and the polymer surface, but the entire bulk. These phenomena do not occur with conventional metals and semiconductors, making CPs appealing candidates for ion and electron transducing materials. Additionally, CPs can be readily functionalized by known standard organic chemistry modifications, processed at low temperature and allow oxide free interfaces with aqueous electrolytes. In contrast, for a conventional silicon to electrolyte interface, an oxide layer formation is certain, which creates a physical barrier for ions across the interface. With oxide-free interfaces, CPs have a significant edge to be used for interactions with biological systems. Other important properties of these materials are that they are biocompatible, mechanically 'soft' and can immobilize biomolecules. These properties together make these materials excellent candidates over conventional materials currently being used to make flexible and tactile bioelectronics devices. [101]

Realizing the advantages of conducting polymers, various groups are focusing their attention to develop novel biomaterials and devices utilizing them. Due the huge potential in bioelectronics, the new area of research 'organic bioelectronics' has been coined.[102] Intrinsically conducting polymers can be broadly classified in certain families: polyanilines, polypyrroles,

polyparaphenylenes and polythiophenes (Figure 1.6).[100] Among all these, polythiophenes especially poly(3,4-thylenedioxythiophene):poly(styrene sulfonate) (PEDOT:PSS) has been of prime interest due to high stability, compatibility in physiological environments and ready availability as an aqueous dispersions.[103]

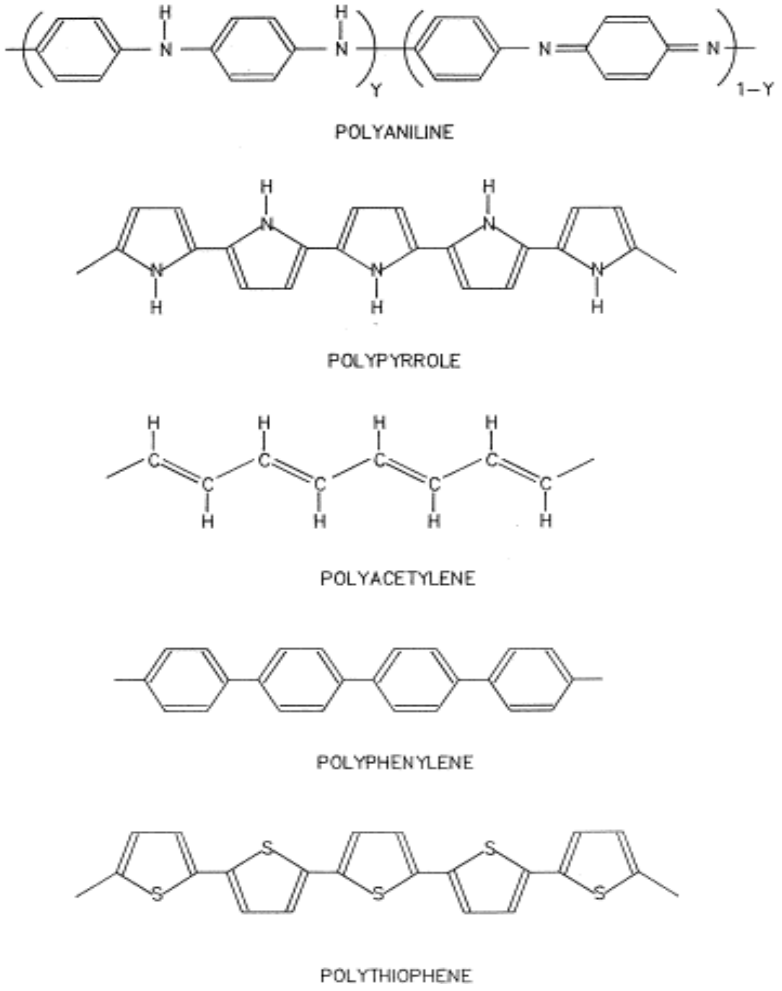

Figure 1.6 *Commonly investigated conducting polymers and their chemical structure. [104]*

Even though CPs such as PEDOT:PSS possess properties that are ideal for development of bioelectronic devices, their application to date with biopolymers has been mostly using bulk scale fabrication techniques in the form of films, fibers, sponges and scaffolds. Precise patterning of conducing polymers has been shown using ink jet printing and screen printing methods. These

methods even though are rapid prototyping methods but lack high precision fabrication. Therefore, the ability to utilize conducting polymers with natural polymers with precise and sustainable fabrication approach is an area ripe for investigation.

1.4 OUTLOOK

From the above discussion, it can be derived that silk proteins have been primarily being used as passive drug delivery and tissue engineering materials. The majority of functionalization approaches to date are focused on such applications. However, the review also suggests that there exist huge possibilities for the development of functional materials and architectures from silk proteins. The research presented in this dissertation seeks to demonstrate the role of silk in establishing "smart" architectures by capitalizing on the fundamental attributes of silk proteins, chemical and physical doping of functional moieties and materials. The aims will be achieved by 1) realizing optical architectures to utilize the intrinsic optical properties, 2) realization of shape specific silk particles for drug delivery and imaging applications, 3) incorporation of conductive materials and facile fabrication of electronic architectures from silk biocomposites and realization of biosensing platforms, 4) developing biodegradable silk based energy storage devices, and 5) developing a nanoscale lithography process for producing precisely tailored, biologically-relevant silk nano-architectures. Therefore, the research will stride forward to create new knowledge and sustainable technologies to realize silk based devices for diverse biomedical applications. The developed materials and techniques will provide immense benefits over the existing materials and techniques for such applications. Moreover, the lessons learned from silk proteins can be applied to other biopolymers as well, enriching the standing of similar materials for interacting with biology.

CHAPTER 2

PHOTOLITHOGRAPHY OF SILK PROTEINS ON FLEXIBLE SUBSTRATES

2.1 INTRODUCTION

As discussed in Chapter 1, recent advances in micro- and nanofabrication technologies have enabled the formation of protein based devices for biological and medical applications.[105] In this chapter, the development of silk proteins towards flexible devices is explored by the initial development of "soft" optical systems. Optical and photonic devices play an important role in biosensing [106], imaging [107], therapeutics [108] and microelectromechanical systems (MEMS).[109] Research in micro optical devices is focused on new materials that can be easily processed, and are robust and soft or flexible. Similarly, inspiration from nature can be utilized to develop novel optical and biophotonic devices.[110] For instance, periodically structured materials commonly found in nature cause physical coloration due to diffraction of light from periodic structures or thin film multilayer interference.[111] While nanoscale periodic structures cause structural color, microscale periodic structures cause angle dependent iridescent colors.[112] Another interesting biomimetic inspiration are compound eyes that enable higher field of view and dual vision in insects.[113] The compound lens feature can be beneficial in medical-imaging systems, where each individual microlens points to a different direction to capture an image of a particular portion of the landscape. The superposition of the images can then be used to form an omnidirectional imaging device. Currently however, optical devices are largely fabricated from glass, semiconductors, metals, and synthetic polymers.[114-116] The intrinsic lack of

biocompatibility and biodegradability of these materials typically render them unsuitable for applications including biophotonics and biointegrated systems.[117, 118]

Natural and recombinant biopolymers such as silk,[24] collagen,[119, 120] chitin, chitosan,[120] and reflectin [121] provide suitable alternatives for the design and fabrication of next generation optical devices. The use of biopolymers in photonic and optoelectronic devices provides an excellent opportunity to take advantage of unique mechanical, chemical, and optical properties. Advantages include the relative abundance, low cost, and biodegradability of proteins and importantly, their biocompatibility and ability to be engineered for external stimuli. Applications include light guiding or concentrating devices for improved imaging, photodynamic treatments, color switching sensors, light propagation to relay physiological signals, and as reading and recording devices used in real time monitoring.[122-124]

Silk proteins in particular, have immense potential to be used as building blocks for optical components. [30, 125] This is owing to their optical transparency, processability into different architectures, and exceptional mechanical properties. Silk films have smooth surfaces and are transparent throughout visible light wavelengths. The reported refractive index of fibroin silk film is 1.54 at 633 nm with approximately 95% transmission of ~30μm films, are slightly higher than glass (n=1.52).[109] To date, these optical properties, and ease in forming micro- and nanostructures have led to the development of holograms, optical gratings, mirrors, waveguides, inverse opals and lenses.[30] Optically iridescent architectures have also been shown by patterning of silk films using a “breath figure approach”.[126] Although this approach can be used to form

cavities ranging from sub-micrometer to micrometer scales, the scalability and limitations on geometry and control of cavity size make these approaches limited. However, many of these techniques can be used only to fabricate devices on flat and rigid substrates.[127] Development of microlens arrays on curved and flexible surfaces is also difficult. The challenge lies in the coupling of silk proteins with accessible fabrication strategies which can form soft micro-optic devices. [128]

There exists an opportunity to expand the application of silk protein lithography discussed in Chapter 1 to develop biomimetic microarchitectures from silk proteins for optical applications. Strategies to micropattern silk proteins on flexible substrates can be used to obtain high fidelity structures in a relatively easy, benign and highly reproducible manner. This can lead to the development of soft micro-optic devices for medical imaging and photon concentrating applications. Investigation of periodic microstructures can provide information required to obtain angle-dependent optical behavior, which can be used to develop iridescent holograms. Similarly, other optical structures such as Fresnel zone plates can be fabricated on flexible membranes.

In this chapter, new ways of inexpensively fabricating photonic devices and architectures, will be shown using a rapid and scalable approach to form microstructures over large (cm) areas. Using photolithography, it is possible to not only accurately control the nature of the patterns formed but also their aspect ratios and periodicity (or aperiodicity). Two specific goals are sought: 1) Demonstration of optical components that can be easily fabricated - biomimetic, structurally iridescent surfaces that can alter the directional pattern of reflected light, and Fresnel zone plates

for the focusing of light, and 2) Development of silk protein lithography procedures whereby silk proteins can be patterned on silk protein films to extend possible device configurations, as well as improve integration with soft or curvilinear substrates. Realization of such devices would lead to simplification and improvements on existing methods for producing soft and flexible silk architectures for use in protein based bio-optics and electronics applications.

2.2 EXPERIMENTAL SECTION

2.2.1 Materials

Silk fibroin protein was obtained from cocoons of *Bombyx mori* (Jhargram Tropical Tasar Farms, West Midnapore, India). Sericin protein was commercially obtained from Wako Chemicals (Richmond, VA). Sodium carbonate (Na_2CO_3) and lithium bromide (LiBr) were employed for fibroin purification from Fisher Scientific (Fair Lawn, NJ). Phosphate buffered saline (PBS, Fisher Scientific, Fair Lawn, NJ) was employed after 0.22 μm filtration at pH 7.4. The reagent 2-isocyanatoethyl methacrylate (IEM, MW = 155.15 Da), 98% with < 0.1% BHT 128 inhibitor was utilized for chemical modification of fibroin. Anhydrous dimethyl sulfoxide, anhydrous lithium chloride (LiCl) and dimethyl sulfoxide-d6 were purchased from Sigma-Aldrich (St. Louis, MO). 1,1,1,3,3,3-Hexafluoro-2-propanol (HFIP) was obtained from Oakwood Chemical (West Columbia, SC). Irgacure 2959 (1-[4-(2-Hydroxyethoxy)-phenyl]-2-hydroxy-2-methyl-1-propane-1-one, Ciba, Tarrytown, NY) was employed as a photoinitiator.

2.2.2 Extraction and purification of fibroin

Fibroin protein was extracted and purified from silk cocoons (*B. mori*) following the protocol described elsewhere.[25] Hot boil degumming was first conducted in order to remove the sericin

glue protein. Silk cocoons (1 g) were cut into small, 1 cm^2 fragments and a solution (400 mL) of 0.02M Na_2CO_3 was prepared and heated until boiling. The silk cocoon pieces were added to the boiling solution of sodium carbonate and intermittently stirred for 30 minutes. The degummed fiber mass was removed from the solution, and immersed for 30 minutes in a stirred solution of cold deionized water, for a total of three rinses. The degummed fiber was then dried overnight at ambient temperature. Regeneration of silk fibroin was achieved via a solution of 9.3M LiBr. The degummed fiber was packed into a small beaker with 9.3M LiBr added to form a 20 % (wt./vol.) solution, and dissolved at 60 °C for 4 hours. The resulting solution was optically transparent, with a dull yellow coloration. This solution was then transferred to 3500 MWCO dialysis tubing, and dialyzed against deionized water for 48 hours, with buffer changes at 1 and 2 hours, and subsequently every 8 hours for total of 6 times. The regenerated fibroin solution was then recovered, and centrifuged at 4200 rpm and 4 °C for 20 minutes to remove insoluble particles. This process was repeated following recovery of the supernatant for a total of three times. The resulting solution (7 – 8 % (wt./vol.)) was then frozen overnight at -20 °C. The frozen silk was then lyophilized for 48 hours to obtain a fibroin foam.

2.2.4 Synthesis and purification of Fibroin and Sericin Photoresists

Photoreactive conjugates of fibroin (FPP) and sericin (SPP) were prepared as described earlier.[28, 129] The solvent system of 1M LiCl in DMSO was used for the dissolution of protein, and reaction with isocyanate-terminated groups. During the reaction, reagents and associated glassware were dried to prevent the moisture-sensitive isocyanate group of IEM from reacting with water and decomposing. Protein was initially added to a round-bottom flask and vacuum-dried for 24 hours at 70°C to remove residual water. LiCl was dried at 120°C for 24 hours before use. Protein was

dissolved at a concentration of 1% (w/v) in 1M LiCl/DMSO, while heating at 60°C for 45 minutes. This mixture was continuously stirred under a dry N_2 purge throughout the dissolution process. A stoichiometric amount of IEM was added to the round bottom flask, and the reaction was maintained at 60°C for 5 hours in a dry N_2 atmosphere. Immediately thereafter, the resulting solution was poured into excess cold ethanol and centrifuged to precipitate the product. The product was then collected and washed in a mixture of cold ethanol/acetone and centrifuged. The remaining precipitated mass was then frozen at -80 ºC and lyophilized for 48 hours to yield an off-white powder (fibroin)/white powder (sericin).

2.2.2 Surface functionalization

Protein micro- and nanopatterns were made on glass substrates to take advantage of optical transparency. To facilitate attachment of the features, substrates were functionalized with acrylate moieties. The glass substrates were initially washed thoroughly with ethanol and deionized water to remove surface contaminants. The surfaces were then cleaned using piranha (3:1 98%H_2SO_4:30%H_2O_2) solution for 30 min in ambient condition to remove organic contaminants and to hydroxylate the surface, in order to present silanol surface groups for further modification (*Caution: Piranha solution reacts violently with organic materials and must be handled with extreme care*). Surfaces were then repeatedly washed with deionized water and ethanol, and dried at 150°C. Functionalization to silanol groups was conducted using 3-(trichlorosilyl)propyl methacrylate (TPM) using chemical vapor deposition (CVD).[130] 100 μL TPM was added to a desiccator containing the substrates. The chamber was then drawn down to 0.4 bar and left for 12 hours for the TPM to react and present covalently bound functional groups. Methacrylate-modified surfaces were extensively washed with hexane and water, and dried before further use.[130] No

further modification was needed to facilitate attachment of the protein patterns.

2.2.3 Silk Protein Photolithography

Micropatterned holograms and Fresnel zone plates (FZPs) of silk proteins (fibroin and sericin) were fabricated on glass using contact photolithography. FPP and SPP were dissolved at 3.75% (w/v) in 1,1,1,3,3,3-hexafluoro-2-propanol (HFIP, Sigma-Aldrich, St. Louis, MO) and 2,2,2-trifluoroethanol (TFE, Acros Organics, NJ), respectively. Photoinitiator (Irgacure 2959, BASF) 0.6% (w/v) was added to the silk photoresist solution and mixed. The solutions were cast on substrates functionalized with TPM. HFIP and TFE were allowed to evaporate for 5 and 10 min, respectively. Contact photolithography was performed in direct contact with SPP films. Substrates were exposed UV light (OmniCure S1000 system, Lumen Dynamics Ontario, Canada) for 4.5 s at 20 mW cm^{-2}, through a chrome mask. Development of uncrosslinked and unexposed protein photoresist was performed using 1 M LiCl/DMSO solution and deionized water (18.2 MΩ·cm) for 2 hours, followed by copious rinsing with de-ionized water and ethanol. To form dark binary phase Fresnel lenses, a dark carbon dye was added to the precursor solutions.

2.2.4 Optical Microscopy and Scanning Electron Microscopy

Optical microscopy was performed on a Nikon Eclipse microscope. Scanning electron microscopy (SEM) was conducted using a JEOL high-resolution field emission microscope, at a 2.0 kV accelerating voltage. Prior to SEM, patterned substrates were sputter coated with 20Å platinum to enhance conductivity (Denton Vacuum Desk V cold sputtering system, Denton Vacuum, Moorestown, NJ).

2.2.5 Atomic Force Microscopy

Atomic Force Microscopy (AFM) analysis of surface morphology was performed on an Asylum Research MFP-3D AFM (Santa Barbara, CA), operating in AC mode with an AC240TS tip (nominal k = 2 nN nm^{-1}, Olympus, Japan).

2.2.4 Proteolytic degradation *in vitro* and imaging

To demonstrate biodegradability of the micropatterned features, enzymatic degradation was followed over time. 100 µm features (1.5 mg of protein cast/cm^2 of substrate) on glass substrate were incubated in 4 mL of protease (Protease XIV from *S. griseus*, ≥3.5U/mg, Sigma-Aldrich) solution (0.25U/ml of PBS buffer) at 37 °C. The enzyme solution was replaced every third day to preserve activity. As negative controls FPP and SPP patterns were incubated in PBS solution containing no enzyme. At different time intervals, samples were removed from solution, washed with deionized water, and imaged. The structures were studied using optical microscopy, SEM and AFM to observe changes in the surface morphology over time.

2.3 RESULTS AND DISCUSSION

Use of biodegradable materials having optical properties can be used to develop next generation soft and biodegradable bio-photonic devices.[131] For instance, periodically structured architectures commonly found in natural systems can form hue or coloration, and display remarkable optical behaviors that are purely physical in nature.[132] Such phenomena occur because of manipulation of light based on photonic crystals, diffraction of light, or multilayer interference and can therefore be adapted to flexible and soft substrates. The photopolymerizable

conjugates of silk proteins used (fibroin protein photoresist (FPP) and sericin protein photoresist (SPP)), behave as negative photoresists that are cross-linked in the presence of UV-radiation through a photomask. This transforms the proteins into water-insoluble, mechanically robust patterns that are covalently attached to the underlying substrates. Following development (removal of un-cross-linked protein), structures of high resolution and fidelity can be patterned over large areas in a few seconds. Here, micropatterning of silk proteins is used to demonstrate structurally induced iridescence and Fresnel zone plates that can be used for light focusing. Importantly, development of protocols to pattern silk proteins a flexible underlying substrate (silk sheet) will be realized to further make the silk protein lithography a more versatile technique.

2.3.1 Structure-induced iridescence

Structural color can be produced by coherent or incoherent light scattering from the surface.[133] Coherent scattering occurs when the photonic structures have periodicity that is less than half of the wavelength of light. Scattered light produces precisely ordered constructive or destructive interference patterns, which results in forbidden wavelengths or photonic bandgaps, and only a few wavelengths of light can be visible.[134] In contrast, incoherent scattering occurs when the photonic structure periodicity is larger than the wavelength of light, where the phase relationship of scattered light is random. Structure-induced iridescence from two-dimensional (2D) periodic arrays of microstructures on a substrate may therefore result because of incoherent scattering of light. The light reflected from the microstructures and diffracted light from the periodically arranged materials creates an interference pattern (Figure 2.1).

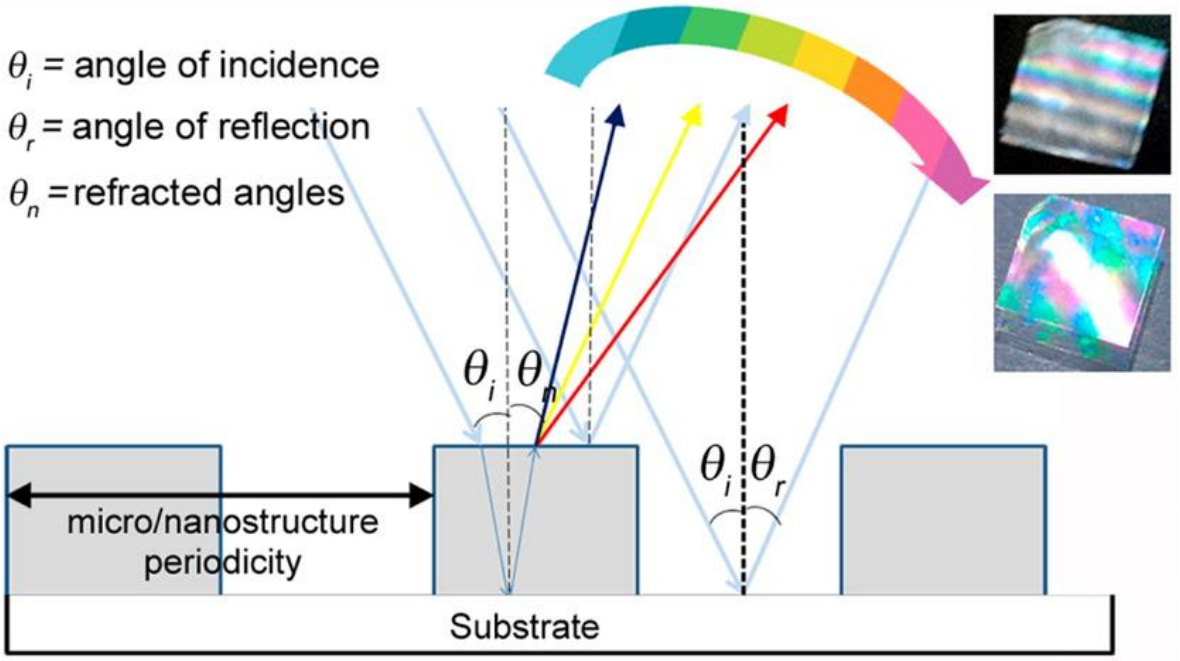

Figure 2.1 *Nature of structural iridescence. The angle of viewing can change the colors observed. Digital camera image showing the micropatterned protein sheet (1 cm^2) with an almost metallic appearance in sunlight.*

At a particular viewing angle only a few particular wavelengths of light produce constructive interference so that those color lights are only visible and a change in hue is observed.[135] To demonstrate that silk protein microstructures can display structure-induced iridescent behavior, a variety of features were patterned as shown in Figure 2.2. Structures ranging from 2 -10 μm of both silk fibroin and sericin patterns are shown. The column on the right shows typical iridescent behavior observed in sunlight. The color changes with viewing angle, and the films present a distinctly metallic appearance. In contrast, patterns of the same design but without constituent microstructures do not show iridescence behavior. This confirms that the iridescence is caused by the diffraction of light from the microstructures, and not by the interference of light from the thin protein films. It is important to note that larger microstructures (>10 μm) or structures that are further apart than 10 μm do not show any iridescence, showing that this effect is indeed caused by

the patterned microstructure.

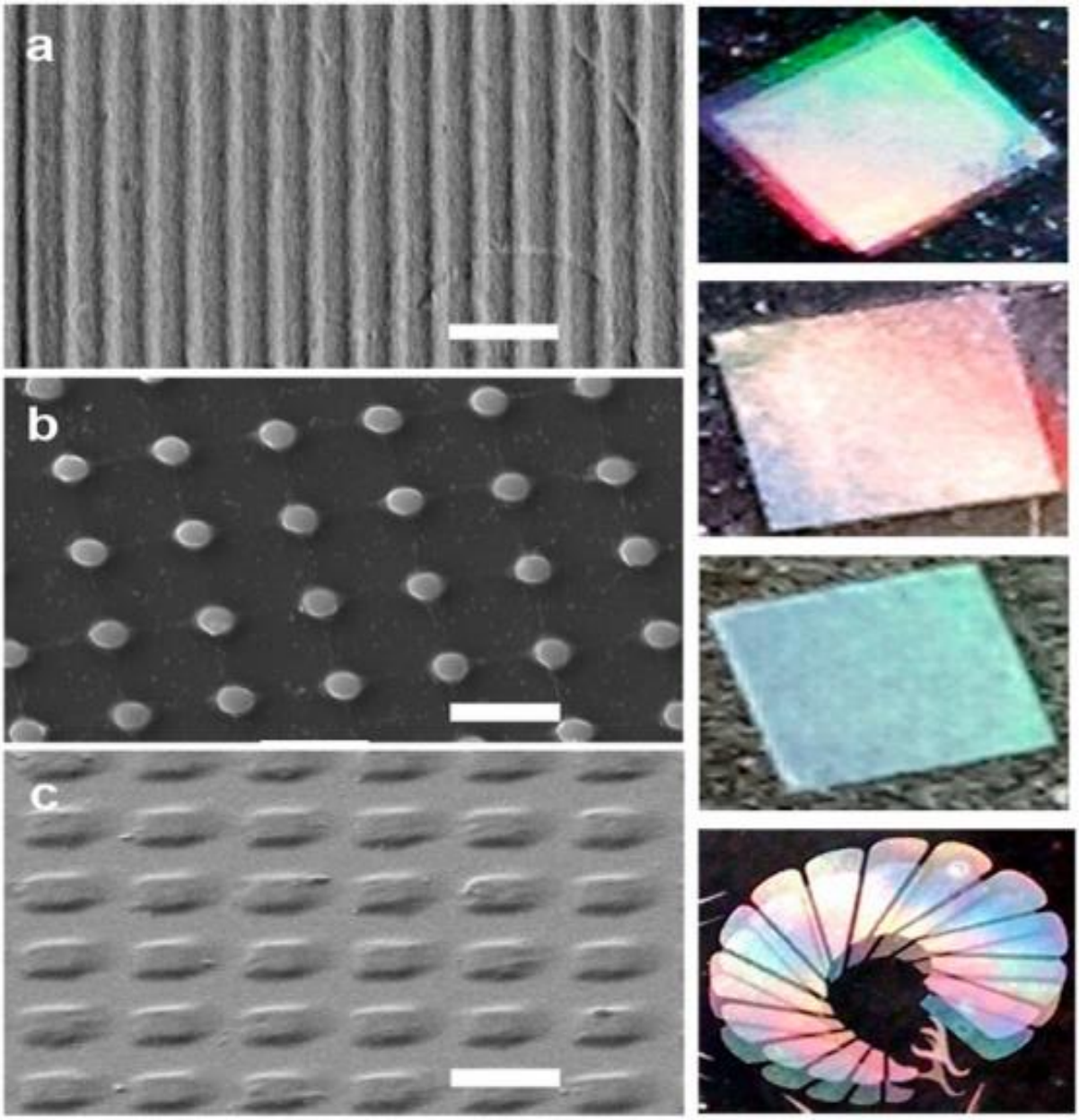

Figure 2.2 *SEM images of various periodic patterns of silk that can form iridescent colors (a) 2 µm lines, (b) 5 µm posts, (c) 10 µm squares (Scale bars=10 µm). Column on the right shows the iridescent microstructures*

Figure 2.3 shows patterns patterned with and without constituent microarchitectures. Using photolithography, any shape including lines, squares, circles, etc. can be patterned. In these structures, the strength of the iridescent behavior is governed not as much by the shape of the microstructure, but by their spacing. As the photonic structure periodicity is 2–10x larger than the wavelength of light, incoherent scattering causes a random phase relationship of scattered light.[136] This is further reflected in the pattern of scattered light from a microstructured film vs. a non-microstructured film (Figure 2.3 e, f). The structure-induced iridescence strengthens the idea of silk biomaterials for soft optics and adds an important functionality to the material.

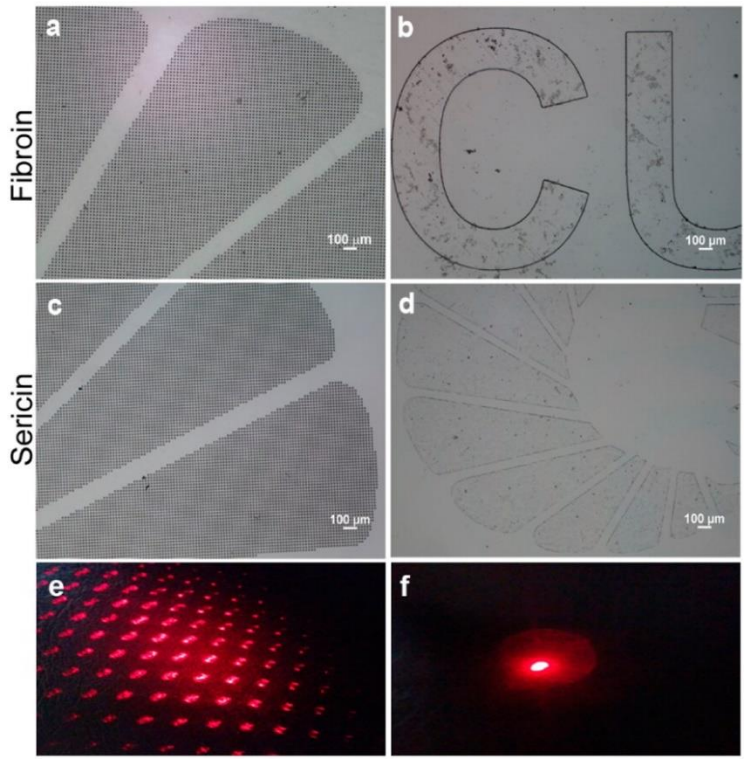

Figure 2.3 *Optical micrographs of micropatterned fibroin (FPP) features on glass (a) with patterns, (b) without patterns and sericin (SPP) features on glass (c) with patterns, (d) without patterns. Features patterned in the absence of periodic microstructures showed no iridescent behavior. This is also (e) observed in the diffraction pattern and (f) absent in an identically formed film with no microstructures*

2.3.2 Fabrication of Fresnel Zone Plates

The second optical component fabricated was a Fresnel zone plate (FZP) that utilizes diffraction of light to focus light. An FZP consists of binary circular opaque and transparent zones. Light passing through radially symmetric transparent zones gets diffracted. The zones are spaced such that constructive interference occurs at a desired focal distance to realize the image.[137] FZP lenses are used for concentrating lasers or X-rays, as well as for environmental and biomedical imaging.[138-140] However, typically the fabrication of FZP lenses has been via techniques such as electroplating, dry etching, and atomic layer deposition.[139] Here, Fresnel plates consisting of 15 opaque and transparent zones were fabricated using silk proteins on glass via photolithography. Successive zone edges were calculated by utilizing the equation $r^2 = fn\lambda$, where r is radius of successive zones, n = 1 - 15, λ = wavelength of light (600 nm), and f = focal length.[141] Three different arrays were fabricated with focal lengths from 1.35 to 13.5 cm. The radially symmetric rings, known as Fresnel zones, alternate between opaque and transparent.

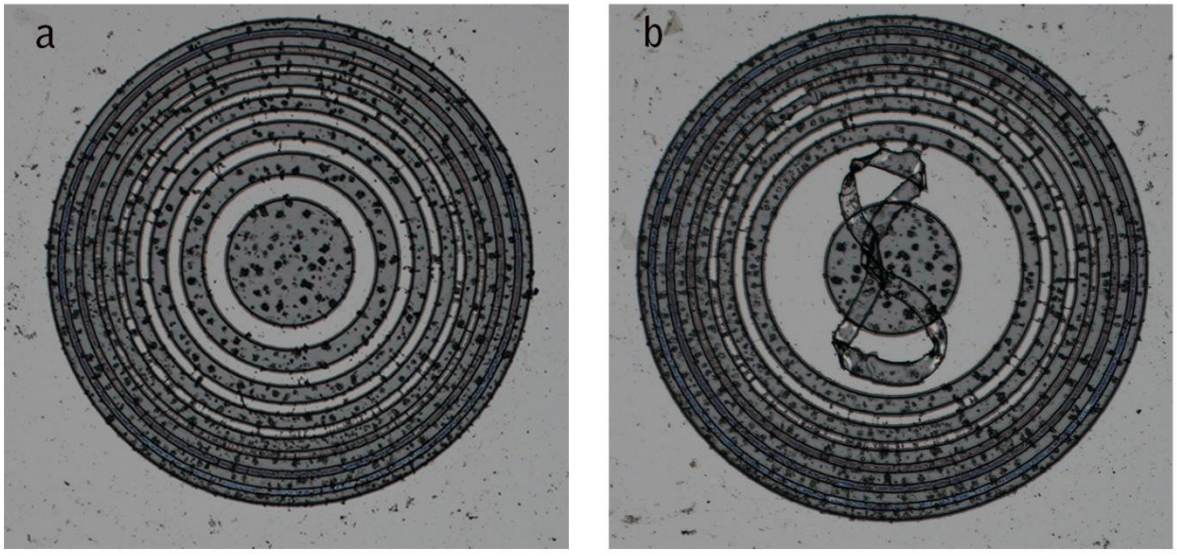

Figure 2.4 *Incomplete development of (a) FZP patterns due to improper thickness of the resist and (b) Delamination caused by extreme sonication.*

During initial fabrication of FZPs, improper development was observed (Figure 2.4 a). It can be seen from the figure that the development of outer rings was poor. Initially, it was assumed that the dissolved proteins were not able to diffuse out into the bulk developing solution owing to the small area. To improve dissolution, sonication was followed. However, strong sonication resulted in dissociation of patterns from the surface (Figure 2.4 b). Another parameter investigated was the aspect ratio of the patterns achieved. Since the FZP has concentric rings of decreasing spacing, the maximum resist thickness was used according to the smallest feature. Thus, it was resolved that the issue was the use of higher thickness of resist films for photolithography. In later experiments resist thickness was reduced to obtain complete development as shown in Figure 2.5.

Once the development issue was solved, alternating FZPs using a dark carbon dye (Figure 2.5a), as well as completely transparent rings without dye (Figure 2.5b) were fabricated. SEM images showing close-ups of the lenses show a clear morphology and the ability to form arrays over large areas (Figure 2.4 c, d). Fabricated FZP lenses having focal length of 13.5 cm were tested under an optical microscope (5x magnification). The transmission image can be seen in Figure 2.4f. The focusing of the light can be seen at center of the Fresnel lens. Better light concentration can be achieved if the opaque zones are perfectly dark and a monochromatic light source is used to perform the experiment. This has been a challenge in the fabrication of such lenses and only recently was the use of carbon nanotubes suggested as a possible solution.[142]

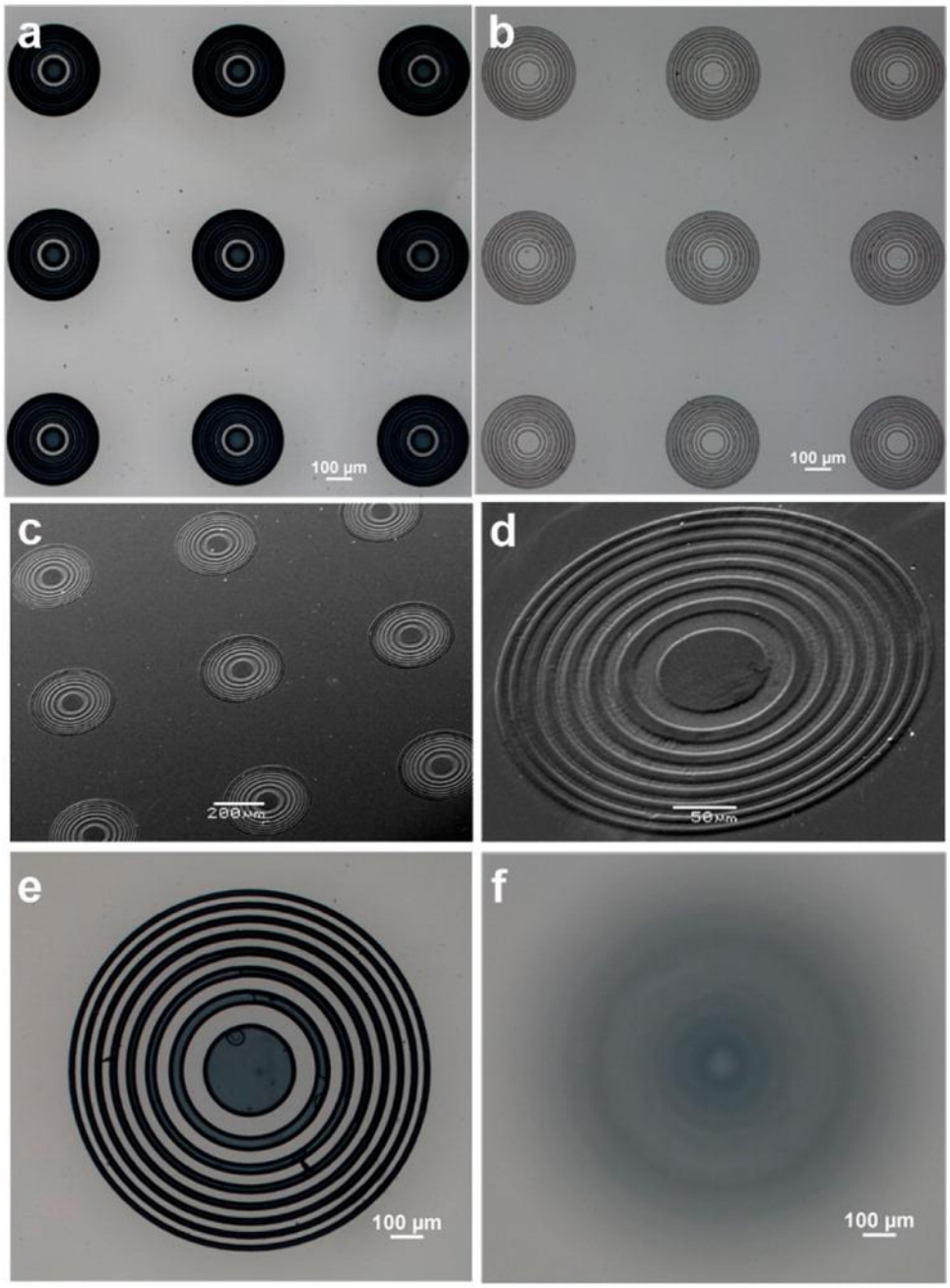

Figure 2.5 *Optical image of (a, b) FZP arrays fabricated from sericin with and without carbon dye to form alternating circles. (c, d) SEM images of Fresnel lenses. (e) Optical image of single lens with a focal length 13.5 cm and (f) light focusing by the lens.*

FZPs have many advantages over refractive lenses, specifically the amount of the material needed for focusing light is less. Second, large *f*-number Fresnel lenses can handle higher magnitude of

ripples of membranes on which they are mounted without appreciable focal spot destruction. This latter advantage makes them particularly suitable for soft and flexible biomedical optics applications. However, typically the optical efficiency of the Fresnel zone plates is low as alternating opaque zones block approximately half of the incident radiation. To date, 12% optical efficiency has been achieved by utilizing vertically aligned carbon nanotube array as a material for opaque zones.[142] Here, optical efficiency is defined as the ratio of light intensity at the focal point to the total light intensity falling at the FZP. Using photolithography, FZPs can easily be patterned on flat surfaces instead of using complicated and expensive gray scale lithography techniques needed to form the structures of a Fresnel refractive lens.[143] The simplicity of fabrication by silk protein photolithography makes silk FZPs a suitable choice for application in implantable optical devices to manipulate light. It opens another avenue for research to be explored and further reinforces the idea of s ilk proteins to be used as optical materials for implantable sensors and devices.

2.3.3 Flexible soft micro-optics

Following the successful demonstration of silk protein photolithography to form optical structures on conventional rigid substrates, the research focused on expanding the ability of this technique to form flexible devices. Given the discussion on its properties above, it is clear that silk forms an excellent substrate for such devices. Therefore, developing a strategy to enable the formation of microstructures of silk proteins on an underlying silk substrate can lead to a fully organic, flexible device comprised solely of silk proteins. In this chapter, we discuss how the silk photolithography technique can be used to fabricate microstructures on a biodegradable elastic sheet to form flexible optical systems. Soft optical systems, which can be folded or stretched repetitively without any

significant loss to their mechanical or optical properties, have applications as adaptive microlenses, paper like displays, and importantly, bio-integrated photonic micro/nanodevices.[90, 144] Because of their biocompatibility, they can be integrated into microfabricated implanted devices as integrated biosensors or as ocular systems.[145, 146]

Initial trials to form FPP patterns on FPP films proved to be unsuccessful due to the high swelling potential exhibited by the carrier HFIP solvent. This results in significant swelling and loss of fidelity of the underlying layer when a subsequent layer of FPP was casted. It should be noted that the sericin protein is water soluble, while fibroin is not. These intrinsic properties of both silk proteins are conserved even after the chemical conjugation. Therefore, to resolve the issue, SPP was chosen to be used for making patterns on flexible FPP substrates, which preserves the idea of an all-protein device. The fabrication steps were as follows: first FPP solution in HFIP was cast on a flexible PDMS substrate. The solution was allowed to dry in air. After drying, the film was exposed to UV light to crosslink the FPP and form a film. The subsequent layer of SPP solution in water was then cast. Here, two problems were observed: 1) due to the hydrophobicity of fibroin polymer uniform spreading of aqueous SPP solution on FPP film was difficult, and 2) due to low evaporation rate of water drying, detachment of FPP films from the PDMS surface was observed. This resulted in uneven stresses and crumbling of the film. This issue was a big obstacle in the development of silk based flexible devices via photolithography. The effect of a crumbled surface on photolithographically developed patterns is shown in Figure 2.6. To overcome this issue, water annealing of FPP films before casting of SPP solutions was investigated. Water annealing is known to increase the beta sheet concentration of fibroin. Here our aim was three-fold: 1) release any stress arising in FPP film during drying, 2) make the FPP surface hydrophilic so that SPP solution

can spread uniformly, and 3) facilitate simultaneous drying of crosslinked FPP film and cast SPP solution so that the delamination could be avoided. This strategy was successful and sericin micropatterns could be realized on fibroin sheets (Figure 2.7)

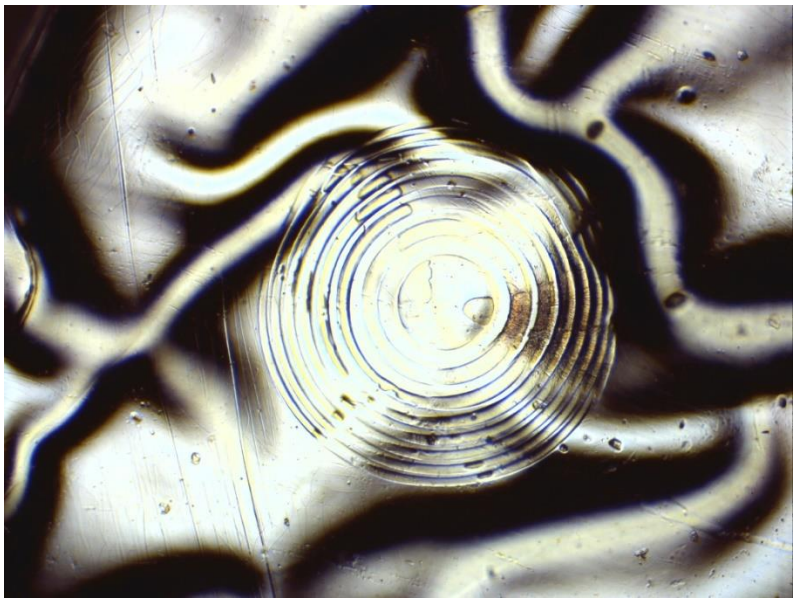

Figure 2.6 *Crumbling of FPP film causing improper patterning of features.*

Both periodic microstructures of SPP and Fresnel lenses were patterned as shown in Figure 2.7. These sheets with lenses and structures can be patterned over large (cm) scales and can be repeatedly twisted or folded as shown in Figure 2.7 b, c. Similar to the patterns on glass, the sheets are mechanically robust and can be stored for several weeks without any degradation. In solutions of protease, the films disintegrate over a period of around 4 weeks. By controlling the degree of cross-linking of the films (MeOH activation of the fibroin sheets, higher cross-linking of the protein photoresist), it will be possible to increase the life of these soft optics for various implantable systems.

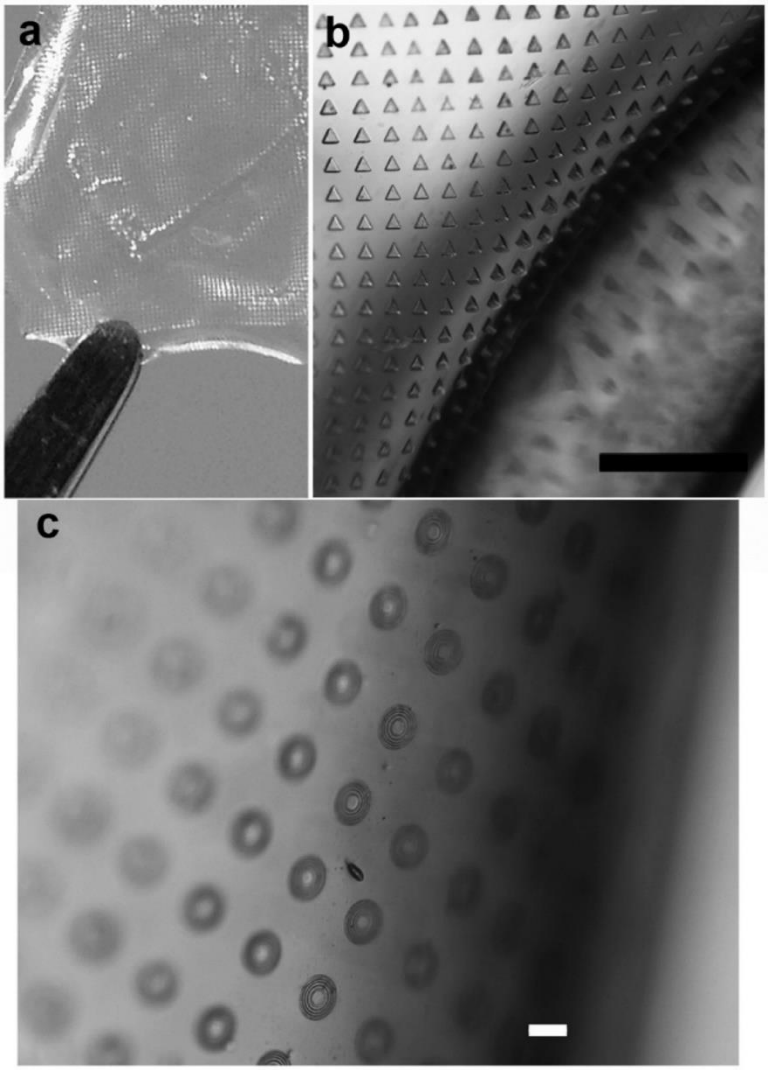

Figure 2.7 *Large-scale flexible micropatterns formed by photolithography. (a) Flexible fibroin sheet with periodic microstructures on the centimeter scale, (b) bending of the films (scale bar = 500 μm), (c) Fresnel lenses patterned on a flexible sheet (scale bar = 100 μm).*

2.3.4 Proteolytic degradation of micropatterns *in vitro*

A significant challenge in the development of micro-optical devices is in the material of choice. Currently, devices are the purview of glass, metals and synthetic polymers. It is in this context that the search for optical biomimetic systems that also utilize natural biopolymers has been initiated.[78, 121, 147] As shown above, silk proteins can be used to make optical

microarchitectures. One of the primary advantage of silk proteins is that they are proteolytically degradable in forms such as silk protein fibers, yarns, freestanding films, and scaffolds.[148-150] Mass loss; reduction of thickness, average molecular weight, and change in surface characteristics, mechanical properties or crystal structure have been studied in these bulk scale arrangements. However, in the formation of microarchitectures, their degradation behavior is largely unknown. When a silk film is studied for analyzing degradation behavior, usually it is open to proteolytic enzyme attack from all sides. Therefore, rate of degradation may be faster than if silk proteins patterns are anchored on a substrate. Here, the objective is 2-fold- (a) demonstrate that the optical microarchitectures can also be completely degraded *in vitro* and, (b) investigate the degradation profiles of micropatterned structures of silk proteins (fibroin and sericin) on glass or silicon substrates. This may be useful in the design of patterns that may be controlled in terms of life span of silk-based optical devices subjected to a challenging or degradation environment.

Optical microscopy, AFM and SEM were used to characterize surface morphology and integrity of silk protein structures. As an example, the optical images of degradation behavior of fibroin patterns on a glass substrate are shown in Figure 2.8. As the top surface was primarily available for the enzyme to act, the surface roughness of the features increased with time. The formed cavities due to degradation increase in size and number. After 5 weeks, the features were almost completely degraded, after which the features delaminated from the surface of glass. The observed degradation behavior was not similar to previous studies. At day 38, the non-uniformity in degradation of microstructures from left to right is possibly due to the slight thickness variation of patterns. In contrast, for the water-soluble sericin, the photo-cross-linked microstructures were completely degraded in around 3 weeks (data not shown). In our earlier reports, free-standing films

of fibroin and sericin were completely degraded in ~2 weeks, showing that the anchoring of the patterns on the substrate affects the kinetics of enzymatic action.[28, 29]

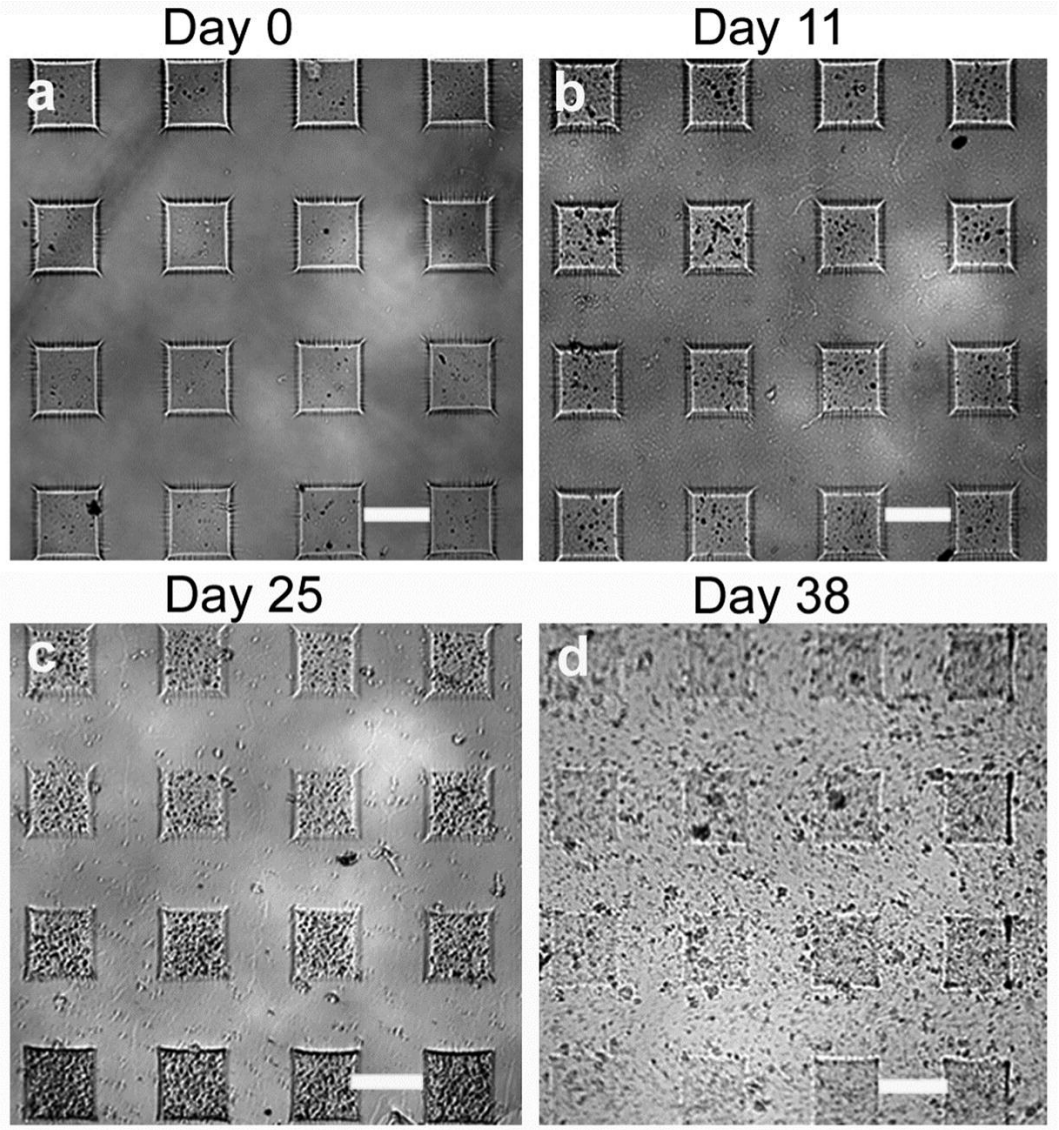

Figure 2.8 *Optical imaging of FPP degradation study (A) day 0, (B) day 11, (C) day 25, (D) day 38 (scale bars = 100 μm).*

To further explore the mechanism of progression of microstructure degradation at the surface, a shorter duration study was conducted, in which both micro- and nanoscale changes are observed. After 1 week, the disintegration can be observed by optical microscopy as discussed above. The

SEM images of the microstructures at Day 0; and at Day 6 in degradation medium and in PBS (control) have been shown in Figure 2.7 (top). The degradation of sericin patterns is higher than the fibroin patterns as evidenced by the higher growth of surface defects. It may be noted that the controls in PBS also show a slight degradation, which are, however, much less compared to the degradation of patterns subjected to the enzyme solution. In contrast, the micropatterned films have maintained their structure for several months during storage in dry condition, showing their overall mechanical stability. Atomic force microscopy (AFM) was done to investigate the surface morphology of the silk protein structures (Figure 2.7, bottom). The results of AFM study are consistent with the results of SEM. At Day 6, fibroin patterns subjected to protease solution shows several micrometer size cavities that were not evident on SEM images. The fibroin control samples increased in roughness, but no observable cavities developed on the surface. The root-mean-square surface roughness data as measured from AFM imaging is shown in Table 2.1. Several microstructures ($n = 5$) were imaged over 10 × 10 μm areas with replicates for this data.

***Table 2.1**: RMS surface roughness (nm) of fibroin and sericin microstructures during enzymatic degradation as measured from AFM imaging.*

		In enzyme solution	In PBS control
Days	**0**	**6**	**6**
Fibroin	5.9 ± 0.3	25.5 ± 1.8	16.0 ± 1.2
Sericin	4.1 ± 1.3	65.2 ± 28.7	15.9 ± 3.9

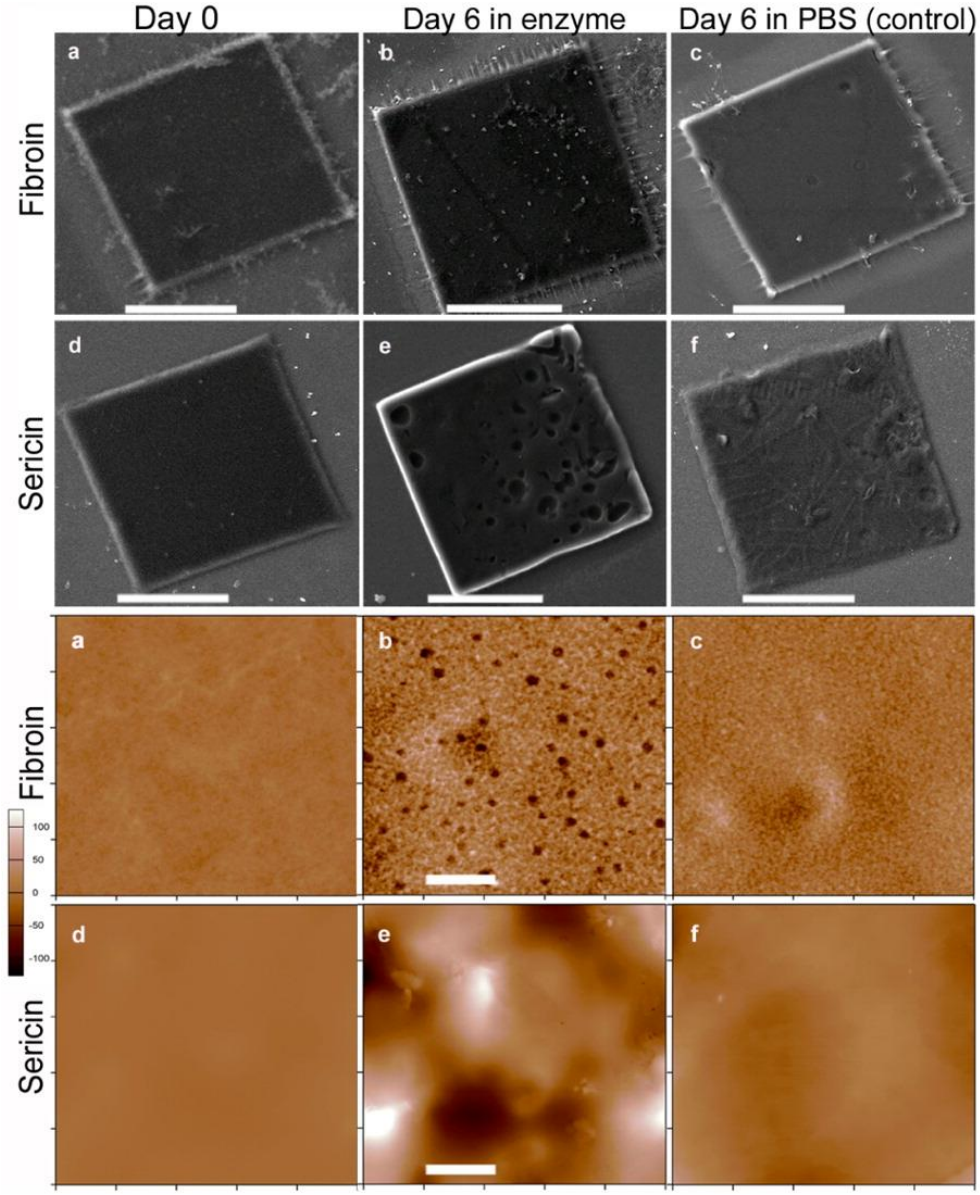

Figure 2.9 *(top) SEM imaging of degradation study of micropatterned fibroin (a) day 0, (b) day 6, (c) day 6 (control); and sericin (d) day 0, (e) day 6, and (f) day 6 (control). Scale bar =50 μm. (bottom). Close-up using AFM images of the degradation study showing the surfaces of photopolymerized fibroin and sericin films. Fibroin: (a) day 0, (b) day 6 in enzyme, (c) day 6 in PBS buffer (control); and sericin: (d) day 0, (e) day 6 in enzyme, (f) day 6 in PBS buffer (control). Scale bar = 2 μm. z-scales are the same on all AFM images.*

The two silk proteins, sericin and fibroin, have different molecular structure. Silk fibroin mostly comprises beta sheets of a highly repetitive sequence of Gly-Ala-Gly-Ala-Gly-Ser, which makes it highly crystalline and thus insoluble in water.[151] On the other hand, sericin is mostly a random coil structure that makes it amorphous and therefore soluble in water.[152] Protease enzymes are more active and tend to bind easily to amorphous regions, in comparison to crystalline regions and low-molecular-weight, non-compact proteins.[153, 154] As most of the regions of sericin are amorphous random coils, the protease is likely to attack and degrade the protein easily. Fibroin with β-sheet crystalline domains is likely to be much more resistant to protease attack. Here, the overall degradation analysis suggests that this is indeed the case, as the sericin degrades faster than the fibroin in the presence of protease, consistent with previous studies. The probable mechanism of degradation of silk protein features is that the enzyme gets adsorbed in very small cavities from where it starts to degrade the protein patterns. These cavities then act as a nucleation sites for enzyme action. Therefore, over time, cavities increase in size and new cavities are created. The observed degradation behavior provides new insight on proteolytic degradation of protein patterns attached to substrates. It is important to note that the degradability of silk proteins can be controlled by changing the degree of cross-linking of silk photoresist.[28, 29] This provides a route to form stable architectures that can be programmed to degrade over a specific time.

2.4 CONCLUSION

In conclusion, the work described in this chapter demonstrates an extension of the earlier developed silk protein photolithography technique. Both proteins in the photoresist form are easily synthesized, and via photolithography can be used in complementary ways for engineered micro- and biophotonic elements. The processing conditions of silk photolithography are relatively benign

in comparison to other micro/nanopatterning techniques reported, and can be conducted rapidly and inexpensively on the benchtop. This method is versatile and can be formed into diverse shapes that can be patterned at the macroscale (several cm) on both rigid substrates and flexible sheets. The 2D array of periodic micropatterns produce angle-dependent structure-induced iridescence, while Fresnel zone plates can be used for the focusing of light. These soft optical systems are mechanically stable in air over several months, and stable in liquids for weeks. They degrade completely in a few weeks because of proteolytic degradation, which can be controlled by controlling the degree of cross-linking of the proteins. Thus, the silk protein lithography route may be a potential route to make precise, biocompatible and biodegradable features rapidly without any limitations on shape and size. The characteristics reported here can lead to further studies where silk can be studied as a potential optical biomaterial. Most importantly, for the first time, a protocol to develop flexible micropatterns based on silk proteins was developed. These results lay the ground work for the next chapters in which this technique is used for the development of flexible functional protein based devices.

[This chapter contains results that have been previously published: R.K. Pal, N.E. Kurland, C. Wang, S.C. Kundu, V.K. Yadavalli, "Biopatterning of silk proteins for micro-optics", ACS Applied Materials and Interfaces, 7, 8809-8816, 2015.]

CHAPTER 3

FABRICATION OF PRECISELY SHAPED PARTICLES USING SILK PROTEIN LITHOGRAPHY

3.1 Introduction

Chapter 2 discussed the extension of the silk protein lithography platform to flexible substrates. Prior to adoption of the technique for the development of devices discussed in subsequent chapters, silk protein lithography was investigated as a tool for the fabrication of precise microscale objects. Manufacturing of high fidelity, shape-specific (i.e. non-spherical) particles in large quantities require novel micro- and nanofabrication techniques, that can enable production in a cost effective manner.[155] Typically fabricated from synthetic polymers, particles ranging from a few nm to hundreds of μm can function as imaging or contrast agents, vehicles to encapsulate and deliver therapeutics with precise control,[156, 157] or intracellular biosensors.[158] New systems are being developed to serve these applications. However, success of nanoparticle delivery *in vivo* is often limited, particularly following systemic administration where less than 5% of the total dose successfully reaches the target site.[159] Improving the delivery efficiency is of prime importance to fully exploit their potential as both a research tool and as a potential pharmaceutical agent.

For these reasons, there has been a focus on engineering particles through modulation of specific physical characteristics such as particle shape, size, mechanical properties, permeability, surface charge and surface chemistry.[160-162] These properties can modulate particle motion in blood

flow, cell-particle collisions, drift and margination propensities, protein adsorption characteristics, adhesion probabilities and strength, rate of internalization, and payload delivery outputs.[162] Several techniques have been reported for the formation of particles, ranging from bottom-up approaches guided by self-assembly,[163] to top-down approaches including spray drying,[164] atomization,[165] milling, grinding,[166] and emulsion solvent evaporation.[167] Bottom-up methods are driven by thermodynamics and kinetics which determines the yield of the desired structures. Limitations include formulation instability, large size distribution, and limited particle shapes.[168] Similarly, the top down approaches have limited control on shape and size of particles, resulting in large variations in particle sizes and distributions.

Control of the shape of the particles formed is challenging, with spherical or near-spherical particles being most commonly formed. A recent addition to considering particle fabrication is the shape of the particle.[169] *Non-spherical* and anisotropic micro and nanoparticles are of great interest to provide functionality not accessible to spherical geometries.[170] For example, engineering particle shape provides the ability to affect cellular interactions and uptake, vascular dynamics and pharmacokinetics.[160, 171] Advantages include improved packing, controllable responses to external stimulus, and unique optical behavior.[172] Particles with unique shape and illustrative patterns can be used to tag various chemistries for multiplexed sensing and bioassays.[155, 173, 174]

Large numbers of monodisperse, non-spherical particles with precisely controlled physical and chemical characteristics, may be fabricated using soft lithography, microfluidic synthesis, stop flow lithography, contact flow lithography, capillary flow lithography and optofluidic

techniques.[174-178] The novel particle replication in nonwetting templates (PRINT®) technique has been one of the most successful and versatile at producing freestanding, high fidelity particles at high throughput.[179] Particles of various synthetic biopolymers like poly(ethylene glycol) (PEG), poly(ethylene glycol) di-acrylate (PEGDA), poly(lactic acid) (PLA), poly(lactic-co-glycolic acid) (PLGA) have been demonstrated.[170, 174, 180] However, to date, free-standing, high fidelity particles made from natural and bioinspired biopolymers, have been relatively unexplored.[181] Natural materials including proteins (silk, collagen, gelatin, elastin, keratin), polysaccharides and nucleotides present alternatives to form particles for various biomedical applications.[147, 182, 183]

Micro and nanostructures of both silk fibroin and sericin have been reported for drug delivery and regenerative medicine. Silk protein have unique advantages over synthetic polymers for drug delivery applications such as suitability with common sterilization techniques, robust mechanical properties, water based processing (in the case of sericin), enzymatic biodegradation, non-toxic degradation products (amino acids), and drug stabilization.[184] However, to date, these have been restricted to films, foams, rods, and spherical geometries formed using self-assembly, emulsification, desolvation, coacervation or electrospray drying.[185-190] Formation of controlled and non-spherical shapes has not been possible due to the significant mismatch between processing and the biomaterials. This part of the research therefore focused on utilizing SPL to form precise microscale architectures of silk proteins in the form of designed shapes and 3D objects. As shown below, freestanding shapes can be formed from both fibroin and sericin, to achieve unabridged use of silk.

Using a non-adhesive monolayer, independent, unattached shapes can be formed at the microscale via photolithography. While this is a mask-based process, the relatively simple processing involved, the rapid nature of particle synthesis, monodisperse and high fidelity architectures produced, makes this suitable to produce large quantities of precise protein shapes. The patterns produced are easily reproducible over large numbers, and the shape of the architectures is only limited to the mask. Silk protein particles possess an important advantage in that they can break down to physiologically compatible amino acids when resorbed, making them suitable choices for *in-vivo* systems over synthetic polymers.[191] Both the protein matrix and the lithography strategy employing benign solvents, are suited for encapsulation of biologically functional agents This provides a route to design of monodisperse protein shapes that may be harvested for the potential delivery or presentation of biologically functional agents.[192]

3.2 EXPERIMENTAL

3.2.1 Materials

Silk fibroin and sericin were sourced as discussed in Chapter 2. 2-isocyanatoethyl methacrylate, 98% with < 0.1% BHT inhibitor (IEM, MW = 155.15 Da) was utilized for chemical modification of fibroin. Anhydrous dimethyl sulfoxide, and anhydrous lithium chloride (LiCl) were purchased from Sigma-Aldrich (St. Louis, MO). 1,1,1,3,3,3-Hexafluoro-2-propanol (HFIP) was obtained from Oakwood Chemical (West Columbia, SC). Irgacure 2959 (1-[4-(2-Hydroxyethoxy)-phenyl]-2-hydroxy-2-methyl-1-propane-1-one, Ciba, Tarrytown, NY) was employed as a photoinitiator. Octadecyltrichlorosilane (OTS) was procured from Sigma-Aldrich (St. Louis, MO).

3.2.2 Synthesis and Purification of Fibroin and Sericin Photoresist

The synthesis and purification of fibroin and sericin photoresist materials were the same as described in Chapter 2.

3.2.3 Surface Functionalization of Silicon and Glass Substrates

Silicon and glass substrates were used for patterning of silk microshapes. Squares of silicon (1 x 1 cm^2) and glass (2 x 2 cm^2) were initially washed thoroughly with ethanol and deionized water to remove surface contaminants. Substrates were treated with Piranha solution (3:1 98% H_2SO_4:30% H_2O_2) for 30 minutes to remove organic contaminants and hydroxylate the surface for further modification (*Caution: Piranha solution reacts violently with organic materials and must be handled with extreme care*). Surfaces were then repeatedly washed with deionized water and ethanol and dried at 150°C. To enable patterning and subsequent delamination of features, surfaces were modified to create a chemically-inert, hydrophobic surface. This was achieved via the modification with a self-assembled monolayer (SAM) of octadecyltrichlorosilane (OTS). Vapor deposition of OTS was conducted in a desiccator (0.4 bar for 12 hours). These substrates were washed alternately with ethanol and water, and dried prior to use.

3.2.4 Silk Protein Photolithography (SPL)

Micropatterns of silk fibroin and silk sericin protein photoresist (FPP, SPP) were fabricated using contact photolithography. FPP was dissolved at 2% (w/v) in HFIP with 0.6% (w/v) of Irgacure 2959 photoinitiator, while SPP was dissolved in water having similar 2% (w/v) concentration with Darocur 1173 (0.05µl/1 mg of SPP) as the photoinitiator. The protein solutions were vortexed at low speed for a period of 30 minutes, at which point no solids remain. The FPP and SPP solution

were cast on clean silicon substrates functionalized with a SAM of OTS. An ambient 'pre-bake' step was then conducted, in a fume hood to allow excess solvent (HFIP)/water to evaporate, and avoid photoresist-to-photomask adhesion. Cast protein films were polymerized via an OmniCure S1000 UV Spot Curing lamp (Lumen Dynamics, Ontario, Canada) equipped with a 320 – 500 nm filter. Substrates were exposed at 365 nm ultraviolet (UV) light (20 mW/cm^2), for 1.5 seconds through a chrome photomask. Development of uncrosslinked and unexposed FPP was performed using 1M LiCl in DMSO, followed by copious rinsing with deionized water. Similarly, SPP features were developed in deionized water, followed by extensive rinsing with water. The developed substrate was briefly sonicated to facilitate particle detachment from substrate. Finally, protein particles were corralled and harvested using a cell scraper while the substrate was still partially hydrated with deionized water. Water behaves as a 'collection' medium, enabling displacement of particles which are observed to aggregate, preventing mechanical damage.

3.2.4 *In vitro* proteolytic degradation and imaging

To demonstrate the biodegradability of the particles, enzymatic degradation was followed over time. "Arrow" shaped FPP particles with a length of 50 μm (1 mg of protein/40 μl of HFIP) were incubated in 3 mL of protease (1 U/mg of protein) at 37°C (Protease XIV from *S. Griseus*, ≥ 3.5U/mg, Sigma-Aldrich). The enzyme solution was replaced every third day to preserve activity. As negative controls, particles were incubated in PBS containing no enzyme. At different time intervals (1, 2 and 3 weeks), samples were removed from solution, washed with deionized water, and dried for further study. The particles were imaged using scanning electron microscopy (SEM) to observe the changes in the surface morphology over time. Scanning electron microscopy (SEM) images were taken on a Jeol (JSM-5610 LV) instrument. The patterns and films for SEM were

first sputter coated in 20 Å platinum Denton vacuum V cold sputtering system (Moorestown, NJ).

3.2.5 Particle interactions with cells

To investigate cell compatibility of the particles, as prepared FPP and SPP particles were first collected in wells. Particles were sterilized by adding 75% ethanol/water solution to the wells and allowing the ethanol solution to evaporate. UV sterilization was followed for 30 min (Labconco (Kansas City, MO) class II, type A2 purifier logic+ biological safety cabinet). No treatment was done to immobilize the particles on well surface. The particles were in suspension with media. Female mouse embryonic fibroblasts (MEFs) was used in the experiment. Cells were cultured in DMEM/F12 (1:1) medium (Thermo Fisher) with 20% fetal bovine serum (Atlanta Biologicals) at 37^{o}C in a 5% CO_2 incubator and fed every 3 days. Detached cells with 0.25% Trypsin EDTA (Sigma-Aldrich). Each well with sterile samples was seeded with 2 x 10^4 cells. Images were taken on days 1, 3 and 5 after being seeded. Following confluence, to understand the adhesion morphology, distribution and cell-to-cell and cell-to-particle interaction, the cells were fixed and stained with phalloidin and DAPI and imaged using a confocal microscopy (Olympus IX81 microscope). Particles also pick up the DAPI stain making them visible.

3.3 RESULTS AND DISCUSSION

Developing sustainable, low-cost and biofriendly techniques for particle fabrication includes adoption of a non-toxic material, green synthesis, and ensuring that the products degrade with a minimal impact to the environment at the end of their useful lifespan.[193] Further, it is desirable for micro and nanoparticles for sensing or delivery applications to possess a number of properties.

These include printability at desirable resolution (nm to mm), throughput, biocompatibility, favorable degradation kinetics and byproducts, and the ability to incorporate active biomimetic components to induce desired structural, functional and dynamic properties. Silk proteins (fibroin and sericin) have proved to be extremely attractive for integration with a biological milieu owing to these advantages as well as outstanding mechanical performance, processability and ease of functionalization.[187, 194-196] However, to date, micro and nanostructures of both silk fibroin and sericin have primarily been in the form of films, rods, or spherical particles.[185-190] Conventional methods result in shapes that are most typically spherical or near-spherical, tend to be polydisperse with size ranges over several orders of magnitude, or that can easily aggregate. The development of techniques with controlled shape and encapsulation using silk proteins would therefore greatly expand the application space for these biomaterials. Here, for the first time, a technique to form non-spherical particles of controllable properties using only a protein as the material of construction is demonstrated.

3.3.1 Photolithography using silk fibroin and sericin to fabricate shapes

The modified SPL process to fabricate monodisperse microparticles using silk proteins involves four primary steps (**Figure 3.1**). First, a substrate (silicon or glass) is functionalized with a sacrificial monolayer that enables a weak attachment of the proteins. This enables the particles to stick to the substrate till they are physically removed. Second, a layer of the photoresist material of which the particles would be made (FPP/SPP) is spin coated on the functionalized substrate. Third, exposure of the UV light through the photomask, having specific patterns of interest. In the presence of UV light, the protein base material, which behaves as a negative tone photoresist is crosslinked. The crosslinked protein is then developed to obtain micropatterns on the substrate.

The final step is the dissolution of the sacrificial layer or mechanical lift-off to corral the freestanding particles of specific shapes.

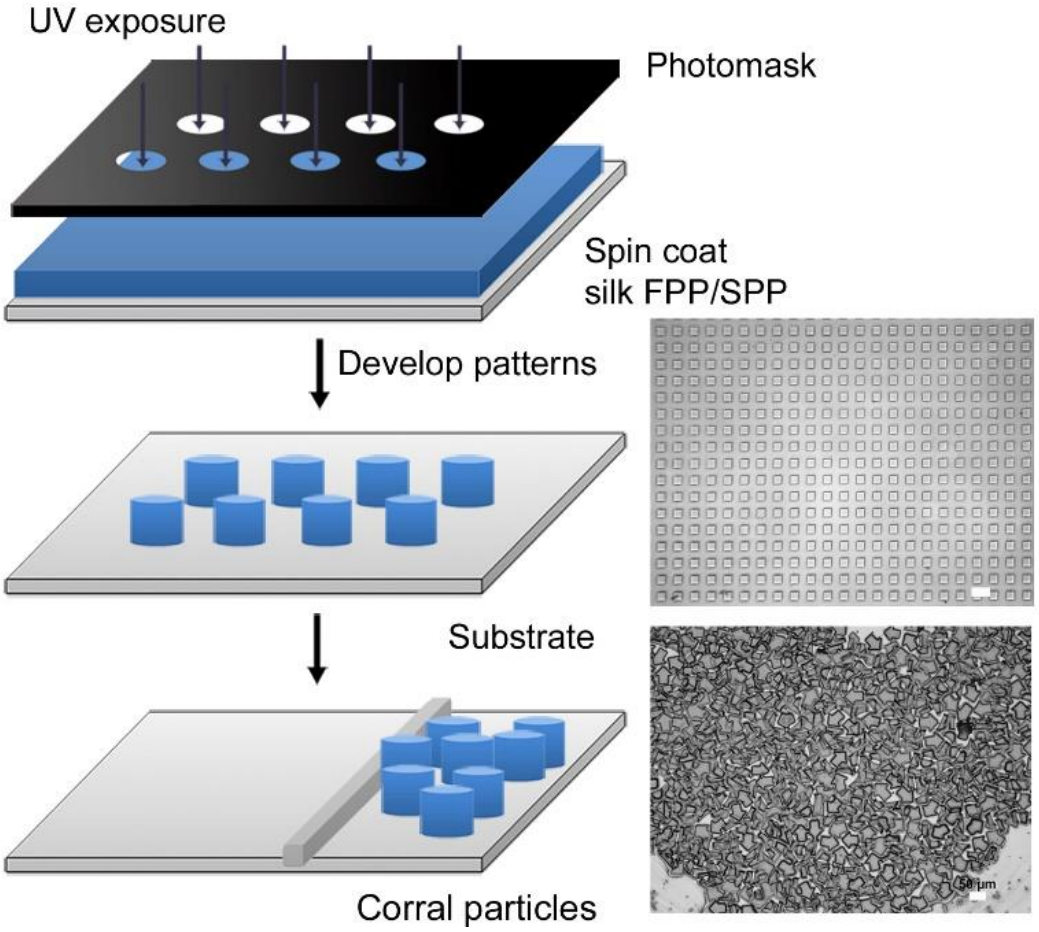

Figure 3.1 *Schematic of precise shapes using silk proteins via photolithography. Optical microscopy shows square particles formed immediately after development and large numbers of arrow shaped particles corralled using a cell-scraper. Scale bars = 50 µm.*

At first, the research focused on a suitable tether for the particles to the surface since the material needs to be strongly attached to the underlying substrate until the development step is completed. Following this step, particles need to be easily detached and collected. In the previous chapter, it was shown that FPP/SPP micro features can be covalent attached to the underlying substrate using functionalization with 3-(trichlorosilyl) propyl methacrylate (TPM). However, TPM results in an

irreversible coupling to the surface via methacrylate groups, and is as such not suitable for free-standing shapes. The use of fluorinated substrates was demonstrated in the PRINT® technique for creating non-wetting substrates, allowing facile delamination and harvesting of architectures [180]. Here, various surface treatments were explored including alkylsilanes with optimum surface hydrophobicity that can preserve adhesion during photoresist application and development, while enabling removal post-development without damage to particles [197]. The effects of some surface treatments are shown in Table 3.1 using silicon as the substrate (the results for glass were similar and are not shown). Trichloro (1H,1H,2H,2H-perfluorooctyl) silane (FOTS) and octadecyltrichlorosilane (OTS) both provide highly hydrophobic surfaces (typical contact angles are ~100-110^{o}). However difficulty in controlling the deposition of monolayers using FOTS, in addition to loss of particles during development, led to OTS being chosen for subsequent surface functionalization.

Initial attempts to form freestanding fibroin particles were hindered by the precipitation of fibroin on the silicon substrate and around the developed particles (Figure 3.2 a**)**. This issue was not observed in earlier works with fibroin patterning or with the development of sercin particles. Due the precipitation issue, the collection of particles were either not possible or resulted in excess debris around the particles after collection. By careful analysis of earlier used protocols and current procedures, it was found that the particles were covalently attached to the substrate (either rigid or flexible) due to the formation of vinyl bonds. Therefore, washing of patterns with a water jet was done after development to remove any residual solvent.

In these experiments, washing with a water jet was not possible to avoid washing away of particles. The samples were therefore directly immersed in water. Since fibroin is water-insoluble, but

DMSO and LiCl are soluble in water, precipitation of fibroin in the solvent is observed. To counter this issue, after complete development, the substrates were soaked in fresh DMSO/LiCl solution and briefly sonicated to reduce the concentration of fibroin. 2x soaking in fresh DMSO/LiCl solution was found to be sufficient to avoid precipitation in subsequent washing steps (Figure 3.2 b).

Table 3.1. *Contact angle values for various surface treatments of silicon. OTS and FOTS both lead to non-adherent, highly hydrophobic surfaces. OTS was chosen due to ease of chemical vapor deposition, and favorable adhesion properties.*

Treatment	**Contact Angle**
Untreated Si	33.4 ± 2.7º
Si treated with piranha solution	6.8 ± 1.3º
3-(trichlorosilyl) propyl methacrylate (TPM)	57º
Octadecyltrichlorosilane (OTS)	100º - 110º
Trichloro(1H,1H,2H,2H-perfluorooctyl)silane (FOTS)	100º - 110º

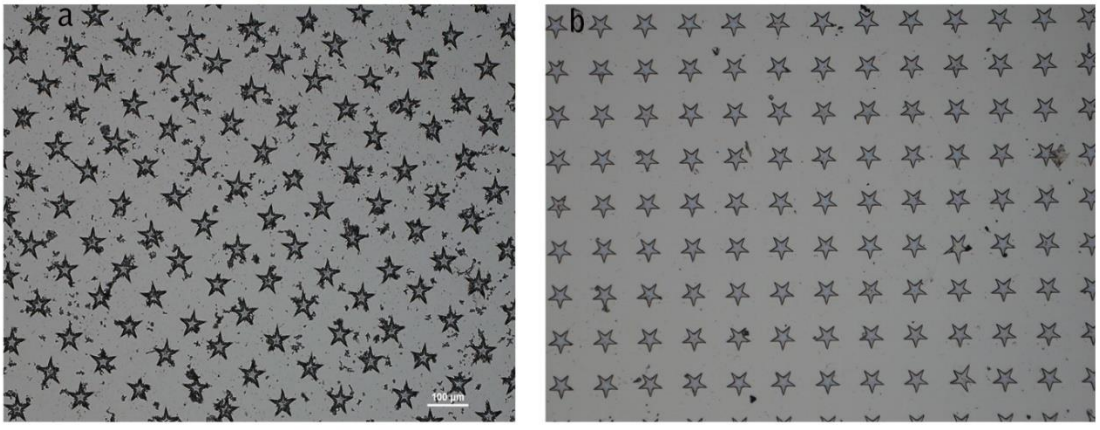

Figure 3.2 *Optical microscope image showing (a) precipitation of fibroin with unmodified protocol and (b) negligible precipitation with modified protocol during the water soaking*

3.3.2 Collection and characterization of shapes

Monodisperse shape specific microparticles were formed using this SPL procedure. Surfaces were modified using an OTS monolayer and development did not result in delamination of particles. To collect the particles from substrate, a cell scraper was used. However, the use of a cell scrapper alone resulted in inefficient particle collection and particle damage (Figure 3.3**).** Brief sonication of ~30 sec prior corralling of particles was then introduced to partially detach the particles. Particles could then be easily corralled using a cell scrapper and harvested (Figure 3.1). Optical microscope images of various shapes and sizes of particles formed from fibroin protein photoresist (FPP) and sericin protein photoresist (SPP) are shown in Figure 3.4. Particles ranging from 5 µm to 500 µm can be easily formed using this process. In this work, sub-micron architectures are not studied, but they are feasible to around 700 nm using suitable photomasks and UV-exposure.

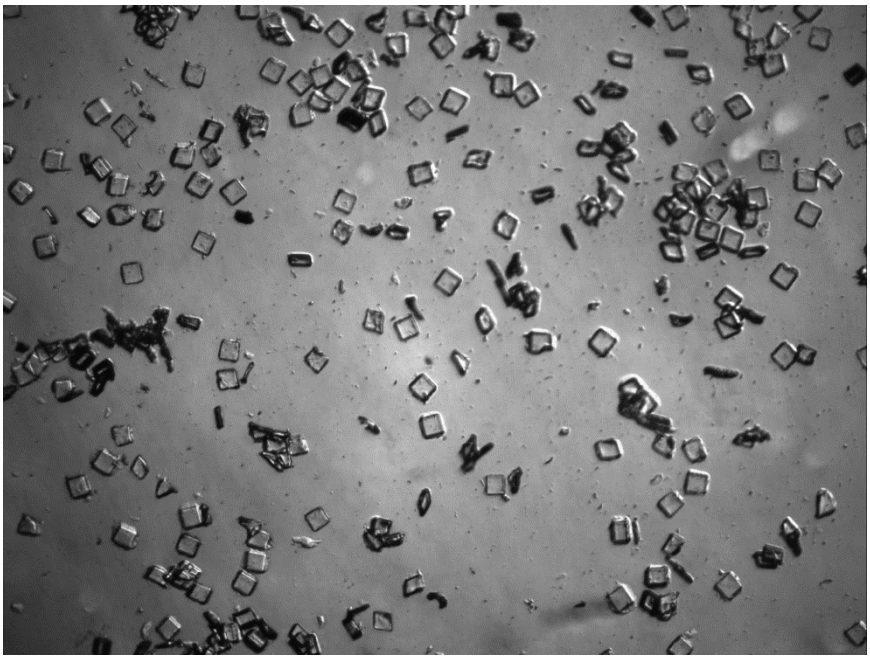

Figure 3.3 *Particle damage due to excessive cell scraper friction*

Once the process was optimized, various shapes (circles/discs, arrows, squares, triangles, stars etc.) can be formed with aspect ratios up to 0.5 (Figure 3.4). This compares well with other reported

techniques including photolithography (0.5),[198] optofluidics (0.1),[199] and contact flow lithography (0.05-0.25),[174] but is lower than that reported by the PRINT® method (1.0-3.0).[180] It may be noted that in these reports, the materials included PEG-DA, PLGA and SU-8 photoresists. In contrast, competitive results using a biopolymer are shown for the first time. The corralled shapes can be easily collected and mixed to form mixtures of different geometry (Figure 3.5). SEM images indicate that the particles formed have sharp edges and flat straight side walls. This process therefore results in particles with high fidelity and very less debris formed during the process.

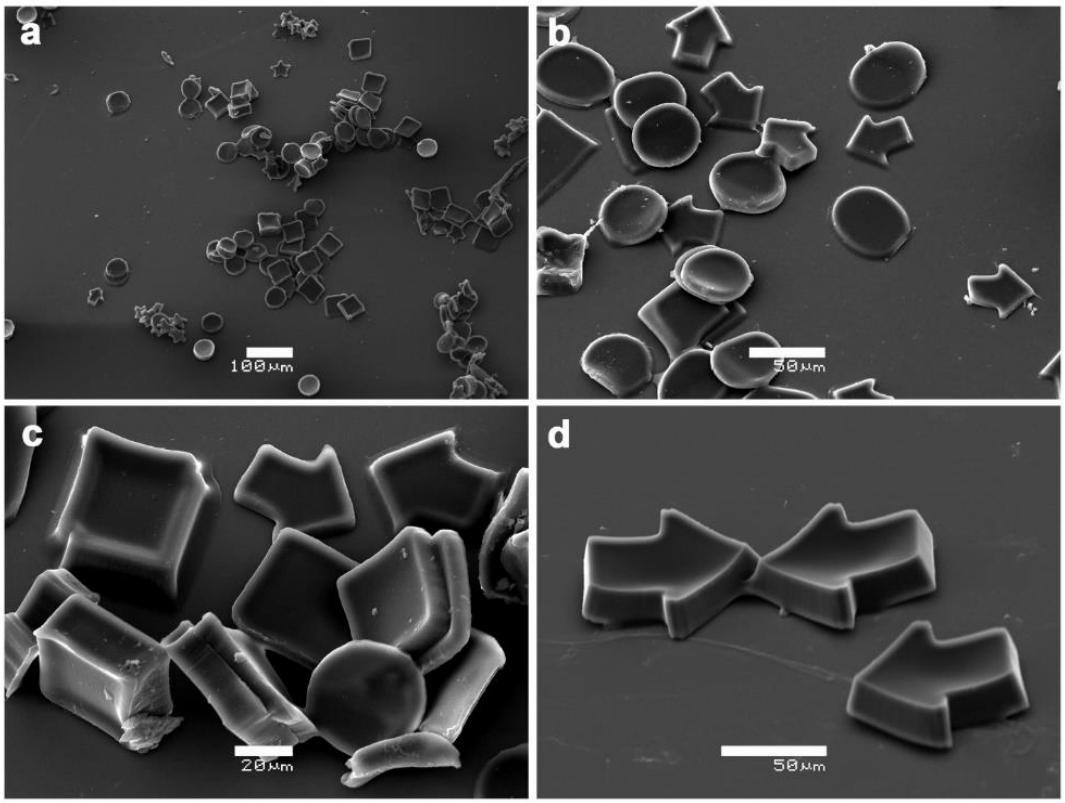

Figure 3.4 *Synthesis of diverse shapes in large numbers corralled using a cell scraper. Here shapes from both fibroin and sericin are shown. (a) Discs/circles, arrow shaped, stars, square fibroin particles. On all panels, scale bar = 50 µm. (b) SEM images of small sericin particles formed using photolithography. Scale bar = 5 µm.*

The photolithographic approach to manufacture protein particles has significant advantages over reported self-assembly processes.[200] First, several self-assembly techniques use ethanol making them unsuitable for the immobilization of enzymes or biomolecules. Second, monodisperse particles of specific shapes can be formed at high throughput. For instance, a 100 x 100 array can form ~10000 particles in a matter of minutes – even considering the time for spin coating, exposure and development. This compares favorably with other reported techniques and can potentially be used for high-throughput, continuous production of large numbers of particles in parallel. It may be noted that the current work uses very short duration, low intensity UV radiation to form the particles. The short exposure of ~1 second makes it less detrimental to enzymes that may be immobilized in the particles. The use of natural polymer, room temperature, and one step fabrication with very low UV exposure makes the process relatively biofriendly than other fabrication process as discussed earlier in Chapter 1.[201]

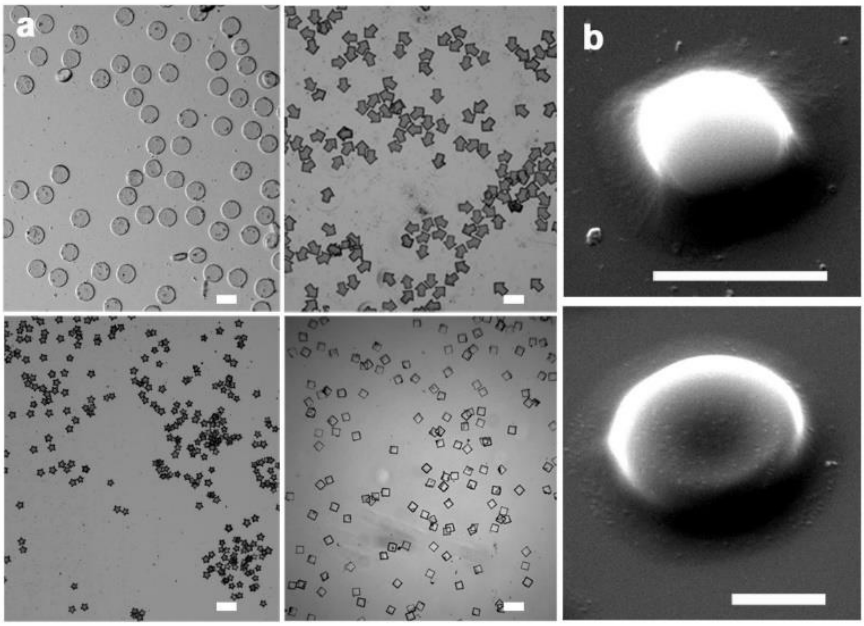

Figure 3.5 *SEM images showing mixtures of independent structures: monodisperse shapes of fibroin in the form of microparticles fabricated through SPL on a non-wetting substrate. Particles of various shapes and thicknesses can be fabricated and mixed.*

The shapes can be applied for the incorporation or delivery of a bioactive payload. To investigate this potential, fluorescent dye loading was used to allow visualization of particles, and effectively demonstrate the ease of incorporation and successful entrapment of functional agents. Fluorescein isothiocyanate (FITC)-conjugated albumin (green fluorescence) and Alexa Fluor® 555 ovalbumin conjugate (red fluorescence) were loaded into 50 µm stars, discs and squares via a 1:10 mass ratio of dye to FPP. UV exposure and development did not show any observed leaching of dye (Figure 3.6) over a period of 1 week. Figure 3.5 shows that variously tagged particles can be used to load different biomarkers as cargo (green stars, red squares, green discs etc.) This strategy establishes the versatility of the SPL platform in incorporating multiple functional materials as a composite without any changes to structure or noticeable degradation.

Biomolecule-loaded particle templates can therefore be potentially used to investigate the efficiency and kinetics of uptake, molecular sensing, and quantitative or qualitative imaging. While small molecule drugs can be released via diffusion, the relatively large 45 kDa proteins were not released via diffusion over a period of a week, but could potentially be released via degradation of the particles as discussed below.[184] Here the focus is on the fabrication procedure and characterization of the particles, and not on release. In contrast to spherical particles, the particles themselves are of different shapes and anisotropic. Further, the swelling and pore sizes of both proteins can be controlled easily by modulating the crosslinking of proteins to achieve controlled release. Therefore, the release is expected to be a complex function of particle size, shape, aspect ratio etc. and would have to be studied separately. Such studies should be followed in future.

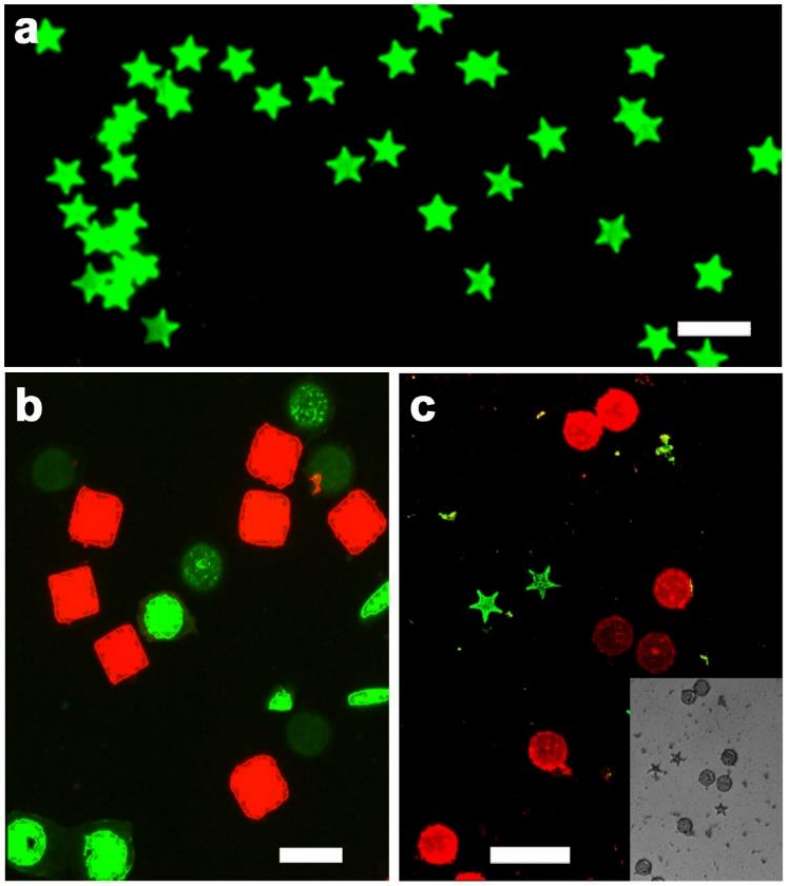

Figure 3.6 *(a) Monodisperse fibroin (FPP) stars, 50 µm, loaded with FITC-albumin at 1:10 FITC-albumin:FPP. Stars, and lack of detectable fluorescence in background, indicates retention of dye through the lithography process. (b) Shapes can be loaded with different dyes and mixed - square FPP shapes loaded with AlexaFluor® 555-ovalbumin + FITC loaded discs and (c) discs loaded with AlexaFluor® 555 (red) + stars loaded with FITC (green). Scale bar = 100 µm.*

3.3.3 Cytocompatibility of silk shapes

Both fibroin and sericin are known to be biocompatible, in their native form as well as in the photo-reactive FPP/SPP forms. To verify that these particles are cytocompatible, fibroin and sericin particles were co-cultured with mouse embryonic fibroblasts (MEFs) over a period of 1 week. 100 and 500 particles of each were incubated with cells in each well and monitored till the cells reach

confluence. Figure 3.6 shows 50 µm FPP and SPP star-shaped particles following actin (green) and DAPI (blue) staining. Control experiments (not shown) consisted of the cells in the absence of particles. The experiment indicate that the materials and fabrication process are biocompatible as shown in previous works.[28, 29] Also, even with large numbers of particles in co-culture with cells, there was no detrimental effect to the cells, demonstrating that this technique can form biocompatible shapes.

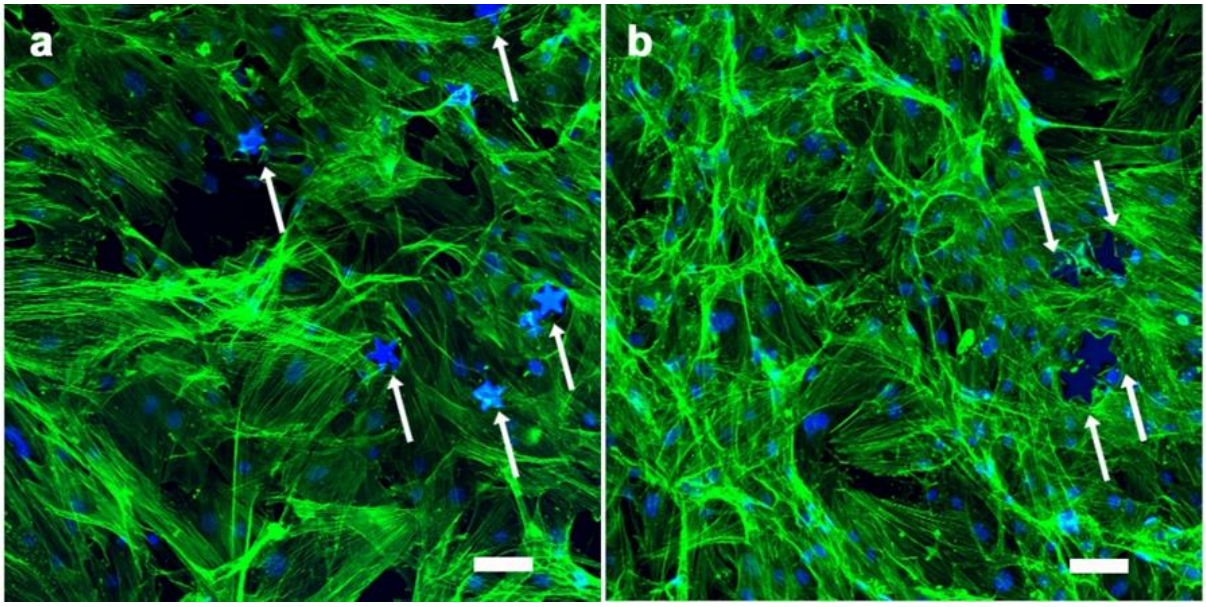

Figure 3.7 *Cytocompatibility experiments.* ***(****a) Fibroin and (b) sericin particles (white arrows) were cultured with mouse embryonic fibroblasts over a period of 7 days. 50 µm star-shaped particles following actin (green) and DAPI (blue) staining are shown. Scale bars = 100 µm.*

3.3.4 Biodegradation of silk shapes and solvent usage

A proteolytic degradation study done on 50 µm fibroin particles showed similar degradation characteristics as reported in earlier works (Figure 3.8)**.** As sericin degrades faster than the fibroin in the presence of protease. The degradation behavior and properties of both proteins can therefore guide the selection and usage of FPP vs. SPP. For instance, fibroin has superior mechanical

properties, with a higher molecular weight than sericin. Sericin is water soluble but fibroin is not. Silk fibroin has been shown as an efficient carrier for various drugs.

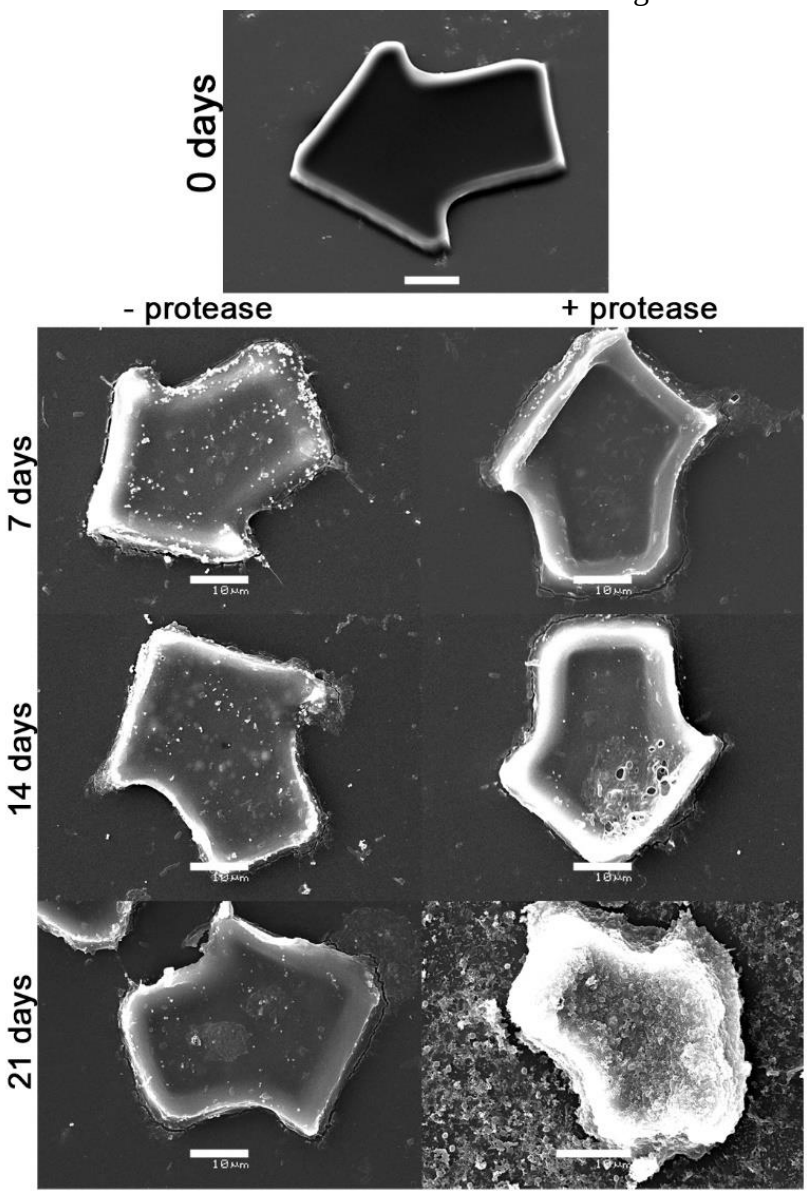

Figure 3.8 *Proteolytic degradation. Sets of fibroin particles were incubated in buffer solutions with (right) and without (left) protease enzyme. Particles were retrieved after 7, 14 and 21 days and imaged via SEM to observe surface morphology. Following 3 weeks, particles in enzyme were almost completely degraded. Scale bars = 10 µm.*

A study showed that the Indomethacin (IDMC) drug could be entrapped in fibroin using HFIP as solvent, and without degradation of the drug.[202] But many drug molecules are susceptible to

HFIP which is being used for the processing of fibroin (and FPP). In those cases, sericin (SPP) micro-shapes may play in important role, since they are fabricated in an all-aqueous process. Therefore, both the proteins have their own advantages for many applications. Recent studies also indicate that formic acid (FA) can be used to dissolve FPP, as a much more benign solvent in comparison to HFIP.[203] Therefore, later studies on formation of fibroin shape specific particles can be done using FA.

3.4 CONCLUSION

In this chapter, the versatility of the SPL technique was explored to fabricate fibroin and sericin into high-precision microscale shapes (of various non-spherical geometries) and sizes ranging from 5 to 100 μm. The processing conditions of the technique are relatively benign in comparison to other micro/nanopatterning techniques reported, and large numbers of particles can be rapidly and inexpensively fabricated at the benchtop. These shapes are mechanically stable in air over several months, and stable in liquids for weeks. The cytocompatibility and degradation experiments suggest that both reported silk shapes are biocompatible and they degrade completely in a few weeks owing to proteolytic degradation. The degradation rates can be controlled by varying the size, thickness and the degree of cross-linking of the proteins, thereby providing a route for controlled release applications. The formation of non-spherical architectures of bioinspired polymers in general, and silk proteins in particular can be enabled by such lithographic techniques which can be used in various applications.

[This chapter contains results that have been previously published: RK Pal, NE Kurland, SC Kundu, VK Yadavalli, "Fabrication of shape-defined particles of silk proteins using photolithography", European Polymer Journal, 85, 421-430, 2016]

"Fabrication of nanoscale patternable films of silk fibroin using benign solvents"- A Bucciarelli, RK Pal, A Quaranta, D Maniglio, V Mulloni, A Motta, VK Yadavalli Macromolecular Materials and Engineering, 2017, 1700110.

CHAPTER 4

MICROFABRICATION USING CONDUCTIVE SILK COMPOSITES

4.1 INTRODUCTION

In previous chapters, development of photolithographic processes to fabricate flexible silk protein architectures and shape-defined silk microparticles were described. The versatile nature of silk protein lithography allows us to envision next generation applications in areas ranging from biosensors to bioelectronics.[204, 205] An insight in the role of electronics in biology suggests several interesting applications. For instance, devices can serve as biosensors for analytes of interest, or measure physical aspects of bioelectric processes such as ion flows and voltage gradients, providing insight into the underpinnings of physiological mechanisms.[206] The application of silk proteins in such devices has been suggested due to their sustainable nature. However, despite having interesting biological and mechanical properties, silk proteins are electrical insulators and therefore "passive" substrates.[207] To realize bioelectronic devices based on silk proteins, electroactive materials are required.[208] This implies that materials with intrinsic electroactivity are needed to form smart biocomposites that facilitate the transduction of events via electrical, electrochemical, electromechanical, and optoelectronic means.

Such materials include dielectrics, piezoelectric, photovoltaic and conductive materials.[209] Traditionally, metals, inorganic semiconductors and oxides are obvious materials of choice for

developing such systems. For instance, zinc oxide nanowires which generates a voltage difference when bent can be used as a pressure sensor, silicon based devices for bio-interfacing applications can form retinal implants, gold and silicon carbide materials can be used as neural sensors and electrodes.[210] However, such materials cannot be used to form composites with silk owing to the fundamental physico-chemical differences in their properties. Therefore, addition of electrochemical function to silk proteins is explored via doping using materials that are closer in structure and chemical properties, specifically polymers.[211, 212]

Polymeric bioelectronics is an emerging research field that exploits the intrinsic properties of polymers and soft organic elements to enable applications at the interface of biology and electronics.[213] The devices formed with such electronic materials are soft, stretchable and mechanically conformable, which are important qualities for interacting with biological systems. Thus, conceptualization is done with a view to making the electronic–biological interface as seamless as possible. It is important note that organic bioelectronics is a field that is currently limited by the materials that transduce signals across the biotic/abiotic interface.[96] As an example, we can consider the case of glucose sensors. A glucose sensor consists of the enzyme glucose oxidase (GOx) that acquires electrons when it converts glucose to gluconic acid. Transfer of the electrons to an electrode is the limiting step, and various approaches have been employed to improve this process. The current state-of-the-art in glucose sensing are third-generation biosensors which employ molecular wiring to shuttle electrons from the enzyme to the electrode.[214] Another example is the electrode-neural tissue interface, where the impedance between the electrode and the cerebrospinal fluid is the key parameter that determines the efficiency of electrical communication.[206] These examples illustrate the need for a class of

materials, which can improve the connection between the ionic current that flows in the electrolyte and the electronic current that flows in the electrode, thereby reducing the net impedance.[215] Current approaches to tackle this problem involve the use of conducting polymer coatings that are not only proven to reduce impedance, but also enhance implant lifetime due to similar mechanical properties with physiological systems.[216]

Conducting polymers (CPs) are a class of conjugated polymers which possess dual ionic and electronic transport properties. CPs are facilitating development of host of new devices that leverage the coupling of these carriers to enable new modes of operation. A discussion on CPs is provided in Chapter 1. Among various CPs, Poly(3,4-ethylenedioxythiophene) doped with poly(styrene sulfonate) (PEDOT:PSS) is currently one of the most important in terms of practical applications.[217] PEDOT has a dioxyalkylene bridging group across the 3- and 4- position of its heterocyclic ring which greatly improves its properties by reducing band gap, redox potential.[218] Therefore, it possesses many unique properties such as good film forming ability, high electrical conductivity (>1,000 S cm^{-1}), intrinsically high work function, and excellent physical and chemical stability in air.[219] PEDOT:PSS is being extensively used for biosensing, cell cultures and neural probe applications, and is chemically stable and biocompatible.[220] Therefore, it forms an ideal material to form composites with silk proteins in order to render electroactive properties. However, strategies are needed to not only develop such composite materials but also enable their usage in bioelectronics. Using the SPL platform, it is clear that high resolution circuits can be formed using FPP and SPP. Therefore, objective of this chapter is to investigate the formation of electroactive composites of silk proteins with the conducting polymer PEDOT:PSS and then to demonstrate application of SPL platform to pattern conducting polymers. As shown

below a ‘photoresist-like’ aqueous conductive blend comprised of PEDOT:PSS and silk proteins can be formed. Here, the term blend is used to specify a physical mixture of the PEDOT:PSS particle dispersion and silk sericin photopolymer in an aqueous medium. The blend composition can be optimized to provide ample electroactivity including the uncompromised biodegradable and patternable characteristics of silk proteins. The work will describe the application of PEDOT:PSS-silk protein composite as a transducer laminate on conventional electrodes, as well as metal free flexible devices for bioelectronic applications. The latter will lead to the development of fully biodegradable, bioelectronic devices. Applications of thus fabricated devices can be in detection of biomolecules as discussed in the next chapter.

4.2 EXPERIMENTAL

4.2.1 Materials

Dry re-dispersible pellets of PEDOT:PSS (Orgacon, Sigma-Aldrich, St. Louis, MO). Polyethylene glycol (PEG) and dimethyl disulfoxide (DMSO) for using as plasticizer and secondary dopant was procured from Alfa Aesar, Ward Hill, MA and Fisher Scientific, Fair Lawn, NJ respectively. All other chemicals are the same as described in previous chapters.

4.2.2 Synthesis and Purification of Fibroin and Sericin Photoresist

Fibroin and sericin photoresists were synthesized as described in Chapter 2.

4.2.3 Formation of SPP-PEDOT:PSS patterns on FPP via photolithography

Dry re-dispersible pellets of PEDOT:PSS were dispersed in water and ultrasonicated for 20 min. The dispersion was then filtered through a 0.45 µm syringe filter to remove particles of bigger

sizes which could create non-homogeneity in the ink and micropatterns. The solution was mixed with SPP, polyethylene glycol (PEG) (Alfa Aesar, Ward Hill, MA) (0.3 mg/mg of SPP), and dimethyl sulfoxide (DMSO) (5% v/v in PEDOT:PSS stock solution) to form the conductive ink. Concentrations were varied as discussed above. Crosslinked films were prepared by dissolving FPP in 1,1,1,3,3,3-hexafluoro-2-propanol (HFIP). Photoinitiator (Irgacure 2959, BASF) 0.6% (w/v) was added to the silk photoresist solution and mixed. The solutions were cast on poly dimethyl siloxane (PDMS) substrates and exposed to UV light (Lumen Dynamics OmniCure 1000 system) for 1 s at 20 mW cm^{-2} at 365 nm. Films were water annealed overnight. The composite SPP-PEDOT:PSS ink was mixed with photoinitiator (0.1 µl/1 mg of SPP) (Darocur 1173, BASF) and cast on the FPP film or glass, and left to air dry in a fume hood. After drying, the sample was exposed to UV for 1–1.5 s through a photomask to form patterns. Patterns were developed in water to remove any un-crosslinked material and form sensors.

4.2.4 Electrical Characterization

The sheet resistance of the conductive ink was measured by a conventional four-point probe technique using an HP 4156B precision semiconductor parameter analyzer (Agilent Technologies). SPP-PEDOT:PSS films (with and without DMSO) were formed on glass slides. To prevent damage, adhesive strips of copper tape of 1 mm thickness were used to provide ohmic contact between the sharp probe and sample. Film thickness was obtained by SEM imaging following cryo-fracturing (Jeol JSM LV-5610). Resistivity and conductivity were calculated from sheet resistance and thickness data. I-V characteristics were measured on a Keithley 4200 semiconductor characterization system (Keithley Instruments, Cleveland, OH). All samples were fabricated in triplicate and at least 3 points were tested for each sample.

4.2.5 Optical Microscopy and Scanning Electron Microscopy

Optical microscopy and Scanning electron microscopy (SEM) were performed as discussed in Chapter 3.

4.2.6 Atomic Force Microscopy and Conductive AFM (ORCA™)

Atomic Force Microscopy (AFM) analysis of surface morphology was performed on an Asylum Research MFP-3D AFM (Santa Barbara, CA), operating in AC mode with an AC240TS tip (nominal k = 2 nN nm^{-1}, Olympus, Japan). Conductive imaging was performed using a conductive AFM technique (ORCA™). A voltage (500mV) is applied to the substrate, and the current is recorded using an internal preamplifier (Asylum Research ORCA model, sensitivity 2 nA V^{-1}). Pt/Ir-coated AFM tips (AC240TM-R3) (Oxford instruments) with a frequency of 2 Nm^{-1} and spring constant of 70 kHz were used for this study.

4.2.6 Proteolytic Degradation *in vitro* and Imaging

To demonstrate biodegradability of the micropatterned structures and devices, enzymatic degradation was followed over time, similar to that described in the above chapters. One hundred micrometer features (1.5 mg of protein cast/cm^2 of substrate) on glass substrate were incubated in 4 mL of protease (Protease XIV from *S. griseus*, ≥3.5U/mg, Sigma-Aldrich) solution (0.25U/ml of PBS buffer) at 37 °C. The enzyme solution was replaced every third day to preserve activity. As negative controls FPP and SPP patterns were incubated in PBS solution containing no enzyme. At different time intervals, samples were removed from solution, washed with deionized water, and imaged. The structures were studied using optical microscopy, scanning electron microscopy,

and atomic force microscopy to observe changes in the surface morphology over time.

4.3 RESULTS AND DISCUSSION

4.3.1 Development of Conductive ink

In order to form a photopatternable silk protein based conductive composite (ink), initially, the idea of combining PEDOT:PSS with FPP as the carrier was explored. However, PEDOT:PSS is only dispersible in water, while FPP is only soluble in HFIP (or formic acid). A derivative of PEDOT having a methacrylate-end group with poly-toluene sulfonate (PTS) as dopant (instead of PSS), dispersed in nitro-methane was investigated. The addition of PEDOT:PTS in the FPP-HFIP solution resulted in precipitation due to the high solubility of nitromethane with HFIP. This resulted in poorly cast films with PEDOT:PTS particles clearly observed in the composite FPP films (Figure 4.1a). As the next option, PEDOT:PSS redispersible pellets were dispersed in HFIP. However, the dispersion of PEDOT:PSS in HFIP was also hampered by several problems. Since HFIP is a highly volatile solvent, handling requires extra care. Further, the particle size of PEDOT:PSS could not be reduced to the optimal scale (Figure 4.1b). In order to form dispersions, particles on the order of ~100 nm are required. Several dispersion techniques such as vortex mixing, sonication, ultra-sonication, and ball-milling were tested. Satisfactory results were not obtained. The improper dispersion of PEDOT:PSS in the FPP matrix/films was also observed in while measuring I-V characteristics (Figure 4.2). PEDOT:PSS cannot be dispersed in HFIP or other organic solvents such as ethanol. Following these trials, it was noted that re-dispersible pellets of PEDOT:PSS were forming very stable dispersions in water as suggested by the manufacturer. Consequently, SPP was chosen as the route to form photopatternable silk protein-based conductive ink. It should to be noted here that the SPP is water soluble and, as demonstrated

in the previous chapter, very precise patterning on rigid as well as flexible substrate can be achieved using it as a photoresist.

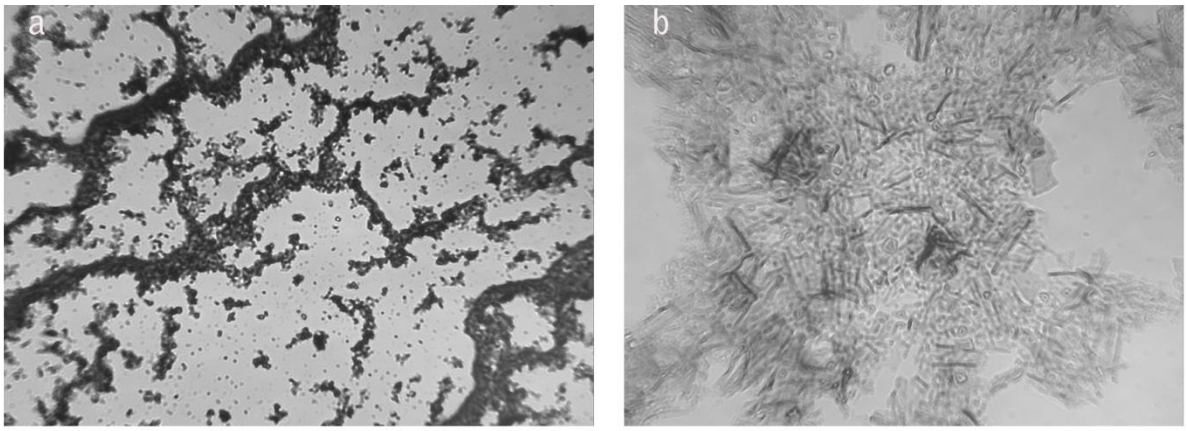

Figure 4.1 *Initial trials of (a) PEDOT:PTS and (b) PEDOT:PSS dispersion in HFIP*

Aqueous dispersions of PEDOT:PSS were successfully blended with photoreactive sericin (SPP) [129] to form a photopatternable, water compatible, conductive protein ink (termed SPP-PEDOT). This protein ink can be spin coated or cast on various substrates including silicon, glass, ITO or PDMS to form homogeneous films. The ink is crosslinked on UV exposure (365 nm) to form stable and water insoluble films, and can be used to form conductive micropatterns down to 1 µm feature size. Initially, even though use of SPP allowed the formation of a stable conductive ink, the films formed were brittle in nature. Plasticizing additives such as glycerol and polyethylene glycol (PEG) were therefore investigated to improve the flexibility of the films.[221] Finally, PEG was as chosen as the plasticizer to improve the bendability of the composites.

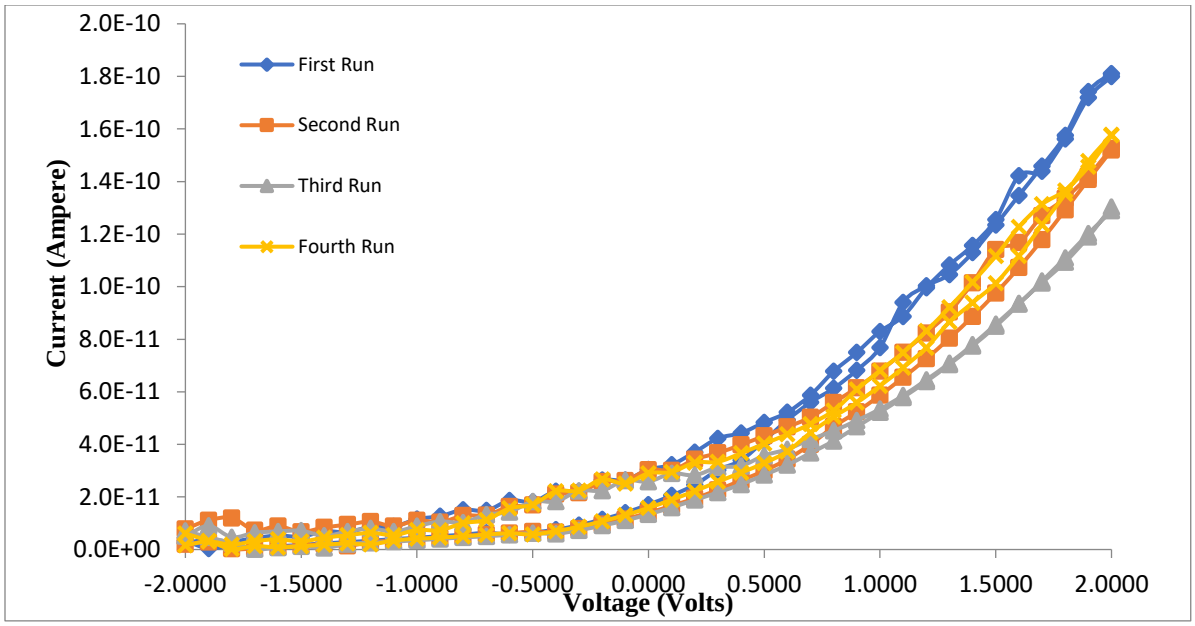

Figure 4.2 *I-V characteristics of films of PEDOT:PSS-FPP*

4.3.2 Electrical characterization

The electrical and electrochemical characteristics of the conductive composite ink were initially evaluated utilizing different characterization techniques. The first step involved optimizing the composition of the ink for desired applications. A two-point probe technique was used to obtain current-voltage (I-V) characteristics of the composite, as a function of the conducting polymer concentration. Initial observations suggested that the SPP-PEDOT:PSS composite ink behaves like an ohmic conductor without any hysteresis, under application of a dual potential sweep in a voltage window from -2 to 2 V. Expectedly, the conductivity increased with an increase in the PEDOT:PSS concentration (PEDOT to sericin), implying that the conductivity of the composite depends on the density of the conductive polymer network inside the silk matrix. Therefore, silk sericin acts as an inactive insulator, but does not trigger any instability.

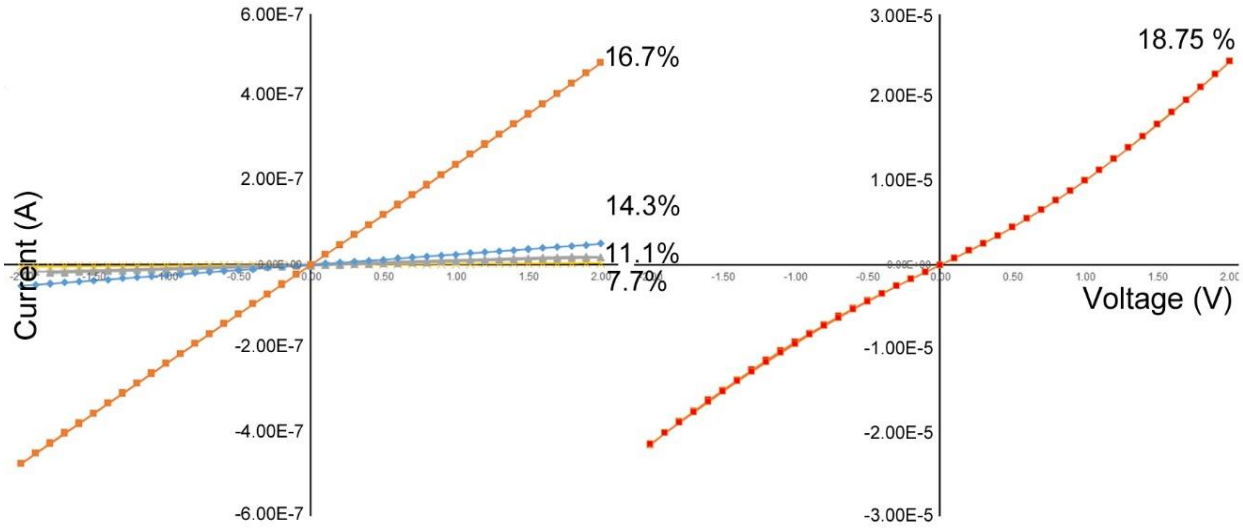

Figure 4.3 *I-V characteristics of the SPP-PEDOT composite ink as a function of the concentration of PEDOT in the SPP (7 % - 19 %). Above 20% concentration of the conducting polymer (PEDOT:PSS) in the silk sericin, the matrix begins to exhibit non-linear I-V behavior.*

Repeated I-V measurements also suggested that the material was stable under the applied voltage range. At ~19% PEDOT:PSS concentration the onset of a slight nonlinear behavior was observed. The µA range of current obtained with the material having 19% PEDOT:PSS provided a good conductivity for further applications (Figure 4.3). Conductive AFM imaging was used to confirm that there is no nanoscale phase separation of the PEDOT:PSS in the silk matrix (Figure 4.4). To understand the relative change in resistivity as a function of PEDOT:PSS concentration, and to observe the effect of secondary dopants, a four-point probe technique was attempted to determine sheet resistance, resistivity and conductivity. Initially, several trials of four-point probe measurements did not provide consistent data. In order to form an ohmic contact, the probes need to be pressed against the films. However, since the probes of the instrument were very sharp, this was either causing holes in the films or their breakage, leading to unstable contact. To solve this problem, copper tape strips were attached to the film at fixed distances, such that the probes could

be used on the films. The copper stripes provide a protective intermediate layer and facilitate ohmic contact. This modification solved the consistency issue and stable data were obtained.

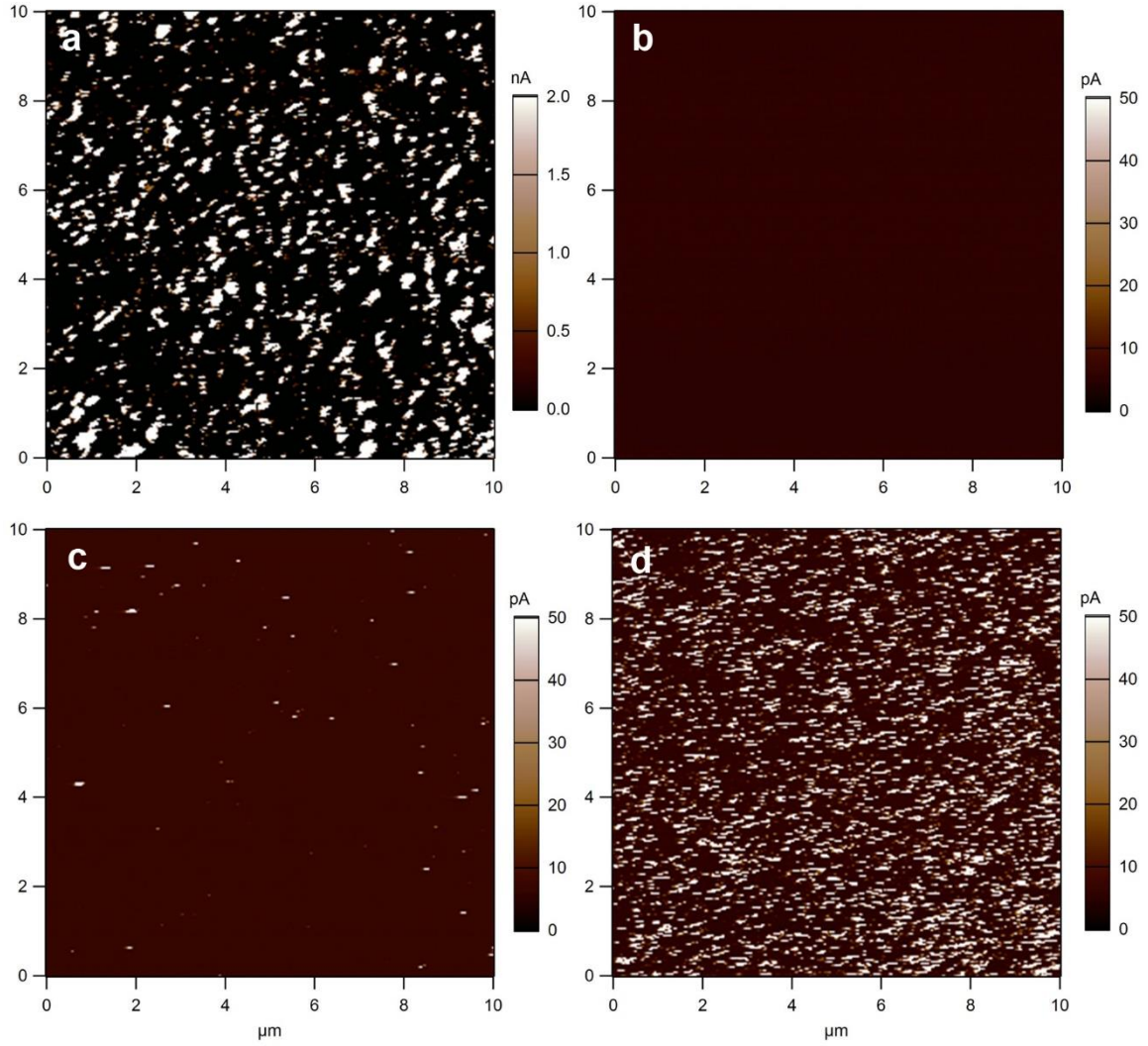

Figure 4.4 *Conductive AFM on films made of (a) pure PEDOT:PSS, (b) pure SPP, (c) SPP with 10% PEDOT:PSS and (d) SPP with 20 % PEDOT:PSS. (note that the scale for PEDOT:PSS films is to 2.0 nA due to the much higher current observed)*

At least three sets of measurements were taken on three separately prepared films. SPP-PEDOT:PSS films were made at 11, 16 and 19% PEDOT:PSS concentration. A positive control of 50% PEDOT:PSS/50% PEG was used. The resistivity data indicated that the material is more conductive as the PEDOT:PSS concentration increases (Figure 4.5a). In another set of experiments, 5% (v/v) DMSO was mixed with the PEDOT:PSS stock solution keeping the other compositions constant. The addition of DMSO at 5% (v/v) was previously shown to positively affect conductivity of PEDOT:PSS by inducing better packing of particles and reducing PSS content from the surface of the film.[222] In this ink, the results indicate that the DMSO improves the conductivity of the composite ink by ~2 orders of magnitude (Figure 4.5b). DMSO may shield the non-conductive silk protein from PEDOT:PSS to obtain better packing, and define a better path for current flow. Overall, the investigations of electrical property of the material suggested that 15 to 20% concentration in the silk matrix provided an optimal PEDOT:PSS range for different applications.

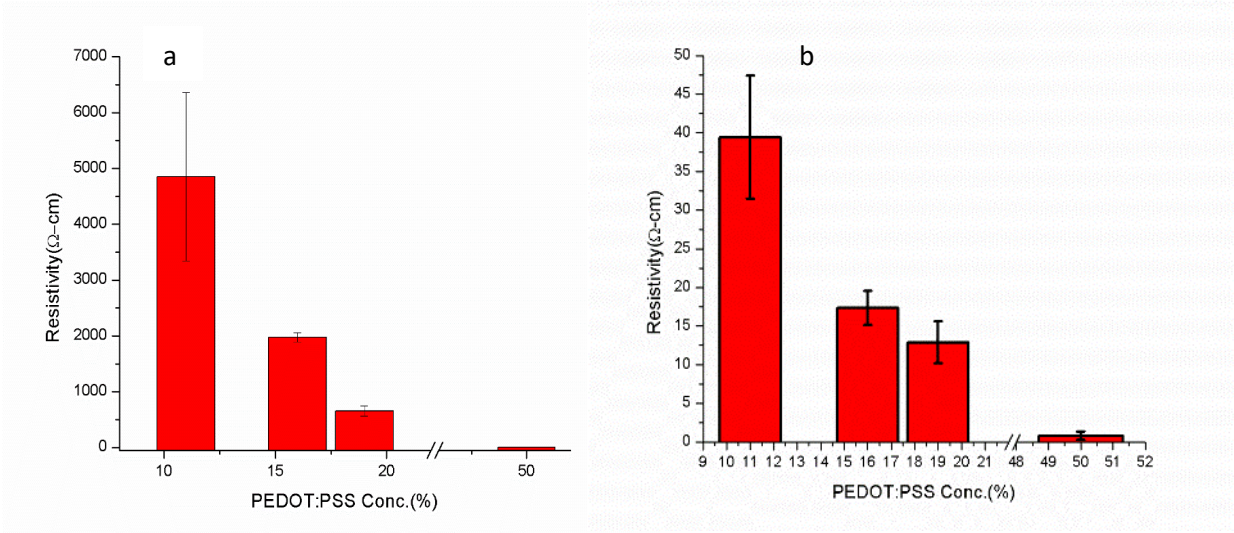

Figure 4.5 *Resistivity of conductive composite films (a) without DMSO and (b) with DMSO*

4.3.3 Patterning of conductive ink on conventional microelectrodes

In order to adopt the composite for bioelectronics the ability to form precise patterns and circuits is critical. Following electrical characterization, the patternability of the conductive ink was initially investigated on conventional electrodes such as indium Tin Oxide (ITO) and gold. Gold is a popular electrode material for bioelectronics due to its inert surface properties.[206] ITO electrodes are widely used in electrochemistry due to stable electrochemical and physical properties, optical transparency, high electrical conductivity, and a wide potential window.[223, 224] Numerous optical, electronic, electrochemical and electro-chemiluminescence biosensors have been shown using ITO.[224-227] While ITO/glass is relatively cheaper than gold, silver and platinum, recent price increases in the material have encouraged the use of other materials to enhance their properties. PEDOT:PSS is often introduced on ITO substrates to provide ohmic contact and transport charges efficiently. It presents a low series resistance and acts as a planarization layer for the ITO surface to avert shorts and increase device yield.

As discussed above, patterning of conducting polymers such as PEDOT:PSS, to date, on ITO/glass, and indeed, most surfaces have been challenging. At the microscales, soft lithography, stamping, inkjet printing etc. have been reported. However, photolithography using PEDOT:PSS has been difficult, particularly over large areas. The micropatterning of PEDOT:PSS using the conductive ink based to define conductive areas on ITO/glass was therefore demonstrated to improve electrochemical performance. Since, ITO/glass is itself conductive, it is necessary to define specific conductive (and insulating) areas on such a substrate in order to form electrode micropatterns. The microscale conductive areas are coated with the conductive composite ink while the insulation is achieved using an epoxy-based photoresist.

The microfabricated hybrid biosensor was fabricated using photolithography using a two-step process: 1) formation of microelectrode lines of ITO/glass on the substrate using the photoresist SU-8, followed by, 2) patterning of the conductive ink on the ITO/glass lines. This is realized via a two-mask process with identical design but a single difference in layout – the first is a bright field mask and the second is a dark field mask (Figure 4.6). Initially, the negative photoresist SU-8 is crosslinked through the first mask to form microelectrode lines of ITO. The conductive ink is then drop casted on the surface and exposed through the second mask (aligned via a contact aligner) with a complementary pattern. The preliminary patterning of conductive ink on pre-patterned substrates were found to be difficult as the conductive ink does not crosslink completely to ITO and gold microelectrodes (Figure 4.7). In later experiments, a conductive ink having 16% PEDOT:PSS could be patterned successfully with an increase in exposure time. The patterning of 16% PEDOT:PSS was used for later sensing experiments with ITO microelectrode.

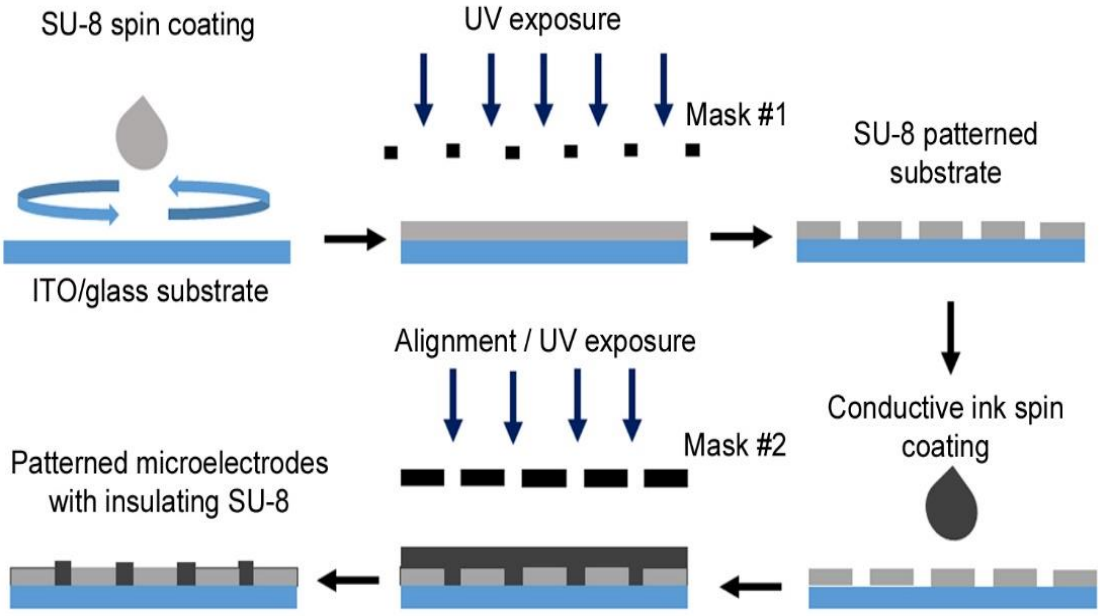

Figure 4.6 *Schematic of photolithography process to form conducting microelectrodes on the conventional rigid electrode materials.*

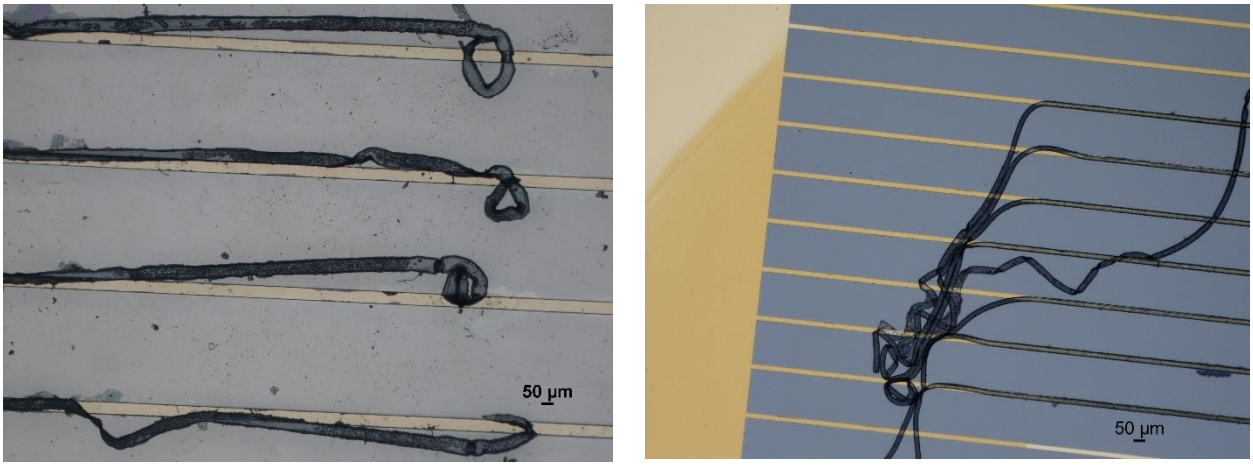

Figure 4.7 *Patterning of conducting ink on conventional rigid microelectrode surfaces (a) ITO, and (b) gold.*

As discussed in next chapter, the benign conditions and ambient temperature of the photolithography process permits the encapsulation of biomolecules such as enzymes within the ink. [228] These microscale patterns can therefore be fabricated in different designs over large (cm) scale areas with high fidelity (Figure 4.8). The conductive ink patterns can be specifically patterned on areas of interest, and other conductive areas can be excluded using specific masks, which is difficult to achieve by electro-polymerization. An important advantage of using this carrier protein (other than to facilitate photolithography and a mechanically conformable matrix) is the ability to conduct the entire patterning process in water. Silk sericin is water-soluble and retains its solubility even after chemical modification. Following crosslinking, the undeveloped material can be easily washed away using water. The second advantage lies in the use of silane/thiol chemistry to chemically bond the conductive ink to the underlying substrate. This is a major improvement over inkjet printing or stamping wherein the ink is physically deposited on the substrate.

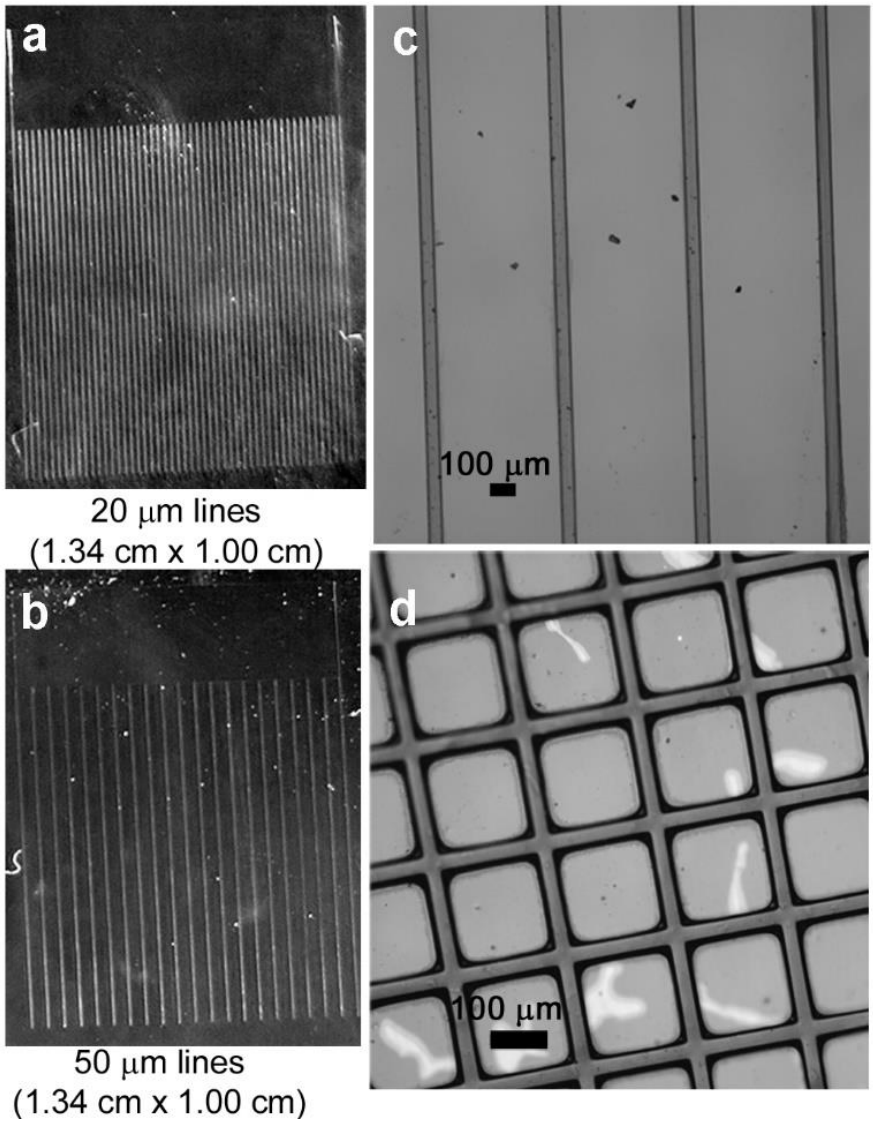

Figure 4.8 *(a, b) Images showing optically transparent sensor pads formed with high fidelity microscale electrodes over large cm scales and (c, d) optical microscopy of the electrode patterns in a variety of designs. The space between the electrodes is insulated using the epoxy photoresist SU-8.*

The stability of the conductive ink micropatterns on ITO was studied using a time course experiment in three different solvents over 5 days. The following solvents were used - 1x PBS buffer (commonly used solution), 1 M KCl (common electrolyte for electrochemical electrode

characterization), and 75% EtOH solution (typically used as a sterilization solvent for cell culture) (Figure 4.9). Images were taken at day 0, day 3 and day 5 and surface roughness calculations were performed with ImageJ software using SurfChar J plugin (Table 4.1). In both PBS and KCl, there was no change in the surface morphology or delamination of the patterns over time. From previous studies, it was known that ethanol poses some problem with silk systems owing to inducing crosslinking. In the case of EtOH, expectedly, the morphology changed. However, the patterns still stay attached to the ITO. The chemical bonding to the substrate therefore results in extremely stable micropatterns that can be stored in aqueous environments or dry for several weeks without delamination of the ink.

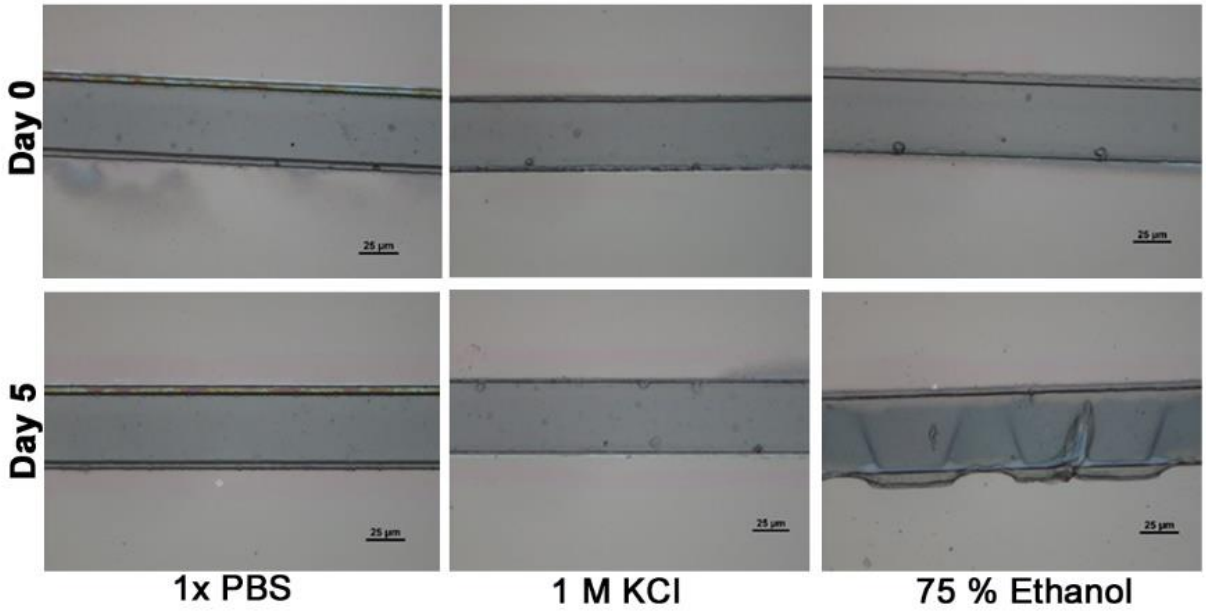

Figure 5.9 *Stability study observing several micropatterns in a challenging solvent over 5 days.*

Table 4.1 *Quantitative study of surface roughness to demonstrate the stability of conductive ink pattern with different solvent.*

	1x PBS		1M KCl		75%EtOH	
Day	R_q(nm)	R_a(nm)	R_q(nm)	R_a(nm)	R_q(nm)	R_a(nm)
0	9.57	7.02	7.96	5.69	6.08	4.49
3	6.9	4.64	9.39	6.68	6.96	4.64
5	9.99	6.92	9.88	7.48	6.78	4.79

4.3.4 Electrochemical characterization of the conducting electrodes

Electrochemical impedance spectroscopy (EIS) is a widely applied electrode characterization technique to obtain information about the absorption characteristics and interaction of molecules on the electrode surface.[229] The observed electrochemical process can be modeled using suitable equivalent circuit models containing parameters that potentially reveal the processes at the electrode surface. In order to show that the patterned electrode surfaces offer higher performance than bare or simply coated surfaces, EIS was conducted on a bare ITO/glass surface and an ITO/glass substrate with varying compositions of conductive ink (containing 11%, 16% and 19% PEDOT:PSS respectively). Figure 4.10a and b shows the Nyquist plots for the conductive ink and bare ITO respectively. Figure 4.10c shows the phase shift plot vs. frequency for the electrode compositions mentioned above.

The phase shifts show that all but bare ITO show three distinct maxima, reflecting the kinetics of three different processes. Hence, a simple equivalent circuit model with two parallel resistances

and a constant phase element connected in series with a resistance could be constructed (Figure 4.11). The second R-CPE block shows the charge transfer resistance and charge double layer capacitance indicative of faradaic processes occurring on the surface. To account for the conductive ink film, a third CPE was incorporated in series. This CPE represents the non-ideal capacitive behavior of the porous conductive ink film. Table 4.2 shows the various parameters obtained from equivalent circuit model fit. The data shows that the inclusion of the conductive ink on the ITO surface decreases the cumulative resistance. It may be observed that the solution resistance obtained for each case is ~11±3 Ω, indicating that the electrolyte imposes a similar resistance to each electrode. The values of charge transfer resistance decrease from 4.5×10^4 Ω to 1.9×10^3 Ω while the electrical double layer non-ideal capacitances do not show any significant difference. On the other hand, the resistance imposed by the ink expectedly decreases with increase in PEDOT:PSS content. The capacitance due to diffusion of ions inside the conductive coating increases with the increase in CP content indicating that there is increase in film-porosity. Furthermore, the ionic contribution becomes more significant with higher concentration of PEDOT:PSS in conductive coating. Therefore, the conductive ink coated electrode shows lower overall impedance and lower charge transfer resistance. This implies that the conductive coating on the electrode facilitates the Faradaic processes and that an *improvement* in biosensing sensitivity is expected with such microelectrodes in comparison to a bare ITO surface. Indeed, this is the case as shown in the next section.

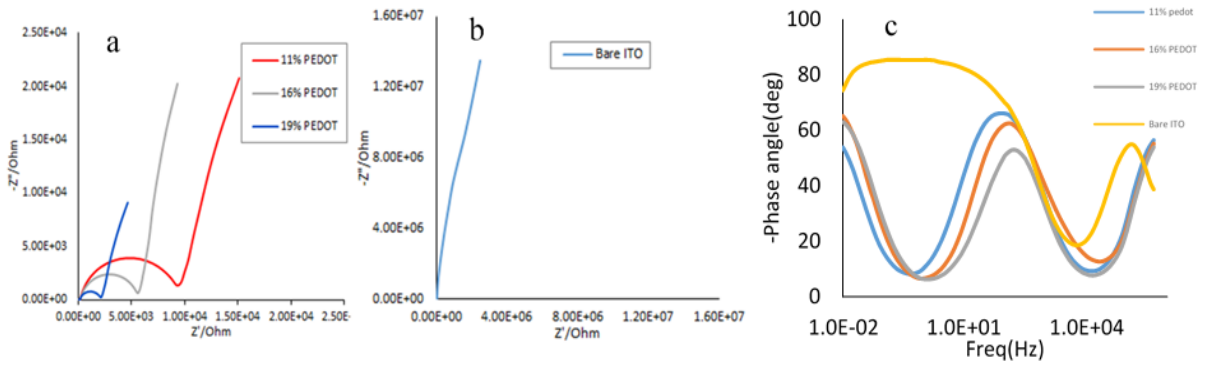

Figure 4.10 (a) *The Nyquist plots for the conductive ink at three compositions of ink containing 11%, 16% and 19% PEDOT:PSS respectively.* ***(b)*** *The Nyquist plots for bare ITO,* ***(c)*** *Phase shift plot vs. frequency for the electrode compositions in comparison to bare ITO.*

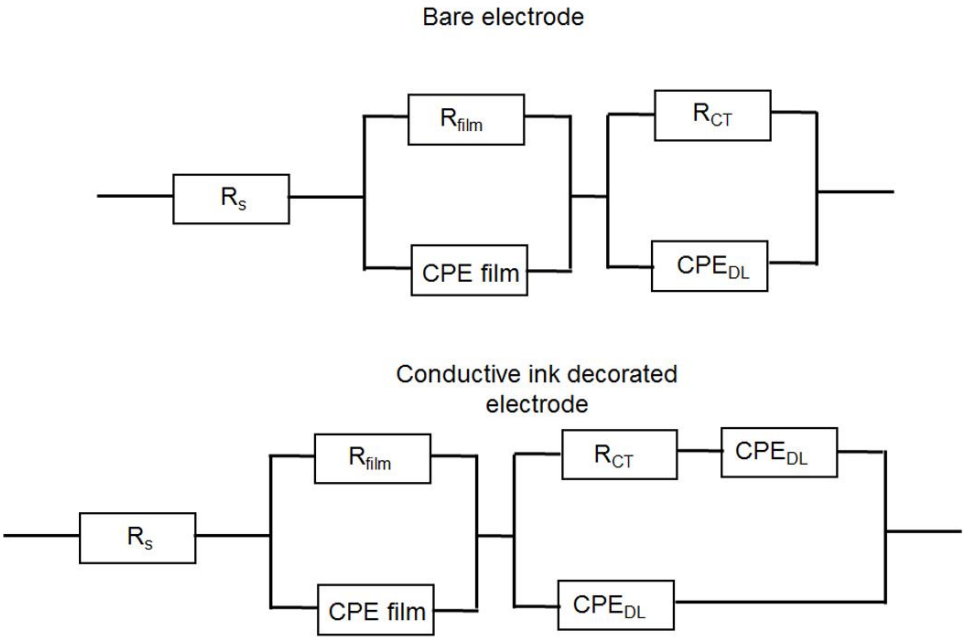

Figure 4.11 *Equivalent circuit model for the sensing electrodes presented. Here, the resistance in series R_s = the intrinsic resistance of solution, the first R-CPE (constant phase element) block indicates the resistance and non-ideal capacitance provided by the self-assembled monolayer on the surface of ITO.*

Table 4.2 *Theoretical equivalent circuit element values obtained from fitting of EIS experimental data. R represents the resistance and CPE = constant phase element in the circuit models*

	R_s (Ω)	CPE film $\mu F.s^{(a-1)}$	a_{film}	R_{film} (Ω)	CPE double layer $\mu F.s^{(a-1)}$	a_{DL}	R_{CT} (Ω)	CPE pore $\mu F.s^{(a-1)}$	a_{pore}
Bare ITO	8.22	1.032	0.9507	126.6	0.379	0.7936	45255		
11% PEDOT	9.8	0.0136	0.954	134.2	3.446	0.8919	9395	499	0.9005
16% PEDOT	14.84	0.00725	0.9979	124.4	3.181	0.8623	5683	571	0.9909
19% PEDOT	11.83	0.00829	0.9668	112.3	4.99	0.8745	1981	1104	0.8438

4.3.5 Fabrication of flexible silk-PEDOT:PSS architectures

After successfully patterning conductive ink on conductive substrates and performing electrochemical characterization, the patternability of the ink on *flexible substrates* was investigated. To form micropatterned devices, the conductive ink may be cast of a variety of substrates using drop casting or spin coating to form a protein based device. The samples are exposed to UV light through a photomask to crosslink the ink and form patterns. Uncrosslinked ink is washed off using water during the development step (Figure 4.12**)**. Microscale patterning is demonstrated on a film around the size of a contact lens (Figure 4.13 a**)**. This process creates high

fidelity structures as depicted in Figure 4.13b. SEM images of the features show the relatively smooth and highly defined patterns (Figure 4.13c), with the smallest feature sizes on the order of 5 µm.

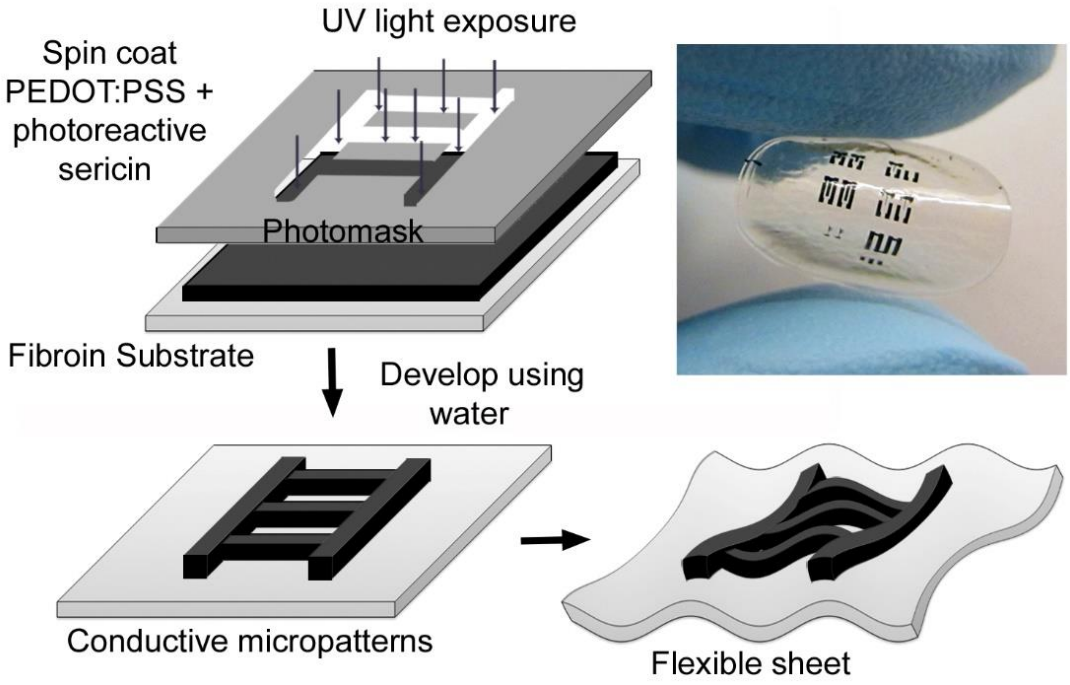

Figure 4.12 *Schematic showing the fabrication of conductive micropatterns on a flexible sheet. The sheet can be repeatedly deformed without delamination of conductive patterns, and can conform to a curvy and extensible surface such as skin as shown.*

The thickness of the support film as well as patterns can be easily controlled by modulating the total material in the solution. Protein patterns formed are flexible and mechanically robust and can withstand bending and twisting while hydrated, without breakage of either the films (substrate) or patterns (conductive ink). Critically, no delamination of the patterns is observed owing to the *covalent linking* of the two components of the system. This addresses a major concern in the design of flexible systems, wherein the active layer and substrate tend to separate due to mechanical stress. The entire device can be stored either dry or wet (in buffer) for weeks without any appreciable

reduction in mechanical integrity or function, as discussed further below. The entire process is carried out on a benchtop setup and involves *all* water based processing at ambient temperature. This gives rise to a facile, high throughput microfabrication process to pattern water dispersible CPs in a relatively green fashion in comparison to earlier reported processes. The electronic microstructures formed by this process are formed via one photolithographic step, in comparison to other strategies where each layer of patterning require multiple steps. This has the problem of increasing complexity and the probability of failures in device manufacturing.[90, 230]

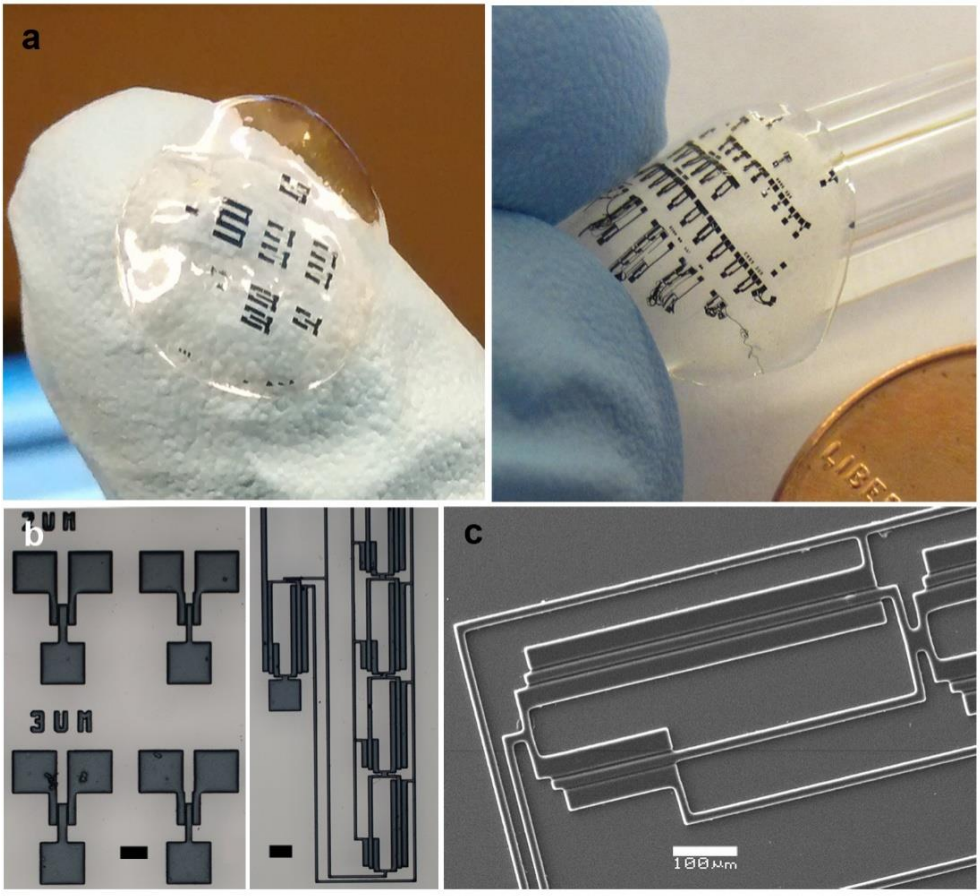

Figure 4.13 *Formation of complex microstructures via photolithography. (a) Large area micropatterns of PEDOT:PSS formed on flexible and conformable silk fibroin sheets, (b) Optical micrographs and (c) SEM images of PEDOT:PSS micropatterns on glass. Scale bars = 100 µm.*

4.3.6 Electrochemical characterization of conductive ink patterns on the non-conductive flexible substrates

To understand the electroactivity and electrochemical stability of the material with no charge carrier support, cyclic voltammetry (CV) and electrochemical impedance spectroscopy (EIS) were performed. Pure sericin (SPP (no PEDOT)) patterns on fibroin (FPP) films were used as a negative control. Films with only PEDOT:PSS (no sericin matrix) on FPP were not stable and tended to delaminate as there is no chemical linkage to attach the PEDOT:PSS to the underlying substrate. Also, the conductive ink was casted on dielectric fibroin films, which means that conductive films did not have a conventional metallic or metal oxide charge collector background. Due to the soft nature of the films, they cannot be directly attached to the potentiostat using alligator clips. Therefore, the films were indirectly connected using interconnects. Initially, films were connected using copper conducting tape. However, copper tape does not form an ohmic contact with the conductive composite film, resulting in a noisy response on the cyclic voltammogram. Subsequently, trials were performed using different interconnecting materials such as carbon tape, carbon paste and silver paste with metal wire. Among these silver paste with metal wire provided best possible connection. The silver paste and metal wire interconnection was masked with epoxy adhesive to provide insulation from electrolyte and providing mechanical rigidity to the connection. All further electrochemical experiments were carried out using silver paste.

A wide stable potential window of -1.0 to 1.6V without water splitting was observed. This wide potential window might therefore be useful to realize detection of various biomolecules having different peak potentials. The electroactivity of the material increased with an increase of PEDOT:PSS concentration (Figure 4.14 a). In a study, 10 cycles of CV were taken each day for 3

days while keeping the samples soaked in PBS (Figure 4.14 a, b and c). The retention of electroactivity was found to be ~80 % (The data are shown in Figure 4.14d). Films with inks containing 19% PEDOT:PSS and DMSO showed a good charge storage capacity (CSC) of ~74 mC/cm^2 on day 0 (Figure 4.14 d), while films without DMSO had CSC ~55mC/cm^2 (scan rate of 0.1 V/s).

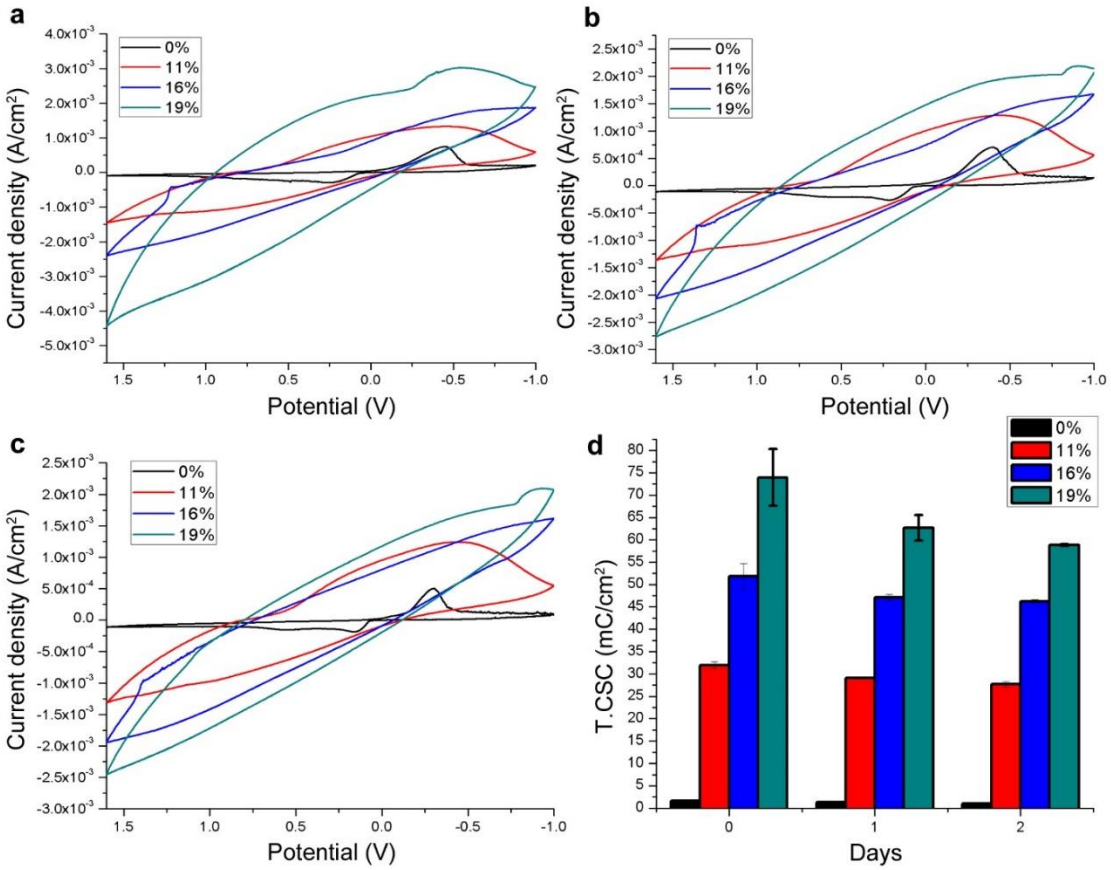

Figure 4.14 *Cyclic voltammograms (A) at day 0, (B) at day 1 and (C) at day 2. (D) Stability of the sensor measured in terms of charge storage capacity (CSC) over days. Legend indicates wt.% of PEDOT:PSS in the conductive ink.*

The electrochemical stability of the material was monitored via long cycling study. In this study, 200 redox cycles at a potential window of -1.0 to 1.6 V and scan rate of 0.1 V/s were performed. A 90.5 % retention of electroactivity was observed (Figure 4.15 a). The CSC measures obtained are comparable, or better than reported values where PEDOT:PSS is within a non-conductive

matrix such as a hydrogel or even in flexible materials without a conductive support.[231, 232] Following the electrochemical stability analysis, the impedance of the material was assessed (Figure 4.7 b). Conductive polymers have the potential to reduce impedance in addition to their high charge storage capacity, when used as an interface between soft tissue and metal electrodes for recording and stimulating applications. [233] One source of noise is the high impedance from the electrolyte-electrode interface.[206] It is therefore an important parameter if the material has to qualify for *in-vivo* sensing and stimulation applications. The impedance spectra of 19% PEDOT:PSS ink showed a flat impedance region from 1 kHz to 1 Hz, which is of importance for neuronal signal recording applications. Films approach a near-resistive region below 1 Hz as the phase angle approaches zero, indicating that the resistance is arising from the solution.[206] These results suggest that the composite has very low impedance (13.6 kΩ) at 1 kHz, which is at par with reported materials for neural recording or stimulation applications, having impedance in range of 10-23 kΩ at a similar frequency. [231, 234-236]

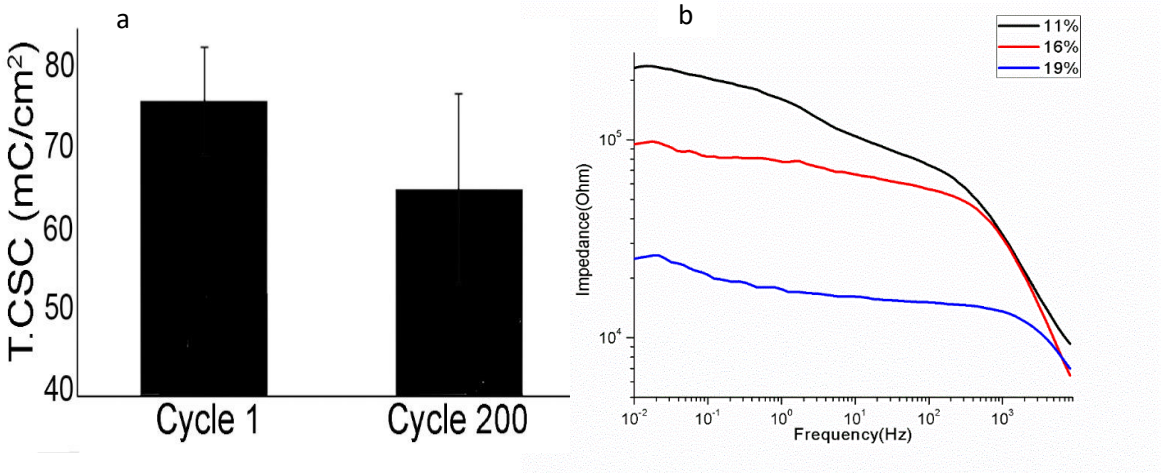

Figure 4.15 *(a) Retention of electroactivity after 200 cycles, and (b) EIS Bode plot showing impedance of the conductive ink films over frequency range.*

Finally, to consider the viability of the composites for electrochemical activities in flexible systems, the effect of mechanical stress on the performance of the conductive patterns was

investigated. The conductive patterns were bent to ~30° degrees and electroactivity was measured using EIS. The bend caused a slight increase in impedance of the material but the order of the impedance remained the same (Figure 4.16 a). Separately, the conductive patterns were subjected to repeated cycles of bending (30^{o}) and release. SEM images of the surfaces showed no damage to the composite or delamination (Figure 4.16b). The CSC values at increasing stress cycles showed only a very slight decrease to 150 cycles (<1.5% loss) (Figure 4.17), indicating a high stability under stress, and the ability to sustain electrical and electrochemical properties under mechanically challenging conditions.

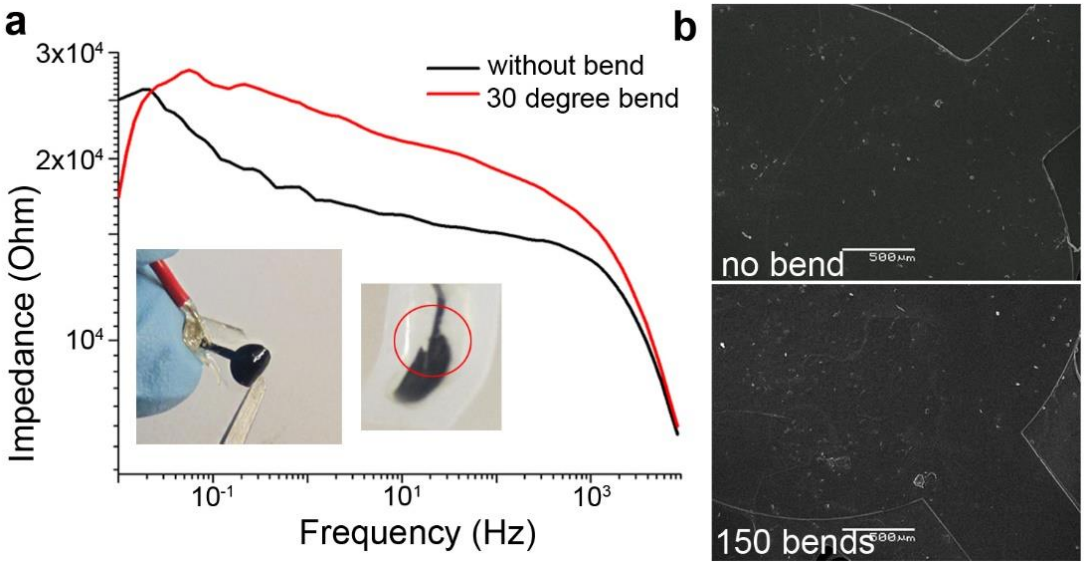

Figure 4.16 *Stability under mechanical stress: (a) Mechanical bending and corresponding effect on impedance after 150 bending cycles. The inset (red circle) shows the region of highest stress during bending that is further explored using (b) SEM images showing the film integrity is retained without any cracks or defects after 150 bending cycles (scale bar = 500 µm).*

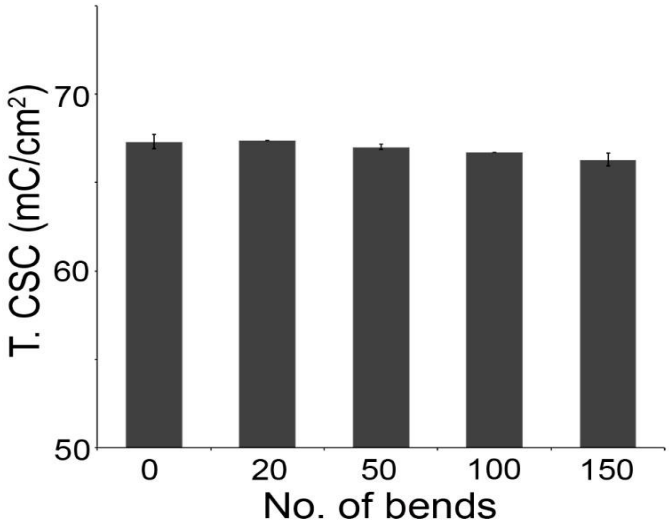

Figure 4.17 *Stability of the sensors (18 % PEDOT:PSS) as a function of redox cycles. Charge storage capacity after the first cycle = 75.99 ± 6.65 mC/cm^2 and at 200 cycles 65.24 ± 11.70 cm^2. (n = 4 sensors).*

4.3.4 Proteolytic degradation

Being mechanically strong, yet intrinsically biodegradable, makes silk biomaterials desirable in implantable bioelectronics and bio-integrated devices.[237] One of the most significant advantages of microfabrication using silk proteins and similar bio-derived materials in comparison to various synthetic polymers currently in use, lies in their biodegradability. It was shown in previous chapters that silk proteins can be proteolytically degraded in enzyme solutions. As the system is comprised of silk protein and PEDOT:PSS, it is also expected to be degradable. Silk-PEDOT (SPP-PEDOT:PSS on FPP) films were incubated in a PBS solution at 37°C with and without protease for several weeks and protease solution was changed every 3 days to retain the enzymatic activity of protease. SEM images of the composite surface at various time points are shown in Figure 4.18. The composite film has a smooth surface on Day 0 (Figure 4.18a). Figure 4.18b and c show the surface profile of negative controls at Day 6 and 21 respectively. Figure

4.18d and e show the surface profile of samples under proteolytic degradation at Day 6 and 21 respectively.

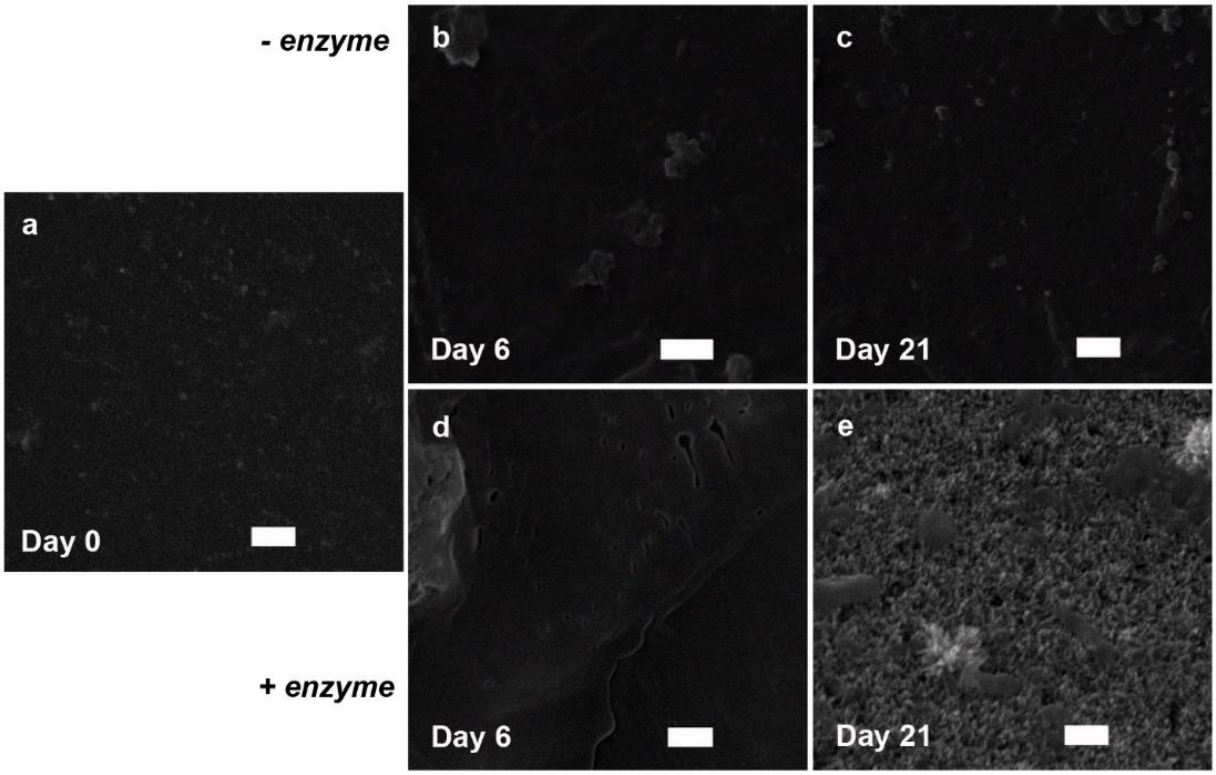

Figure 4.18 *Proteolytic degradation PEDOT:PSS-Silk biosensor devices: SEM images of PEDOT:PSS-silk films (a) at day 0, (b and c) at day 6 and 21 in PBS buffer respectively, and (d and e) at day 6 and 21 in protease enzyme solution respectively.*

It is clear from the figures that at Day 6, both the samples have comparable surfaces. However, after 21 days, while the control sample is minimally affected, the sample in protease solution is significantly degraded. Quantitatively, the roughness of the films in PBS buffer changes from ~12 nm to ~67nm in comparison to ~355nm for the protease solution (Table 4.3). (AFM images showing the nanoscale surface morphology of the films are presented in Figure 4.19). Following a period of ~4 weeks, the samples degrade completely and preclude imaging. The mass loss is

shown in Figure 4.20. Both the fibroin (FPP) support film and sericin (SPP) matrix degrade almost completely in the enzyme solution. It should be noted that even though PEDOT:PSS is biocompatible, it is not biodegradable. In the case of micropatterns of conductive ink, the samples under proteolytic degradation lost PEDOT:PSS in the form of fine fibrous strands, which is intuitive given that the PEDOT:PSS is blended with SPP instead of being formed electrochemically. Thus, by controlling the film crosslinking, it is possible to fabricate a device that is completely degraded over a specified period. The PEDOT:PSS does not escape from the crosslinked matrix, but when the carrier and support degrade, they break down as well.

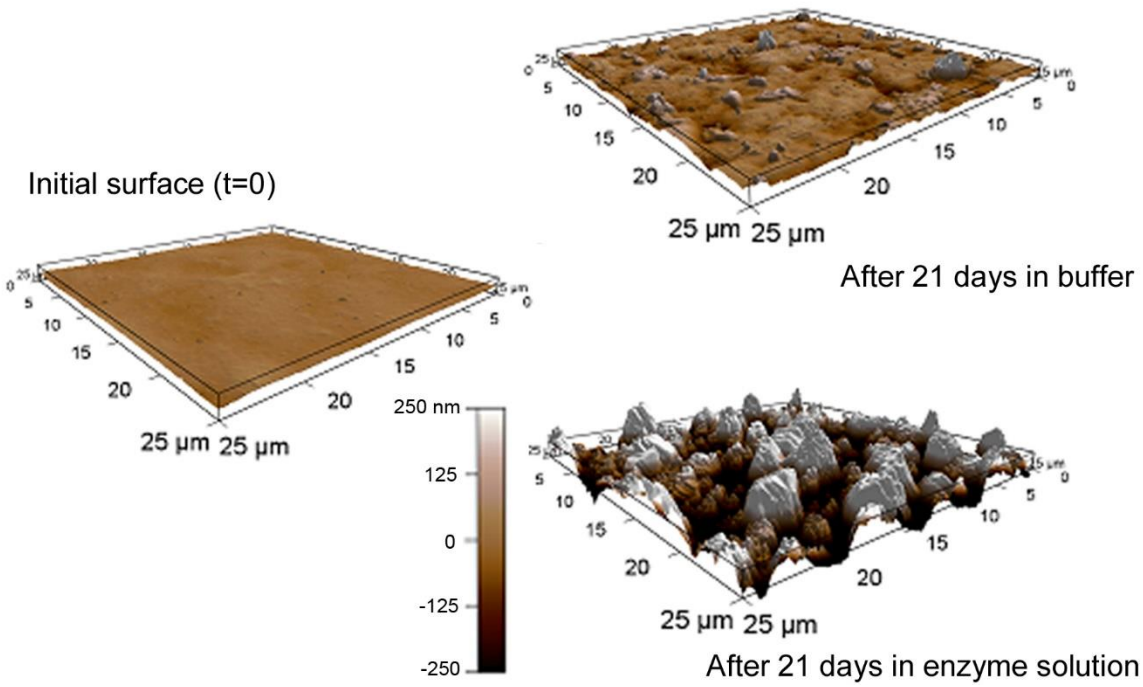

Figure 4.19 *25 µm x 25 µm scans taken via AFM showing the degradation in the sensor surface following 21 days of incubation in a buffer and enzyme (protease) solution respectively. All images are presented to the same scale for clarity. Following 4 weeks, the sensors were completely degraded preventing the use of AFM for scanning.*

Table 4.3. *Surface roughness of SPP-PEDOT surface measured from 5 µm x 5 µm atomic force microscopy images.*

	Day 0	Day 21 (no protease)	Day 21 (protease)
RMS roughness over 25 µm^2 area (nm)	**12.4 ± 0.4**	**67.5 ± 9.6**	**355.0 ± 43.4**

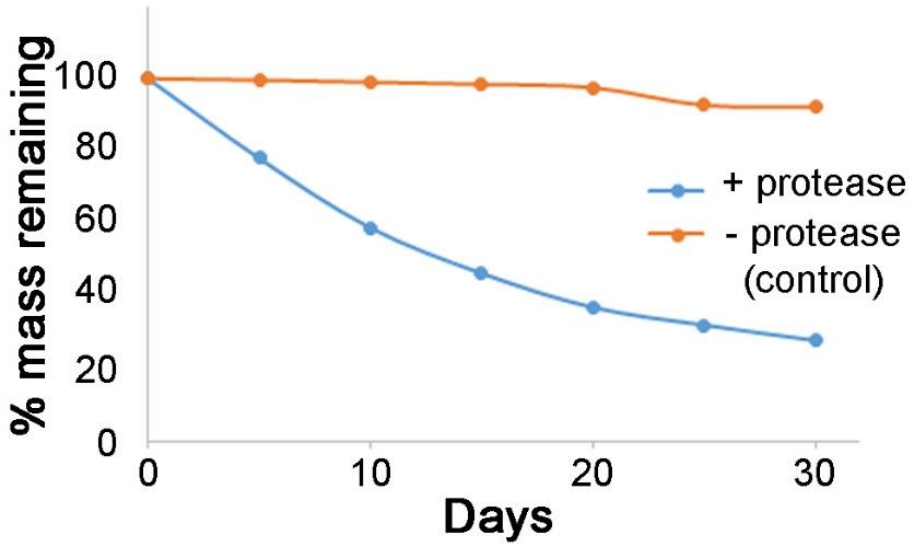

Figure 4.20 *Observed degradation profile of the SS-PEDOT/FMA films.*

4.4 CONCLUSION

In this chapter, an important functionality (electroactivity) was successfully imparted in the silk protein matrix by the combination of conductive polymers with sericin protein. Using the protein photolithography technique developed above, all organic, flexible conducting devices with features across four orders of magnitude (1 µm to cm) can be formed. A substrate/carrier complex for the conducting polymer PEDOT:PSS is shown using photoreactive silk proteins. Devices formed are mechanically stable, optically transparent, flexible, biocompatible, and degradable. The

inherent simplicity of the photolithography process, and development using only water allow for green microfabrication. Flexible patterned SPP-PEDOT electrode matrices may offer suitable environments for the encapsulation of proteins and enzymes, and can be used for electrochemical biosensing with high sensitivity and selectivity. Enzymatic degradation of the devices over a period of weeks shows that tunable mechanical strength and degradation characteristics present opportunities for transient bioelectronics with programmable loss of function. Optimizing materials and processing to form high resolution structures in flexible and biocompatible formats can therefore address current challenges in OEs. Integrated devices such as organic thin-film, electrochemical transistors, or with coupled organic and inorganic molecules can enhance applications for cell guidance, stimulation, or biosensing as shown in the next chapter.

[This chapter contains results that have been previously published: R.K. Pal, A.A. Farghaly, M.M. Collinson, S.C. Kundu, V.K. Yadavalli, "Conducting polymer-silk biocomposites for flexible and biodegradable electrochemical sensors", Biosensors & Bioelectronics, 81, 294-302, 2016

R.K. Pal, A.A. Farghaly, M.M. Collinson, S.C. Kundu, V.K. Yadavalli, "Photolithographic micropatterning of conducting polymers on flexible silk matrices", Advanced Materials, 28, 1406-1412, 2015

R.K. Pal, S.C. Kundu, V.K. Yadavalli, "Biosensing using photolithographically micropatterned electrodes of PEDOT:PSS on ITO substrates", Sensors and Actuators B: Chemical, 242, 140-147, 2017]

CHAPTER 5

SILK PROTEIN-CONDUCTIVE POLYMER BASED BIOSENSING DEVICES

5.1 INTRODUCTION

In Chapter 4, the development and characterization of electroactive silk biocomposites and microfabrication using these materials was shown. One of the major application of such composites is in the area of biosensing.[238] There has been extensive interest in development and exploitation of biosensors for detection, quantification and monitoring of specific chemical species. Biosensors, in general, are analytical devices that convert a change in physical parameters such as pH, temperature and concentration of a specific chemical or set of chemicals into a physical readout.[239] Biosensors need to be specific, rapid, simple to operate, easily fabricated, and ideally require minimal sample pretreatment. Electrochemical biosensors form an important class of biosensors which depend upon the Faradaic reactions occurring at the interface of the electrode and analyte.[240, 241] The ability to provide sensitive, selective, cost effective and fast detection capabilities have made electrochemical biosensing a popular choice for monitoring physiological events.[242] Owing to the nature of the inks developed in Chapter 4, the use of silk devices as an electrochemical biosensor is discussed in this chapter.

Depending on the sensing mechanism, electrochemical biosensors for detection biomolecules can be of two type: 1) direct biosensing of electroactive biomolecules, 2) indirect biosensing of non-

electroactive biomolecules (Figure 5.1). Moreover, depending on the application, biosensors can be *in vitro* biosensors such as lab-on-a-chip device, or implantable biosensors. Both these systems have different requirement. Lab on a chip systems can be fabricated on a traditional rigid substrate, whereas implantable systems should be preferably flexible and adaptable to the shape of soft tissue. Towards this end, various electrode materials have been investigated for electrochemical biosensors such as metals: gold, and platinum, carbon based materials: carbon nanotubes, graphite, and graphene, metal oxides: zinc oxide and indium tin oxide, and conducting polymers.[243] Due to their unique ability of transporting electrons as well as ions, conducting polymers act as sensitive transducer elements for fast readout of Faradaic events at the interface. Further, the porous nature of CPs provide large interfacial area for reactions, resulting in a lower impedance in comparison to metallic or metal oxide planar electrodes.[243]

As shown in the previous chapter, silk based conductive composites are suitable for both systems. The EIS study clearly showed that the conductive coating on a conventional substrate can significantly decrease impedance of the electrode. In addition, the conductive composites could be efficiently patterned on flexible fibroin sheets. The electrochemical study also indicated a stable electrochemical property. In this chapter, the silk-CP biocomposites will be investigated as biosensing elements. Since silk based conductive polymer patterning involves water based and room temperature benign processes, therefore, the intrinsic properties of silk proteins such as biomolecule entrapment can be utilized for developing enzyme based biosensing. Therefore, it is possible to conceptualize a framework where micropatterned biosensors (either for direct biosensing or indirect biosensing or for *in vitro* or implantable applications) using silk biocomposites can be developed.

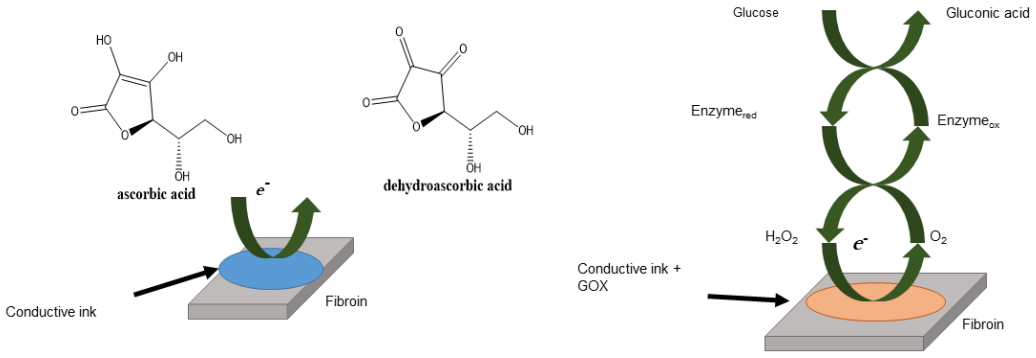

Figure 5.1 *Schematic showing (a) direct and (b) indirect detection of biomolecules.*

To develop a biosensing platform using silk based conductive ink, some general performance parameters need to be met. [244] An important set of requirements are specificity and sensitivity for the analyte of interest. Specificity of a biosensor determines if the biosensor can perform in presence of interfering species. It is considered that a "perfect" biosensor will not be perturbed by the concentration of another analyte in the ambient tissue or fluid. Sensor sensitivity must be sufficient to overcome the noise present in the system. Another highly desired attribute is stability of under cyclic loading and over time. The ability to entrap biosensing elements such as enzymes is also important for indirect biosensors (Figure 5.1).

To study the efficacy of silk-PEDOT:PSS in biosensing, initially the conductive ink patterned laminate was used as a transducer layer. The aim was to investigate the enhancement of sensing characteristics of a conventional electrode (in this case ITO on glass). The study also looked at the patternability of conductive ink on conventional microelectrodes and stability of ink patterns on these electrodes. The second study focused on the development of conductive ink patterned flexible electrodes as biosensing elements. The aim was to show that the conductive inks could be

used for biosensing without using any conductive charge carriers. This is therefore one of the few studies where non-conventional electrode materials are used for sensing in a flexible format.

5.2 EXPERIMENTAL SECTION

5.2.1 Materials

Glucose oxidase (from *A. Niger*) and Ferrocenyl methyl trimethyl ammonium iodide were procured from Sigma-Aldrich and Strem Chemicals, Newburyport, MA respectively. All other chemicals and materials are same as discussed in previous chapters. The synthesis of FPP, SPP and formation of photopatternable conductive ink and fabrication of micropatterned ITO coated glass electrodes and flexible fibroin devices was as discussed in Chapter 4.

5.2.2 Electrochemical sensing

Cyclic voltammetry (CV), Differential pulse voltammetry (DPV), Electrochemical impedance spectroscopy (EIS) and Chronoamperometric (*I-t*) techniques were used. The electrolyte used was PBS buffer (0.1 M, 7.4 pH). A standard three cell setup used Ag/AgCl (in 2M KCl) and Pt electrodes as reference and counter electrodes respectively, while the as-prepared samples formed the working electrode. CV experiments were done on a CHI 401 instrument (CH Instruments, Inc., Austin, TX) at a scan rate of 0.1 V/s over a -1.0 to 1.6 V potential window. DPV and *I-t* measurements were conducted on a CHI 660 workstation. The DPV parameters were as follows: step size 2 mV, pulse size 50 mV, sample period 0.02 s, pulse time 0.2 s. DPV response for dopamine and ascorbic acid were recorded. The *I-t* response for dopamine was measured at 0.28V constant potential.

For the sensing experiments described, the devices did not use conventional electrode charge collecting electrodes such as carbon cloth, metal or metal oxide layers. Chronoamperometric (*I-t*) response was measured for electrochemical sensing of glucose, dopamine hydrochloride (DA) and ascorbic acid (AA). A 10 ml of stirred solution of PBS (0.1 M PBS buffer pH 7.4) was used with a polarization potential of 0.3 and 0.6 V for SPP/PEDOT:PSS patterns on FPP. For glucose sensing experiments, the conducting ink was loaded with 200 U of glucose oxidase. 0.1 mM ferrocenyl methyl trimethyl ammonium iodide was added to the buffer to shuttle electrons from the enzyme active site to the conducting polymer. Fructose, sucrose and galactose were used as negative controls for the glucose sensor. 0.1 M glucose, 0.1 M fructose, 0.1 M sucrose, 0.1 M galactose, 0.01 M ascorbic acid, and 0.01 M dopamine stock solutions were freshly prepared for each experiment. After stabilization of the background current, increasing amounts of analytes were added to the stirred solution at regular intervals to obtain *I vs. t* response curves. Limit of detection (LOD), limit of quantitation (LOQ) and sensitivity were calculated as per ICH guidelines:

$LOD = \frac{3.3 \times S_{y/x}}{m}\ \mu\text{M}$, $LOQ = \frac{10 \times S_{y/x}}{m}\ \mu\text{M}$ and $\text{Sensitivit y} = \frac{m}{A}\ \mu A/\mu M.cm^2$, where, $S_{y/x}$= Standard error at y-intercept, m= slope of the calibration curve ($A/\mu M$). Both values are obtained from regression analysis of calibration curves. A = area of sensor exposed to electrolyte (cm^2).[245]

5.3 RESULTS AND DISCUSSION

5.3.1.1 Rigid biosensors using ITO/glass as electrode material

The use of ITO as a biosensing platform has been previously reported.[246] In the previous chapter

the fabrication of site-specific patterns of silk based conductive ink on ITO electrodes were discussed in detail. The fabrication of conductive ink on the ITO substrate was obtained by functionalizing the surface first. These functional moieties crosslink with the conductive ink to make the patterns more stable than simple electrostatic adhesion. Moreover, the surface functionalization techniques are very well developed and can applied to most conventional electrodes depending on the application. Here, the study of biosensing is discussed. Dopamine, ascorbic acid, and glucose were tested as analytes in this set up. Dopamine, a catecholamine neurotransmitter, is physiologically found in the central nervous system (CNS), peripheral nervous system (PNS) and blood. In plasma, the reported dopamine concentration is ~0.1 nM.[247] In extracellular region of brain striatum, the reported concentration of dopamine is 10-20 nM.[248] It is important to note that the dopamine concentration can be spiked to micromolar concentrations by pharmacological stimuli.[249, 250] In many biological fluids, for example in CNS extracellular fluid, dopamine (DA) tends to be found in the presence of an excess of ascorbic acid (AA).[251, 252] AA itself is an important antioxidant in metabolic processes and its reported concentrations in plasma and extracellular fluid are ~2 µM and 60-70 µM respectively.[249, 253]

5.3.1.2 Oxidation potentials of DA and AA on conducting ink coated ITO microelectrodes

Direct sensing of electroactive biomolecules relies on the oxidation occurring at electrode-electrolyte interface. Initially, cyclic voltammetry was conducted to determine the oxidation potential of DA and AA for our system, which were observed to be 0.3 V and 1.3 V respectively. Figure 5.2 shows the oxidation potentials of AA and DA on bare ITO electrodes. The usage of the ITO electrode therefore provides a wide oxidation potential gap for simultaneous sensing of DA and AA. Interestingly, the AA peak appeared at higher positive potential while the DA peak was

consistent. This behavior is unlike other conventional electrodes such as glassy carbon (GCE), planar gold or planar platinum. Therefore, to further explore the oxidation peak of AA on various substrates, CV experiments with different electrodes were performed – ITO, GCE, Pt disk and planar gold electrodes (Figure 5.3).

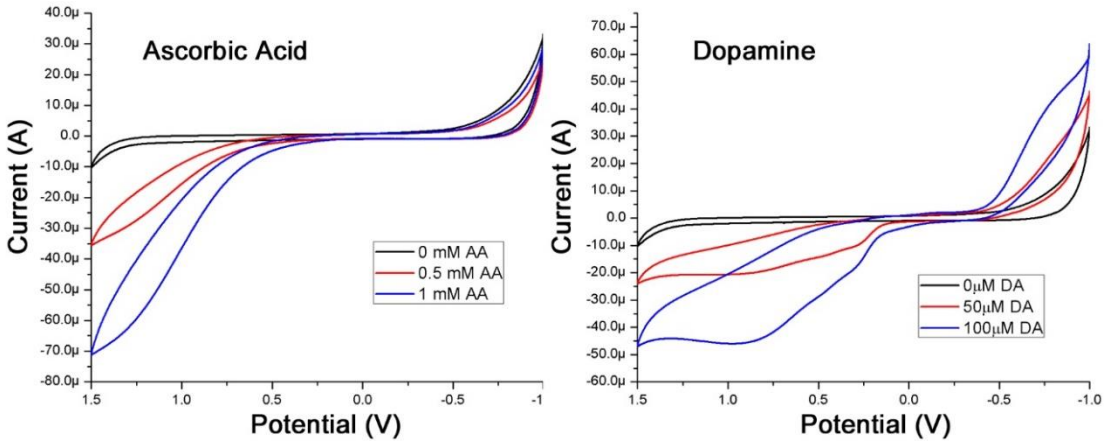

Figure 5.2 *Oxidation potentials of ascorbic acid and dopamine on bare ITO surfaces at a scan rate of 0.1 V/s and in 0.1 M PBS at room temperature*

It is observed that the oxidation potential of AA depends strongly on the electrode material, and the AA peaks shifts towards negative potential. For Pt electrodes, even though very sharp peak is obtained, the peak (0.275V) almost overlaps with the DA peak of 0.306V. On the other hand, ITO provides a wide stable potential window in comparison to these conventional electrodes, with an efficient separation of the oxidation peaks of DA and AA. The oxidation peaks were not as sharp as Pt, implying the need to improve the sensitivity of ITO electrodes to be used as biosensors. The oxidation potential was similarly observed to shift towards negative values by usage of differential pulse voltammetry (DPV) instead of CV. This is to be expected since pulse voltammetric techniques minimize the charging current, whereby peak potentials are clearly distinguished from CV oxidation peaks.[254] Previous reports suggest that conductive ink coating on electrodes improve their sensitivity.[255, 256] EIS characterization of conductive ink coated ITO substrate

showed lower charge transfer resistance and lower charged double layer capacitance. The conductive ink patterned ITO microelectrodes were further investigated to confirm the hypothesis. These initial experiments suggest that the conductive ink coated electrodes do indeed have a significant increase in the peak current of DA and AA over bare ITO microelectrodes (Figure 5.4), justifying the initial hypothesis that micropatterning of ITO with the conducting polymer is useful for biosensing.

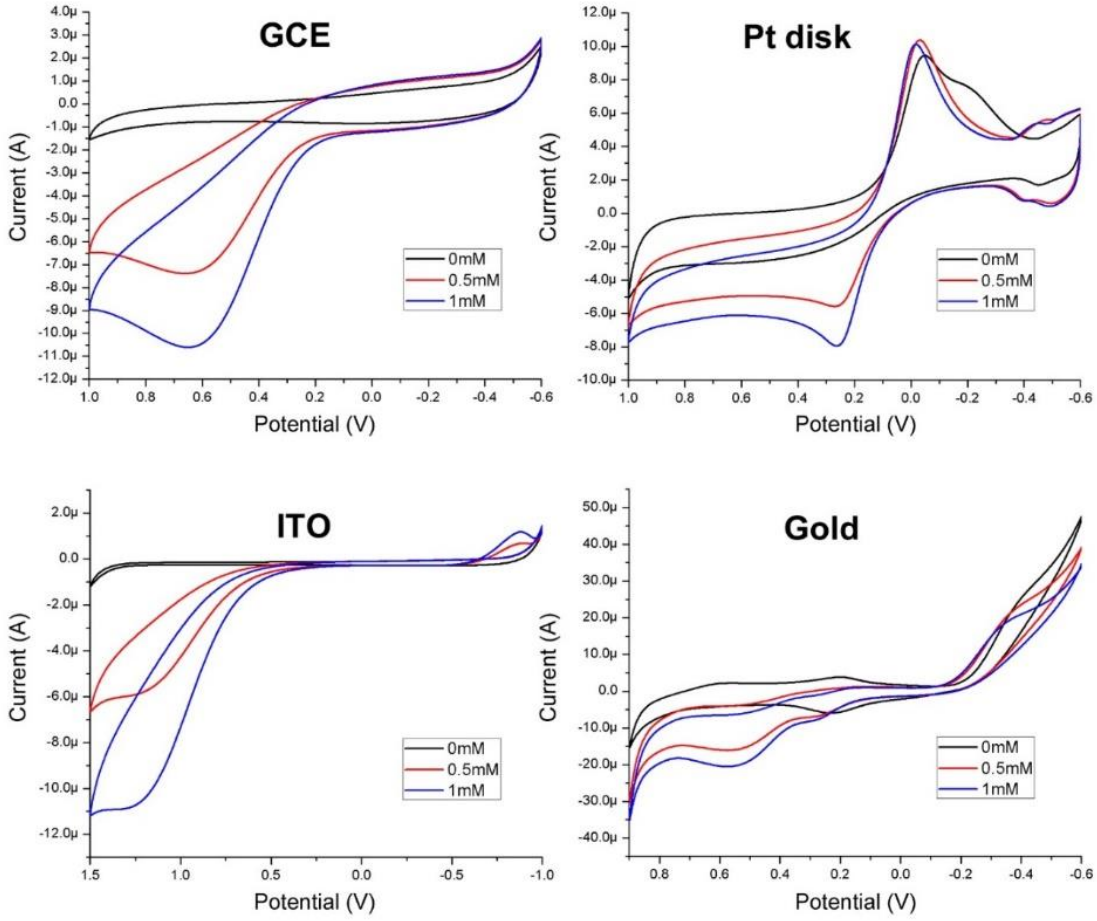

Figure 5.3 *Oxidation potential of ascorbic acid as a function of the electrode material at a scan rate of 0.1 V/s and in 0.1 M PBS at room temperature*

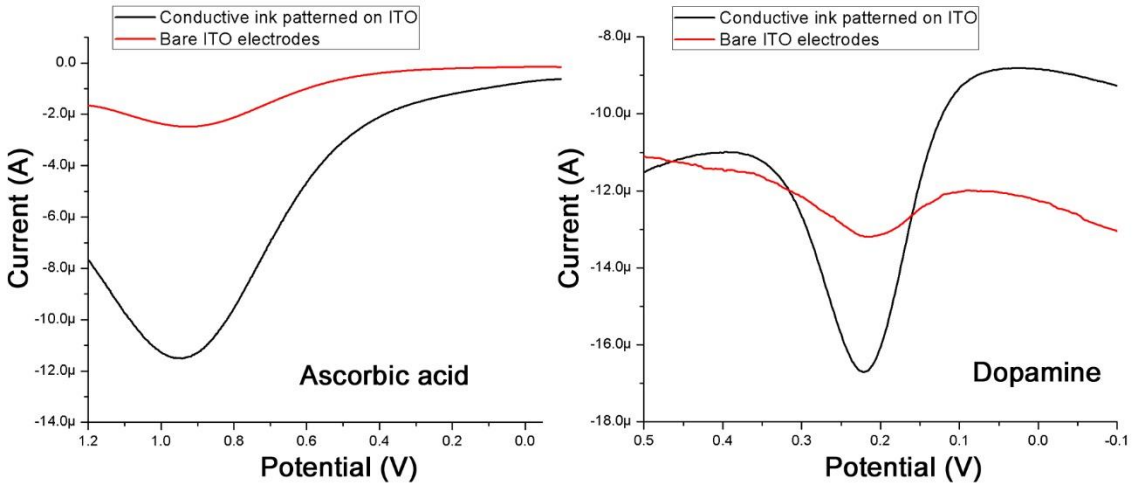

Figure 5.4 *Differential pulse voltammograms (DPVs) of bare ITO and conductive ink coated electrodes in 0.1 M PBS (7.4 pH) showing peak potentials of ascorbic acid and dopamine. The increase in peak current shows that the idea of forming micropatterned electrodes on ITO using conductive composites is valid.*

DA is positively charged in PBS buffer (pH 7.4), and therefore has an electrostatic attraction to anionic molecules. PEDOT:PSS has two components - the cationic PEDOT and the anionic surfactant PSS, which exists in large excess to the PEDOT. The overall abundance of anionic charges over the cationic charges, results in an overall attraction force for DA in the conductive ink coated electrodes. This can cause a "pre-concentration" effect whereby dopamine can diffuse inside conductive ink matrix and accumulate.[257, 258] The PSS acts as an electron transfer facilitator between the electrode surface and the dopamine target. Therefore, pre-concentration effect might lead to more sensitive detection of DA over AA. To verify this, CV experiments were conducted by adding 20 µM DA in an electrochemical cell. Measurements were taken over time - after 30 seconds and 5 minutes (Figure 5.5a). An increase in the peak after 5 minutes in comparison to 30 seconds indicates the increased DA present for oxidation. In contrast, over the second cycle of CV at 5 minutes, the peak current reduced to the same value as observed in the CV at 30 seconds.

This reduction of peak current indicates that the increase in peak current at the longer time interval is indeed due to the pre-concentration effect – over the second cycle only the diffused DA is oxidized resulting in a peak similar to that observed at 30 seconds. Further, to confirm that the pre-concentration effect is not an artifact of electrolyte. The experiment was repeated in 1 M KCl solution (Figure 5.5b). Here also, the pre-concentration effect is clearly observed. Thus, the anionic PEDOT:PSS presents an interesting of pre-concentration behavior which can be coupled with pulse voltammetric procedures to provide a sensitive biosensing of dopamine without the need for separate anionic membranes.[257, 258]

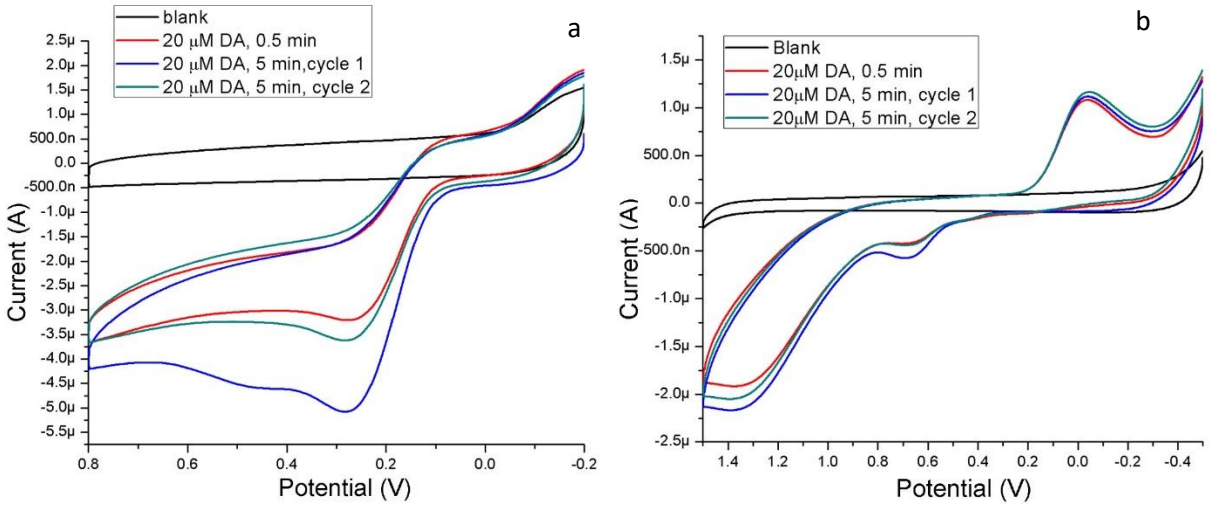

Figure 5.5 *Time course cyclic voltammograms with a scan rate of 0.1 V/s in (a) 0.1 M PBS (pH 7.4) and (b) 1 M KCl, taken at 30 s and 5 minutes in the presence of dopamine showing the pre-concentration effect.*

5.3.1.3 Detection of dopamine in the presence of ascorbic acid

To add to the physical presence of AA, in many conventional electrode systems, the oxidation potential of AA is very close to that of DA.[259-261] Therefore, AA acts as an interferent for DA

electrochemical sensing. As discussed above, the use of ITO based electrodes can minimize AA interference by effective separation of the peak potential. In order to explore the biosensing capabilities of the conductive ink decorated ITO micropatterns, individual DPV sensing experiments with DA and AA were initially conducted. Representative voltammograms of DA and AA sensing are shown in Figure 5.6 showing that the peaks obtained for dopamine are sharper, likely owing to the pre-concentration effect described earlier.

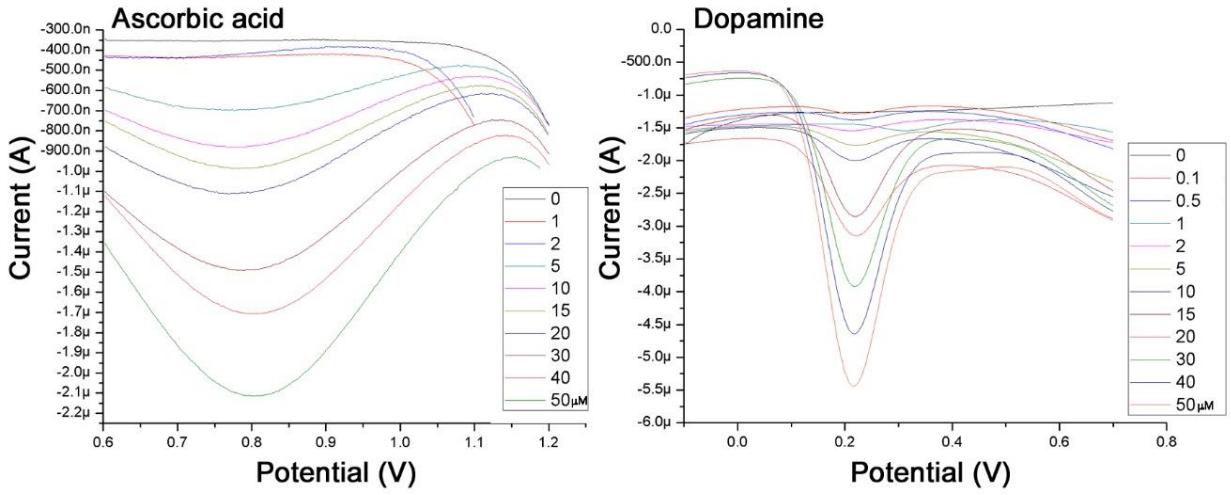

Figure 5.6 *Representative differential pulse voltammograms for sensing of ascorbic acid and dopamine at conductive ink coated microelectrodes in 0.1 PBS (7.4 pH)*

The calibration curves are shown in Figure 5.7. The corresponding calibration curves of DA (Figure 5.8a) and AA (Figure 5.8b) show the linear response of the sensors with a high R^2. To further explore the effect of AA interference on DA sensing, DA sensing was studied in the presence of a large excess of AA (100 μM). 100 μM was chosen as the upper limit of the physiologically relevant range. The calibration curves of dopamine in the presence of ascorbic acid are shown in with a representative voltammogram in Figure 5.8 c and d.

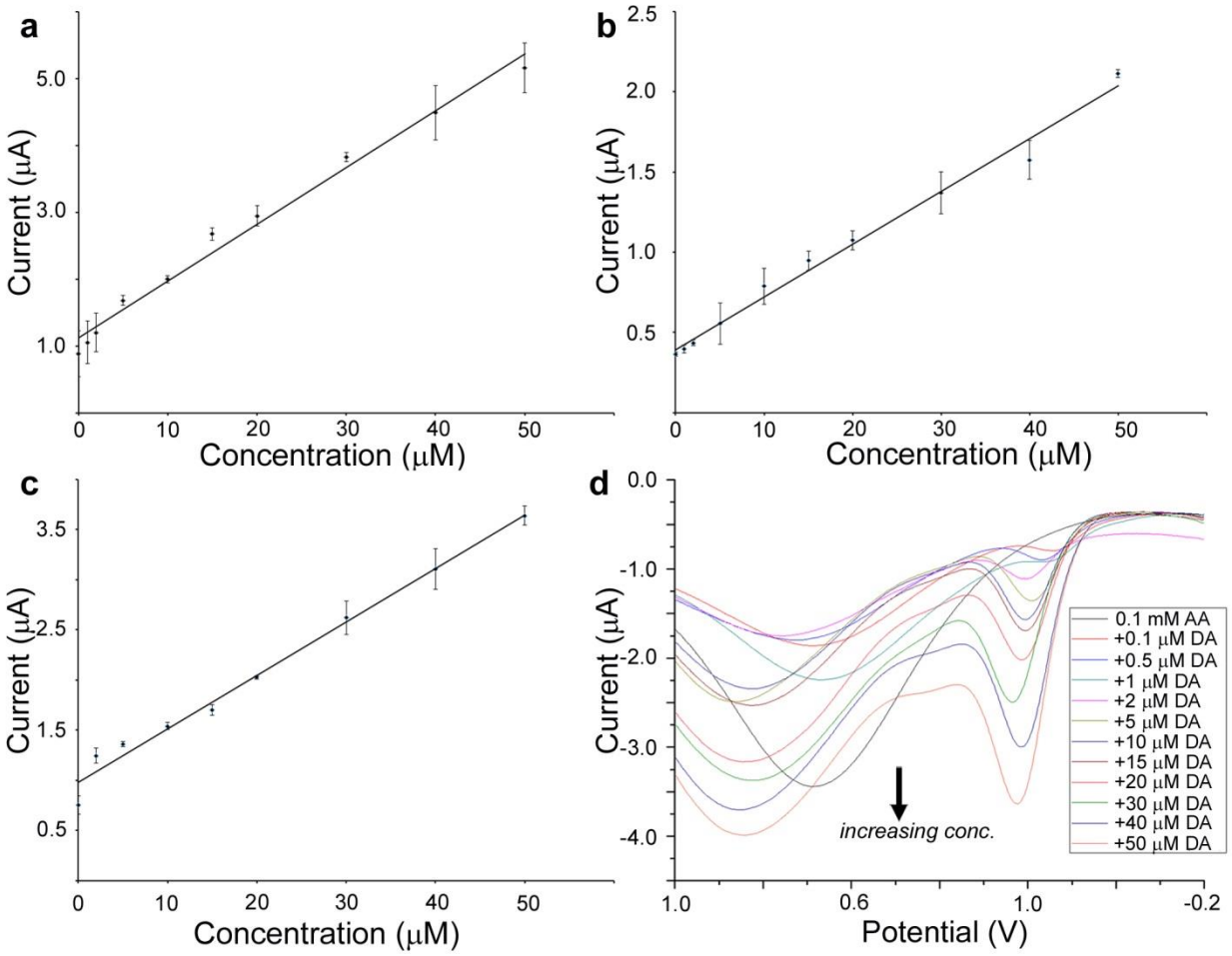

Figure 5.7 *Calibration plots for the sensing of (a) dopamine alone (R^2 = 0.9867), (b) ascorbic acid alone (R^2 =0.9885) and (c) dopamine in the presence of a large excess (100 μM) of ascorbic acid (R^2 = 0.9861). (d) representative differential pulse voltammogram of the dopamine detection in the presence of ascorbic acid. (n=3)*

The metrics of the biosensor - limit of detection, limit of quantitation and sensitivity of the sensor for DA, AA, and DA in presence of AA are shown in Table 5.1. The lowest detection limit of DA in both sensing setups either in absence or in presence of AA is very similar ~6.7 μM. AA can be detected as low as 6.6 μM, which is only a slightly lower sensitivity than for DA. In order to establish the consistency of results, experiments were run in triplicate. The sensitivity of AA

sensing was 313 nA/(cm^2.µM), lower than DA sensing. Interestingly, the sensitivity of DA sensing in the presence of AA is 523 nA/(cm^2.µM), which is lower than the sensitivity 826 nA/(cm^2.µM) when only DA was present in the system. However, given that the order of sensitivity is the same for both cases, indicating that these microfabricated sensors can be used for efficient DA sensing even with the presence of large amounts of AA. It may be noted that these values are comparable to, or exceed other sensors using dopamine sensing on ITO based electrodes.[262, 263] In a comparative sensor, the enzyme tyrosinase was used to improve the dopamine sensing resulting in a detection limit 1.04 µM which is only slightly better than our sensor.[264] However, the sensors shown have a superior linear range and sensitivity than the earlier reported figures. As discussed further below, the biofriendly processing enables enzymes to be efficiently entrapped in the conductive ink matrix. Therefore, further improvements in DA detection can be performed with the incorporation of suitable enzymes and electroactive species.

Table 5.1 *Analytical parameters of the microelectrode biosensors*

	Limit of detection (µM)	Limit of quantitation (µM)	Sensitivity (nA/µM.cm^2)
Dopamine alone	6.84	20.73	826
Ascorbic acid alone	6.6	20	313
Dopamine in the presence of ascorbic acid	6.77	20.52	523

An important characteristic for biosensors is the ability to perform under cyclic loading and unloading of targets of interest. An amperometric electrochemical technique was used to study the detection of dopamine in a cyclic fashion. The concentration of DA was increased from 0 to 20 µM in steps of 5 µM, 10 µM and 20 µM and then reduced back to 5 µM in similar steps by diluting

the sample buffer. Figure 5.8 shows the amperometric response over time with several loadings and unloading cycles. The sensor is stable with fluctuating dopamine concentration with only a slight change in current response. The current recovery with change in dopamine concentration is shown in Table 5.2. This study therefore indicates the potential for the sensor to be used in real world systems where the concentration of dopamine can fluctuate.

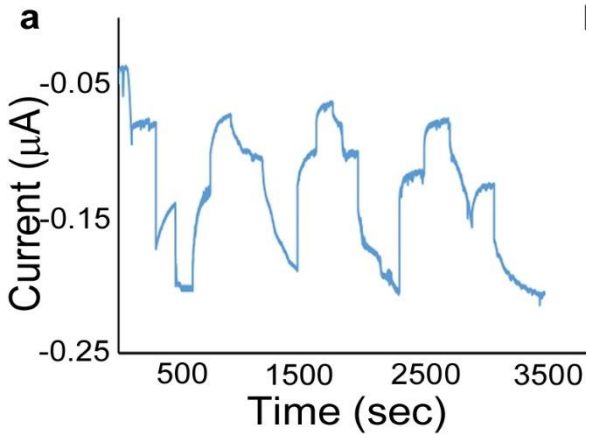

Figure 5.8 *Amperometric (I-t) sensing of dopamine using the microelectrode sensors under cyclic loading and unloading of Dopamine in 0.1 M PBS solution at 0.3 V potential. The same sensor was cycled 4 times through concentrations up to 20 µm.*

Table 5.2 *Hysteresis of biosensor with DA addition and dilution*

Concentration (µM)	**5**	**10**	**20**	**10**	**5**
Current(µA)	0.07933	0.1407	0.1983	0.1323	0.074
Concentration (µM)	**10**	**20**	**10**	**5**	**10**
Current (µA)	0.1042	0.187	0.1009	0.06608	0.1026
Concentration (µM)	**20**	**10**	**5**	**10**	**20**
Current (µA)	0.2053	0.1174	0.07765	0.1257	0.207

5.3.2 Biosensor in a flexible format

For continuous or real time monitoring of physiological activities, biosensors that can be operated *ex vivo* (such as bionic contact lenses, and skin wearable devices) and *in vivo* (such as implantable devices) conditions are desirable. In case of implantable systems, controlled biodegradability is another additional requirement achieving 'implant and forget' capabilities. A transient or bioresorbable biosensor that can lose function in a programmable fashion over time can therefore be realized. In the previous chapter, the silk based conductive architectures was shown to be bioresorbable. Thus, the goal of this part is to study was to translate the biosensing capabilities of the conductive ink architectures on *flexible* fibroin substrates.

5.3.2.1 Detection of DA and AA with conductive ink patterned electrode on fibroin

Initially, direct and non-specific sensing of biomolecules ascorbic acid (AA) and dopamine (DA) were done. In separate experiments, 0.01 M DA and AA were added to a 10 ml PBS buffer system at various intervals after stabilization of background current. SPP-PEDOT:PSS (on fibroin films), Ag/AgCl and platinum were used as working, reference and counter electrode respectively in a chronoamperometric setup at 0.3 V constant potential. Each experiment was replicated with at least 3 different sensors. The lowest detectable concentration was 15.21 µM and 15.47 µM of DA and AA respectively, whereas the limit of quantitation was 46.1 µM and 46.87µM of DA and AA respectively, calculated from linear regression analysis of calibration curve. The amperometric response curve of the dopamine and ascorbic acid reveal a linear range from 10 µM to 200 and 700 µM respectively, having a sensitivity of 45.9 nA/(µM.cm^2) and 256.5 nA/(µM.cm^2) (Figure 5.9). The response time of the sensors (time taken to reach 95% of steady state current) for DA

and AA is ~30 seconds respectively.

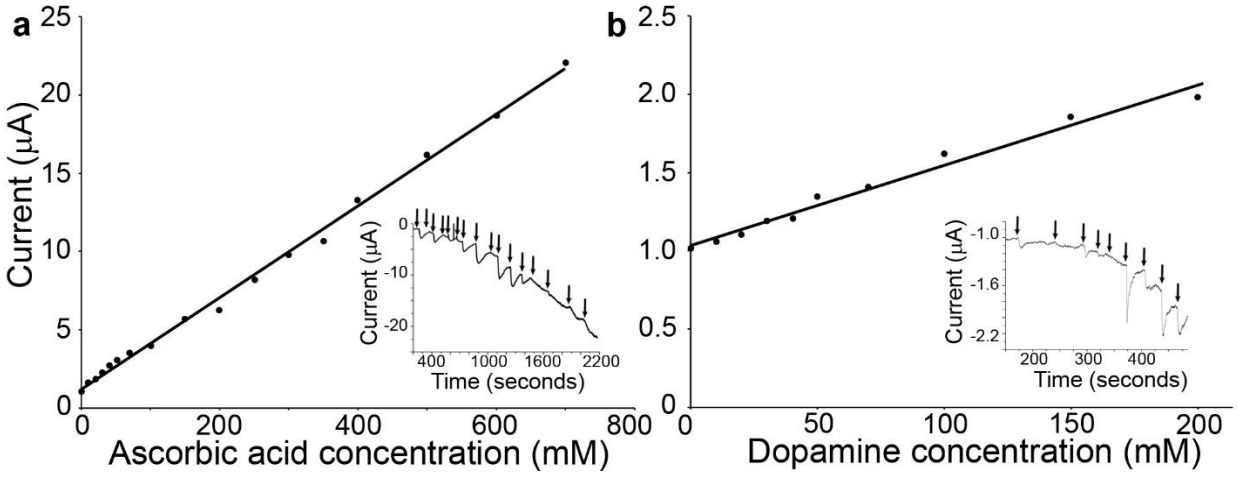

Figure 5.9 *SPP-PEDOT:PSS biosensor: Non-specific sensing of (a) ascorbic acid (at 0.6 V) and (b) dopamine (0.3 V) biosensing in 0.1 M PBS, showing the linear ranges of both sensors (R^2 = 0.996 and 0.980 respectively). The insets show the chronoamperometric response with addition. Both sensors start from the same baseline current. Downward arrows indicate point of addition. The current data noted just before addition of next increment of analyte.*

The data are presented for one sensor each, starting at the same baseline. Another example of sensor response for each analyte is presented in Figure 5.10, showing the reproducibility of these sensors. The linear and dynamic ranges are comparable with reported sensors, for instance a flexible graphite-paper sensor [251]. The patterns contain only PEDOT:PSS (19%), and neither the sensor nor the electrolyte solution contain any other electroactive species to enhance the electrochemical response of the sensor. With the addition of suitable biocompatible electroactive species, it is possible to enhance sensitivity and detection limits.

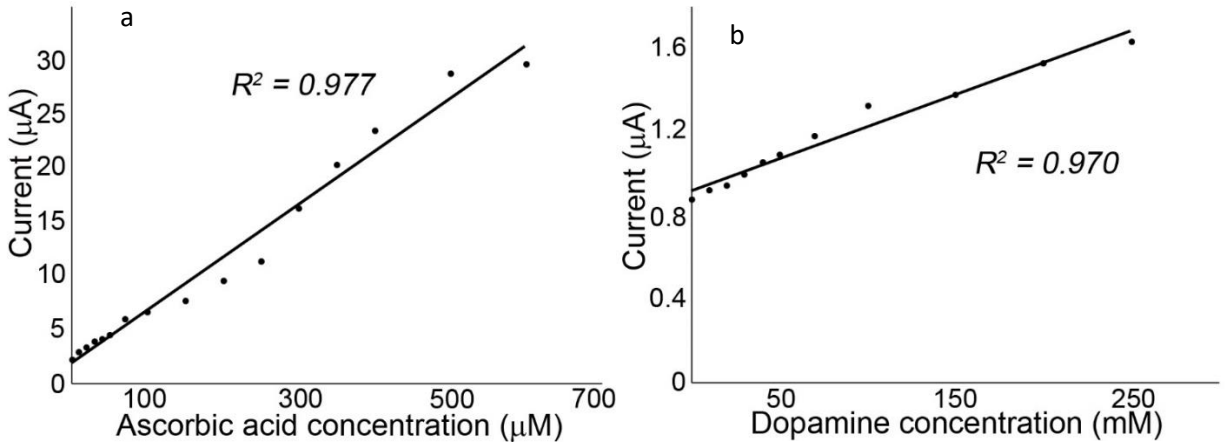

Figure 5.10 *Linear response of a second set of (a)ascorbic acid (at 0.6 V) and (b) dopamine (0.3 V) sensors over the range of 0-600 mM (ascorbic acid) and 0-250 mM (dopamine) in 0.1 M PBS. Beyond these concentrations, the sensors became saturated. Note that both sensors start from the same baseline (~ 1 μA).*

5.3.2.2 Enzyme encapsulation and glucose biosensing

The benign nature of the photolithography using only water and at ambient temperature and the natural silk matrix further provide the possibility to encapsulate proteins, enzymes, therapeutics and other active biomolecules [185, 265]. Silk proteins are themselves known to be promising for the stabilization of biomolecules [265]. The patterned silk-PEDOT:PSS sensors were subsequently demonstrated as a biosensor specific to glucose via the encapsulation of the enzyme, glucose oxidase (GOx) [266]. To date, most conductive polymer based enzymatic biosensors have shown that the conductive polymer plays a role to transduce electrons from analyte recognition enzymes to active electrode. Here, the glucose sensor is demonstrated by immobilizing the GOx directly in the SPP-PEDOT:PSS composite ink itself, to work as both the transducer and active electrode. The fully water-based processing enables dissolution of the enzyme directly in the SPP-

PEDOT:PSS composite to form a photopatternable enzyme ink. 0.1 M glucose solution were added to sensors in PBS, under continuous stirring at different intervals. The amperometric response of the glucose sensor is shown in Figure 5.11a. The mediator (ferrocene derivative) efficiently shuttled/carried electrons from enzyme FAD center to the electrode surface.[266] The sensor shows a rapid linear response throughout the dynamic range which is from 0 to 10 mM, which covers physiologically relevant blood glucose concentrations. The selectivity of the sensor was tested by adding solutions of galactose, fructose, and sucrose. It is clear from the Figure 5.11 that the sensors do not detect any other sugar except glucose. The limit of detection and quantitation of the sensor is 1.16 mM and 3.52 mM respectively, with a sensitivity of 7.57 µA/mM.cm^2. The average response time of the sensor (time taken to reach 95% of steady state current) is ~15 seconds. Such biosensors may be potentially used for epidermal sweat sensing as shown in Figure 5.11b.

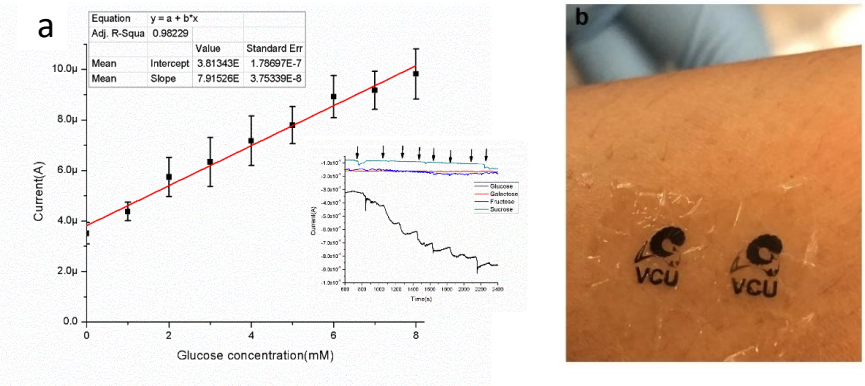

Figure 5.11 *SPP-PEDOT:PSS enzyme biosensor: (a) Glucose sensing (at 0.6 V) shown by immobilizing glucose oxidase (GOx) in the microfabricated sensor (R^2 = 0.98). The inset shows I vs. t response of the sensor and the specificity control experiment showing that it does not detect other sugars.(n=3)* ***(b)*** *The flexible micropatterned sensors may be placed on skin. The dark patterns are formed from the conductive ink (SPP-PEDOT:PSS) on the underlying crosslinked fibroin sheet*

Sensor response was tested as a function of ionic strength using 0.2x and 0.5x PBS as the electrolyte (Figure 5.12). The sensors were linear with comparable metrics as those reported above for 1x PBS. The encapsulated GOx sensors were extremely stable over time and could be used several days after fabrication. Samples with entrapped GOx in the SPP-PEDOT:PSS matrix and those without enzyme were soaked in a PBS buffer for 3 days to study possible loss of the enzyme due to leaching. Aliquots of the buffer collected and analyzed using UV/Vis absorbance (A_{280}) showed that both sets of films showed a negligible amount of protein leaching (<0.5%). The glucose oxidase has extinction coefficient ($E^{1\%}$) of 16.7 (at 280 nm). The ability to encapsulate enzymes without any leaching can therefore lead to multifunctional devices; for instance, where drug delivery can be integrated with sensing of different target analytes.

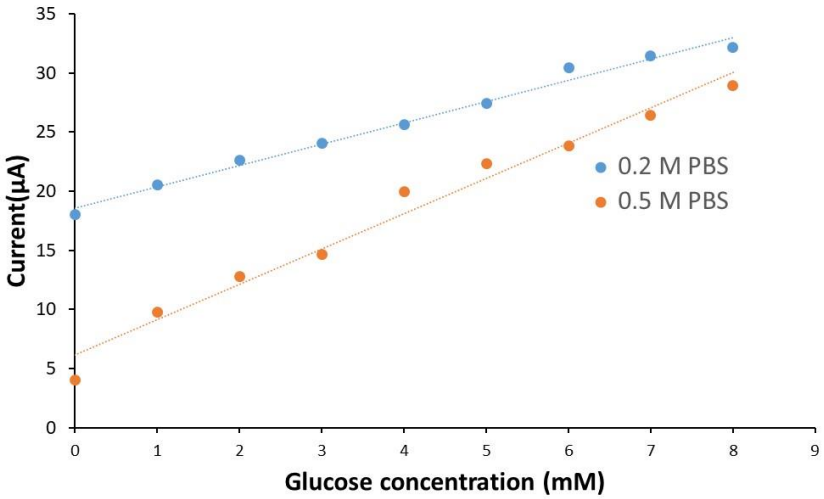

Figure 5.12 *Effect of ionic strength on the sensing of glucose using the SPP-PEDOT:PSS on FPP sensor. (R^2 = 0.950 and 0.988 at a 0.2x and 0.5x PBS respectively). The sensitivity of 1.3 and 1.5 µA/mM.cm^2. The average response time of the sensor (time taken to reach 95% of steady state current) is ~15 seconds which is comparable to 1x PBS.*

To the best of our knowledge, this is the first study showing a functional fully organic biosensor device formed by a green microfabrication technique that can also be degraded in a targeted manner. Such biosensors display conformability as seen in Figure 5.11b. It should be noted that the degree of crosslinking and thickness of films can be varied to precisely modulate the degradation. This gives an opportunity to realize organic bioelectronic devices, which can be programmed to specific levels of transience.

5.4 CONCLUSIONS

In summary, this chapter demonstrates biosensing application of silk based conductive composites on rigid and flexible substrates. The ITO microelectrodes functionalized using a silk protein based conductive ink improves the biosensing performance over a bare ITO surface. The conductive ink acts as a transducer layer and facilitates faster ion transport than the bare ITO electrodes, thereby improving the biosensing ability of the ITO electrodes. Conductive ink biosensors on fibroin films were then successfully shown as nonspecific and sensitive biosensors for dopamine and ascorbic acid *in vitro*. In the first part of study done on ITO based electrodes, the micropatterned sensors can detect dopamine in highly sensitive manner even in presence of excess amounts of ascorbic acid. This sensor can detect fluctuations in dopamine concentrations and be used over repeated cycles. The second part of the study shows sensitive detection of biomolecules even without a charge carrying background. By encapsulating enzymes such as glucose oxidase at biological pH and ambient temperature, a highly sensitive and selective glucose biosensor is demonstrated. The conductive ink-based micropatterned electrodes present a fully aqueous, green technique, suitable for biomolecule immobilization inside the conductive matrix. Therefore, the present work opens new directions for microfabricated biosensing using conductive polymers and silk proteins.

[This chapter contains results that have been previously published: R.K. Pal, A.A. Farghaly, M.M. Collinson, S.C. Kundu, V.K. Yadavalli, "Conducting polymer-silk biocomposites for flexible and biodegradable electrochemical sensors", Biosensors & Bioelectronics, 81, 294-302, 2016

R.K. Pal, A.A. Farghaly, M.M. Collinson, S.C. Kundu, V.K. Yadavalli, "Photolithographic micropatterning of conducting polymers on flexible silk matrices", Advanced Materials, 28, 1406-1412, 2015

R.K. Pal, S.C. Kundu, V.K. Yadavalli, "Biosensing using photolithographically micropatterned electrodes of PEDOT:PSS on ITO substrates", Sensors and Actuators B: Chemical, 242, 140-147, 2017]

CHAPTER 6

SILK PROTEIN-CONDUCTIVE POLYMER BASED MICROSUPERCAPACITORS

6.1 INTRODUCTION

Most portable and implantable transient (bio)electronic devices further require energy storage and supply systems to function independently.[267] The development of compatible energy storage systems as part of integrated devices forms another piece of the puzzle. This has led to the development of lithium-ion batteries, fuel cells, and supercapacitors in flexible formats.[268, 269] However, the realization of these systems involves a different set of challenges such as energy storage (and delivery) in a flexible format, necessitated by the soft and conformal nature of the biological working environments, light-weight, and controlled biodegradability. Conventional batteries cause biocompatibility problems such as immune rejection, inflammatory reactions, and secondary biological toxicity due to corrosion and leakage.[270] Supercapacitors (SCs) and micro-supercapacitors (μSCs) are emerging as an important alternative energy storage systems due to their fast charge-discharge rate, high power density, and long cycling life.[271]

To date, there have been significant efforts to fabricate flexible SCs in various geometries including planar [272], fiber, and wire-shaped, [273] to achieve properties such as ultra-flexibility, compactness, light weight, mechanical, and electrochemical stability. A traditional supercapacitor primarily comprises four components: the active electrode, carrier flexible substrate, gel electrolyte and charge collectors. Various active electrode materials have been identified including

oxides: such as MnO_2, and SnO_2, carbon-based materials: such as carbon nanotubes, graphite, graphene oxide and reduced graphene oxide, and conjugated polymers: such as polypyrrole (PPy), polyaniline (PANI), and poly(3,4-ethylenedioxythiophene) polystyrene sulfonate (PEDOT:PSS).[267, 274, 275] These materials have shown a great promise as active materials for flexible SCs, and are usually deposited or printed on inert, flexible carrier substrates such as Kapton, polypropylene, PET, or paper.[276] Gel electrolytes are used as electrode separators and ion conductors. A typical gel electrolyte consists of a polymer matrix such as polyvinyl alcohol, polyethylene glycol and gelatin, and ion conducting electrolytes such as H_2SO_4, H_3PO_4, KCl, KOH, and ionic liquids.[277] The electrodes are usually fabricated on metallic conductors for charge collection and transport. Finally, the fourth component is the encapsulation in which the entire device is built. Since devices involved for *in vivo*, subcutaneous or deep tissue implantable operations require additional properties such as biocompatibility, biodegradability, and sustainable processing, [278] it is clear that many of these materials do not qualify.

In previous chapters, the extension of the silk photolithography platform towards the fabrication of flexible optical devices and biosensors was discussed. Based on the capacitive nature of the silk protein-conductive polymer composites developed in Chapter 4 *without* the use of a conductive metal/metal oxide background, the possibility to form energy storage devices using the techniques discussed is therefore considered. The materials possess distinct advantages in terms of flexibility and degradability that could provide a new class of biocompatible super and micro capacitors.[228] The focus of this chapter is the development of techniques to fabricate and characterize a SC using the biocompatible, non-toxic silk protein-CP composite. Using the photolithography platform, it is possible to fabricate miniaturized SC devices (μSCs) using a facile, room temperature approach

with water as the solvent. Via the doping of very small amounts of reduced graphene oxide (rGO) with the conductive ink, a tunable increase in the capacitive nature of the electrodes can be achieved.[279] The use of an agarose biopolymer and sodium chloride based gel electrolyte is also investigated to form a benign, completely biomaterial based, biocompatible micro-supercapacitor system that can potentially be used in a biological microenvironment.[280]

6.2 EXPERIMENTAL

6.2.1 Materials

Agarose, graphene oxide (GO) solution and ascorbic acid were purchased from Sigma-Aldrich, St. Louis, MO, University wafer, South Boston, MA, and Fisher Scientific, Asheville, NC respectively. All other materials used were same as described in the previous chapters.

6.2.2 Synthesis of silk protein photoresist

The synthesis of photoreactive silk proteins is the same as described in Chapter 2.

6.2.3 Formation of modified photocrosslinkable conductive ink

The conductive ink is formed by mixing together four components: sericin protein photoresist (SPP), PEDOT:PSS, reduced graphene oxide (rGO) and DMSO. First, dry re-dispersible pellets of PEDOT:PSS (Orgacon™) were dispersed in water, ultrasonicated for 20 min and filtered with 0.25 µm syringe filter to obtain 1.0% w/v solution. 5 % (v/v) DMSO was added to PEDOT:PSS to enhance the conductivity and improve plasticity of conductive ink. In the second step, graphene

oxide (GO) was reduced to rGO at room temperature following a procedure reported elsewhere with slight modification. [281] rGO is commonly obtained after the reduction of commercially available GO in aqueous dispersions. There have reports to reduce GO either thermally, chemically or electrochemically.[282] All these processes either uses harsh conditions or chemicals, thus, making them unworthy to be used to develop a sustainable technology. In this work we utilized an earlier shown biofriendly reduction process of GO with ascorbic acid.[281] GO was shown to be reduced by ascorbic acid, a natural organic molecule (vitamin C). The reduction of GO to rGO was confirmed by observing shift of UV-vis absorption peak from 230 to 264 nm. Thus, obtained rGO was directly mixed SPP-PEDOT:PSS conductive ink to obtain rGO doped conductive ink. Briefly, 2 mg/ml graphene oxide (GO) solution was reduced with ascorbic acid at 5 mg per 1 mg of GO under continuous stirring at room temperature for 1 hour. The reduction of GO to rGO was confirmed by UV-Vis absorption spectra which shifted from 230 nm to 262 nm. The freshly reduced rGO was always used to avoid precipitation of rGO. Sericin and rGO solution were added to PEDOT:PSS solution to form conductive ink to have required % of each in conductive ink. The photoinitiator Darocur 1173 at 0.1 µl/1mg of SPP was added to conductive ink before use.

6.2.4 Fabrication of conductive ink patterns and imaging of devices

Microfabrication of devices using the conductive ink is the same as described in Chapter 4. Optical microscopy and SEM were as described above.

6.2.5 Electrolyte gel development

First NaCl was dissolved in 10 ml of DI water to form a 5M NaCl solution. 100 mg agarose (Sigma-Aldrich, St. Louis, MO) added in NaCl solution. The agarose was melted and dissolved in solution

by heating the solution in water bath at 90° C for 2 hours. To form a PVA-H_3PO_4 electrolyte, first 0.2 gram PVA (9000 MW, 80% hydrolyzed) (Fisher Scientific, Asheville, NC) was first mixed with 2 ml of water and heated under continuous stirring until the solution became clear. Then 0.16 grams of H_3PO_4 was added.

6.2.6 Electrochemical experiments

Cyclic voltammetry (CV), galvanostatic charge-discharge (C-D) and electrochemical impedance spectroscopy (EIS) were used. All electrochemical characterizations were conducted with two-electrode cell configuration. 5 M NaCl-Agarose or 0.8 M H_3PO_4-PVA gel electrolytes were used within the potential range of 0 to 0.5 V and 0 to 1.0 V for C-D or CV experiments. The EIS data were collected in a frequency range of 0.01 Hz to 10^4 Hz with a 5 mV AC amplitude. The capacitance of the device was calculated from the galvanostatic charge-discharge (C-D) curves following the equations are shown below:[283]

$$C_{device} = \frac{i_{app}}{-\Delta E / \Delta t} \quad (1)$$

where i_{app} is the discharge current (A), ΔE is discharging voltage and Δt is the discharge time.

The various specific capacitance was calculated by following equations:

$$C_s = \frac{C_{device}}{m} \quad (2)$$

$$C_a = \frac{C_{device}}{a} \quad (3)$$

$$C_v = \frac{C_{device}}{v} \quad (4)$$

where C_s, C_a and C_v are gravimetric, areal and volumetric specific capacitance respectively. m, a and v are the mass, area and volume of active material on the electrode. The energy density (E, Wh kg^{-1}) and the power density (P, W kg^{-1}) of a supercapacitor in two cell-electrode configurations are obtained by the following equations:

$$E = \frac{1}{2} C_s \Delta V^2 \quad (5)$$

$$P = \frac{E}{\Delta t} \quad (6)$$

6.2.7 Biodegradation studies

The bioresorption and degradation studies of the devices via proteolytic degradation were conducted as described in Chapter 4.

6.3 RESULTS AND DISCUSSION

There have been earlier reports on energy storage devices for bioelectronic applications having natural polymers or biomolecules to improve biocompatibility and electrochemical stability in physiological media.[284-287] These works have been crucial for the advancement of energy storage systems and can be used in flexible, and or wearable formats. However, use of metal and harsh electrolyte limit the applicability of such systems. Thus, apart from few reports, there has been limited work on the development of biocompatible, and biodegradable miniaturized and microfabricated SCs. The use of non-biodegradable configuration such as the use of metal or metal

oxide charge collectors make these systems applicable where the implants need to stay for very long time like for an year.[286] At the other end, there have been reports of ingestible energy storage system that can be degraded with in few hours after ingestion.[288] Therefore, both type of systems are unsuitable for implant and forget type of systems, where a relatively moderate implant life (~1 month) is required. Here the work is intended to develop a completely metal/metal-oxide free, ultralight weight, and biodegradable supercapacitor.

6.3.1 Biofriendly conductive inks and gel electrolytes for supercapacitors

PEDOT:PSS is considered a suitable electrode material due to its electrical and ionic conductivity, and electrical and electrochemical stability for long period. Nanoscale carbon materials, such as graphene have also attracted a lot of attention due to high capacitance, high surface area and double layer properties, and electrochemical stability. Graphene has theoretical electrical double layer capacitance values up to 550 F/g.[289] However, the parallel stacking of graphene sheets limits its capacitance values to low levels. Incorporation of rGO with PEDOT:PSS greatly reduces the re-stacking of rGO and improves flexibility of the electrode at the same time.[279] Composites made of conductive polymers and rGO therefore can have very high specific capacitances of ~300 F/g.[290] Combining these materials with the silk protein photoresists therefore provides a unique opportunity to form a biofriendly conductive ink. Here, biofriendly term is used to indicate the water based and room temperature process for the formation and application of conductive ink.

A recent approach to improve performance and integration with microfabricated devices involves optimizing electrode packaging. Instead of two planar electrodes with sandwiched gel electrolyte, an interdigitated alternating microelectrode array is used.[275, 291] Performance improvement is

achieved due to shortened diffusion path without problems of short-circuiting of electrodes. In a flexible format, with interdigitated micro-supercapacitor configuration, an impressive specific capacitance value of 338 F g^{-1} at a constant current density of 0.5 mA/cm^2 has been reported using metal oxides on a non-biodegradable format.[292] Even though inkjet printing and stencil printing are primarily being used for fabrication of interdigitated supercapacitors, only sub millimeter scale feature sizes have been shown.[293, 294] Developing photolithographic techniques can therefore pave the way for miniaturization of these systems.

There are numerous ion conducting materials - either acidic, basic or neutral and gel matrix forming materials to obtain high capacitive performance. Most of them alone, or in combination are unsuitable for biological applications. Therefore, in the present work, agarose, a polysaccharide and NaCl, a neutral salt were used to form a green electrolyte gel.[280] Agarose is a hydrophilic polymer, often obtained from seaweed that is widely used due to its non-immunogenic and anti-fouling properties. Agarose has the ability to maintain resistance to non-specific adsorption of proteins or biofouling that can lead failure of electrodes. This electrolyte was chosen for its superior biocompatibility, even considering a slight compromise in performance as discussed below.

The fabrication of supercapacitor device is similar to that shown in Chapter 4, with a modification in ink composition. 2 mg/ml rGO stock solution and 1% (wt./vol.) PEDOT:PSS solution with 5% (vol.) DMSO were prepared separately. The two solutions were mixed together with SPP and photoinitiator to form a conductive ink. Initial trials of adding rGO with the previously developed

conductive ink which contained PEG as plasticizer resulted in precipitation of rGO. FPP films were prepared by drop casting the FPP solution in formic acid (FA) on a glass/ silicon substrate, followed by crosslinking using UV light. Patterning of the conductive electrodes was performed using photolithography as discussed above. Initially, strip electrodes were patterned, while the interdigitated patterns were used for stability testing.

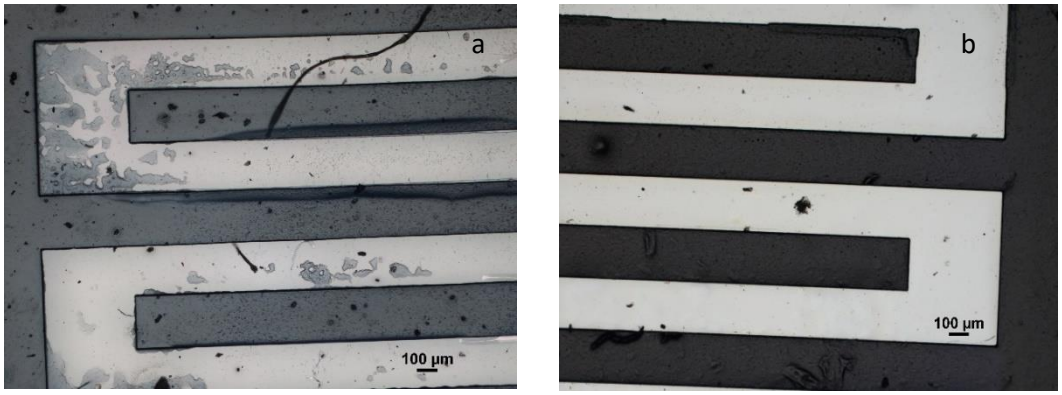

Figure 6.1 *Fabrication of supercapacitor patterns on fibroin with (a) glass, and (b) silicon as the underlying base.*

Glass was initially used as a flat rigid support during photolithography. However, this resulted in short circuited electrodes. Careful investigation revealed that the transparent nature of glass led to the combination of refraction and scattering of UV light from the bottom of the glass surface. This scattering resulted in crosslinking of a very thin layer of ink leading to the short (Figure 6.1a). To overcome the issue, silicon wafers were used as the flat rigid support for fabrication. Since silicon is an opaque and has a polished reflective surface, no refraction issues were observed. The patterns thus formed were distinct and conductive (Figure 6.1b, and 6.2c and d). The fabricated devices on fibroin sheets are flexible and can be rolled and bent (Figure 6.2 b). The devices are also ultralight weight (Figure 6.2 and b) and has an average mass of ~3.9 mg/cm^2 which is 27 fold lighter than general office paper (130 µm thick, 8 mg/cm^{-2}).[288] The ultra-light weight nature is an added

advantage for such systems. It is to be noted that incorporation of gel electrolyte further increases weight for the device therefore form an overall light weight device, each component of the device should be kept at minimum possible mass loading to keep the overall device relevant for implantable or wearable applications.

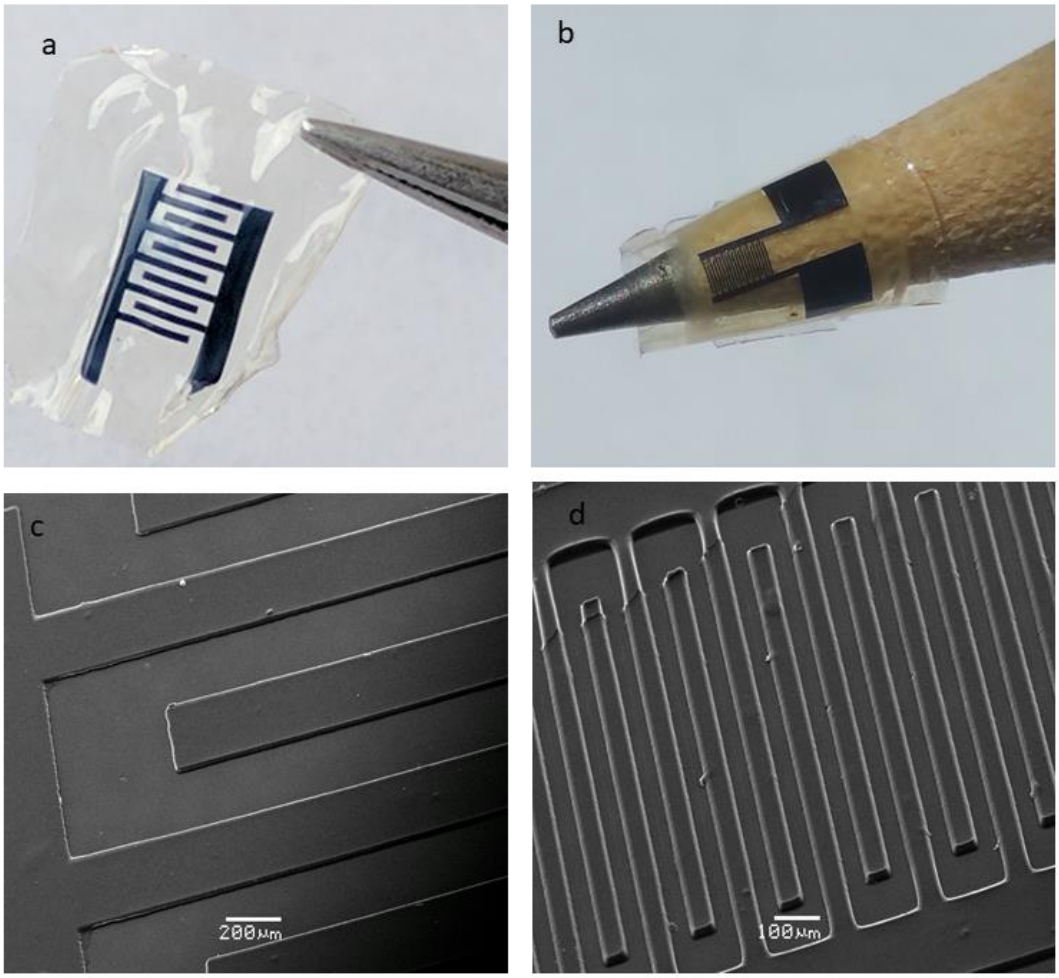

Figure 6.2 *Interdigitated micro supercapacitors of two sizes: optical images of (a) large and (b) small electrodes. (c, d) Corresponding SEM images showing complete development.*

6.3.2 Electrochemical Characterization of rGO doped conductive ink

Important performance parameters of an SC are its capacitance, charge-discharge characteristics, capacitance retention over cycling, and the ratio of energy density to power density.[283] Capacitance values can be normalized over active material loaded (mass), area or volume of the electrode. Improvement in capacitance performance is typically driven by approaches to combine active electrode materials and enhance porosity to increase active area.[274] Reported specific capacitance values for such systems range from 150-300 F g^{-1} which is still far from reported values (700-2223 F g^{-1}) when using metal oxides.[295-297]

Table 6.1 *Conductive ink compositions*

Composition	SPP (%)	PEDOT:PSS (%)	rGO (%)
1	70.6	28	1.4
2	66.6	28	5.4
3	49.8	48	2.2
4	43.84	48	8.16

To characterize the rGO-doped conductive ink's capacitive properties, electrochemical impedance spectroscopy (EIS) and cyclic voltammetry (CV) were conducted. Four conductive ink compositions shown in Table 6.1, were first cast on ITO/glass substrate and the electrode area was defined by covering the electrode by PTFE tape and keeping 1/8″ diameter size hole open. EIS measurements were done in three-electrode electrochemical cell having 0.1 M PBS buffer solution as electrolyte. The frequency response of electrode/electrolyte system is usually being shown as a plot of the imaginary component (Z″) of the impedance against the real component (Z′) and these types of plots are being called Nyquist plots. The Nyquist plots obtained for all four composition of conductive ink are shown in Figure 6.3a. Each data point is obtained at a different frequency with the lower left portion of the curve corresponding to the higher frequencies. The more vertical

the curve at lower frequency regime, the more closely an ideal capacitor behavior is observed. The real part of the complex impedance (Z′) obtained by linear interpolation of the low frequency part of the Nyquist curve to Z″ = 0 represents the internal or equivalent series resistance (ESR) of the cell which limits the rate the cell can be charged/ discharged (power performance). The slope of the 45° portion of the curve signifies the Warburg resistance, and is caused due to the frequency dependence of ion diffusion/transport in the electrolyte. In Figure 6.2a, increase of conductive polymer and rGO content in ink causes lower ESR and therefore, better capacitive performance. The sample having 8.16% rGO shows a very low ESR of ~130 Ω. The ESR values for all compositions are reported in Table 2. As the conductive material content is increased, the spectra become more vertical at lower frequency regime further indicative of higher capacitive nature.

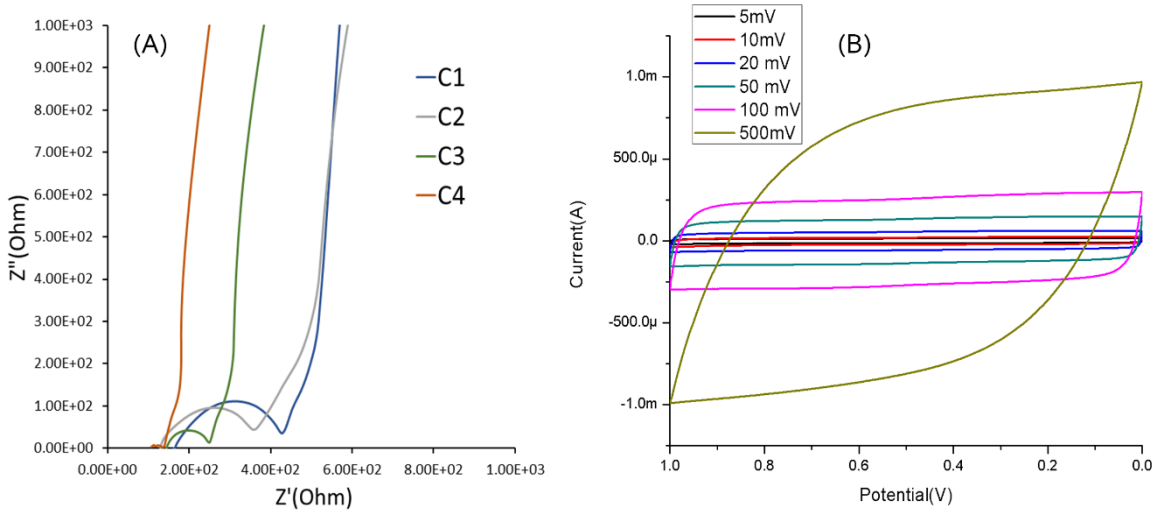

Figure 6.3 *Electrochemical characterization of all conductive ink compositions with (A) electrochemical impedance spectroscopy (EIS), and (B) Effect of scan rate on capacitance behavior of fourth composition.*

Table 6.2 *ESR values from EIS*

Composition	1	2	3	4
ESR (Ω)	425.1	245.3	247.6	130.7

To confirm the capacitive nature of the conductive ink, two parallel electrodes were patterned on silk fibroin films. The Agarose/NaCl gel electrolyte was used to perform CV experiments. Figure 6.3b shows the cyclic voltammograms of composition 4 at scan rate varying from 5 mV/s to 500 mV/s. Figure 6.2b portrays the characteristic symmetric and square shape of voltammogram up to 500 mV/s scan rate, indicative of a typical double layer supercapacitor charge injection mechanism. Comparative CV measurements conducted for all four compositions, acquired at a scan rate of 50 mV/s also depict that the increase of conductive material in ink improves the capacitance behavior (Figure 6.4). An important point to note that the capacitive performance can be further increased by reducing silk sericin content in the composite ink. However, further reduction of sericin content renders the ink unsuitable for patterning. The composite material developed here can be used without adding any sericin if micropatterning is not required. The above characterization indicate that the conductive inks show a very good capacitive behavior either as capacitive coating, or as a standalone electrode material. The versatility of the material is augmented by the fact that it can be photolithographically patterned on any functionalized substrate. Since, we are only interested in completely biodegradable systems, he later performance characterization was performed only with flexible all polymer supercapacitor patterns.

6.3.3 Performance of supercapacitors

The capacitive performance was evaluated by galvanostatic charge/discharge experiments. Parallel strip electrodes made from all four composition of ink show similar behavior observed with CV. The SCs made from composition 4 with 48% PEDOT:PSS and 8.16% rGO, provide impressive specific gravimetric capacitance of 148.28 F/g. The sp. capacitance obtained for the device is very competitive. The highest reported sp. capacitance for similar conductive composite system is ~380 F/g .[298] However, the use of H_2SO_4 electrolyte and carbon cloth charge collectors, makes the system unsuitable for biological applications. Other reports show much lower sp. capacitance ranging from 100-200 F/g.[279, 299, 300] The charge-discharge curves for all four compositions at current density of 1A/g are shown in Figure 6.5a. Charge-discharge experiments were done in triplicates and their rate performance are shown in Figure 6.5b. The linear profile of galvanostatic charge and discharge curves of all compositions and their symmetric triangular shapes are indicative of nearly ideal capacitive characteristics.

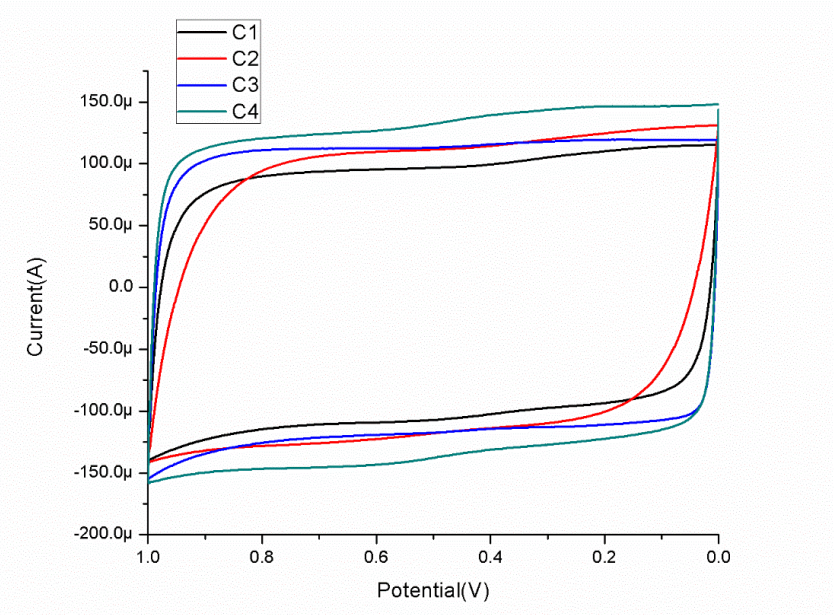

Figure 6.4 *Cyclic voltammogram of all conductive ink compositions at a scan rate of 50 mV/s*

Since the intended application of SC is for potentially wearable or implantable environments, a potential window of 0-0.5V was used, away from the water electrolysis window. It must be noted here that the patterns were made of fibroin films and did not have conventional metallic or metal oxide charge collectors. The strip patterns were connected to silver wires with silver paste at on end, the sealed using hermetic epoxy to avoid noise due to metal electrolyte interface. Further, the material has found to be stable up to 5A/g current density (Figure 6.5c). As the current density is increased, the discharge time decreases but no appreciable change in specific capacitance of the system is observed (Table (6.3)). The independence of specific capacitance on current density is a characteristic of ideal capacitor behavior. The electroactivity of a material depends on the speed of loading-unloading of charges through its matrix, and the number of active sites offered by the electrode. The increase in i-R drop from low to high current density show that the effect of internal resistance plays a role at higher loading-unloading of charges. Still, the charge-discharge curves at all current density remains mostly triangular and symmetric indicative of stability of system at various current load.

Table 6.3 *Effect of current density on capacitance of supercapacitor*

Current density (A/g)	0.2	0.5	1	2.5	5
Sp. Capacitance(F/g)	141	142.8	144.7	143	141.4

The application of semiconducting materials such as conducting polymers and rGO to form all polymer metal-free supercapacitors or with NaCl electrolytes, have not been very common. To further compare the conductive ink with other systems two type of experiments were conducted. In first experiment, conductive ink having 8.14% rGO was casted on ITO/glass substrate and tested

with agarose-NaCl electrolyte system. PVA-H_3PO_4 electrolyte was tested with strip patterns with 8.14% rGO. The sp. capacitance of the supercapacitors increase to ~221 F/g and ~178 F/g for experiments with ITO and PVA H_3PO_4 system respectively (Figure 6.6). These experiments are indicative of possibility of achieving better capacitive properties with this material with conventional supercapacitor configuration.

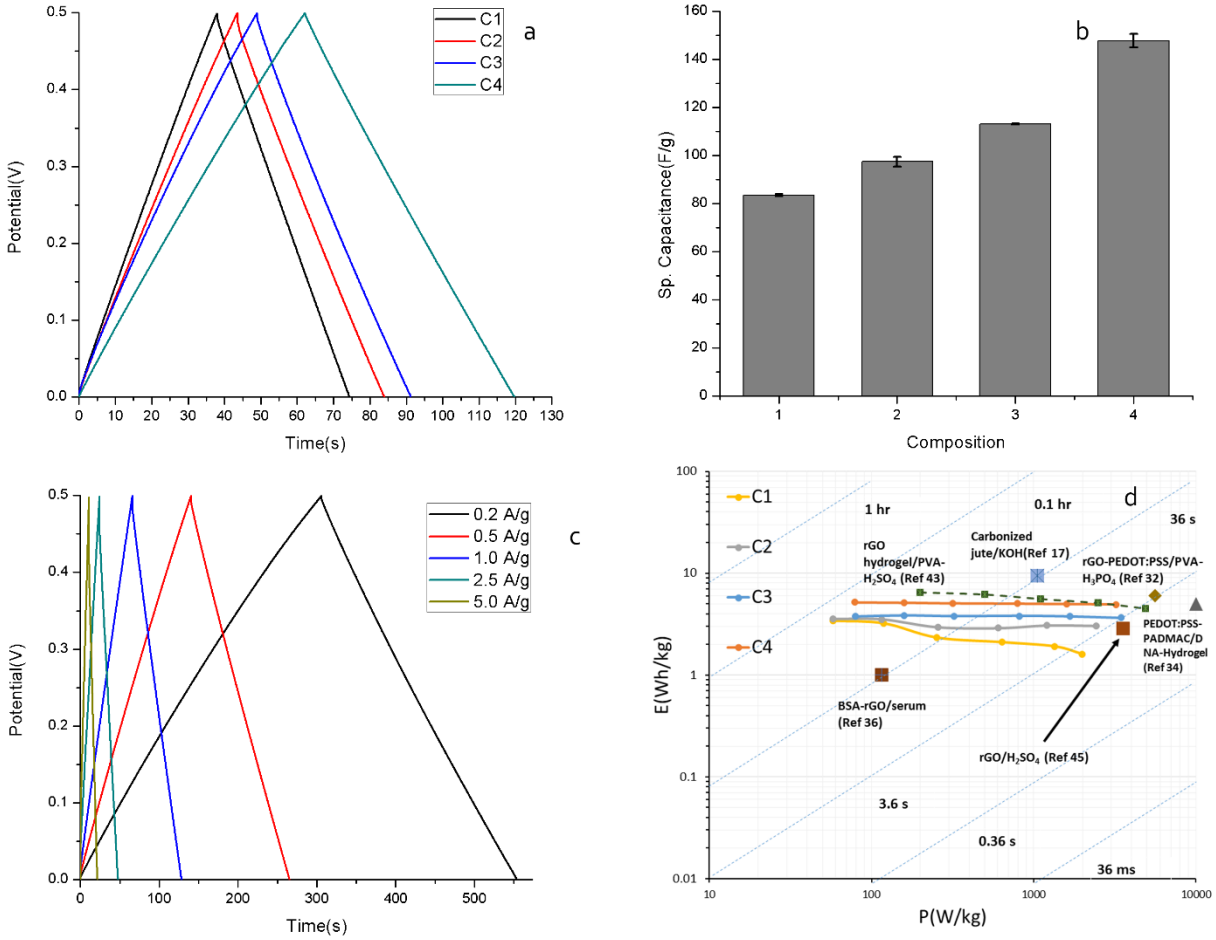

Figure 6.5 *Performance evaluation of supercapacitors (a) galvanostatic charge-discharge for compositions all compositions, (b) Sp. capacitance values for all compositions, (c) stability of supercapacitor over various current density, and (d) Ragone plot*

The overall performance of any energy storage material is shown via a Ragone plot (Figure 6.5d). Electrodes with highest PEDOT:PSS-rGO content can achieve a maximum power and energy densities ~3229 W/kg and 5.19 Wh/kg respectively. The energy and power density obtained in this work is similar or better than previous works having conductive material on non-conductive matrix or having combination of rGO/PEDOT:PSS supercapacitor system.[279, 286, 299, 301-303] The comparison with recently published supercapacitor works, suggest that the capacitance of the present system is very competitive (Table 6.4).

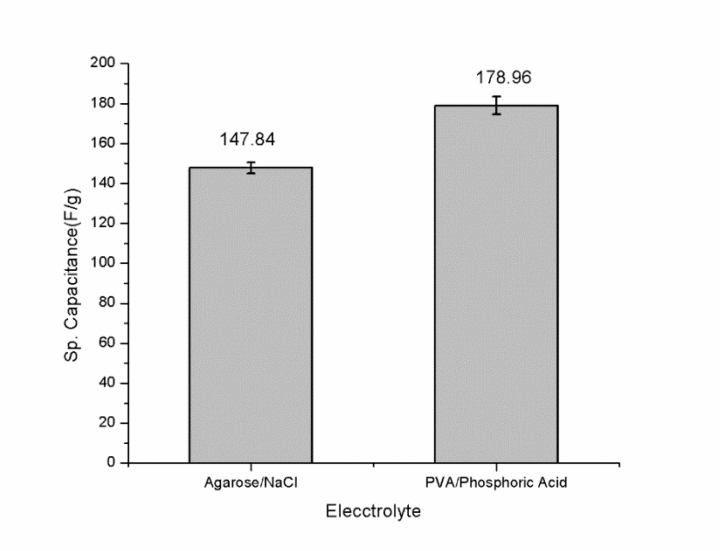

Figure 6.6 *Effect of electrolyte on capacitor performance*

Finally, the interdigitated supercapacitor design was tested and found to be displaying similar charge storage capacity as when the patterns were only two parallel strips. Interdigitated patterns were fixed with silver wires at the very end and insulated with epoxy. This was done to ensure that the supercapacitor device stays metal free and to avoid any false enhancement in capacitive behavior due to contact of electrolyte with silver. To test the long-term stability of the SCs, 500 cycles of run were performed on three samples. Assuming 10 charge-discharge cycles a day, the device only needs to be stable for 300 runs. The stability experiment reveals

capacity retention of ~ 91% after 500 cycles, and the charge-discharge curve remain symmetric and triangular without increase in I-R drop (Figure 6.7a and b).

Table 6.4 *Comparison of recently reported conductive polymer-rGO composite based supercapacitor performance*

Ref	Electrode material	SC configuration	Electrolyte	Highest gravimetric sp. capacitance(F/g)	Highest areal sp. capacitance (mF/cm^2)	Highest volumetric sp. capacitance(F/cm^3)
[304]	rGO	mSC	PVA/H_2SO_4		1.5	1.6
[286]	rGO/BSA/Myoglobin	sSC	Serum	306	1.5	
[299]	PEDOT:PSS/rGO	mSC	PVA/H_2SO_4		5.4	27
[301]	rGO hydrogel	sSC	PVA/H_2SO_4	186	372	
[302]	PPY/rGO/cellulose	sSC	PVA/H_3PO_4		0.51	8.5
[305]	Mesoporous carbon	mSC	PVA/H_2SO_4		9.05	12.92
[306]	rGO	mSC	PVA/H_2SO_4		19.8	41.8
[307]	Graphene	mSC	Ionic liquid			~20
[303]	rGO	mSC	PVA/H_2SO_4	43	0.7	
This work	**PEDOT:PSS/rGO/Protein**	**mSC**	**NaCl/Agarose**	**148.28**	**9.85**	**5.94**

Where, sSC= sandwiched supercapacitor, mSC= micro-interdigitated supercapacitors

Conductive polymers have been found to be unstable during the long-term charge/discharge processes, which is a major drawback in using for supercapacitor applications.[308] After 200 electrochemical cycles the electroactivity retention of the material was 90.5%.[228] In the present system the electroactivity retention after 500 cycles is similar to our previously reported values. Therefore, an improvement in electrochemical stability is observed with the addition of rGO in the conductive ink. rGO doping might further enhance the mechanical properties of the ink, causing a reduction in swelling and shrinking during long-term cycling. Therefore, the rGO doped composite ink exhibits an improved stability compared to our earlier developed conductive ink. In fact, four supercapacitors in series can light up a LED lamp of 20 mW for a few seconds showing the real-life applicability of such devices. (Figure 6.8)

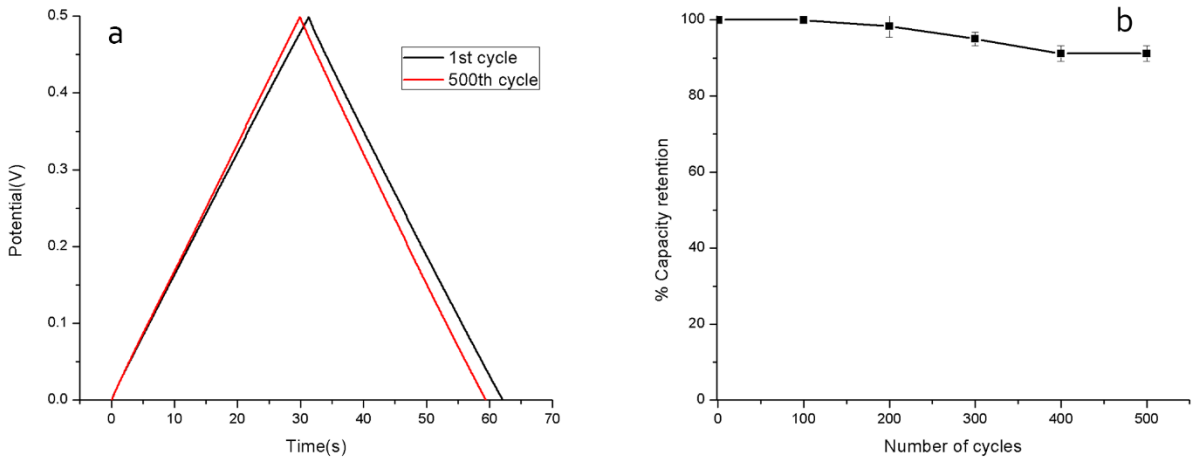

Figure 6.7 *Stability of supercapacitor, (a) change in charge-discharge curve after 500 cycles, and (b) change in capacitance over number cycles.*

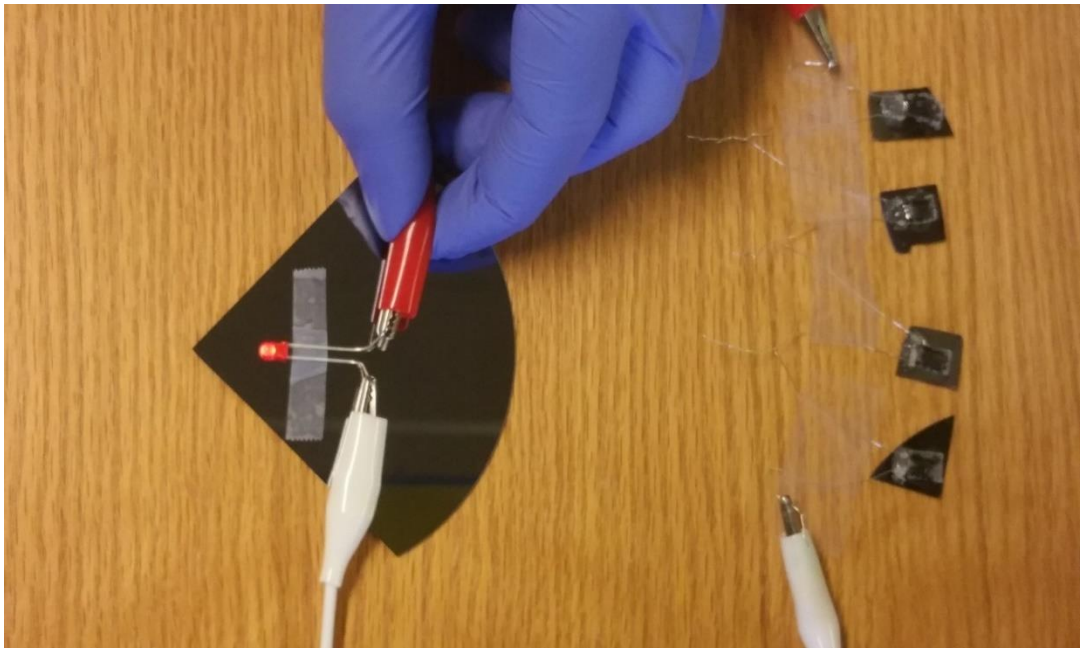

Figure 6.8 *Powering an LED lamp using 4 SCs in series.*

6.3.4 Bendability of the supercapacitors

The nature of implantable bioelectronics application can involve movement inside the body. Therefore, an important performance criterion is to evaluate device stability under different mechanical deformation states. The SC shows a negligible decrease in capacitance after 180° steady bend. The i-R drop increased slightly from 3 mV (flat) to 6 mV (180° bend) (Figure 6.9a). We further studied the capacitance retention of device during cyclic bending, where the device was bent up to 90° and flexed back in a cyclic manner. An impressive capacitance retention of 97.5% even after 450 cycles (Figure 6.9b) suggests that the device has excellent stability under applied mechanical stress. The overall results establish that all polymer-silk based supercapacitors show an electrical double layer capacitance behavior with fast, reversible capacitive nature. The fact that the device can deliver power densities comparable to the devices having toxic electrolyte and/or conventional charge collectors, also including green water based processing with readily

available material and techniques, provide a suitable alternative for powering emerging implantable flexible devices.

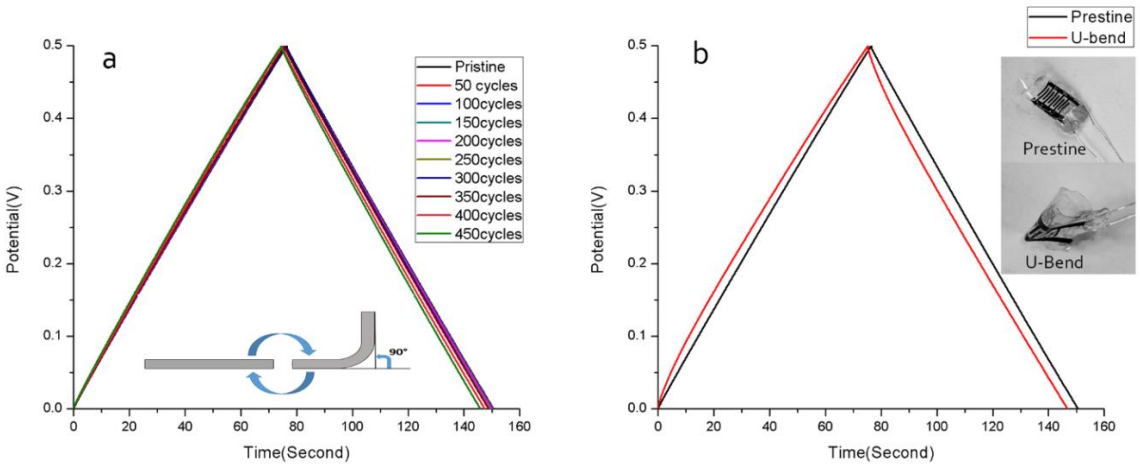

Figure 9 *Galvanostatic charge discharge curve showing stability under, (a) cyclic stress, and (b) static stress.*

6.3.5 Stability in liquid electrolyte medium

Survival of the supercapacitors in liquid environments is essential for the device to qualify for implantable applications. Therefore, the stability of the flexible device was studied in 0.1 M PBS buffer medium for 5 days. During this period, three samples were kept in PBS medium and galvanostatic C-D experiments were carried out each day. It should be noted that the supercapacitor system was not packaged, wherein PBS acted as the liquid electrolyte. Therefore, the observed capacitance of the system is lower than the earlier mentioned values. However, no physical delamination of the functional architecture from the FPP support is observed, indicating the mechanical stability of the device in liquid. The mechanical stability of the system resulted in stable capacitive performance of the system. C-D curves shown in Figure 6.10a is suggestive of the fact as the C-D curves stay symmetric over the period of 5 days with an unnoticeable increase

in i-R drop. The device retains ~99% of its initial capacitance performance even after 5 days soaking in PBS (Figure 6.10b).

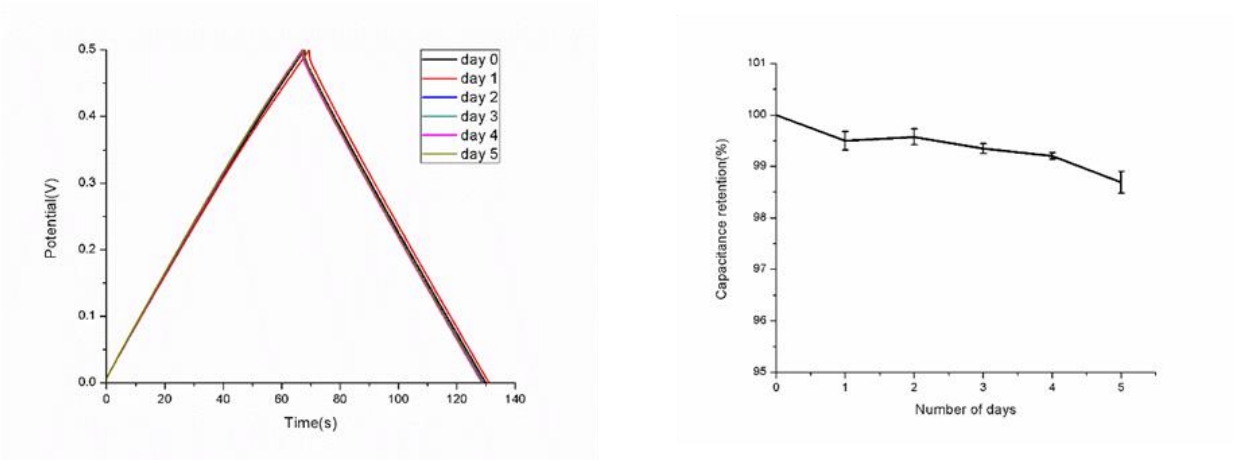

Figure 6.10 *Stability of supercapacitor in PBS over 5 days (a) C-D curves showing stable performance of the material, and (b) decrease in capacitance over 5 days.*

6.3.6 Biodegradability of supercapacitors

In previous chapters, proteolytic degradation experiments showed that the modified silk proteins and conductive ink composite could be degraded under protease action over a month.[309] Since the system now also contains rGO in matrix, a similar enzymatic degradation essay was studied. 3 samples were kept in protease medium and 3 samples in 0.1 M PBS medium (control) at 37° C. One sample from each set was taken out and washed. These samples were imaged using SEM to investigate degradation. Figure 6.11 shows the SEM images of degradation over three weeks. No appreciable degradation was observed on samples kept in PBS medium even after three weeks. Samples kept in protease medium were at different stage of degradation in each successive week. At the end of three weeks, the film breaks down as the film nanoscale morphology became fibrous from almost flat. This suggests that the degradation characteristics of conductive ink are not

hampered by rGO doping, and the conductive ink structures can be fully degraded over the period of 1 month. It should be noted that the crosslinking of SPP and FPP films/patterns can be controlled very readily by modulating the pendant reactive moieties in the protein backbone, therefore, bioresorption can be tuned as per the need.

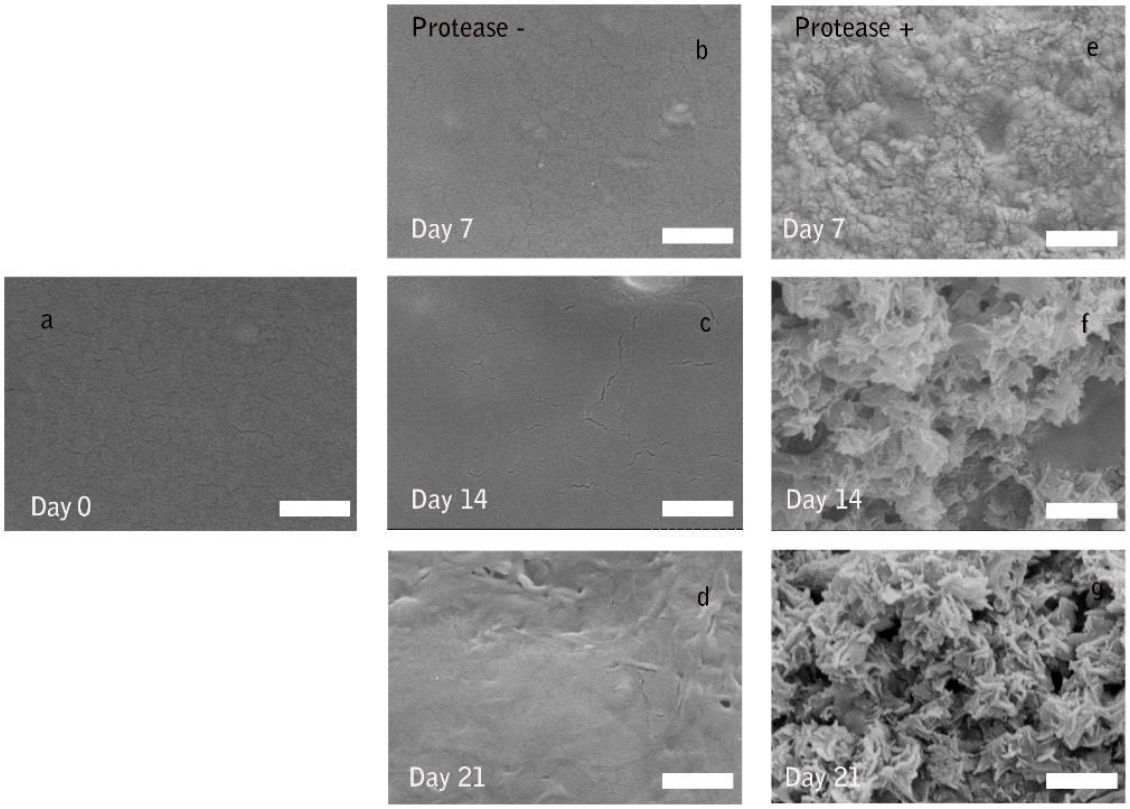

Figure 6.11 *Proteolytic degradation PEDOT:PSS-Silk supercapacitor devices: SEM images of conductive ink-silk proteins (A) at day 0, (B and D) at day 7, 1 and 21 in PBS buffer respectively, and (e and g) at day 7, 14 and 21 in protease enzyme solution respectively.*

6.4 CONCLUSION

In summary, this chapter describes an extension of the SPL technique and functional inks towards the development of lightweight, flexible energy storage devices based on silk proteins. This unique

approach involves the development of rGO doped conductive inks for SC electrodes, and gel electrolyte with benign and readily available materials. The composite of PEDOT:PSS and rGO in the silk protein matrix show impressive charge storage and excellent performance with high energy density and power density, without use of harsh electrolytes or metal contacts. The device is stable under static as well as dynamic mechanical deformations, and in liquid electrolytes over several days. The in-series connected supercapacitors can even power a commercial red LED. The fact that most of the device mass is comprised of proteins and polysaccharides (agarose), implies that the device can be degraded inside body over a period of time. Therefore, the system is suitable for implant-and-forget kind of configuration. There exist possibilities to further modify the device configuration and performance by using biological fluids as electrolytes and redox polymer materials.

[This chapter contains results that have been submitted for publication: R.K. Pal, S.C. Kundu, V.K. Yadavalli, "Fabrication of an organic, flexible, and biodegradable micro-supercapacitor", 2017]

CHAPTER 7

NANOSCALE PATTERNING OF SILK BIOCOMPOSITES

7.1 INTRODUCTION

Patterning of functional materials at different length scales in a precise fashion plays a key role in various research fields such as material science, optics, electronics, medicinal science, cell biology, and tissue engineering.[310] In the previous chapters, microscale patterning of silk proteins and conductive composites at length scales from micron to centimeter on various formats have been shown using photolithography. Even though the photolithography technique is very versatile, the feature resolution is a function of the wavelength of the light used. Taking the diffraction limit into consideration, the minimum resolvable feature size achieved through photolithography is determined by the equation: [311]

$$R = \frac{3}{2}\sqrt{\lambda\left(s + \frac{z}{2}\right)}$$

where, λ is the wavelength of light, s is the gap between the mask and photoresist surface (μm) and z is photoresist thickness. Depending upon the mode of photolithography, the minimum resolution can vary from 3 μm (s=10 μm) to a low of 0.6 μm (s=0). Following the successful development of microscale patterning of silk proteins and conductive polymers, the next logical step forward is to develop a process that can be used to manufacture *nanoscale* functional features beyond light based lithography. Nanoscale protein patterns are particularly advantageous in many

application areas such as proteomics, cell research, and pharmaceutical screening. Device miniaturization can also open other application areas which are not possible by microscale patterns such as field effect transistor based nano-biosensor and nano-optics/-photonic architectures (e.g. dielectric metamaterials).[312-314]

To date, different patterning techniques have been shown to pattern proteins, biopolymers and conducting polymers such as nanoimprint lithography, dip pen lithography (DPN), femtosecond laser direct writing (FsLDW), polymer pen lithography (PPL) and electron beam lithography (EBL).[87, 315-319] However, each of these techniques have pros and cons. For instance, nanoimprinting allows for rapid generation of patterns, but requires a suitable template. The use of toxic chemicals for processing, and often, high temperature and pressure requirements are some disadvantages. Preparation of dense patterns is also difficult due to loss of fidelity, or incomplete molding during transfer steps, limiting biomedical applications.[81, 86] DPN and PPL enable direct write methods with nanoscale pitch, but are relatively slow and often limited to simple dot arrays.[320, 321] In contrast, EBL is a serial process and requires significantly longer exposure times. However, this technique allows for the generation of user-defined shapes with high resolution and fidelity. EBL provides nanoscale alignment allowing multiplexing and high density patterning.[322, 323] Furthermore, the integration of EBL with photolithography protocols are well developed, making it easy to realize nanoscale active systems. [324]

Similarly, patterning of conducting polymers at nanoscale has been rare.[325] The nanoscale patterning of conducting polymers by EBL often requires complex multistep processes and harsh

chemical which might render it unsuitable for biological applications.[326] Direct writing of silk proteins by EBL has been shown recently, where silk fibroin was used as a positive or negative resist for protein patterning.[87] Even though the process was all water based, the use of high energy irradiation with electrons for patterning is not ideal for protein patterning. Therefore, there is a need to develop a low-energy EBL process that can pattern silk proteins and conducting polymer is required for biological applications. It should be noted that most negative EBL resists such as ZEP (Nippon Zeon) are based on acrylate chemistry for crosslinking which require lower energy.[327] Given that the silk protein photoresists developed in this work possess methacrylate moieties as pendent groups, there exists the possibility to employ them as EBL resists and form nanoscale architectures. This chapter focuses on these studies.

Several design considerations are needed to enable this process. For instance, the development of EBL for patterning of silk protein resists and conducting polymer composites needs to be performed on silicon substrates since they enable better change dissipation and formation of high fidelity patterns. Optimization of EBL parameters such as acceleration voltage and peak current are needed to obtain the dosage to fabricate negative/positive silk patterns. Next, the composition of the inks in the composite which can be used to form nanoscale patterns need to be optimized. Since, the aim is to form nanoscale patterns, the particle size of PEDOT:PSS used in the process can be a limiting factor. Finally, the conductivity of the nanoscale patterns can be characterized using a technique such as conductive-AFM. Previous reports have shown the dual tone nature of silk proteins, which is also studied.[87] The work discussed will lead to the development of a low energy, intensive, photoinitiator free and water-based one step EBL process for patterning of silk proteins and their conductive polymer composites.

7.2 EXPERIMENTAL

7.2.1 Materials, synthesis of photoresists and surface functionalization.

Materials and chemicals were the same as described in Chapter 4. The synthesis and purification of fibroin and sericin photoresist materials (FPP/SPP) were the same as described in Chapter 2. Functionalization of Si was the same as shown in Chapter 4.

7.2.2 Electron beam lithography (EBL)

FPP (1 mg) in formic acid (40 µl) solution or conductive ink solution containing 10% PEDOT:PSS was spin coated on functionalized silicon wafers at 2000 RPM with ramp up of 100 RPM/second^2 for 30 seconds. The thickness of the resist was ~100 nm. EBL was performed in a Hitachi SU-70 FE SEM equipped with a Nibity Nanometer Pattern Generation System (NPGS). The electron beam was used at an accelerating voltage of 30 kV and 60 pA beam current. An accelerating voltage of 20 kV and 40 pA beam current were used for obtaining positive and negative tone behavior. As a preliminary step for EBL processing, the electron beam dosage for efficient cross-linking of silk resist was optimized. A range of dosage exposures (10–20000 µC cm^{-2}) were tested to obtain the optimum dosage required to generate stable micropattern array features without excessive degradation and overexposure.

7.2.3 Characterization of nanoscale patterns

Optical microscopy was performed on a Nikon Eclipse microscope. Atomic Force Microscopy (AFM) analysis of surface morphology was performed on an Asylum Research MFP-3D AFM

(Santa Barbara, CA), operating in AC mode with an AC240TS tip (nominal k = 2 nN nm^{-1}, Olympus, Japan). Conductive imaging was performed using a conductive AFM technique (ORCA^{TM}). A voltage (500mV) is applied to the substrate, and the current is recorded using an internal preamplifier (Asylum Research ORCA model, sensitivity 2 nA V^{-1}). Pt/Ir-coated AFM tips (AC240TM-R3) (Oxford instruments) with a frequency of 2 N m^{-1} and spring constant of 70 kHz were used. I-V characteristics were measured on a Keithley 4200 semiconductor characterization system (Keithley Instruments, Cleveland, OH).

7.3 RESULTS AND DISCUSSION

7.3.1 Development of EBL protocol

Both modified silk proteins (fibroin and sericin) were considered as candidates for nanoscale patterning via EBL. However, fibroin was ultimately chosen for optimizing the EBL parameters owing to its mechanical stability. Initially, FPP was dissolved in HFIP and the solution were spin coated on silicon wafer. Previous reports on EBL patterning of silk proteins suggested very high dosages of electron beam 2,250 µC cm^{-2} (positive) and 25,000 µC cm^{-2} (negative). As a point of reference, this is 2.5 times higher dosage than that required for PMMA.[87] which is primarily used as a positive resist.[328] As a starting point, optimized EBL parameters of PMMA for SU-70 FE SEM were used. The parameter used were: center to center (C to C) spacing = 5.82nm, line spacing 5.82 nm, point dosage: 0.35 to 0.85 fC (Area dosage), acceleration. Voltage= 30KeV, magnification =1000x, Peak current: 60 pA. The initial design was 400 nm x 5µm line array. The optical images of these pattern did not show any patterns, but indistinct blobs at the exposure site (Figure 7.1). The images indicate overexposure of the patterns. Consequently, in the next

experiment, the dosage was lowered and the pattern design was updated with 10 µm posts, 400nm ×1µm line array and 400 nm dot array. With a lowered point dosage 0.05 fC (area dosage 147.74 µC/cm^2) (Figure 7.2a), the optical images show features with overexposure. However, the AFM images show that the features were *positive* instead of *negative*. The overexposed area was negative. It should be noted that these features are obtained in the absence of a photoinitiator. Outside the overexposed area, a good development was observed. These experiments suggested that higher doses cause the FPP to behave as a positive photoresist and to obtain a negative pattern, lower dosages are required. Meanwhile, the high volatility of the HFIP solvent also renders control of thickness using spin coating very difficult. Due to this, the optimization of various dosages proved difficult. Recent work from our group showed that nanoscale thin films could be obtained using formic acid(FA) as a solvent due to its lower volatile nature than HFIP.[203] Therefore, later experiments were conducted using FA as a solvent.

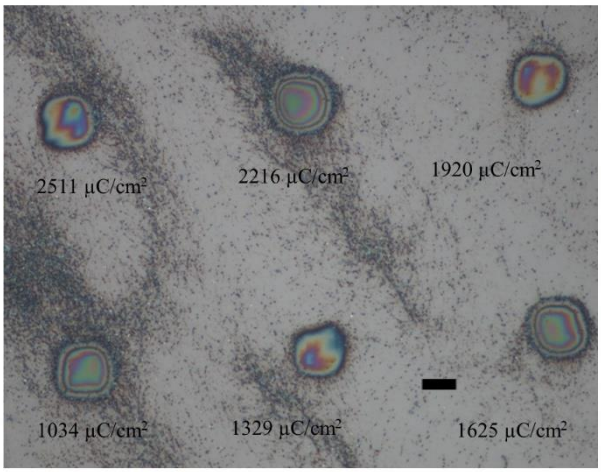

Figure 7.1 *First EBL experiment area dosage written below of each pattern (scale bar =5µm)*

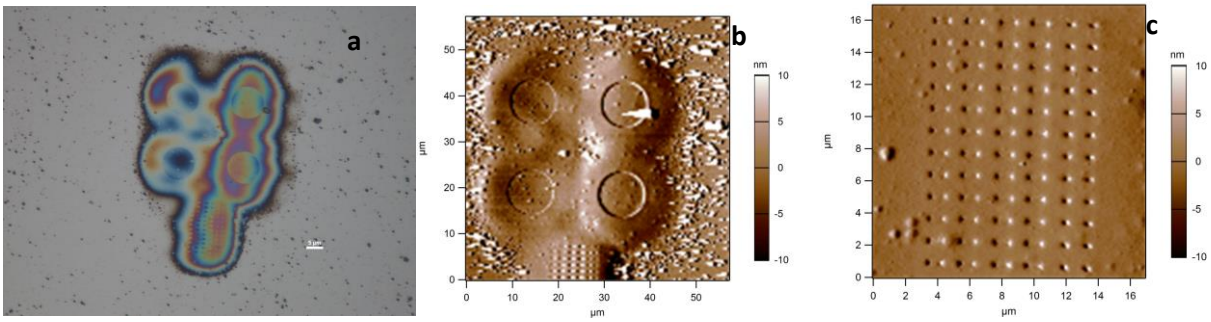

Figure 7.2 *Second EBL experiment with lower dosage. (a) Optical image of pattern, AFM image of (b) microscale dots, and (c) nanoscale patterns.*

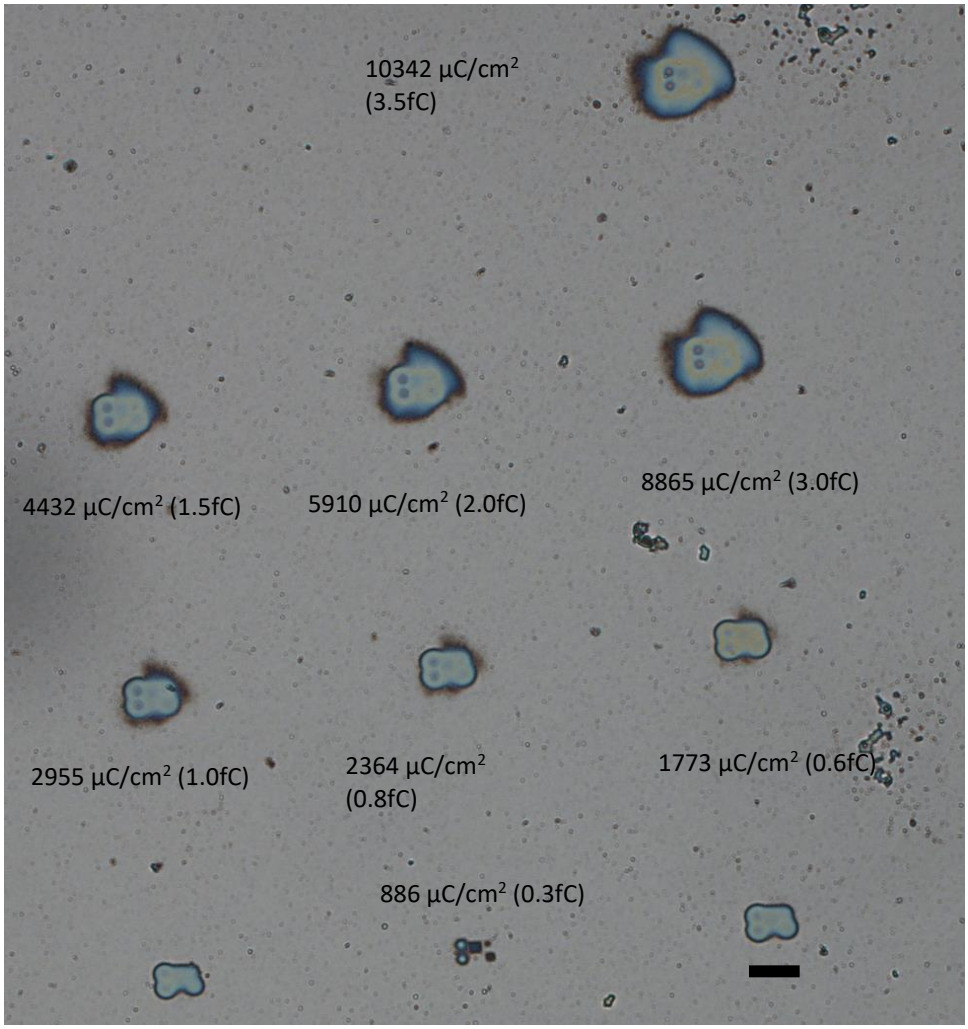

Figure 7.3 *EBL dosage optimization for FPP patterns of ~100 nm thick film. The area dosage and point dosage (in small bracket) shown adjacent to each pattern (Scale bar=20 µm).*

Using FA as the solvent a 100-nm thick film was obtained. A new design was made having 5 µm dots, and 400 nm, 300 nm, 200 nm and 100 nm dot array having same periodicity. The dosage was varied over three orders of magnitude to understand the effect of dosage on the patterning (Figure 7.3). It was observed that the lowest area dosage (44 µC/cm^2) resulted in better developed patterns. However, further lowering of dosage were not possible at 30 KeV. Therefore, the next experiment was conducted with an acceleration voltage of 25 KeV and peak current of 45 pA.

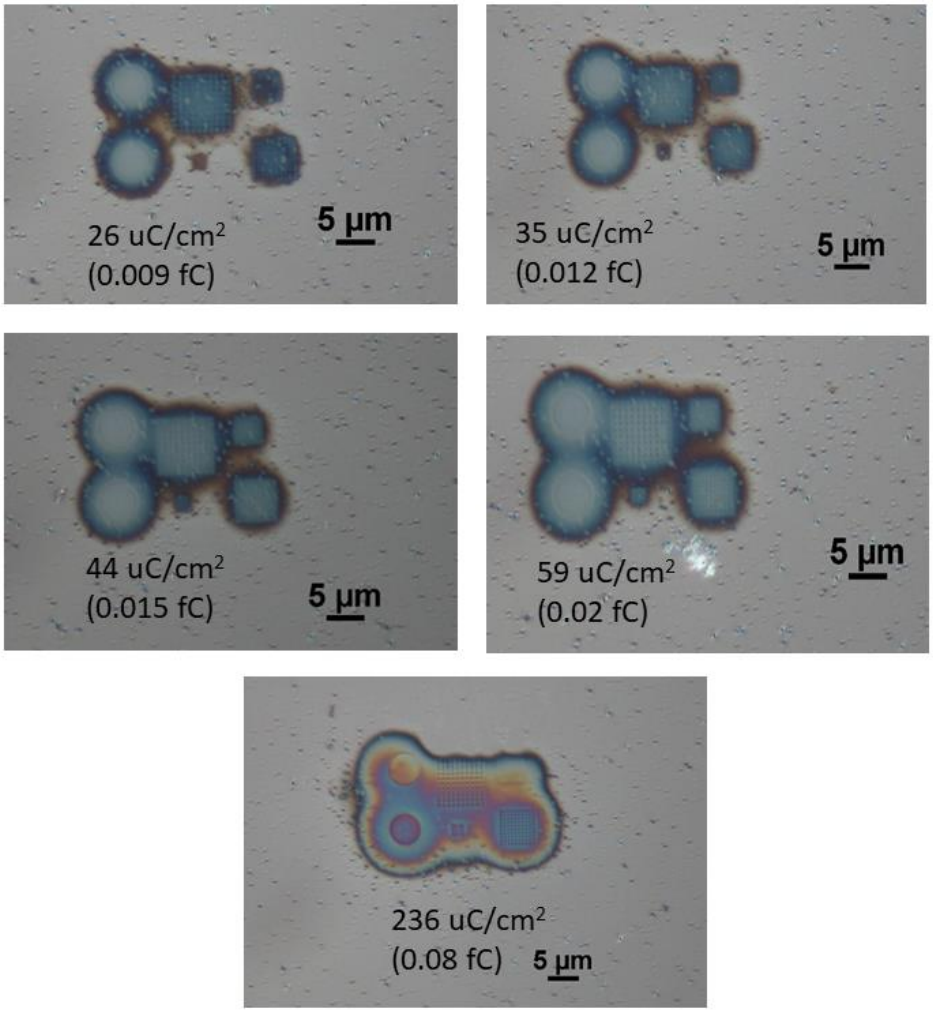

Figure 7.4 *EBL of FPP with varying dosage at 25 KeV acceleration voltage and 45 pA peak current.*

Comparing the dosage of 44 μC/cm^2 with the acceleration voltages of 30 KeV and 25 KeV show that the patterns are better developed at *higher* acceleration voltage. This counterintuitive result show may be due to the increased reaction time of the low energetic beam with the resist layer leading to more secondary electrons. The study also suggests that even lower dosages are required to achieve proper development. A report on optimization of EBL parameters for negative resists show 20 KeV acceleration voltage as optimal.[329] Thus, in the next experiment 20 KeV acceleration voltage and 40 pA peak current were used with resist thickness of ~100nm. In this experiment, the lowest possible point dosage was used with varying point to point distance.

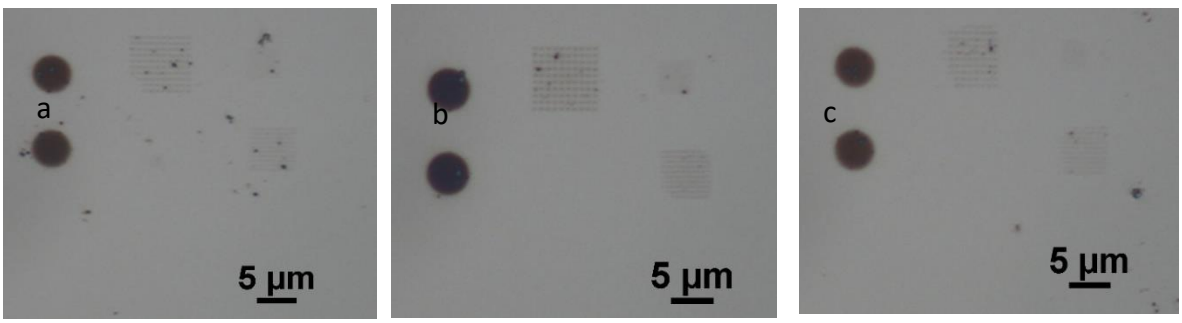

Figure 7.5 *EBL parameter optimization with point doze of 0.008 fc with varying point to point distance (a) 11.63 nm, (b) 13.09 nm, and (c) 16.00 nm*

The area dosage obtained with 11.63 nm, 13.09 nm and 16.00 nm were 5.91, 4.67 and 3.12 μC/ cm^2 respectively. Since the 13.09 nm point to point spacing show best development to confirm the parameters, 400 nm arrays with 400 nm pitch were fabricated using same conditions (Figure 7.6). The optimization process reveal that a very low dosage (4.67 μC/ cm^2) is required to obtain patterns by EBL. The dosage is ~5000 times lower than the previously reported EBL work with silk proteins.[87] Another report on EBL patterning using PEG shows a dosage requirement of 100 μC/cm^2 for 6.8 kDa PEG and 3 μC/cm^2 for 200 kDa PEG, indicating that the dosage depends on the degree of polymerization.[324]

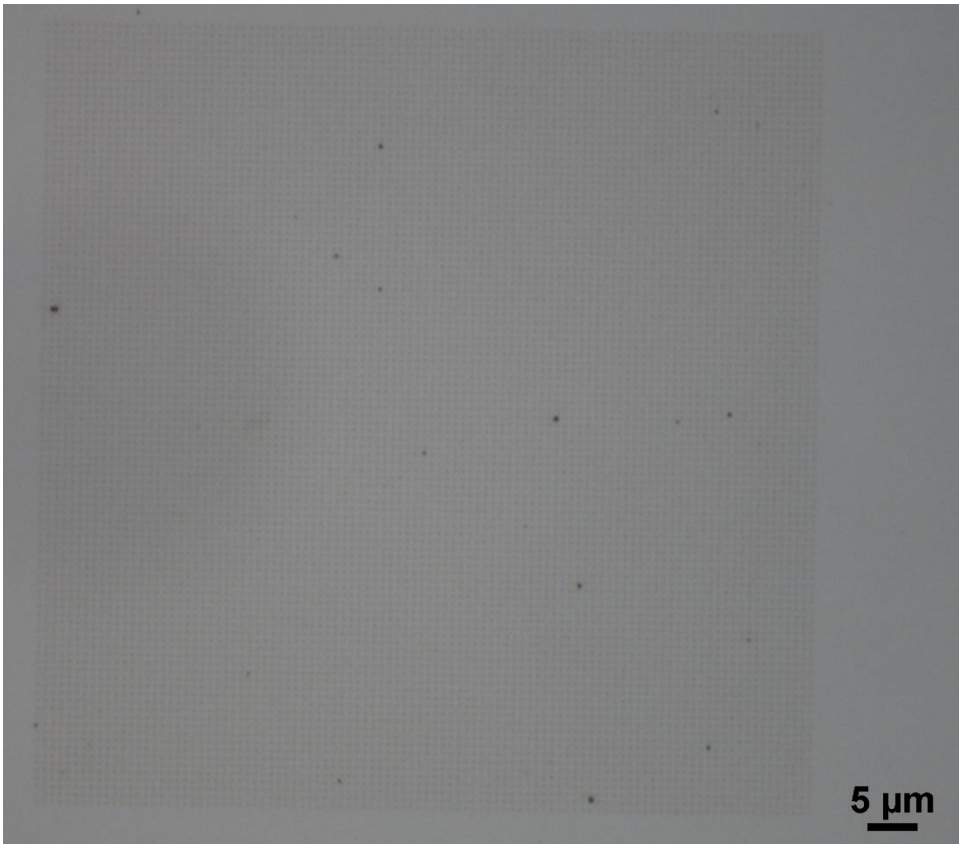

Figure 7.6 *400 nm FPP dot array with optimized parameters.*

7.3.2 Dual tone nature of silk protein resist

Initial experiments with FPP resists show that negative patterns can be obtained using lower beam dosage. Based on prior reports, silk proteins can behave as dual tone resists (i.e. it is possible to obtain both negative and positive patterns). In order to obtain positive patterns on FPP films, the FPP in FA solution with photoinitiator was initially crosslinked using UV light. This film can be used to form positive patterns by de-crosslinking the protein using energetic electrons in EBL. Figure 7.6 shows the patterns obtained with ~2500 µC/cm^2 at 30 KeV acceleration voltage and 60 pA peak current. Here, the dosage required to form positive pattern are similar to the earlier reported dosage for silk. [87] The results are expected since the positive tone is obtained by

breaking down the silk proteins into short polypeptides by incident electron beam.[87] It may be noted that the mechanism of negative pattern formation is due to crosslinking of methacrylate moieties which is a less energy intensive reaction. The lower energy in comparison to earlier reports can be explained by considering that negative tones can also be obtained by amorphous-to-helix folding of the silk fibroin, coupled with formation of intermolecular crosslinks via radiolysis, which in turn made the protein water-insoluble.[87]

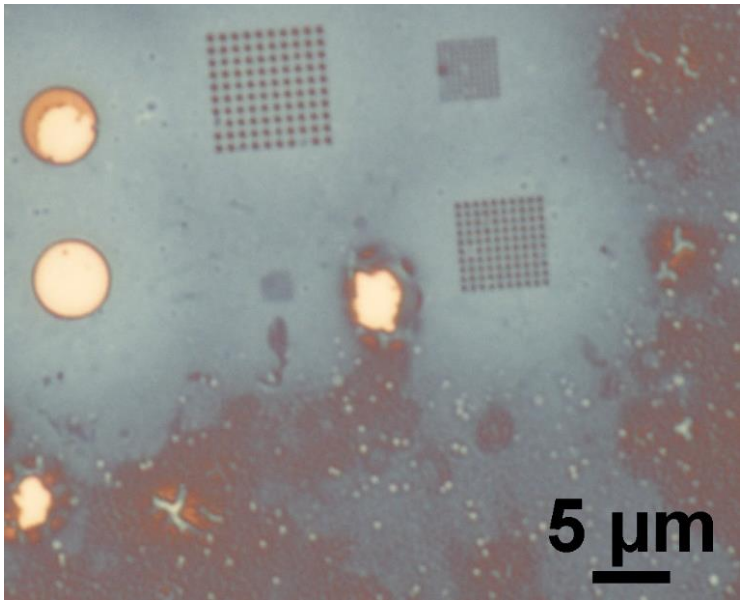

Figure 7.6 *Positive patterns on crosslinked FPP film*

7.3.3 Nanopatterning of conductive ink

In previous chapters, silk sericin and PEDOT:PSS based conductive composites were reported. Thus, the idea of using EBL to form conductive nanowires was explored. Due to the presence of methacrylate groups in the SPP, patterning of the conductive inks described previously via EBL is theoretically possible. However, keeping in mind the scale of the patterns, the PEDOT:PSS used in this case was 0.2 nm filtered instead of 0.45 nm filtered. Similar EBL parameters were used to pattern conductive composites. Initial experiments with 19% PEDOT:PSS did not form any

patterns, presumably because of lower crosslinkable components (SPP). Therefore, in the next experiment, conductive ink containing 10% PEDOT:PSS was used to form 400 nm, 300 nm, 200 nm and 100 nm width lines. It is interesting to note that the dosage required to form conductive composites is similar to that using FPP.

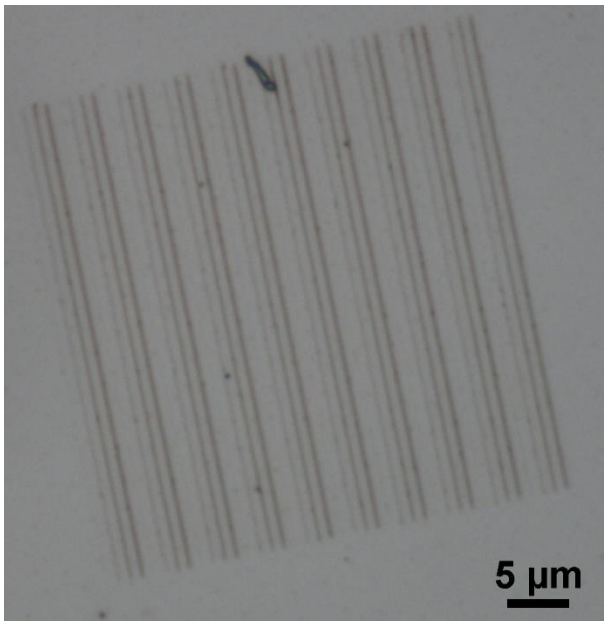

Figure 7.7 *Nanopatterns of conductive ink via EBL*

7.3.4 Electrical characterization of conductive ink nanowires

Electrical characterization was then performed to verify that the conducting polymer is retained in the nanowires and not leaching out. Several trials were performed with conductive nanowires on metal pads to measure I-V characteristics (Figure 7.8). However, due to lack of functionalization on metal pads, the patterns did not adhere to pads and failed to form an ohmic contact for I-V measurements.

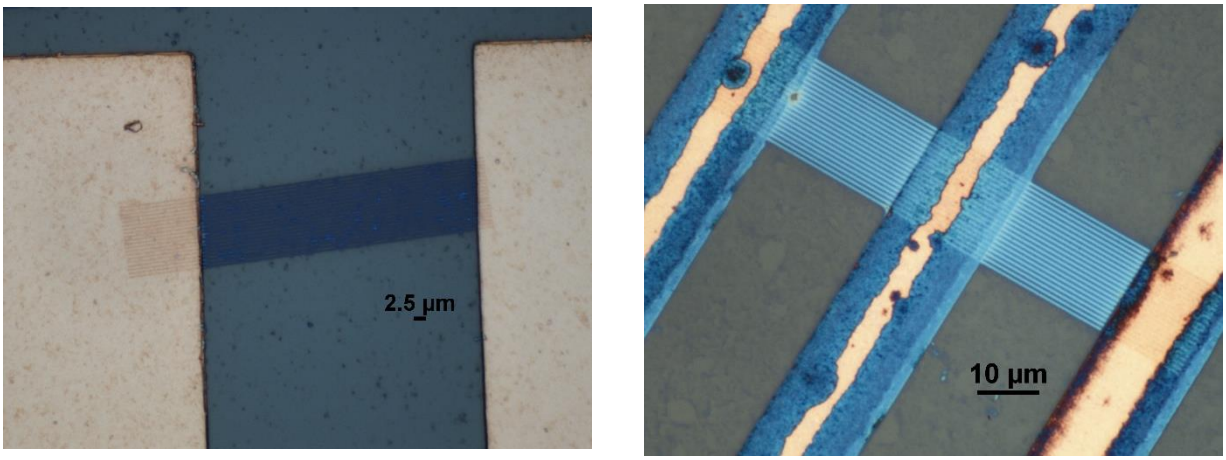

Figure 7.8 *Unsuccessful patterning on copper pads for I-V measurements.*

Silver paste was then explored to form pads after patterning of conductive ink. The challenge was that the EBL instrument has a maximum line with of 90 µm/exposure window. Given the length scales, multiple partially overlapped patterns of conductive ink were formed by precisely moving the EBL beam from one exposure to other (Figure 7.9a). The silver paste pads formed on the patterns are shown in Figure 7.9b.

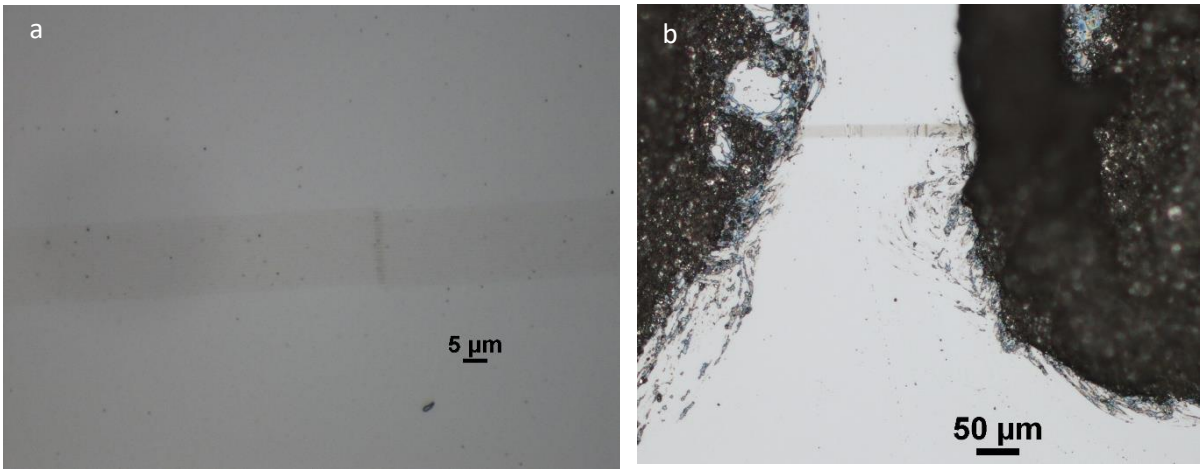

Figure 7.9 *Patterning of conductive ink in series, and (b) connection by silver paste.*

However, even with this setup, the I-V characteristics did not show an stable response, presumably due to the ineffficent contact in between patterns or silver paste and patterns (Figure 7.10).

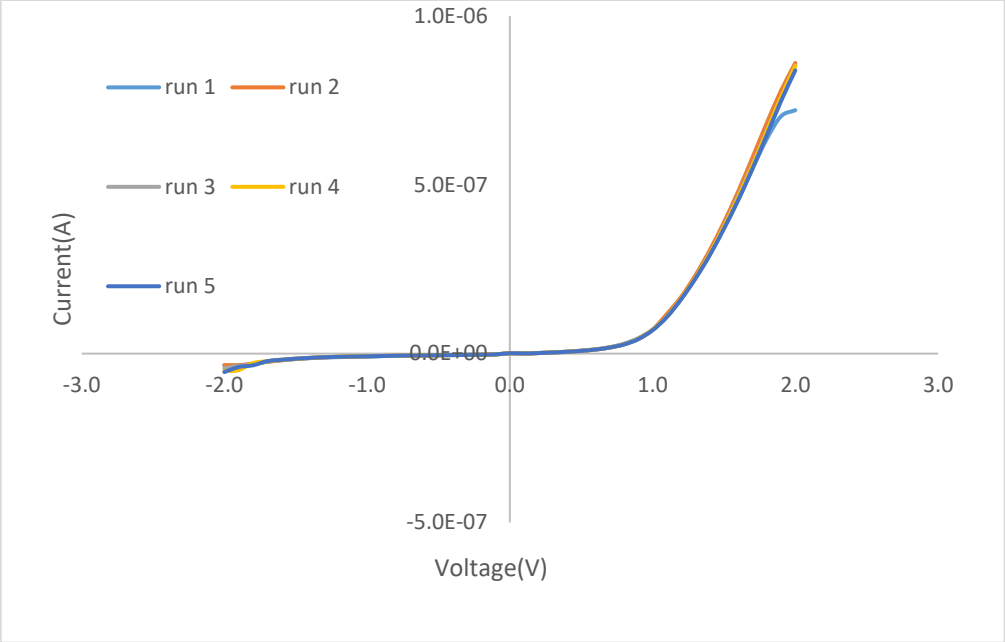

Figure 7.10 *I-V characteristics of conductive ink nanopattern lines.*

Finally, conductive ink patterns with conductive pads were fabricated for conductive AFM measurements which proved successful (Figure 7.11).

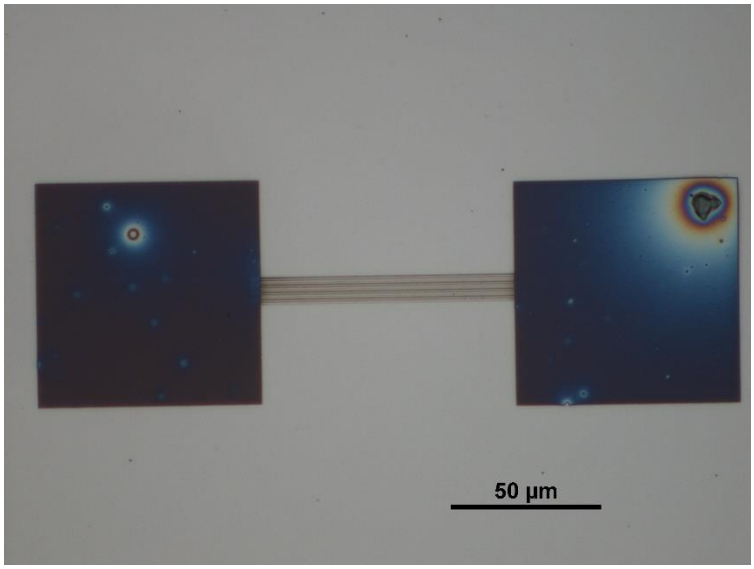

Figure 7.11 *Conductive ink patterns with conductive ink pads for C-AFM study.*

The conductive nature of nanoscale patterns can be clearly observed. While the study affirms qualitatively that even at nanoscale silk sericin can entrap conductive polymer particles of similar length scale (Figure 7.12), it is clear that further trials are necessary to optimize the formation of nanowires and their structure to obtain better performance metrics.

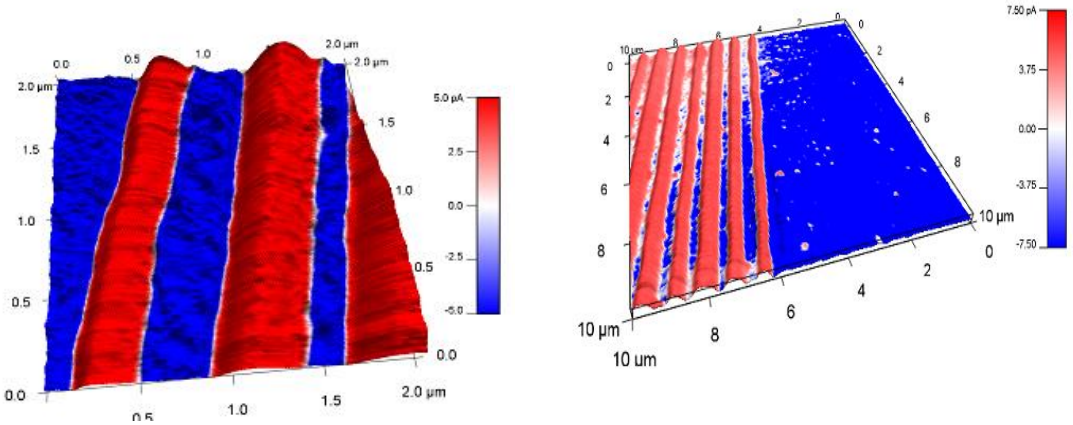

Figure 7.12 *C-AFM images showing conductive nature of the nanoscale wires.*

Overall the work shows that a relatively less energy intensive EBL can be performed using modified silk proteins. Also, the approach can be extended to pattern conductive polymers such as PEDOT:PSS in all water-based one step fabrication at the nanoscale. The dimensions of the lines fabricated (down to 100 nm) have never been shown using a protein based material before. Formation of a conductive nanowire using a protein + conducting polymer at this length scale is also unprecedented. This study therefore opens up new avenues to form biodegradable nanowires for green bioelectronics which can be investigated.

7.4 CONCLUSION

The present chapter shows the successful development of a low-energy electron beam lithography (EBL) procedure. For the first time, it is shown that EBL can be used to form silk protein features

of 100-200 nm in a precise manner. The work also show that previously developed conductive ink composites can be patterned to form precise and dense nanoscale conductive architectures. Conductive AFM study of the nanoscale features show that the silk proteins can entrap conductive polymer particles, resulting in water-based conductive polymer patterning at the nanoscale. Further, the technique shows the dual tone nature of the silk resist materials, whereby both positive and negative features can be patterned by simply varying the energy of the electron beam used. While quantitative characterization and performance optimization are currently being studied, it can be envisioned that the developed EBL protocols can be used for various life science applications involving nanoscale protein patterning.

CHAPTER 8

CONCLUSIONS AND FUTURE DIRECTIONS

8.1 CONCLUSIONS

The techniques discussed in this research for the functionalization and fabrication of natural materials to impart properties that result in applications in therapeutics, bio-optics and bioelectronics are still in nascent stages. There are unique opportunities to develop a number of systems such as smart and targeted drug delivery, real-time biological sensing, and recording, stimulation and modulation applications for future health care and study. As discussed above, the nature of such applications poses challenges for ensuring properties such as biocompatibility, bio-resorbability, flexibility/conformability, along with the ability to combine specific electrical, optical and biochemical functionalities. Silk proteins, among various biopolymers are unique in the ability to address the compatibility issues present at the biotic-abiotic interface. These materials therefore require specific functionalization and fabrication approaches to allow processing into functional devices for execution in therapeutics and bioelectronics.

To meet these goals, the research described in this dissertation is focused on fundamental and applied investigations on functionalization of silk proteins (sericin and fibroin) and their fabrication to realize functional devices. These studies led to the development of smart doping processes and new fabrication strategies to enable the control of complex architectures and

functionality across multiple length scales – from the nanoscale to the macroscale and on different formats (rigid to flexible).

The research outlined in this dissertation can be summarized as below:

1. *Development of photolithographic fabrication methods to micropattern silk proteins in flexible formats*. The biochemically modified silk protein photoresists were used to develop a photolithographic technique in prior research. This work extended the SPL technique towards flexible and functional formats. Initially, photolithographically micropatterned silk proteins produced angle-dependent structure-induced iridescence and light focusing devices. These optical systems were printed on flexible protein sheets to form soft, degradable systems that are nonetheless mechanically stable in air over several months, and stable in liquids for weeks. The proteolytic degradation can be controlled by the degree of cross-linking of the proteins.
2. *Utilizing the unique immobilizing properties of silk proteins to form functional composites*. To harness and facilitate these properties, initially free-standing high-precision microscale shapes (of various non-spherical geometries) and sizes ranging from 5 to 100 μm was demonstrated. The benign fabrication process can be used to manufacture large numbers of biodegradable particles rapidly and inexpensively at the benchtop without any cleanroom requirement. Again, degradation rates can be controlled by varying the size, shape, thickness and the degree of cross-linking of the proteins. Silk photoresists were then explored for functional biocomposites by mixing with conducting polymers and dopants to induce electrochemical activity.
3. *Application of silk-based devices to next-generation bioelectronics:* Based on the biocomposites developed, new electronic materials could be exploited without hampering the intrinsic biocompatibility and biodegradability of silk proteins. The SPL technique was then

used to electrode patterns on rigid and flexible formats with features across four orders of magnitude (1 μm to cm). Devices formed are mechanically stable, optically transparent, flexible, biocompatible, and degradable using all water based, green microfabrication processing. The electrode matrices offer suitable environments for the encapsulation of proteins and enzymes and shown to be useful for electrochemical biosensing with high sensitivity and selectivity. The approach can be extended to attain capacitive properties in the composite matrix by the benign addition of graphene resulting in a flexible microsupercapacitor. Opportunities for transient bioelectronics with a programmable loss of function can therefore address pressing challenges in organic (bio) electronics for applications in cell guidance, stimulation, recording, biosensing, and smart therapeutics.

4. *Patterning of functional materials at different length scales:* Development of multiscale, high fidelity microfabrication can enable precise functional devices in different areas. This research explored patterning from the nanoscale (EBL) to micro and macroscale patterning (photolithography). A low energy electron beam lithography (EBL) procedure was developed to form nanoscale architectures of silk proteins and silk-conductive polymer nanowires. Characterization of the features show entrapment of conductive polymer particles even at the nanoscale leading to conductive nanowires. Further, the technique shows the dual tone nature of silk-methacrylate resist.

Considered together, these experimental investigations portray a clear picture of the path taken to develop functional materials and devices considering earlier knowledge and by creating new knowledge. The work is a step towards the realization of the ultimate goal of completely biocompatible, biodegradable functional devices for biomedical applications. Further development

of shown approaches will extend the utility of silk proteins within the fields of therapeutics, bio-optics and -electronics. The implications of the work go beyond the scope of the tested applications. For instance, the approaches may also be applied to other natural and synthetic biopolymers that are recently being developed. However, the conclusions and technical advancement achieved from the work represent only incremental steps to the original challenges present in the biomedical field. The next section will suggest extensions of the work to provide a path forward towards addressing bigger challenges.

8.2 FUTURE DIRECTIONS

8.2.1 Patterning of fibroin on flexible fibroin sheets

In Chapter 2, it was mentioned that the fabrication of fibroin microarchitectures on fibroin was challenging due to the use of HFIP as a solvent. The formation of devices that are fully fabricated using fibroin will have application in the development of flexible optics and where the microarchitecture rigidity is important. Recent experiments suggest that the fibroin on fibroin patterning is possible by using a two-solvent strategy. Formic acid and HFIP can be used to form films and patterns respectively. A successful patterning of fibroin on fibroin is shown in Figure 8.1, which can create new opportunities for flexible devices such as multilayer patterning and flexible optical waveguides.

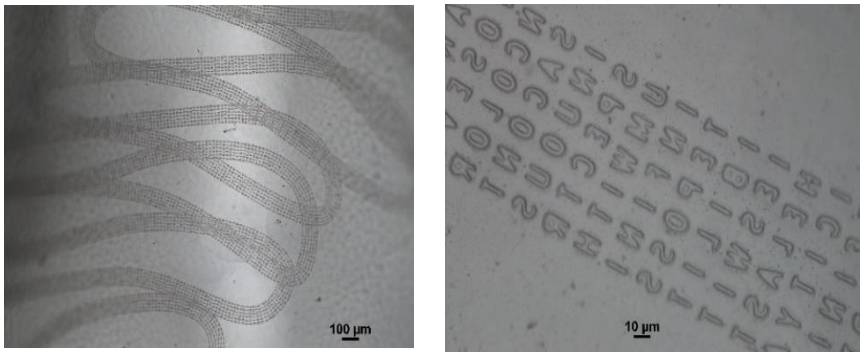

Figure 8.1 *Fibroin alphabets on flexible fibroin sheet*

8.2.2 Use of alternative natural photoinitiators for photolithography

The current SPL process involves synthetic photoinitiators (PI) that are α-hydroxyketones. These PIs are generally considered to be toxic in nature. In the work shown, the devices were washed thoroughly to remove any residual PI from the system. However, use of natural organic molecules can allow for safe implantation or use in sensitive tissue environments without any danger of toxicity. Recently, studies show that riboflavin (Vitamin B2) can be used to crosslink polyethylene glycol-di(meth)acrylate (PEGDA) and as well as silk.[330, 331] Since the chemically modified silk protein contains methacrylate moieties and their crosslink chemistry is similar to that of PEGDA, investigation with riboflavin as PI for silk protein lithography could lead to the development of a fully biofriendly process.

8.2.3 Silk protein based antibacterial surface

Towards incorporating functional properties by fabrication, investigations can be directed towards active biomimetic antimicrobial surfaces. Examples include the fabrication of “shark skin” like

surfaces with specific micropatterns on the surface to impart antimicrobial properties.[332] To date, such surfaces have only been formed on rigid surfaces using synthetic polymers. However, using the SPL technique, it is possible to visualize applications with antimicrobial properties for implantable and flexible environments. Effects of surface topography and feature sizes on bacterial adhesion are needed. An example of shark skin patterned silk protein film is shown in Figure 8.2.

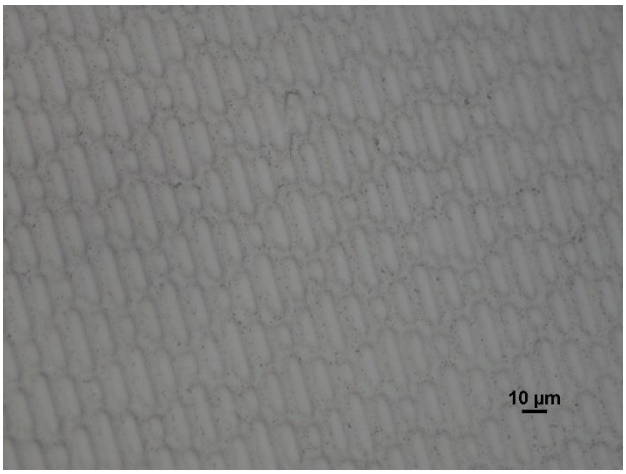

Figure 8.2 *Biomimetic shark-skin patterns of silk protein*

8.2.4 Development of silk-based organic field effect transistor

Similar to the biosensors and SCs shown, it is possible to visualize various forms of organic bioelectronics device components including organic field effect transistors (OFET), and electronic skin. The OFET may be conceived to transduce mechanical and chemical stimuli to electrical signals.[333, 334] However, a key obstacle in the development of such devices for biosensing applications is the development of suitable fabrication processes to form these devices on flexible formats. In addition, the development of suitable composites with semiconducting and dielectric properties are needed. The fabrication platform can be easily extended to develop an FET array on

flexible fibroin sheet. However, there are few challenges in realization of such devices including the development of three-step fabrication for fabricating channel dielectric and gate electrode layers, optimization of channel dimensions, and overcoming the low mobility of charge carriers resulting in huge ratio between driving voltage and modulated current (leading to a high vulnerability to noise effects).[333]

8.2.5 Multianalyte biosensing and neural recording devices.

The research field of biosensors is now moving towards parallel detection of multiple analytes on the same platform. Multiplexed assays that are integrated with portable devices and wearable devices are desired to obtain results of high scientific quality within short time and at low cost. These can be conceived of as wearable or implantable devices that can operate under dynamic and transient conditions. Studying time-resolved responses often requires continuous read-out to ensure that occurrences of important events are not missed. Highly sensitive multi-node sensor devices where each node is specific for an analyte are required. Thus, the fabrication of such sensors on flexible formats, making each node selective by means of enzyme immobilization, enhancing sensitivity for obtaining fast response and study the effect of interferent molecules are important problems to be solved.

Another interesting application of developed platform can be in a realization of stretchable biosensors. Human skin can be stretched 30-50%, [335, 336] implying that, to use sensors in an epidermal setting, the sensor has to be stretchable at least to that extent or more. Even though the

conductive patterns shown here, are flexible, however, they might fail when subjected to tensile stress during a stretch. A possible approach to obtain stretchability is to form space filling curve designs of these conductive patterns on sensor pads. These space filling curves designs will also provide higher effective surface coverage compared to simple node designs. Another important aspect is the adherence of the flexible devices onto a skin. Previous reports suggest that the flexible film supports having a thickness below 7µm show better conformation with skin.[337] Therefore, FPP film thickness and interconnects have to be reduced to form a completely conformable ultrathin electronics for on-skin sensors. Therefore, patterning of composite conductive ink on ultrathin flexible FPP films will be developed. And better interconnection methods to connect a sensor to external electronics will be explored.

Recent advances in neural prostheses, urge for high-resolution and site-specific stimulation. Currently, commercial neural stimulation devices are made of platinum, iridium oxide, or titanium nitride electrodes.[338] However, the mechanical mismatch between solid metal and soft tissue, and impedance values are undesirable. Conducting polymers offer the organic, improved bionic interface that is necessary to promote biocompatibility in neural stimulation applications. While conducting polymers hold much promise in biomedical applications, the fabrication of these was difficult. The work shows a benign approach to pattern conducting polymers in micro-/nanoscale. Therefore, the technique shows a great promise for the development of such electrodes.

REFERENCES

1. Hardy, J.G. and T.R. Scheibel, *Composite materials based on silk proteins.* Progress in Polymer Science, 2010. **35**(9): p. 1093-1115.
2. Saini, M., et al., *Implant biomaterials: A comprehensive review.* World Journal of Clinical Cases: WJCC, 2015. **3**(1): p. 52.
3. O'brien, F.J., *Biomaterials & scaffolds for tissue engineering.* Materials today, 2011. **14**(3): p. 88-95.
4. Bozukova, D., et al., *Improved performances of intraocular lenses by poly (ethylene glycol) chemical coatings.* Biomacromolecules, 2007. **8**(8): p. 2379-2387.
5. Sell, S.A., et al., *Electrospinning of collagen/biopolymers for regenerative medicine and cardiovascular tissue engineering.* Advanced drug delivery reviews, 2009. **61**(12): p. 1007-1019.
6. Pal, S., *Design of artificial human joints & organs*2013: Springer Science & Business Media.
7. Beutner, D. and K.-B. Huttenbrink, *Passive and active middle ear implants.* GMS current topics in otorhinolaryngology, head and neck surgery, 2009. **8**: p. Doc09.
8. Elmqvist, R., *Review of early pacemaker development.* Pace-Pacing and Clinical Electrophysiology, 1978. **1**(4): p. 535-536.
9. Boretius, T., M. Schuettler, and T. Stieglitz, *On the Stability of Poly-Ethylenedioxythiopene as Coating Material for Active Neural Implants.* Artificial Organs, 2011. **35**(3): p. 245-248.

10. Black, J. and G. Hastings, *Handbook of biomaterial properties*2013: Springer Science & Business Media.

11. Sakiyama-Elbert, S.E. and J.A. Hubbell, *Functional biomaterials: Design of novel biomaterials.* Annual Review of Materials Research, 2001. **31**: p. 183-201.

12. Katti, K.S., *Biomaterials in total joint replacement.* Colloids and Surfaces B: Biointerfaces, 2004. **39**(3): p. 133-142.

13. Griffith, L., *Polymeric biomaterials.* Acta materialia, 2000. **48**(1): p. 263-277.

14. Martiradonna, L., *Soft implants for long-term use.* Nature Materials, 2015. **14**(3): p. 267-267.

15. Lacour, S.P., *Epidermal electronics: Skin health monitoring.* Nature Materials, 2015. **14**(7): p. 659-660.

16. AlGhatrif, M. and J. Lindsay, *A brief review: history to understand fundamentals of electrocardiography.* Journal of community hospital internal medicine perspectives, 2012. **2**(1).

17. Hassler, C., T. Boretius, and T. Stieglitz, *Polymers for neural implants.* Journal of Polymer Science Part B: Polymer Physics, 2011. **49**(1): p. 18-33.

18. Sionkowska, A., *Current research on the blends of natural and synthetic polymers as new biomaterials: Review.* Progress in Polymer Science, 2011. **36**(9): p. 1254-1276.

19. Bhatia, S., *Natural Polymers vs Synthetic Polymer*, in *Natural Polymer Drug Delivery Systems*2016, Springer. p. 95-118.

20. Sun, H.S., Y.C. Chiu, and W.C. Chen, *Renewable polymeric materials for electronic applications.* Polymer Journal, 2017. **49**(1): p. 61-73.

21. Khan, R. and M. Dhayal, *Chitosan/polyaniline hybrid conducting biopolymer base impedimetric immunosensor to detect Ochratoxin-A.* Biosensors and Bioelectronics, 2009. **24**(6): p. 1700-1705.

22. Nyström, G., et al., *Ultrafast all-polymer paper-based batteries.* Nano Letters, 2009. **9**(10): p. 3635-3639.

23. Esquivel, J., et al., *Microfluidic fuel cells on paper: meeting the power needs of next generation lateral flow devices.* Energy & Environmental Science, 2014. **7**(5): p. 1744-1749.

24. Kundu, B., et al., *Silk proteins for biomedical applications: Bioengineering perspectives.* Progress in Polymer Science, 2014. **39**(2): p. 251-267.

25. Rockwood, D.N., et al., *Materials fabrication from Bombyx mori silk fibroin.* Nature Protocols, 2011. **6**(10): p. 1612-1631.

26. Altman, G.H., et al., *Silk-based biomaterials.* Biomaterials, 2003. **24**(3): p. 401-416.

27. Murphy, A.R. and D.L. Kaplan, *Biomedical applications of chemically-modified silk fibroin.* Journal of materials chemistry, 2009. **19**(36): p. 6443-6450.

28. Kurland, N.E., et al., *Precise patterning of silk microstructures using photolithography.* Advanced Materials, 2013. **25**(43): p. 6207-6212.

29. Kurland, N.E., et al., *Silk protein lithography as a route to fabricate sericin microarchitectures.* Advanced Materials, 2014. **26**(26): p. 4431-4437.

30. Omenetto, F.G. and D.L. Kaplan, *A new route for silk.* Nature Photonics, 2008. **2**(11): p. 641-643.

31. Smela, E., *Conjugated polymer actuators for biomedical applications.* Advanced Materials, 2003. **15**(6): p. 481-494.

32. Heim, M., D. Keerl, and T. Scheibel, *Spider silk: from soluble protein to extraordinary fiber.* Angewandte Chemie International Edition, 2009. **48**(20): p. 3584-3596.

33. Vepari, C. and D.L. Kaplan, *Silk as a biomaterial.* Progress in Polymer Science, 2007. **32**(8-9): p. 991-1007.

34. Lotz, B. and F.C. Cesari, *The chemical structure and the crystalline structures of Bombyx mori silk fibroin.* Biochimie, 1979. **61**(2): p. 205-214.

35. Pérez-Rigueiro, J., et al., *Mechanical properties of single-brin silkworm silk.* Journal of Applied Polymer Science, 2000. **75**(10): p. 1270-1277.

36. Qi, Y., et al., *A Review of Structure Construction of Silk Fibroin Biomaterials from Single Structures to Multi-Level Structures.* International Journal of Molecular Sciences, 2017. **18**(3).

37. Melke, J., et al., *Silk fibroin as biomaterial for bone tissue engineering.* Acta Biomaterialia, 2016. **31**: p. 1-16.

38. Perez-Rigueiro, J., et al., *Silkworm silk as an engineering material.* Journal of Applied Polymer Science, 1998. **70**(12): p. 2439-2447.

39. Minoura, N., et al., *Attachment and growth of fibroblast cells on silk fibroin.* Biochemical and Biophysical Research Communications, 1995. **208**(2): p. 511-516.

40. Li, M.Z., M. Ogiso, and N. Minoura, *Enzymatic degradation behavior of porous silk fibroin sheets.* Biomaterials, 2003. **24**(2): p. 357-365.

41. Gamo, T., T. Inokuchi, and H. Laufer, *Polypeptides of fibroin and sericin secreted from the different sections of the silk gland in Bombyx mori.* Insect Biochemistry, 1977. **7**(3): p. 285-295.

42. Cao, T.T. and Y.Q. Zhang, *Processing and characterization of silk sericin from Bombyx mori and its application in biomaterials and biomedicines.* Materials Science & Engineering C-Materials for Biological Applications, 2016. **61**: p. 940-952.

43. Kundu, S.C., et al., *Natural protective glue protein, sericin bioengineered by silkworms: Potential for biomedical and biotechnological applications.* Progress in Polymer Science, 2008. **33**(10): p. 998-1012.

44. Dewair, M., X. Baur, and K. Ziegler, *USE OF IMMUNOBLOT TECHNIQUE FOR DETECTION OF HUMAN IGE AND IGG ANTIBODIES TO INDIVIDUAL SILK PROTEINS.* Journal of Allergy and Clinical Immunology, 1985. **76**(4): p. 537-542.

45. Aramwit, P., et al., *Monitoring of inflammatory mediators induced by silk sericin.* Journal of Bioscience and Bioengineering, 2009. **107**(5): p. 556-561.

46. Panilaitis, B., et al., *Macrophage responses to silk.* Biomaterials, 2003. **24**(18): p. 3079-3085.

47. Wang, Z., et al., *Exploring natural silk protein sericin for regenerative medicine: an injectable, photoluminescent, cell-adhesive 3D hydrogel.* Scientific Reports, 2014. **4**.

48. Zhang, Y.Q., *Applications of natural silk protein sericin in biomaterials.* Biotechnology Advances, 2002. **20**(2): p. 91-100.

49. Ersel, M., et al., *Effects of Silk Sericin on Incision Wound Healing in a Dorsal Skin Flap Wound Healing Rat Model.* Medical Science Monitor, 2016. **22**: p. 1064-1078.

50. Kundu, B. and S.C. Kundu, *Silk sericin/polyacrylamide in situ forming hydrogels for dermal reconstruction.* Biomaterials, 2012. **33**(30): p. 7456-7467.

51. Yang, M.Y., *Silk-based biomaterials.* Microscopy Research and Technique, 2017. **80**(3): p. 269-271.

52. Thurber, A.E., F.G. Omenetto, and D.L. Kaplan, *In vivo bioresponses to silk proteins.* Biomaterials, 2015. **71**: p. 145-157.

53. You, R., et al., *The degradation behavior of silk fibroin derived from different ionic liquid solvents.* Natural Science, 2013. **Vol.05No.06**: p. 10.

54. Steven, E., et al., *Carbon nanotubes on a spider silk scaffold.* Nature Communications, 2013. **4**.

55. Kang, M., P. Chen, and H.J. Jin, *Preparation of multiwalled carbon nanotubes incorporated silk fibroin nanofibers by electrospinning.* Current Applied Physics, 2009. **9**: p. S95-S97.

56. Yoon, S.H., et al., *Electrically conducting silk fibroin microspheres by incorporation of multiwalled carbon nanotubes on their surfaces*, in *Eco-Materials Processing and Design Viii*, H. Kim, J. Hojo, and S.W. Lee, Editors. 2007. p. 977-+.

57. Hosseini, S.H. and A. Pairovi, *Preparation of conducting fibres from cellulose and silk by polypyrrole coating.* Iranian Polymer Journal, 2005. **14**(11): p. 934.

58. Tsukada, S., H. Nakashima, and K. Torimitsu, *Conductive polymer combined silk fiber bundle for bioelectrical signal recording.* Plos One, 2012. **7**(4): p. e33689.

59. Samal, S.K., et al., *Biomimetic Magnetic Silk Scaffolds.* ACS applied materials & interfaces, 2015. **7**(11): p. 6282-6292.

60. Wang, J.T., et al., *Directly obtaining pristine magnetic silk fibers from silkworm.* International Journal of Biological Macromolecules, 2014. **63**: p. 205-209.

61. Chu, M. and Y. Sun, *Self-assembly method for the preparation of near-infrared fluorescent spider silk coated with CdTe nanocrystals.* Smart Materials and Structures, 2007. **16**(6): p. 2453.

62. Lammel, A.S., et al., *Controlling silk fibroin particle features for drug delivery.* Biomaterials, 2010. **31**(16): p. 4583-4591.

63. Hofer, M., G. Winter, and J. Myschik, *Recombinant spider silk particles for controlled delivery of protein drugs.* Biomaterials, 2012. **33**(5): p. 1554-1562.

64. de Araujo, A.D., et al., *Diels-Alder ligation and surface immobilization of proteins.* Angewandte Chemie-International Edition, 2006. **45**(2): p. 296-301.

65. Florczak, A., A. Mackiewicz, and H. Dams-Kozlowska, *Functionalized Spider Silk Spheres As Drug Carriers for Targeted Cancer Therapy.* Biomacromolecules, 2014. **15**(8): p. 2971-2981.

66. Zheng, K., et al., *Chemically Functionalized Silk for Human Bone Marrow-Derived Mesenchymal Stem Cells Proliferation and Differentiation.* ACS applied materials & interfaces, 2016. **8**(23): p. 14406-14413.

67. Chen, I., et al., *Site-specific labeling of cell surface proteins with biophysical probes using biotin ligase.* Nature Methods, 2005. **2**(2): p. 99-104.

68. Huang, W., et al., *Improving the activity of immobilized subtilisin by site-specific attachment to surfaces.* Analytical Chemistry, 1997. **69**(22): p. 4601-4607.

69. Stephanopoulos, N. and M.B. Francis, *Choosing an effective protein bioconjugation strategy.* Nature Chemical Biology, 2011. **7**(12): p. 876-884.

70. Cai, K.Y., et al., *Poly(D,L-lactic acid) surfaces modified by silk fibroin: effects on the culture of osteoblast in vitro.* Biomaterials, 2002. **23**(4): p. 1153-1160.

71. Gotoh, Y., et al., *Synthesis of poly(ethylene glycol)-silk fibroin conjugates and surface interaction between L-929 cells and the conjugates.* Biomaterials, 1997. **18**(3): p. 267-271.

72. Manchineella, S., et al., *Surface-Functionalized Silk Fibroin Films as a Platform To Guide Neuron-like Differentiation of Human Mesenchymal Stem Cells.* ACS applied materials & interfaces, 2016. **8**(35): p. 22849-22859.

73. Teramoto, H., K.-i. Nakajima, and C. Takabayashi, *Chemical modification of silk sericin in lithium chloride/dimethyl sulfoxide solvent with 4-cyanophenyl isocyanate.* Biomacromolecules, 2004. **5**(4): p. 1392-1398.

74. Hofmann, S., et al., *Silk fibroin as an organic polymer for controlled drug delivery.* Journal of Controlled Release, 2006. **111**(1): p. 219-227.

75. Liu, H., et al., *Immobilization of glucose oxidase in the composite membrane of regenerated silk fibroin and poly (vinyl alcohol): application to an amperometric glucose sensor.* Bioelectrochemistry and bioenergetics, 1996. **39**(2): p. 303-308.

76. Qian, J.H., et al., *Immobilization of horseradish peroxidase with a regenerated silk fibroin membrane and its application to a tetrathiafulvalene-mediating H2O2 sensor.* Biosensors & Bioelectronics, 1997. **12**(12): p. 1213-1218.

77. Guo, C.C., et al., *Gold nanoparticle-doped silk film as biocompatible SERS substrate.* Rsc Advances, 2015. **5**(3): p. 1937-1942.

78. Kim, S., et al., *Silk inverse opals.* Nature Photonics, 2012. **6**(12): p. 817-822.

79. Hu, X., J. Li, and Y. Bai, *Fabrication of high strength graphene/regenerated silk fibroin composite fibers by wet spinning.* Materials Letters, 2017. **194**: p. 224-226.

80. Tsioris, K., et al., *Rapid Transfer-Based Micropatterning and Dry Etching of Silk Microstructures.* Advanced Materials, 2011. **23**(17): p. 2015-2019.

81. Sarrat, B., et al., *Bioinspired Material Based on Femtosecond Laser Machining of Cast Sheet Micromolding as a Pattern Transfer Process.* Langmuir, 2011. **27**(6): p. 3174-3179.

82. Wu, D., et al., *A facile approach for artificial biomimetic surfaces with both superhydrophobicity and iridescence.* Soft Matter, 2010. **6**(2): p. 263-267.

83. Bettinger, C.J., et al., *Silk fibroin microfluidic devices.* Advanced Materials, 2007. **19**(19): p. 2847-+.

84. Brenckle, M.A., et al., *Protein-Protein Nanoimprinting of Silk Fibroin Films.* Advanced Materials, 2013. **25**(17): p. 2409-2414.

85. Gates, B.D., et al., *New approaches to nanofabrication: Molding, printing, and other techniques.* Chemical reviews, 2005. **105**(4): p. 1171-1196.

86. White, R.D., et al., *Rapid nano impact printing of silk biopolymer thin films.* Journal of Micromechanics and Microengineering, 2011. **21**(11).

87. Kim, S., et al., *All-water-based electron-beam lithography using silk as a resist.* Nature nanotechnology, 2014. **9**(4): p. 306-310.

88. De Silva, A. and C.K. Ober, *Patterning by photolithography.* Functional Polymer Films: 2 Volume Set, 2011: p. 475-499.

89. Kargl, R., et al., *Functional Patterning of Biopolymer Thin Films Using Enzymes and Lithographic Methods.* Advanced Functional Materials, 2013. **23**(3): p. 308-315.

90. Hwang, S.W., et al., *A Physically Transient Form of Silicon Electronics.* Science, 2012. **337**(6102): p. 1640-1644.

91. Hwang, S.W., et al., *High-Performance Biodegradable/Transient Electronics on Biodegradable Polymers.* Advanced Materials, 2014. **26**(23): p. 3905-3911.

92. Yin, L., et al., *Dissolvable metals for transient electronics.* Advanced Functional Materials, 2014. **24**(5): p. 645-658.

93. Fu, K.K., et al., *Transient electronics: materials and devices.* Chemistry of Materials, 2016. **28**(11): p. 3527-3539.

94. Di Mario, C., et al., *Drug-eluting bioabsorbable magnesium stent.* Journal of interventional cardiology, 2004. **17**(6): p. 391-395.

95. Hwang, S.-W., et al., *Dissolution chemistry and biocompatibility of single-crystalline silicon nanomembranes and associated materials for transient electronics.* Acs Nano, 2014. **8**(6): p. 5843-5851.

96. Rivnay, J., R.M. Owens, and G.G. Malliaras, *The Rise of Organic Bioelectronics.* Chemistry of Materials, 2014. **26**(1): p. 679-685.

97. Chiang, C.K., et al., *ELECTRICAL-CONDUCTIVITY IN DOPED POLYACETYLENE.* Physical Review Letters, 1977. **39**(17): p. 1098-1101.

98. MacDiarmid, A.G., *Synthetic metals: a novel role for organic polymers.* Synthetic Metals, 2001. **125**(1): p. 11-22.

99. Shirakawa, H., *Nobel Lecture: The discovery of polyacetylene film - the dawning of an era of conducting polymers.* Reviews of Modern Physics, 2001. **73**(3): p. 713-718.

100. Guimard, N.K., N. Gomez, and C.E. Schmidt, *Conducting polymers in biomedical engineering.* Progress in Polymer Science, 2007. **32**(8): p. 876-921.

101. Svennersten, K., et al., *Organic bioelectronics in nanomedicine.* Biochimica Et Biophysica Acta-General Subjects, 2011. **1810**(3): p. 276-285.

102. Berggren, M. and A. Richter-Dahlfors, *Organic bioelectronics.* Advanced Materials, 2007. **19**(20): p. 3201-3213.

103. Ludwig, K.A., et al., *Chronic neural recordings using silicon microelectrode arrays electrochemically deposited with a poly (3, 4-ethylenedioxythiophene)(PEDOT) filmThis*

work was supported by the Center for Wireless Integrated Microsystems NSF EEC-9986866 and the Whitaker Foundation. Journal of neural engineering, 2006. **3**(1): p. 59.

104. Gerard, M., A. Chaubey, and B.D. Malhotra, *Application of conducting polymers to biosensors.* Biosensors & Bioelectronics, 2002. **17**(5): p. 345-359.

105. Voldman, J., M.L. Gray, and M.A. Schmidt, *Microfabrication in biology and medicine.* Annual Review of Biomedical Engineering, 1999. **1**(1): p. 401-425.

106. Baldini, F., et al., *Fiber Optic Sensors for Biomedical Applications.* Current Analytical Chemistry, 2008. **4**(4): p. 378-390.

107. Grayson, A.C.R., et al., *A BioMEMS review: MEMS technology for physiologically integrated devices.* Proceedings of the Ieee, 2004. **92**(1): p. 6-21.

108. Contag, C.H. and B.D. Ross, *It's not just about anatomy: in vivo bioluminescence imaging as an eyepiece into biology.* Journal of magnetic resonance imaging, 2002. **16**(4): p. 378-387.

109. West, J.L. and N.J. Halas, *Engineered nanomaterials for biophotonics applications: improving sensing, imaging, and therapeutics.* Annual Review of Biomedical Engineering, 2003. **5**(1): p. 285-292.

110. Lee, L.P. and R. Szema, *Inspirations from biological optics for advanced photonic systems.* Science, 2005. **310**(5751): p. 1148-1150.

111. Gu, Z.Z., et al., *Structural color and the lotus effect.* Angewandte Chemie International Edition, 2003. **42**(8): p. 894-897.

112. Pfaff, G. and P. Reynders, *Angle-dependent optical effects deriving from submicron structures of films and pigments.* Chemical reviews, 1999. **99**(7): p. 1963-1982.

113. Jeong, K.-H., J. Kim, and L.P. Lee, *Biologically inspired artificial compound eyes.* Science, 2006. **312**(5773): p. 557-561.

114. He, Y., X. Li, and L. Que, *A Transparent Nanostructured Optical Biosensor.* Journal of Biomedical Nanotechnology, 2014. **10**(5): p. 767-774.

115. Kanellos, G.T., et al., *Two dimensional polymer-embedded quasi-distributed FBG pressure sensor for biomedical applications.* Optics Express, 2010. **18**(1): p. 179-186.

116. Kim, D.H., et al., *Thin, Flexible Sensors and Actuators as 'Instrumented' Surgical Sutures for Targeted Wound Monitoring and Therapy.* Small, 2012. **8**(21): p. 3263-3268.

117. Smart, S.K., et al., *The biocompatibility of carbon nanotubes.* Carbon, 2006. **44**(6): p. 1034-1047.

118. Lawrence, B.D., et al., *Bioactive silk protein biomaterial systems for optical devices.* Biomacromolecules, 2008. **9**(4): p. 1214-1220.

119. Sun, Y.-L., et al., *Stretching type II collagen with optical tweezers.* Journal of biomechanics, 2004. **37**(11): p. 1665-1669.

120. Azofeifa, D.E., H.J. Arguedas, and W.E. Vargas, *Optical properties of chitin and chitosan biopolymers with application to structural color analysis.* Optical Materials, 2012. **35**(2): p. 175-183.

121. Qin, G.K., et al., *Recombinant reflectin-based optical materials.* Journal of Polymer Science Part B-Polymer Physics, 2013. **51**(4): p. 254-264.

122. Domachuk, P., et al., *Bioactive "self-sensing" optical systems.* Applied Physics Letters, 2009. **95**(25).

123. Der, A., et al., *Protein-based all-optical sensor device.* Sensors and Actuators B-Chemical, 2010. **151**(1): p. 26-29.

124. Sznitko, L., et al., *Biopolymer based system doped with nonlinear optical dye as a medium for amplified spontaneous emission and lasing.* Applied Physics Letters, 2011. **99**(3).

125. Kwon, H. and S. Kim, *Chemically Tunable, Biocompatible, and Cost-Effective Metal-Insulator-Metal Resonators Using Silk Protein and Ultrathin Silver Films.* Acs Photonics, 2015. **2**(12): p. 1675-1680.

126. Galeotti, F., et al., *Precise surface patterning of silk fibroin films by breath figures.* Soft Matter, 2012. **8**(17): p. 4815-4821.

127. Kang, D.Y., et al., *Scalable microfabrication procedures for adhesive-integrated flexible and stretchable electronic sensors.* Sensors, 2015. **15**(9): p. 23459-23476.

128. Bhushan, B., *Biomimetics: lessons from nature - an overview.* Philosophical Transactions of the Royal Society a-Mathematical Physical and Engineering Sciences, 2009. **367**(1893): p. 1445-1486.

129. Kurland, N.E., et al., *Silk Protein Lithography as a Route to Fabricate Sericin Microarchitectures.* Advanced Materials, 2014. **26**(26): p. 4431-+.

130. Brzoska, J.B., I. Benazouz, and F. Rondelez, *SILANIZATION OF SOLID SUBSTRATES - A STEP TOWARD REPRODUCIBILITY.* Langmuir, 1994. **10**(11): p. 4367-4373.

131. Parker, A.R. and H.E. Townley, *Biomimetics of photonic nanostructures.* Nature nanotechnology, 2007. **2**(6): p. 347-353.

132. Vukusic, P. and J.R. Sambles, *Photonic structures in biology.* Nature, 2003. **424**(6950): p. 852-855.

133. Glover, B.J. and H.M. Whitney, *Structural colour and iridescence in plants: the poorly studied relations of pigment colour.* Annals of Botany, 2010. **105**(4): p. 505-511.

134. Prum, R.O., et al., *Coherent light scattering by blue feather barbs.* Nature, 1998. **396**(6706): p. 28-29.

135. Seago, A.E., et al., *Gold bugs and beyond: a review of iridescence and structural colour mechanisms in beetles (Coleoptera).* Journal of the Royal Society Interface, 2009. **6**: p. S165-S184.

136. Bagnara, J.T., P.J. Fernandez, and R. Fujii, *On the blue coloration of vertebrates.* Pigment Cell Research, 2007. **20**(1): p. 14-26.

137. Baez, A.V., *Fresnel zone plate for optical image formation using extreme ultraviolet and soft X- radiation.* Journal of the Optical Society of America, 1961. **51**(4): p. 405-&.

138. Pang, S., et al., *Fluorescence microscopy imaging with a Fresnel zone plate array based optofluidic microscope.* Lab on a Chip, 2011. **11**(21): p. 3698-3702.

139. Wu, S.-R., Y. Hwu, and G. Margaritondo, *Hard-X-ray zone plates: recent progress.* Materials, 2012. **5**(10): p. 1752-1773.

140. Sakdinawat, A. and D. Attwood, *Nanoscale X-ray imaging.* Nature Photonics, 2010. **4**(12): p. 840-848.

141. Fan, Y.H., H.W. Ren, and S.T. Wu, *Switchable Fresnel lens using polymer-stabilized liquid crystals.* Optics Express, 2003. **11**(23): p. 3080-3086.

142. Rajasekharan, R., et al., *Can nanotubes make a lens array?* Advanced Materials, 2012. **24**(23).

143. Morgan, B., et al., *Development of a deep silicon phase Fresnel lens using gray-scale lithography and deep reactive ion etching.* Journal of Microelectromechanical Systems, 2004. **13**(1): p. 113-120.

144. Hu, J.J., et al., *Flexible integrated photonics: where materials, mechanics and optics meet Invited.* Optical Materials Express, 2013. **3**(9): p. 1313-1331.

145. Khademhosseini, A., et al., *Microscale technologies for tissue engineering and biology.* Proceedings of the National Academy of Sciences of the United States of America, 2006. **103**(8): p. 2480-2487.

146. Ainslie, K.M. and T.A. Desai, *Microfabricated implants for applications in therapeutic delivery, tissue engineering, and biosensing.* Lab on a Chip, 2008. **8**(11): p. 1864-1878.

147. Tao, H., D.L. Kaplan, and F.G. Omenetto, *Silk Materials - A Road to Sustainable High Technology.* Advanced Materials, 2012. **24**(21): p. 2824-2837.

148. Horan, R.L., et al., *In vitro degradation of silk fibroin.* Biomaterials, 2005. **26**(17): p. 3385-3393.

149. Zhao, C.X., et al., *Enzymatic degradation of Antheraea pernyi silk fibroin 3D scaffolds and fibers.* International Journal of Biological Macromolecules, 2011. **48**(2): p. 249-255.

150. Arai, T., et al., *Biodegradation of Bombyx mori silk fibroin fibers and films.* Journal of Applied Polymer Science, 2004. **91**(4): p. 2383-2390.

151. Zhou, C.Z., et al., *Silk fibroin: structural implications of a remarkable amino acid sequence.* Proteins: Structure, Function, and Bioinformatics, 2001. **44**(2): p. 119-122.

152. Teramoto, H. and M. Miyazawa, *Molecular orientation behavior of silk sericin film as revealed by ATR infrared spectroscopy.* Biomacromolecules, 2005. **6**(4): p. 2049-2057.

153. Zuo, B., L. Dai, and Z. Wu, *Analysis of structure and properties of biodegradable regenerated silk fibroin fibers.* Journal of Materials Science, 2006. **41**(11): p. 3357-3361.

154. Cao, Y. and B.C. Wang, *Biodegradation of Silk Biomaterials.* International Journal of Molecular Sciences, 2009. **10**(4): p. 1514-1524.

155. Caldorera-Moore, M., et al., *Designer nanoparticles: incorporating size, shape and triggered release into nanoscale drug carriers.* Expert Opinion on Drug Delivery, 2010. **7**(4): p. 479-495.

156. Kumari, A., S.K. Yadav, and S.C. Yadav, *Biodegradable polymeric nanoparticles based drug delivery systems.* Colloids and Surfaces B-Biointerfaces, 2010. **75**(1): p. 1-18.

157. Orive, G., et al., *Drug delivery in biotechnology: present and future.* Current Opinion in Biotechnology, 2003. **14**(6): p. 659-664.

158. Kim, S.-H., et al., *Encapsulation of Enzymes within Polymer Spheres To Create Optical Nanosensors for Oxidative Stress.* Analytical Chemistry, 2005. **77**(21): p. 6828 -6833.

159. Bae, Y.H. and K. Park, *Targeted drug delivery to tumors: Myths, reality and possibility.* Journal of Controlled Release, 2011. **153**(3): p. 198-205.

160. Mitragotri, S. and J. Lahann, *Physical approaches to biomaterial design.* Nature Materials, 2009. **8**(1): p. 15-23.

161. Champion, J.A., Y.K. Katare, and S. Mitragotri, *Particle shape: A new design parameter for micro- and nanoscale drug delivery carriers.* Journal of Controlled Release, 2007. **121**(1-2): p. 3-9.

162. Sen Gupta, A., *Role of particle size, shape, and stiffness in design of intravascular drug delivery systems: insights from computations, experiments, and nature.* Wiley Interdisciplinary Reviews-Nanomedicine and Nanobiotechnology, 2016. **8**(2): p. 255-270.

163. Li, Y., et al., *Self-Assembled Nanoparticles Based on Amphiphilic Anticancer Drug-Phospholipid Complex for Targeted Drug Delivery and Intracellular Dual-Controlled Release.* Acs Applied Materials & Interfaces, 2015. **7**(32): p. 17573-17581.

164. Sunderland, T., J.G. Kelly, and Z. Ramtoola, *Application of a novel 3-fluid nozzle spray drying process for the microencapsulation of therapeutic agents using incompatible drug-polymer solutions.* Archives of Pharmacal Research, 2015. **38**(4): p. 566-573.

165. Hariyadi, D.M., et al., *Diffusion loading and drug delivery characteristics of alginate gel microparticles produced by a novel impinging aerosols method.* Journal of Drug Targeting, 2010. **18**(10): p. 831-841.

166. Merisko-Liversidge, E. and G.G. Liversidge, *Nanosizing for oral and parenteral drug delivery: A perspective on formulating poorly-water soluble compounds using wet media milling technology.* Advanced Drug Delivery Reviews, 2011. **63**(6): p. 427-440.

167. Iqbal, M., et al., *Double emulsion solvent evaporation techniques used for drug encapsulation.* International Journal of Pharmaceutics, 2015. **496**(2): p. 173-190.

168. Liddle, J.A. and G.M. Gallatin, *Nanomanufacturing: a perspective.* Acs Nano, 2016. **10**(3): p. 2995-3014.

169. Shum, H.C., et al., *Droplet Microfluidics for Fabrication of Non-Spherical Particles.* Macromolecular Rapid Communications, 2010. **31**(2): p. 108-118.

170. Xu, J., et al., *Future of the Particle Replication in Nonwetting Templates (PRINT) Technology.* Angewandte Chemie-International Edition, 2013. **52**(26): p. 6580-6589.

171. Wang, J., et al., *More Effective Nanomedicines through Particle Design.* Small, 2011. **7**(14): p. 1919-1931.

172. Kim, S.H., et al., *Self-assembled colloidal structures for photonics.* Npg Asia Materials, 2011. **3**(1): p. 25-33.

173. Cederquist, K.B., S.L. Dean, and C.D. Keating, *Encoded anisotropic particles for multiplexed bioanalysis.* Wiley Interdisciplinary Reviews-Nanomedicine and Nanobiotechnology, 2010. **2**(6): p. 578-600.

174. Le Goff, G.C., et al., *High-Throughput Contact Flow Lithography.* Advanced Science, 2015. **2**(10): p. n/a-n/a.

175. Higuita-Castro, N., et al., *Soft Lithography-Based Fabrication of Biopolymer Microparticles for Nutrient Microencapsulation.* Industrial Biotechnology, 2012. **8**(6): p. 365-371.

176. Hassan, N., et al., *Flow Chemistry to Control the Synthesis of Nano and Microparticles for Biomedical Applications.* Current Topics in Medicinal Chemistry, 2014. **14**(5): p. 676-689.

177. Dendukuri, D. and P.S. Doyle, *The Synthesis and Assembly of Polymeric Microparticles Using Microfluidics.* Advanced Materials, 2009. **21**(41): p. 4071-4086.

178. Hyun, D.C., *Fabrication of monodisperse poly (ε-caprolactone)(PCL) particles using capillary force lithography (CFL).* Rsc Advances, 2015. **5**(93): p. 76321-76329.

179. Gratton, S.E.A., et al., *Nanofabricated particles for engineered drug therapies: A preliminary Biodistribution study of PRINT (TM) nanoparticles.* Journal of Controlled Release, 2007. **121**(1-2): p. 10-18.

180. Perry, J.L., et al., *PRINT: A Novel Platform Toward Shape and Size Specific Nanoparticle Theranostics.* Accounts of Chemical Research, 2011. **44**(10): p. 990-998.

181. Kelly, J.Y. and J.M. DeSimone, *Shape-specific, monodisperse nano-molding of protein particles.* Journal of the American Chemical Society, 2008. **130**(16): p. 5438-+.

182. Mohanty, A.K., M. Misra, and L.T. Drzal, *Sustainable bio-composites from renewable resources: Opportunities and challenges in the green materials world.* Journal of Polymers and the Environment, 2002. **10**(1-2): p. 19-26.

183. Nair, L.S. and C.T. Laurencin, *Biodegradable polymers as biomaterials.* Progress in Polymer Science, 2007. **32**(8-9): p. 762-798.

184. Yucel, T., M.L. Lovett, and D.L. Keplan, *Silk-based biomaterials for sustained drug delivery.* Journal of Controlled Release, 2014. **190**: p. 381-397.

185. Mottaghitalab, F., et al., *Silk fibroin nanoparticle as a novel drug delivery system.* Journal of Controlled Release, 2015. **206**: p. 161-176.

186. Yucel, T., et al., *Silk fibroin rods for sustained delivery of breast cancer therapeutics.* Biomaterials, 2014. **35**(30): p. 8613-8620.

187. Sundar, S., J. Kundu, and S.C. Kundu, *Biopolymeric nanoparticles.* Science and Technology of Advanced Materials, 2010. **11**(1).

188. Zhang, S.G., *Fabrication of novel biomaterials through molecular self-assembly.* Nature Biotechnology, 2003. **21**(10): p. 1171-1178.

189. Zhang, S.G., *Emerging biological materials through molecular self-assembly.* Biotechnology Advances, 2002. **20**(5-6): p. 321-339.

190. Leong, T.G., A.M. Zarafshar, and D.H. Gracias, *Three-Dimensional Fabrication at Small Size Scales.* Small, 2010. **6**(7): p. 792-806.

191. Wang, Y., et al., *In vivo degradation of three-dimensional silk fibroin scaffolds.* Biomaterials, 2008. **29**(24-25): p. 3415-3428.

192. Petros, R.A. and J.M. DeSimone, *Strategies in the design of nanoparticles for therapeutic applications.* Nature Reviews Drug Discovery, 2010. **9**(8): p. 615-627.

193. Macleod, J. and F. Rosei, *Photonic crystals: Sustainable sensors from silk.* Nature Materials, 2013. **12**(2): p. 98-100.

194. Altman, G.H., et al., *Silk-based biomaterials.* Biomaterials, 2003. **24**(3): p. 401-416.

195. Zhang, Y.F., et al., *In Vitro and In Vivo Evaluation of Adenovirus Combined Silk Fibroin Scaffolds for Bone Morphogenetic Protein-7 Gene Delivery.* Tissue Engineering Part C-Methods, 2011. **17**(8): p. 789-797.

196. Srisawasdi, T., et al., *Electromechanical response of silk fibroin hydrogel and conductive polycarbazole/silk fibroin hydrogel composites as actuator material.* Materials Science & Engineering C-Materials for Biological Applications, 2015. **56**: p. 1-8.

197. Herzer, N., S. Hoeppener, and U.S. Schubert, *Fabrication of patterned silane based self-assembled monolayers by photolithography and surface reactions on silicon-oxide substrates.* Chemical Communications, 2010. **46**(31): p. 5634-5652.

198. Hernandez, C.J. and T.G. Mason, *Colloidal alphabet soup: Monodisperse dispersions of shape-designed LithoParticles.* Journal of Physical Chemistry C, 2007. **111**(12): p. 4477-4480.

199. Paulsen, K.S., D. Di Carlo, and A.J. Chung, *Optofluidic fabrication for 3D-shaped particles.* Nature Communications, 2015. **6**.

200. Shi, P. and J.C.H. Goh, *Self-assembled silk fibroin particles: Tunable size and appearance.* Powder Technology, 2012. **215-16**: p. 85-90.

201. Canelas, D.A., K.P. Herlihy, and J.M. DeSimone, *Top-down particle fabrication: control of size and shape for diagnostic imaging and drug delivery.* Wiley Interdisciplinary Reviews-Nanomedicine and Nanobiotechnology, 2009. **1**(4): p. 391-404.

202. Zhao, Z., et al., *Fabrication of silk fibroin nanoparticles for controlled drug delivery.* Journal of Nanoparticle Research, 2012. **14**(4).

203. Bucciarelli, A., et al., *Fabrication of Nanoscale Patternable Films of Silk Fibroin Using Benign Solvents.* Macromolecular Materials and Engineering, 2017.

204. Zhang, A.Q. and C.M. Lieber, *Nano-Bioelectronics.* Chemical reviews, 2016. **116**(1): p. 215-257.

205. Kostov, I. and F. Filipov, *Bioelectronics - Status and prospectives.* Biotechnology & Biotechnological Equipment, 1999. **13**(1): p. 81-90.

206. Cogan, S.F., *Neural stimulation and recording electrodes*, in *Annual Review of Biomedical Engineering*2008. p. 275-309.

207. Torculas, M., et al., *Protein-Based Bioelectronics.* Acs Biomaterials Science & Engineering, 2016. **2**(8): p. 1211-1223.

208. Lanzani, G., *MATERIALS FOR BIOELECTRONICS Organic electronics meets biology.* Nature Materials, 2014. **13**(8): p. 775-776.

209. Carpi, F. and E. Smela, *Biomedical applications of electroactive polymer actuators.* 2009.

210. Choi, S., et al., *Recent Advances in Flexible and Stretchable Bio-Electronic Devices Integrated with Nanomaterials.* Advanced Materials, 2016. **28**(22): p. 4203-4218.

211. Simon, D.T., et al., *Organic Bioelectronics: Bridging the Signaling Gap between Biology and Technology.* Chemical reviews, 2016. **116**(21): p. 13009-13041.

212. Muskovich, M. and C.J. Bettinger, *Biomaterials-Based Electronics: Polymers and Interfaces for Biology and Medicine.* Advanced Healthcare Materials, 2012. **1**(3): p. 248-266.

213. Someya, T., Z.N. Bao, and G.G. Malliaras, *The rise of plastic bioelectronics.* Nature, 2016. **540**(7633): p. 379-385.

214. Heller, A. and B. Feldman, *Electrochemical glucose sensors and their applications in diabetes management.* Chemical reviews, 2008. **108**(7): p. 2482-2505.

215. Abidian, M.R. and D.C. Martin, *Multifunctional Nanobiomaterials for Neural Interfaces.* Advanced Functional Materials, 2009. **19**(4): p. 573-585.

216. Fattahi, P., et al., *A Review of Organic and Inorganic Biomaterials for Neural Interfaces.* Advanced Materials, 2014. **26**(12): p. 1846-1885.

217. Sun, K., et al., *Review on application of PEDOTs and PEDOT: PSS in energy conversion and storage devices.* Journal of Materials Science-Materials in Electronics, 2015. **26**(7): p. 4438-4462.

218. Balint, R., N.J. Cassidy, and S.H. Cartmell, *Conductive polymers: Towards a smart biomaterial for tissue engineering.* Acta Biomaterialia, 2014. **10**(6): p. 2341-2353.

219. Elschner, A., et al., *PEDOT: principles and applications of an intrinsically conductive polymer*2010: CRC Press.

220. Kaur, G., et al., *Electrically conductive polymers and composites for biomedical applications.* Rsc Advances, 2015. **5**(47): p. 37553-37567.

221. Turbiani, F.R., et al., *Properties of sericin films crosslinking with dimethylolurea.*

222. Thomas, J.P., et al., *High-efficiency hybrid solar cells by nanostructural modification in PEDOT:PSS with co-solvent addition.* Journal of Materials Chemistry A, 2014. **2**(7): p. 2383-2389.

223. Fang, A.P., et al., *Soft-lithography-mediated submicrometer patterning of self-assembled monolayer of hemoglobin on ITO surfaces.* Langmuir, 2000. **16**(12): p. 5221-5226.

224. Wang, L. and E.K. Wang, *A novel hydrogen peroxide sensor based on horseradish peroxidase immobilized on colloidal Au modified ITO electrode.* Electrochemistry communications, 2004. **6**(2): p. 225-229.

225. Deng, J.J., et al., *Label-free optical biosensor based on localized surface plasmon resonance of twin-linked gold nanoparticles electrodeposited on ITO glass.* Biosensors & Bioelectronics, 2010. **26**(2): p. 615-619.

226. Zhang, L., et al., *A novel alcohol dehydrogenase biosensor based on solid-state electrogenerated chemiluminescence by assembling dehydrogenase to Ru (bpy) 3 2+–Au nanoparticles aggregates.* Biosensors and Bioelectronics, 2007. **22**(6): p. 1097-1100.

227. Rodriguez, M.C., A.N. Kawde, and J. Wang, *Aptamer biosensor for label-free impedance spectroscopy detection of proteins based on recognition-induced switching of the surface charge.* Chemical Communications, 2005(34): p. 4267-4269.

228. Pal, R.K., et al., *Conducting polymer-silk biocomposites for flexible and biodegradable electrochemical sensors.* Biosensors & Bioelectronics, 2016. **81**: p. 294-302.

229. Moisel, M., M. de Mele, and W.D. Muller, *Biomaterial Interface Investigated by Electrochemical Impedance Spectroscopy.* Advanced Engineering Materials, 2008. **10**(10): p. B33-B46.

230. Ouyang, S., et al., *Photolithographic Patterning of Highly Conductive PEDOT:PSS and Its Application in Organic Light-Emitting Diodes.* Journal of Polymer Science Part B-Polymer Physics, 2014. **52**(18): p. 1221-1226.

231. Guo, L., et al., *Stretchable Polymeric Multielectrode Array for Conformal Neural Interfacing.* Advanced Materials, 2014. **26**(9): p. 1427-1433.

232. Patton, A.J., R.A. Green, and L.A. Poole-Warren, *Mediating conducting polymer growth within hydrogels by controlling nucleation.* APL Materials, 2015. **3**(1).

233. Green, R.A., et al., *Conducting polymers for neural interfaces: Challenges in developing an effective long-term implant.* Biomaterials, 2008. **29**(24-25): p. 3393-3399.

234. Gerwig, R., et al., *PEDOT-CNT Composite Microelectrodes for Recording and Electrostimulation Applications: Fabrication, Morphology, and Electrical Properties.* Frontiers in neuroengineering, 2012. **5**: p. 8-8.

235. Sessolo, M., et al., *Easy-to-Fabricate Conducting Polymer Microelectrode Arrays.* Advanced Materials, 2013. **25**(15): p. 2135-2139.

236. Williamson, A., et al., *Localized Neuron Stimulation with Organic Electrochemical Transistors on Delaminating Depth Probes.* Advanced Materials, 2015. **27**(30): p. 4405-4410.

237. Hwang, S.W., et al., *Materials and Fabrication Processes for Transient and Bioresorbable High-Performance Electronics.* Advanced Functional Materials, 2013. **23**(33): p. 4087-4093.

238. Birkholz, M., et al., *Continuously Operating Biosensor and Its Integration into a Hermetically Sealed Medical Implant.* Micromachines, 2016. **7**(10).

239. Thévenot, D.R., et al., *Electrochemical biosensors: recommended definitions and classification.* Biosensors and Bioelectronics, 2001. **16**(1): p. 121-131.

240. Turner, A.P., *Biosensors: sense and sensibility.* Chemical Society Reviews, 2013. **42**(8): p. 3184-3196.

241. Hammond, J.L., et al., *Electrochemical biosensors and nanobiosensors,* in *Biosensor Technologies for Detection of Biomolecules*, P. Estrela, Editor 2016. p. 69-80.

242. Grieshaber, D., et al., *Electrochemical biosensors - Sensor principles and architectures.* Sensors, 2008. **8**(3): p. 1400-1458.

243. Aydemir, N., J. Malmstrom, and J. Travas-Sejdic, *Conducting polymer based electrochemical biosensors.* Physical Chemistry Chemical Physics, 2016. **18**(12): p. 8264-8277.

244. Ward, W.K., *How to Design a Biosensor.* Journal of Diabetes Science and Technology, 2007. **1**(2): p. 201-204.

245. Shrivastava, A. and V.B. Gupta, *Methods for the determination of limit of detection and limit of quantitation of the analytical methods.* Chronicles of Young Scientists, 2011. **2**(1): p. 21.

246. Tahir, Z.M., E.C. Alocilja, and D.L. Grooms, *Indium tin oxide-polyaniline biosensor: Fabrication and characterization.* Sensors, 2007. **7**(7): p. 1123-1140.

247. Goldstein, D.S. and C. Holmes, *Neuronal Source of Plasma Dopamine.* Clinical Chemistry, 2008. **54**(11): p. 1864-1871.

248. Keefe, K.A., M. Zigmond, and E. Abercrombie, *In vivo regulation of extracellular dopamine in the neostriatum: influence of impulse activity and local excitatory amino acids.* Journal of Neural Transmission/General Section JNT, 1993. **91**(2-3): p. 223-240.

249. Brazell, M., et al., *Acute administration of nicotine increases the in vivo extracellular levels of dopamine, 3, 4-dihydroxyphenylacetic acid and ascorbic acid preferentially in the nucleus accumbens of the rat: comparison with caudate-putamen.* Neuropharmacology, 1990. **29**(12): p. 1177-1185.

250. Goto, Y., S. Otani, and A.A. Grace, *The Yin and Yang of dopamine release: a new perspective.* Neuropharmacology, 2007. **53**(5): p. 583-587.

251. Cai, W., et al., *Electrochemical determination of ascorbic acid, dopamine and uric acid based on an exfoliated graphite paper electrode: A high performance flexible sensor.* Sensors and Actuators B-Chemical, 2014. **193**: p. 492-500.

252. Wightman, R.M., et al., *Methods to improve electrochemical reversibility at carbon electrodes.* Journal of the Electrochemical Society, 1984. **131**(7): p. 1578-1583.

253. Harrison, F.E. and J.M. May, *Vitamin C function in the brain: vital role of the ascorbate transporter SVCT2.* Free Radical Biology and Medicine, 2009. **46**(6): p. 719-730.

254. Bard, A.J., et al., *Electrochemical methods: fundamentals and applications*. Vol. 2. 1980: wiley New York.

255. Yang, G., K.L. Kampstra, and M.R. Abidian, *High-Performance Conducting Polymer Nanofiber Biosensors for Detection of Biomolecules.* Advanced Materials, 2014. **26**(29): p. 4954-4960.

256. Nambiar, S. and J.T.W. Yeow, *Conductive polymer-based sensors for biomedical applications.* Biosensors & Bioelectronics, 2011. **26**(5): p. 1825-1832.

257. Hou, S.F., et al., *Highly Sensitive and Selective Dopamine Biosensor Fabricated with Silanized Graphene.* Journal of Physical Chemistry C, 2010. **114**(35): p. 14915-14921.

258. Tsakova, V., G. Ilieva, and D. Filjova, *Role of the anionic dopant of poly(3,4-ethylenedioxythiophene) for the electroanalytical performance: electrooxidation of acetaminophen.* Electrochimica Acta, 2015. **179**: p. 343-349.

259. Sun, C.L., et al., *The simultaneous electrochemical detection of ascorbic acid, dopamine, and uric acid using graphene/size-selected Pt nanocomposites.* Biosensors & Bioelectronics, 2011. **26**(8): p. 3450-3455.

260. Zhang, M.N., et al., *Layer-by-layer assembled carbon nanotubes for selective determination of dopamine in the presence of ascorbic acid.* Biosensors & Bioelectronics, 2005. **20**(7): p. 1270-1276.

261. Ali, S.R., et al., *Interference of ascorbic acid in the sensitive detection of dopamine by a nonoxidative sensing approach.* Journal of Physical Chemistry B, 2007. **111**(42): p. 12275-12281.

262. Aldana-Gonzalez, J., et al., *Gold nanoparticles modified-ITO electrode for the selective electrochemical quantification of dopamine in the presence of uric and ascorbic acids.* Journal of Electroanalytical Chemistry, 2013. **706**: p. 69-75.

263. Celebanska, A., et al., *Film electrode prepared from oppositely charged silicate submicroparticles and carbon nanoparticles for selective dopamine sensing.* Biosensors & Bioelectronics, 2011. **26**(11): p. 4417-4422.

264. Roychoudhury, A., S. Basu, and S.K. Jha, *Dopamine biosensor based on surface functionalized nanostructured nickel oxide platform.* Biosensors & Bioelectronics, 2016. **84**: p. 72-81.

265. Pritchard, E.M., et al., *Review physical and chemical aspects of stabilization of compounds in silk.* Biopolymers, 2012. **97**(6): p. 479-498.

266. Wang, J., *Electrochemical glucose biosensors.* Chemical reviews, 2008. **108**(2): p. 814-825.

267. Dong, L.B., et al., *Flexible electrodes and supercapacitors for wearable energy storage: a review by category.* Journal of Materials Chemistry A, 2016. **4**(13): p. 4659-4685.

268. Pushparaj, V.L., et al., *Flexible energy storage devices based on nanocomposite paper.* Proceedings of the National Academy of Sciences of the United States of America, 2007. **104**(34): p. 13574-13577.

269. Li, L., et al., *Advances and challenges for flexible energy storage and conversion devices and systems.* Energy & Environmental Science, 2014. **7**(7): p. 2101-2122.

270. Chae, J.S., et al., *A biocompatible implant electrode capable of operating in body fluids for energy storage devices.* Nano Energy, 2017. **34**: p. 86-92.

271. Gonzalez, A., et al., *Review on supercapacitors: Technologies and materials.* Renewable & Sustainable Energy Reviews, 2016. **58**: p. 1189-1206.

272. Shi, Y. and G.H. Yu, *Designing Hierarchically Nanostructured Conductive Polymer Gels for Electrochemical Energy Storage and Conversions.* Chemistry of Materials, 2016. **28**(8): p. 2466-2477.

273. Qu, G.X., et al., *A Fiber Supercapacitor with High Energy Density Based on Hollow Graphene/Conducting Polymer Fiber Electrode.* Advanced Materials, 2016. **28**(19): p. 3646-3652.

274. Wang, G.P., L. Zhang, and J.J. Zhang, *A review of electrode materials for electrochemical supercapacitors.* Chemical Society Reviews, 2012. **41**(2): p. 797-828.

275. Zheng, Y., et al., *Smart, stretchable and wearable supercapacitors: prospects and challenges.* Crystengcomm, 2016. **18**(23): p. 4218-4235.

276. Beidaghi, M. and Y. Gogotsi, *Capacitive energy storage in micro-scale devices: recent advances in design and fabrication of micro-supercapacitors.* Energy & Environmental Science, 2014. **7**(3): p. 867-884.

277. Zhong, C., et al., *A review of electrolyte materials and compositions for electrochemical supercapacitors.* Chemical Society Reviews, 2015. **44**(21): p. 7484-7539.

278. Irimia-Vladu, M., *"Green" electronics: biodegradable and biocompatible materials and devices for sustainable future.* Chemical Society Reviews, 2014. **43**(2): p. 588-610.

279. Liu, Y.Q., et al., *High-Performance Flexible All-Solid-State Supercapacitor from Large Free-Standing Graphene-PEDOT/PSS Films.* Scientific Reports, 2015. **5**.

280. Moon, W.G., et al., *A Biodegradable Gel Electrolyte for Use in High-Performance Flexible Supercapacitors.* ACS applied materials & interfaces, 2015. **7**(6): p. 3503-3511.

281. Zhang, J.L., et al., *Reduction of graphene oxide via L-ascorbic acid.* Chemical Communications, 2010. **46**(7): p. 1112-1114.

282. Compton, O.C. and S.T. Nguyen, *Graphene oxide, highly reduced graphene oxide, and graphene: versatile building blocks for carbon-based materials.* Small, 2010. **6**(6): p. 711-723.

283. Zhang, S.L. and N. Pan, *Supercapacitors Performance Evaluation.* Advanced Energy Materials, 2015. **5**(6).

284. Hur, J., et al., *DNA hydrogel-based supercapacitors operating in physiological fluids.* Scientific Reports, 2013. **3**.

285. Milroy, C.A. and A. Manthiram, *Bioelectronic Energy Storage: A Pseudocapacitive Hydrogel Composed of Endogenous Biomolecules.* Acs Energy Letters, 2016. **1**(4): p. 672-677.

286. Mosa, I.M., et al., *Ultrathin Graphene–Protein Supercapacitors for Miniaturized Bioelectronics.* Advanced Energy Materials: p. 1700358-n/a.

287. Jia, X., et al., *A Biodegradable Thin-Film Magnesium Primary Battery Using Silk Fibroin–Ionic Liquid Polymer Electrolyte.* Acs Energy Letters, 2017. **2**(4): p. 831-836.

288. Wang, X., et al., *Food-Materials-Based Edible Supercapacitors.* Advanced Materials Technologies, 2016. **1**(3).

289. Liu, C.G., et al., *Graphene-Based Supercapacitor with an Ultrahigh Energy Density.* Nano Letters, 2010. **10**(12): p. 4863-4868.

290. Zhang, J.T. and X.S. Zhao, *Conducting Polymers Directly Coated on Reduced Graphene Oxide Sheets as High-Performance Supercapacitor Electrodes.* Journal of Physical Chemistry C, 2012. **116**(9): p. 5420-5426.

291. Niu, Z.Q., et al., *All-Solid-State Flexible Ultrathin Micro-Supercapacitors Based on Graphene.* Advanced Materials, 2013. **25**(29): p. 4035-4042.

292. Xue, M.Q., et al., *Microfluidic etching for fabrication of flexible and all-solid-state micro supercapacitor based on MnO2 nanoparticles.* Nanoscale, 2011. **3**(7): p. 2703-2708.

293. Ervin, M.H., L.T. Le, and W.Y. Lee, *Inkjet-printed flexible graphene-based supercapacitor.* Electrochimica Acta, 2014. **147**: p. 610-616.

294. Wang, Y., et al., *Printed all-solid flexible microsupercapacitors: towards the general route for high energy storage devices.* Nanotechnology, 2014. **25**(9): p. 094010.

295. Zequine, C., et al., *High Performance and Flexible Supercapacitors based on Carbonized Bamboo Fibers for Wide Temperature Applications.* Scientific Reports, 2016. **6**.

296. Armelin, E., et al., *Current status and challenges of biohydrogels for applications as supercapacitors and secondary batteries.* Journal of Materials Chemistry A, 2016. **4**(23): p. 8952-8968.

297. Zhou, C., et al., *Construction of High-Capacitance 3D CoO@Polypyrrole Nanowire Array Electrode for Aqueous Asymmetric Supercapacitor.* Nano Letters, 2013. **13**(5): p. 2078-2085.

298. Shi, Y., et al., *Nanostructured conductive polypyrrole hydrogels as high-performance, flexible supercapacitor electrodes.* Journal of Materials Chemistry A, 2014. **2**(17): p. 6086-6091.

299. Liu, Z.Y., et al., *Ultraflexible In-Plane Micro-Supercapacitors by Direct Printing of Solution-Processable Electrochemically Exfoliated Graphene.* Advanced Materials, 2016. **28**(11): p. 2217-2222.

300. Yang, K., et al., *Bendable solid-state supercapacitors with Au nanoparticle-embedded graphene hydrogel films.* Scientific Reports, 2017. **7**.

301. Xu, Y.X., et al., *Flexible Solid-State Supercapacitors Based on Three-Dimensional Graphene Hydrogel Films.* Acs Nano, 2013. **7**(5): p. 4042-4049.

302. Wan, C.C., Y. Jiao, and J. Li, *Flexible, highly conductive, and free-standing reduced graphene oxide/polypyrrole/cellulose hybrid papers for supercapacitor electrodes.* Journal of Materials Chemistry A, 2017. **5**(8): p. 3819-3831.

303. Jung, H., et al., *Direct printing and reduction of graphite oxide for flexible supercapacitors.* Applied Physics Letters, 2014. **105**(5).

304. Zhang, L., et al., *Flexible Micro-Supercapacitor Based on Graphene with 3D Structure.* Small, 2017. **13**(10).

305. Yadav, P., et al., *Highly Stable Laser-Scribed Flexible Planar Microsupercapacitor Using Mushroom Derived Carbon Electrodes.* Advanced Materials Interfaces, 2016. **3**(11).

306. Sun, G.Z., et al., *Layer-by-layer printing of laminated graphene-based interdigitated microelectrodes for flexible planar micro-supercapacitors.* Electrochemistry communications, 2015. **51**: p. 33-36.

307. El-Kady, M.F. and R.B. Kaner, *Scalable fabrication of high-power graphene micro-supercapacitors for flexible and on-chip energy storage.* Nature Communications, 2013. **4**.

308. Snook, G.A., P. Kao, and A.S. Best, *Conducting-polymer-based supercapacitor devices and electrodes.* Journal of Power Sources, 2011. **196**(1): p. 1-12.

309. Pal, R.K., et al., *Photolithographic Micropatterning of Conducting Polymers on Flexible Silk Matrices.* Advanced Materials, 2016. **28**(7): p. 1406-1412.

310. Nie, Z. and E. Kumacheva, *Patterning surfaces with functional polymers.* Nature Materials, 2008. **7**(4): p. 277-290.

311. Madou, M.J., *Fundamentals of microfabrication: the science of miniaturization*2002: CRC press.

312. Jeong, C.K., et al., *Electrical Biomolecule Detection Using Nanopatterned Silicon via Block Copolymer Lithography.* Small, 2014. **10**(2): p. 337-343.

313. Lin, J.Y., et al., *Nanopatterned Substrates Increase Surface Sensitivity for Real-Time Biosensing.* Journal of Physical Chemistry C, 2013. **117**(10): p. 5286-5292.

314. Jahani, S. and Z. Jacob, *All-dielectric metamaterials.* Nature nanotechnology, 2016. **11**(1): p. 23-36.

315. Falconnet, D., et al., *A novel approach to produce protein nanopatterns by combining nanoimprint lithography and molecular self-assembly.* Nano Letters, 2004. **4**(10): p. 1909-1914.

316. Lee, K.B., S.J. Park, and C.A. Mirkin, *Protein nanoarrays generated by Dip-Pen Nanolithography.* Abstracts of Papers of the American Chemical Society, 2002. **223**: p. C94-C94.

317. Sun, Y.L., et al., *Aqueous multiphoton lithography with multifunctional silk-centred bio-resists.* Nature Communications, 2015. **6**.

318. Petti, L., et al., *Fabrication of Novel Two-Dimensional Nanopatterned Conductive PEDOT:PSS Films for Organic Optoelectronic Applications.* ACS applied materials & interfaces, 2013. **5**(11): p. 4777-4782.

319. Rickard, J.J.S., I. Farrer, and P.G. Oppenheimer, *Tunable Nanopatterning of Conductive Polymers via Electrohydrodynamic Lithography.* Acs Nano, 2016. **10**(3): p. 3865-3870.

320. Salaita, K., Y. Wang, and C.A. Mirkin, *Applications of dip-pen nanolithography.* Nature nanotechnology, 2007. **2**(3): p. 145-155.

321. Huo, F., et al., *Polymer pen lithography.* Science, 2008. **321**(5896): p. 1658-1660.

322. Pease, R., *Electron beam lithography.* Contemporary Physics, 1981. **22**(3): p. 265-290.

323. Norman, J.J. and T.A. Desai, *Methods for fabrication of nanoscale topography for tissue engineering scaffolds.* Annals of biomedical engineering, 2006. **34**(1): p. 89-101.

324. Kolodziej, C.M. and H.D. Maynard, *Electron-beam lithography for patterning biomolecules at the micron and nanometer scale.* Chemistry of Materials, 2012. **24**(5): p. 774-780.

325. Jiang, L., X. Wang, and L. Chi, *Nanoscaled surface patterning of conducting polymers.* Small, 2011. **7**(10): p. 1309-1321.

326. Persson, S., P. Dyreklev, and O. Inganäs, *Patterning of poly (3-octylthiophene) conducting polymer films by electron beam exposure.* Advanced Materials, 1996. **8**(5): p. 405-408.

327. Gangnaik, A.S., Y.M. Georgiev, and J.D. Holmes, *New Generation Electron Beam Resists: A Review.* Chemistry of Materials, 2017. **29**(5): p. 1898-1917.

328. Tseng, A.A., et al., *Electron beam lithography in nanoscale fabrication: recent development.* IEEE Transactions on Electronics Packaging Manufacturing, 2003. **26**(2): p. 141-149.

329. Leitao, D.C., et al. *Optimization of exposure parameters for lift-off process of sub-100 features using a negative tone electron beam resist*. in *Nanotechnology (IEEE-NANO), 2012 12th IEEE Conference on*. 2012. IEEE.

330. Hao, Y., et al., *Visible light cured thiol-vinyl hydrogels with tunable degradation for 3D cell culture.* Acta Biomaterialia, 2014. **10**(1): p. 104-114.

331. Applegate, M.B., et al., *Photocrosslinking of silk fibroin using riboflavin for ocular prostheses.* Advanced Materials, 2016. **28**(12): p. 2417-2420.

332. Mann, E.E., et al., *Surface micropattern limits bacterial contamination.* Antimicrobial resistance and infection control, 2014. **3**(1): p. 28.

333. Goetz, S., et al., *Organic field-effect transistors for biosensing applications.* Organic Electronics, 2009. **10**(4): p. 573-580.

334. Sokolov, A.N., et al., *Chemical and engineering approaches to enable organic field-effect transistors for electronic skin applications.* Accounts of chemical research, 2011. **45**(3): p. 361-371.

335. Park, J., et al., *Tactile-Direction-Sensitive and Stretchable Electronic Skins Based on Human-Skin-Inspired Interlocked Microstructures.* Acs Nano, 2014. **8**(12): p. 12020-12029.

336. Agache, P.G., et al., *Mechanical-properties and youngs modulus of human-skin in vivo.* Archives of Dermatological Research, 1980. **269**(3): p. 221-232.

337. Kim, D.H., et al., *Epidermal Electronics.* Science, 2011. **333**(6044): p. 838-843.

338. Zhou, D.D., et al., *Conducting Polymers in Neural Stimulation Applications*, in *Implantable Neural Prostheses 2: Techniques and Engineering Approaches*, D.D. Zhou and E. Greenbaum, Editors. 2010. p. 217-252.

Vita

Ramendra Kishor Pal was born on 6th of February 1985 in Kanpur, Uttar Pradesh, India. He grew up in Kanpur, India and graduated from H.N. Inter College in 2003. He received an associate (of Institution of Engineers) degree in 2011. In 2013, he earned a Master of Technology in Chemical Engineering at the Indian Institute of Technology, Kharagpur. Doctoral work was carried out under the supervision of Dr. Vamsi Yadavalli at Virginia Commonwealth University.